University of Southern Queensland

Faculty of Health, Engineering & Sciences

CFD Analysis of a Primary Nozzle Vortex Generator on Steam Ejector Performance

A dissertation submitted by

Brodie Cooper

in fulfilment of the requirements of

ENG4112 Research Project

towards the degree of

Bachelor of Mechanical Engineering (Honours)

Submitted: October, 2022

Abstract

Ejectors are considered by many researchers a promising replacement for compressors in air-conditioning and refrigeration applications. They are more economical due to having no moving parts, giving them the advantage of requiring less maintenance and having fewer potential points of failure. With concern surrounding the effects of global warming rapidly increasing, the jet ejector's ability to operate using environmentally friendly refrigerants and low-grade thermal energy is highly appealing. The main disadvantage observed throughout research is that the ejector has a poor coefficient of performance attributed to the effects of supersonic turbulent mixing.

The University of Southern Queensland commissioned a steam ejector refrigeration apparatus for the purpose of providing flow visualisation for ongoing research aimed at understanding ejector mixing behaviour and factors influencing the coefficient of performance (Al-Doori 2013). This study focuses on improving the performance of the ejector by incorporating a vortex generator into the design of the primary flow nozzle, with the findings of this dissertation intended to contribute to a technical paper currently being prepared by the University of Southern Queensland. Computational fluid dynamics software is capable of providing reliable results at an acceptable level of accuracy with significantly lower associated costs and risks compared to experimental techniques. For this reason, the operation of the steam ejector has been characterised in this study through an entirely computational approach, using ANSYS Fluent.

To achieve this, the dimensions of the UniSQ steam ejector were obtained through previous work completed by Al-Manea (2019) and Al-Doori (2013); these papers also provided the boundary conditions corresponding the UniSQ steam ejector apparatus necessary for the CFD analysis. The key parameters of the CFD simulations were the use of the realisable k-ϵ turbulence model coupled with advanced wall functions and specified primary, secondary and condenser pressures. Use of the species transport model enabled water-vapour and nitrogen to be assigned to the primary and secondary inlets to remain consistent with the real system; the refrigerants were treated as ideal gases for the purpose of simplicity.

Initially, a 2D ejector model was generated and the geometry was validated by comparing the results obtained through ANSYS Fluent simulations against the existing experimental and CFD results of Al-Manea (2019). A 3D model of the ejector was developed through external CAD software to be used as a standard for comparison for the models equipped with vortex generators. The primary and secondary pressures were set constant at 150kPa and 2.4kPa, respectively, and the condenser pressure was adjusted between 1.8 - 2.8kPa to simulate the operating range of the ejector. The 3D model recorded less than 1% error in choked conditions and up to 10% in unchoked conditions compared to the 2D model.

Following the verification of the standard model, a parametric study was conducted investigating different variations of vortex generators in the primary nozzle. A series of ejector models were created with modified nozzles varying in the vortex generator pitch, profile and quantity. Due to the limited volume of the nozzle and supersonic steam velocity, the models were limited to a maximum of three generators with helical pitches ranging from 17.5 - 53mm, and profiles of 1mm. The influence of the generators geometric characteristics was identified by simulations of the operating range over the same boundary conditions as those used for baseline ejector model.

The results obtained from the simulations revealed that the induced swirling effect decayed rapidly in the mixing chamber and that the presence of the vortex generators reduced primary flow velocity by between 3 and 43.3 m/s. The minimum pressure at the nozzle exit increased over the standard nozzle by between 161.7 and 639.8 Pa for the modified nozzle variations. The combination of these effects resulted in a decreased entrainment ratio of between $0.67 - 2\%$ and an increased calculated mixing efficiency of between $0.22 - 3.7\%$. Overall, the generator variations resulted in increased recirculation and turbulence that contributed to producing a lower quality primary-secondary mixture. It was determined that, in general, the performance of the ejector was decreased as the quantity of vortex generators increased and the helical pitch was reduced.

University of Southern Queensland

Faculty of Health, Engineering & Sciences

ENG4111/2 *Research Project*

Limitations of Use

Certification of Dissertation

I certify that the ideas, designs and experimental work, results, analyses and conclusions set out in this dissertation are entirely my own effort, except where otherwise indicated and acknowledged.

I further certify that the work is original and has not been previously submitted for assessment in any other course or institution, except where specifically stated.

Brodie Cooper

[redacted]

Acknowledgments

Above all, I extend my deepest appreciation to my supervisor Dr Khalid Saleh for offering the opportunity to take on this project, and for his unwavering guidance and support over its duration. For his patience through countless meetings and emails regarding the use of software and details of the project. This research presented a huge learning curve that has undoubtedly elevated me as a developing engineer.

Secondly, I would like to acknowledge Mr Richard Young for the significant effort required in granting undergraduate access to the University's High Performance Computer. Furthermore, the endless advice and information he offered saved a significant amount of time and is immensely appreciated.

Finally, to my family and friends who have constantly believed in me not just throughout my dissertation, but the whole degree. If not for their encouragement and overwhelming support, the achievements I have made would not have been possible.

Brodie Cooper

Contents

List of Figures

List of Tables

Nomenclature

CFD	Computational Fluid Dynamics
UniSQ	University of Southern Queensland
1D	One Dimensional
2D	Two Dimensional
3D	Three Dimensional
COP	Coefficient of Performance
HPC	High Performance Computer
SST	Shear Stress Transport
PLMS	Planar Laser Mie Scattering
TDLAS	Tunable Diode Laser Absorption Spectroscopy
RSM	Reynolds Stress Model
LES	Large Eddy Simulation
NXP	Primary Nozzle Exit Position
SOI	Sphere of Influence
SSH	Secure Shell
STRUDEL	Scientific Remote User Desktop Launcher
VNC	Virtual Network Computer
STFP	Secure File Transfer Protocol
VPN	Virtual Private Network
ICT	Information and Communications Technology
STD	Standard

Notation

h	Enthalpy in J
$\dot{m}$	Mass flow rate in m^3/s
ω_0	Entrainment ratio
Ω_{span}	Spanwise vortex
Ω_{stream}	Streamwise vortex
$\dot{m}_p$	Primary mass flow rate in m^3/s
$\dot{m}_s$	Secondary mass flow rate in m^3/s
v_{pe}	Velocity at primary nozzle exit in m/s
v_{se}	Velocity at secondary inlet in m/s
v_{mix}	Velocity at the end of the mixing chamber in m/s
D	Diameter of the primary nozzle in mm
U_0	Primary nozzle inlet flow velocity in m/s
L	Length of the mixing chamber in mm
d	Diameter of the mixing chamber in mm

Chapter 1

Introduction

1.1 Outline of Study

This study focuses on improving the coefficient of performance (COP) of a steam ejector by incorporating a vortex generator into the design of the primary flow nozzle. The steam ejector will be modelled and visualised in ANSYS Fluent 2022 Revision 1 Computational Fluid Dynamics (CFD) software and verified against existing research conducted by Al-Doori (2013) and Al-Manea (2019). It is widely known that the advantages of ejectors in refrigeration and air-conditioning applications are hindered by poor efficiency. Ejector performance is an intricate topic that is heavily influenced by the low pressure created in the fluid at the primary nozzle exit that entrains secondary flow from the evaporator into the mixing chamber. Literature reviewed surrounding the application vortex generators for the purpose of creating a vacuum effect indicates that the adaption of this method to steam jet ejectors will yield performance benefits.

It is theorised that by introducing a vortex generating element into the primary flow nozzle, a stronger vacuum effect will be produced resulting in an increased entrainment ratio and an improved coefficient of performance. Other foreseeable benefits of incorporating a vortex generator in the primary nozzle include reduced recirculation in the mixing chamber, and improved mixing of the primary and secondary steams. The broader focus of the study will investigate the use of CFD software to analyse the influence of a variety different vortex generator geometries on flow behaviour. The modification of certain geometric characteristics of the vortex generator will be experimented with based on research discovered throughout a literature review.

1.2 Research Aims and Objectives

The aim of this project is to investigate, through CFD software, whether the coefficient of performance of a jet steam ejector will be improved by generating a vortex in the steam exiting the primary flow nozzle. The project specification, provided in Appendix A, outlines the primary objectives of this research project of which is formed into seven main sections:

1. Become competent in ANSYS software and form an understanding of the fundamental concepts of steam ejectors.
2. Develop a 2-dimensional (2D) model of the University of Southern Queensland's (UniSQ) existing steam ejector in ANSYS Design Modeller and simulate its operation using ANSYS Fluent, verifying its accuracy against previous studies.
3. Conduct background research regarding the optimisation of steam ejector and the application of vortex generators in different flow conditions. Identify geometric characteristics for the vortex generators that will be suitable for the primary flow nozzle of the ejector.
4. Create a 3-dimensional (3D) model of the existing UniSQ steam ejector in ANSYS Fluent, run simulations and analyse the performance characteristics of the ejector prior to modification of the primary nozzle.
5. Create multiple 3D ejector models with modified primary nozzles varying in a) number of vortex generators, b) generator helix angles, and c) generator shape profiles.
6. Familiarise with the High Performance Computer (HPC) environment and apply it to conduct simulations for all variations of the vortex inducing nozzle using ANSYS Fluent.
7. Analyse the simulation results and identify: a) whether the vortex generators enhance or hinder ejector performance, and b) the influence of the vortex generator characteristics on flow behaviour in the ejector.

1.3 Overview of the Dissertation

This dissertation is organised as follows:

Chapter 2: Background and Literature Review - This chapter investigates the research conducted on ejector optimisation with particular focus on literature regarding the modification of the primary nozzle and previous attempts to influence flow within the nozzle to increase ejector performance. The operation and applications of the jet steam ejector is reviewed in depth and important considerations relevant to the CFD analysis are detailed.

Chapter 3: Research Methodology - The methodology process for this research project is explained in this chapter which details the creation of the ejector geometries, the grid independence study and set-up of ANSYS Fluent for simulations. This chapter also discusses the methods used to validate the models and optimise the accuracy of the simulations to ensure they are reliable and reflect reality. A guide to accessing and applying the UniSQ HPC for CFD research is also presented in this section.

Chapter 4: Parametric Study of Vortex Generators - The various configurations and characteristics of vortex generators applied to the primary nozzle of the ejector are defined in this chapter. Justification for the vortex generator geometries are also discussed in detail.

Chapter 5: Results - This chapter presents the results from the parametric study and shows how each of the vortex generator geometries impacted the performance of the ejector. The results for the standard ejector model are also delivered and compared to the modified variations.

Chapter 6: Discussion - This chapter provides a more detailed analysis of the results presented in Chapter 5. The implications of the results are discussed and are analysed against initial expectations.

Chapter 7: Conclusion - The conclusions found throughout this research project are presented in this chapter. Complications and limitations encountered over the duration of the project are discussed and recommendations for future work are also included.

1.4 Summary of Methodology

Detailing a structured methodology for which will guide the project is integral for ensuring a transparent and replicable approach is taken and constant progress is maintained. Following a detailed literature review that collates important information and builds a foundation of knowledge on the subject area, the models required for the CFD simulations must be created. This begins with generating the existing 2D shape of the USQ steam ejector – as documented by Al-Doori (2013) and Al-Manea (2019) – using ANSYS Design Modeller. This 2D model will be used to confirm consistency with previous CFD studies of the ejectors and become a baseline model for the rest of this research. Once the 2D geometry is created an appropriate mesh element size will need to be determined through a mesh independence study such that the simulation of the model produces performance characteristics that reflect those determined in (Al-Doori 2013).

Once the accuracy of the 2D geometry is confirmed, a 3D model of the baseline ejector will be generated using Creo-Parametric 3D modelling software and transferred to ANSYS Workbench. A grid independence study is conducted to determine the mesh set up for the model and the flow through the ejector is simulated and analysed in ANSYS Fluent CFD software. The results of these simulations are used as the standard for comparison with those obtained for the modified ejector models.

Next, the vortex generator element is incorporated into the design of the primary flow ejector nozzle. This will be achieved by creating several versions of the baseline 3D model using Creo-Parametric and adding the different vortex generator designs into the primary nozzle. Each vortex generator design tests a different combination of geometric variables such that the final analysis will reveal which characteristics have the greatest influence on ejector performance. Once the 3D models have been created, they are transferred to ANSYS and the mesh is further refined for the modified nozzle until results stop changing. The UniSQ HPC is used to perform simulations for each variation in ANSYS Fluent, and the results are analysed and recorded. The findings from the research will then be discussed in detail and presented in the final chapter of this dissertation along with a conclusion on the research topic.

The general methodology for this project has been devised as following:

- Develop a 2D model of the steam ejector in ANSYS Workbench using geometries obtained from previous research.

- Simulate supersonic flow through the 2D model using ANSYS Fluent and compare with results obtained from the literature review to validate the geometry.

- Generate a baseline 3D model of the ejector and perform a CFD analysis to determine the operating range and performance characteristics of the ejector prior to modification.

- Create multiple 3D ejector models with vortex generators incorporated in the primary nozzle and varying in:

  1. Number of vortex generators
  2. Helix angle
  3. Shape profile

- Using the UniSQ High Performance Computer (HPC), perform simulations for each modified ejector design, maintaining consistent boundary conditions to ensure a valid comparison can be made.

- Analyse simulation results for the modified designs and compare with the results from the baseline ejector model.

1.5 Resource Requirements and Project Timeline

1.5.1 Resource Requirements

In order for successful completion of this project there are a number of essential resources. Since the majority of the project is carried out using computer software there are very few physical resources required. The CFD simulation process is highly time consuming, which makes time the most important resource that must be managed carefully. Other significant resources include:

- ANSYS Fluent Student Access.

- ANSYS Tutorials and Users Guide.

- Guidance of Project Supervisor.
- Time to Conduct Research
- Unlimited Internet Access.
- Vehicle for Travelling to University.
- Remote Access to UniSQ HPC.

1.5.2 Project Timeline

The schedule for this project is presented in Appendix C – Project Timeline in the form of a Gantt Chart. This graph outlines the key components that make up the dissertation and identifies the time frames of which they must be completed to ensure constant progress is made towards achieving the project objectives.

1.6 Consequential Effects

It is an expectation that professional engineers act with safety and sustainability at the forefront of their work. The Code of Ethics developed by Engineers Australia was developed as a guideline for engineering practitioners to ensure they fulfil their responsibility of demonstrating due diligence and professionalism.

1.6.1 Ethical Considerations

The intention for this research is to contribute to the development of a more reliable and efficient replacement for the compressors in air-conditioning and refrigeration systems. If the coefficient of performance is improved, it could help fast-track the transition of the jet steam ejector into mainstream applications.

Ejectors consist of less parts than alternative options thus they require less energy and resources to manufacture, and operate effectively using environmentally friendly refrigerants. Common refrigerants including chlorofluorocarbons, hydro-chlorofluorocarbons and hydro-fluorocarbons have high global warming and ozone depletion potential ratings. For this reason, it has been a focal point in modern research to find alternatives that are both economical and have a minimal effect on the environment.

Whilst limiting environmental damage is a major priority, it is equally important that the safety of those who will utilise the research is considered. Every aspect of this project must be completed with integrity and engineering rigour to ensure it is reliable and safe for others to use.

1.6.2 Risk Assessment

When undertaking any engineering task, it is important to consider the risks that are associated with it. Neglecting to acknowledge the potential dangers of a project can result in the injury or illness of those involved and the possibility of legal and financial consequences. It is the responsibility of the engineer leading the project to put measures in place to mitigate the risks involved and ensure the task can be completed with an acceptable level of safety. In the case of this research project there are very few activities involving substantial risk, however, a detailed risk assessment has been performed and is included in Appendix B – Risk Assessment.

The risk encountered most frequently throughout this project is the extensive use of a computer system which can result in a number of health associated consequences. Some more immediate or short-term issues can include neck and back pain, eye strain and headaches whilst overuse injuries of the shoulders, arms and hands can be long-term (Victoria State Government 2015). With the majority of this research project being performed while being seated at a computer station, the risk of developing these injuries is high. A strategy for effectively reducing the risk of muscle and joint related injuries or discomfort could be creating a workstation that allows for good posture to be maintained, paired with frequent exercise and stretching breaks. Adjusting the computers contrast and brightness settings and ensuring the source of light in the room is not producing glare on the screen will help mitigate eye strain and fatigue (Victoria State Government 2015). The strategies mentioned are considered mandatory for any activity involving extended computer use across the period of this research project.

Another prominent risk encountered on a daily basis is driving between the university and place of residency which increases the probability of a potential car accident that could result in serious injury or death. This kind of incident cannot completely be controlled by a single vehicle operator; however, steps can be taken to minimise the risk of being at fault for a car accident. First and foremost, it is important that the driver is fit to operate the vehicle; this includes being well rested and capable of maintaining full concentration. Secondly, the vehicle should be compliant with the standards and safety requirements enforced by the Queensland Department of Transport and Main Roads. The road rules must be followed at all times and the vehicle operator must drive to the road conditions; consequences for being involved in an accident, whether at fault or a victim, can be severe.

The risks associated with adopting the findings from this research as the basis for further studies should also be acknowledged. Serious financial damages could come as a result should this project not completed with integrity and rigour. It is important that reputable sources are used and that appropriate professional guidance is obtained throughout the project to ensure that the outcome is reliable.

Chapter 2

Background and Literature Review

2.1 Chapter Overview

Understanding the complex flow behaviours and improving the coefficient of performance of ejectors has been a major focus of research for many decades. Despite intensive study on the subject, the multi-phase turbulent flow occurring inside an ejector is yet to be fully understood and many difficulties remain unresolved. A number of methods have been used to analyse ejector operation and predict performance characteristics including: (1) theoretical models with a numerical approach; (2) experimental models using a physical system; 3) flow visualisation approaches; 4) computational fluid dynamics. This chapter will review literature exploring all of these analysis methods, with particular focus on studies that have attempted to modify the ejector to increase performance. An in-depth core understanding of ejectors will be developed in this chapter, identifying the fundamental factors influencing ejector operation. Relevant information regarding computational fluid dynamics necessary for this research project will also be explored.

2.2 Background

2.2.1 Ejector Applications

The history of injectors can be traced back as far as 1958 when French engineer Henri Giffard invented an ejector for the purpose of delivering water to the boilers of steam engines (Elbel 2011). The Giffard ejector (figure 2.1)was designed as a replacement for mechanical pumps that were driven directly by the steam engine; this meant that when the engine was stalled there was no water replenishing the reservoir (Elbel 2011). Gifford's ejector resolved this issue, as the steam that was used as the motive fluid was available even when stationary, so the ejector could still pump fluid.

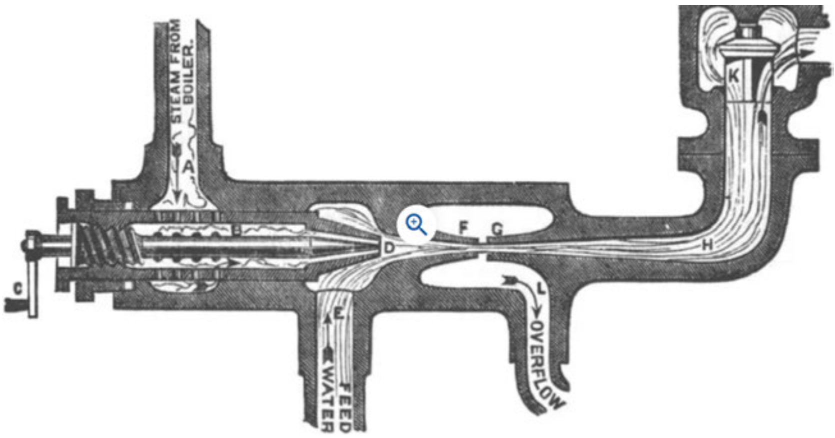

Figure 2.1: Giffards ejector with a screw to adjust the motive steam flow rate (Britannica 2019).

The use of converging-diverging nozzles to develop supersonic flow at the exit of the primary flow nozzle wasn't implemented until 1869 and was based on the venturi effect discovered by Giovanni Venturi (Elbel 2011). Inventor Gustaf de Laval began experimentation with converging-diverging steam nozzles in 1890. Ejectors have since been extensively studied and considered for use in a multitude of applications. Vacuum degassing systems in steel production utilise steam ejectors for the purpose of removing hydrogen from the molten steel to decrease the defects such as hydrogen flaking (Valenti 1998). Refineries often adopt vacuum distillation systems equipped with steam ejectors to draw out the associated unwanted gases and saturated vapours from the distillation column (Ghorbanian & Nejad 2011). Other existing applications for ejectors include space simulations, petrochemical processes, edible oil deodorisation, refrigeration, and air-conditioning systems (Graham Corporation 2022).

Ejectors are often considered in place of compressors due to consisting of no moving parts, thus, they are more economical, require less maintenance and have less points of potential failure. They are also capable of operating in dangerous environments where alternative methods cannot. They can operate using a variety of motive and secondary vapours and fluids including highly corrosive refrigerants. Ejectors are typical configured in either single stage or multi-stage arrangements (see figure 2.2); single stage ejectors are the most common for use in industry applications whilst multi-stage are typically only implemented in circumstances where a stronger vacuum is required (Berk 2009).

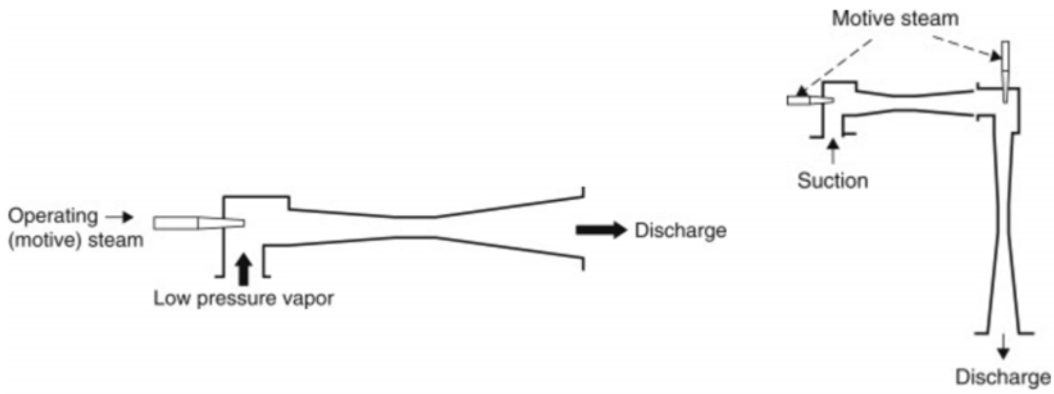

Figure 2.2: Diagram of a single stage ejector (Left) and a multi-stage ejector connected in series (Right) (Berk 2009).

2.2.2 Solar Refrigeration Systems

With the world acknowledging the seriousness of stratospheric ozone layer depletion and global warming, it is a high priority to transition into refrigeration systems that utilise environmentally friendly working fluids and renewable energy. It has been estimated that the use of refrigeration and air-conditioning systems is responsible for 17% of global energy consumption and as a result has a substantial contribution to greenhouse gas emissions (International Institute of Refrigeration 2015). As the world transitions into a low-carbon future through renewable energy sources, solar refrigeration systems are a promising development.

Existing refrigeration systems using absorption, adsorption and desiccant methods can utilise the otherwise wasted heat from the sun in their cooling process. These systems also have the ability to operate on a range of working fluids allowing for environmentally refrigerants to be considered (Sahlot & Riffat 2016) (Alsagri, Alrobaian & Almohaimeed 2020). The main disadvantage off these systems is that they are often larger and more expensive than alternatives such as the traditional vapour-compression refrigeration systems. Another option is the evaporative cooling system, however, this design has high energy and water consumption requirements that make it unfeasible for many applications (Ariafar 2016).

Ejector refrigeration systems are also compatible with sustainable refrigerants and can be driven by solar power. An ejector uses a high-pressure motive stream to entrain a low-pressure secondary stream, resulting in a fluid mixture with a pressure in between the two streams (Elbel 2011). The effect created by the ejector is similar to that of a compressor in a typical vapour compression system with the benefit of having no mechanical components. A standard steam ejector system is shown in figure 2.3, where solar energy would be utilised in the steam generator to reduce the overall energy requirements of the system (Ariafar 2016).

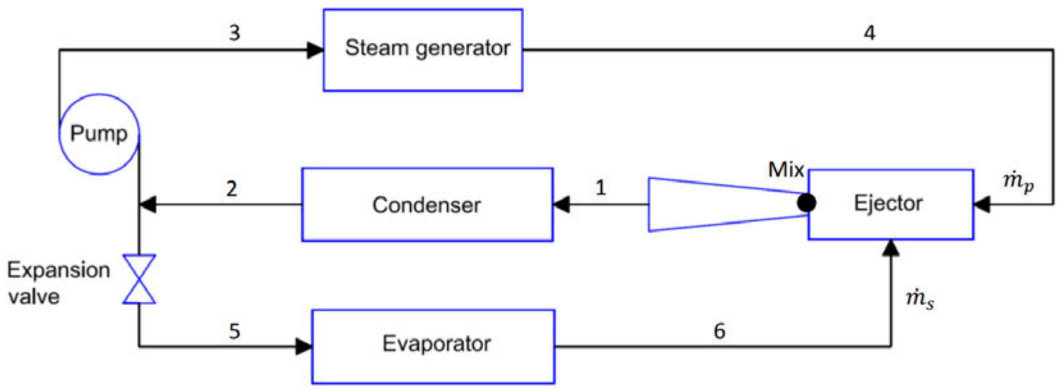

Figure 2.3: Diagram of a steam ejector refrigeration system (Ariafar 2016).

Solar energy is typically harnessed in two ways; through photovoltaic cells to generate electricity, or through thermal collectors to collect heat. Photovoltaic cells are highly accessible and can be used to power pumps, heaters, compressors, and other electric components in any air-conditioning system. Thermal collectors are typically implemented in systems that involve a steam generator (Abdulateef, Sopian, Alghoul & Sulaiman 2009). The steam ejector refrigeration apparatus constructed at the University of Southern Queensland (see figure 2.4) uses electric heaters to power the system (Al-Doori 2013). Since the primary use of this system is for studying ejector performance and due to thermal collectors being heavily dependent on environmental factors, they were considered too unreliable for this application.

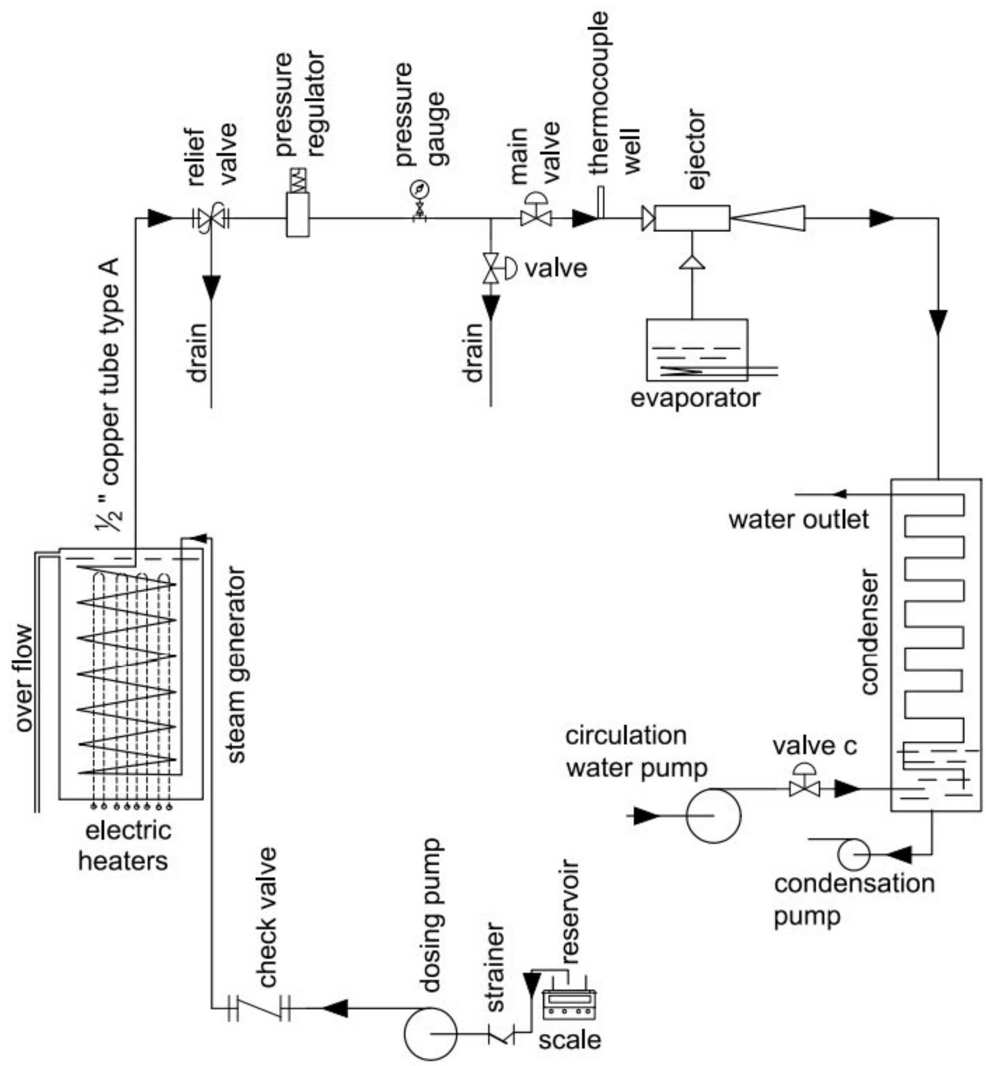

Figure 2.4: Single stage steam ejector refrigeration apparatus constructed at the University of Southern Queensland (Al-Doori 2013).

The T-s diagram shown in figure 2.5 shows the cycle of a steam ejector refrigeration system. A high-pressure and high temperature steam is created in the generator and sent through the ejector which draws through the lower pressure and lower temperature fluid from the evaporator. The ejector produces an increased pressure and reduced temperature mixture at the diffuser exit (Al-Manea 2019). This mixture then enters the condenser, and the temperature is reduced further before finally the low temperature of the refrigerant is transferred to the heat sink as it passes through the evaporator (Ariafar 2016).

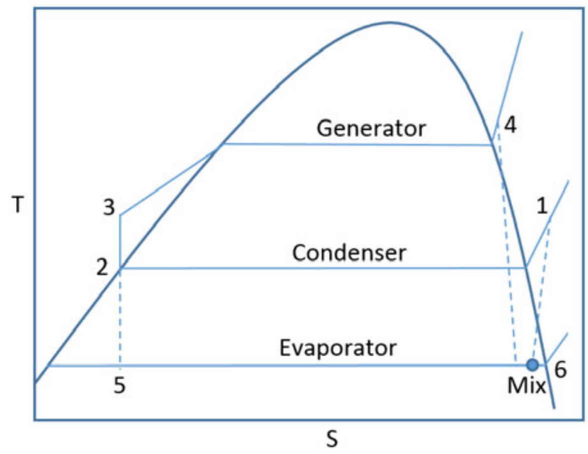

Figure 2.5: T-s diagram of the closed cycle of an ejector refrigeration system (Ariafar 2016).

2.2.3 Steam Ejector Operation

Ejectors follow compressible flow theory and function on Bernoulli's Principle, where the primary flow of high-pressure refrigerant is forced through a converging-diverging nozzle creating a high velocity low pressure flow at the nozzle exit (Varga, Oliveira & Diaconu 2009*a*) (Ariafar 2016). Referring to figure 2.6, the supersonic condition of the primary fluid (G) at nozzle exit (point 1) creates a pressure that is lower than that of the secondary flow (E) from the evaporator (point 2). This results in a vacuum effect that entrains the fluid from the evaporator into the mixing chamber (point 3) (Al-Doori 2013). Mixing of the primary and secondary flows first commences at the nozzle exit and is considered complete at the beginning of the diffuser convergent (point 4). The supersonic mixing of the fluids causes shock waves to occur inside the mixing chamber and the velocity becomes subsonic as the mixture passes through the constant area section (Al-Manea 2019) (Sun, Ma, Zhang, Jia & Xue 2021). The primary-secondary flow mixture is then re-compressed as it flows through a converging-diverging diffuser, reducing the refrigerants velocity and increasing its pressure at the diffuser exit before leading to the condenser (C).

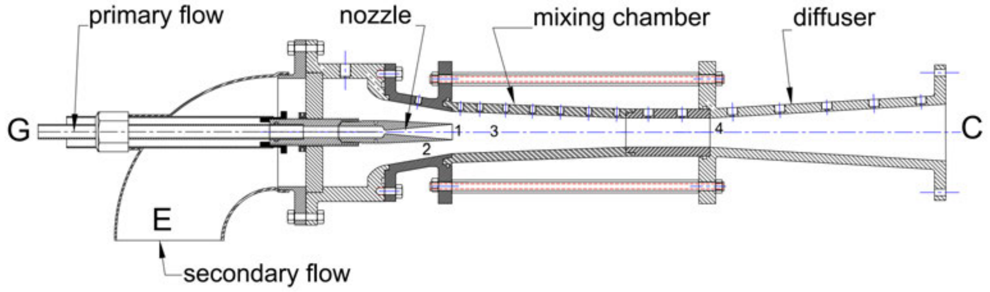

Figure 2.6: Stage diagram of a modern steam ejector (Al-Doori 2013).

The supersonic flow from the nozzle results in shock waves in the mixing chamber that reduce the velocity of the refrigerant and lower the entrainment ratio, thus, decreasing the coefficient of performance of the ejector. Ejector performance can be expressed in simplified terms as the ratio between the effective refrigeration output and the energy input consumed by the cycle (Yu, Ren, Chen & Li 2007). The coefficient of performance of a jet ejector is described by the equation:

$$COP = \frac{\dot{m}_s(h_6 - h_5)}{\dot{m}_p(h_4 - h_3)} \tag{2.1}$$

Where the refrigeration output and energy input are defined as the secondary mass flow rate multiplied by the change in enthalpy across the evaporator and the mass flow rate of the primary flow multiplied by the change in enthalpy across the steam generator, respectively (Giacomelli, Biferi, Mazzelli & Milazzo 2016). These variables are illustrated in figures 2.3 and 2.5. The entrainment ratio is described as the ratio between the primary and secondary mass flow rates (Ariafar 2016) (Varga et al. 2009*a*). Thus, the equation for coefficient of performance for the ejector can be simplified to:

$$COP = \omega_0 \frac{\Delta h_E}{\Delta h_G} \tag{2.2}$$

From equation 2.2, it is clear that the entrainment ratio is a driving factor influencing the performance of an ejector. At specific thermodynamic states during operation, the entrainment ratio and coefficient of performance can be equivalent, meaning that by increasing the entrainment ratio an increase in performance will also be observed (Sun et al. 2021). This is consistent amongst the literature, with the entrainment ratio regularly being used as the main indicator of ejector performance in studies. Factors such as

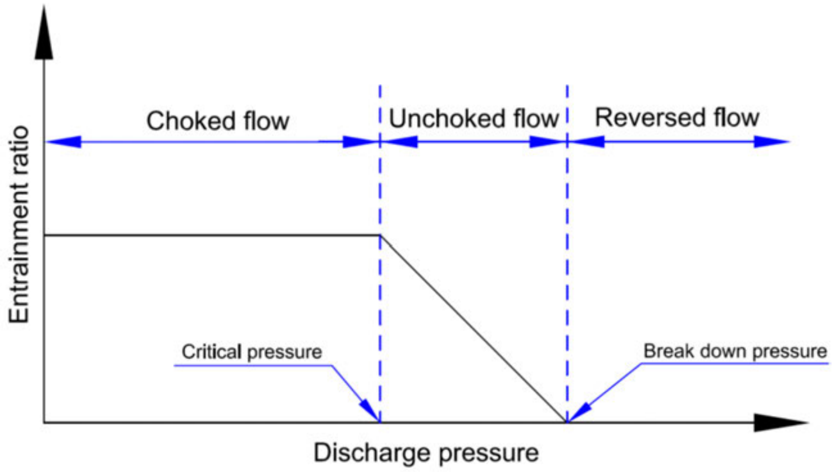

Figure 2.7: Steam ejector performance characteristics (Ariafar 2016).

nozzle geometry and primary flow pressure have been found to have a significant impact on the entrainment ratio (Sun et al. 2021) (Aravind, Reddy & Baserkoed 2014) (Varga et al. 2009*a*).

An ejector typically operates within three performance regions, shown in figure 2.7, which are dependent on the variation between the discharge pressure of the ejector and the backpressure created upstream of the ejector at the condenser (Ariafar 2016). When the condenser pressure is sufficiently low both the primary and secondary flows experience choking effect that limits the mass flow rates, thus, producing a constant entrainment ratio (Han, Wang, Yuen, Li, Guo, Yeoh & Tu 2020). If the upstream pressure is too high the mass flow rate is reduced, and discharge pressure is increased above the critical pressure resulting in an unchoked flow. In this region, the entrainment ratio decreases rapidly as supersonic fluid velocity is not achieved (Al-Doori 2013). If the discharge pressure exceeds the unchoked flow region and reaches the break down pressure the secondary flow will reverse, and the system will fail (Han et al. 2020).

2.2.4 Steam Condensation in Ejectors

When selecting a refrigerant there is a criterion that defines how the system will perform. The working fluid should have a high latent heat of vaporisation, low cost, high availability, non-corrosive, non-flammable and non-toxic. The working fluid should ideally have viscosity and thermal conductivity properties that allow for heat transfer. Selecting a refrigerant with a higher molecular weight will result in better system performance (Abdulateef et al. 2009). The types of refrigerants can be categorised based on their thermodynamic properties as either a wet, isentropic or dry. It is found that while dry and isentropic fluids have similar behaviours, wet fluids can change phase and condensate, potentially blocking flow path and eroding the ejector walls (Giacomelli et al. 2016). This is overcome by superheating the primary flow before the ejector; however, this has been shown to hinder efficiency.

Research conducted by testing the cooling characteristics of various refrigerants on ejector performance has revealed that typically halocarbons, and often dry fluids, produce greater coefficient of performance in most operating conditions (Chen, Havtun & Palm 2014) (Chunnanond & Aphornratana 2004*a*) (Sun 1999). Water (R178) was the first working fluid to be applied in ejector refrigeration and is being experimented with and used in modern systems (Meyer, Harms & Dobson 2009) (Giacomelli et al. 2016) (Al-Doori 2013). The appeal of R178 as a working fluid is due to its extremely high latent heat of vaporisation, it is inexpensive and plentiful, non-flammable and non-toxic and has zero global warming and ozone depletion ratings (Chunnanond & Aphornratana 2004*a*). There are some disadvantages of water, however, it requires a much higher boiler temperature than other refrigerants (Abdulateef et al. 2009), this means that when using low-grade thermal energy such as solar, water is often not the optimal working fluid. Due to its thermodynamic properties, systems utilising R178 are limited to operating temperatures of greater than $0\,^{\circ}\mathrm{C}$. The large specific volume of water means that a much larger area ratio is required compared to other synthetic refrigerants (Sun 1999).

In the ideal operating conditions with low condenser pressures and high boiler temperatures significant improvements in entrainment ratio, enthalpy ratio and compression ratio are observed, which are factors that contribute to a high coefficient of performance (Sun 1999). In some cases, it has been found that ejector systems utilising water can operate at a higher performance that alternative halocarbon-based systems (Milazzo & Rocchetti 2015).

Form observing figure 2.5 it is clear that the cycle of the steam ejector system involves operations within the saturation zone. The expansion process begins as the high-pressure steam in dry superheated form flows through the convergent side of the nozzle (point 1) to the throat of the nozzle (point 2) in a isentropic manner; gradually decreasing in pressure over the axial distance as shown in figure 2.8 (Ariafar 2016). Typically, condensation only occurs after passing through the throat and the fluid has reached sonic velocity, however, supersaturation can occur before the throat (Yang, Zhu, Yan, Ding & Wen 2019). Expansion continues beyond the throat and the low residence time and temperature reduction causes the flow to become a saturated vapour at point 3.

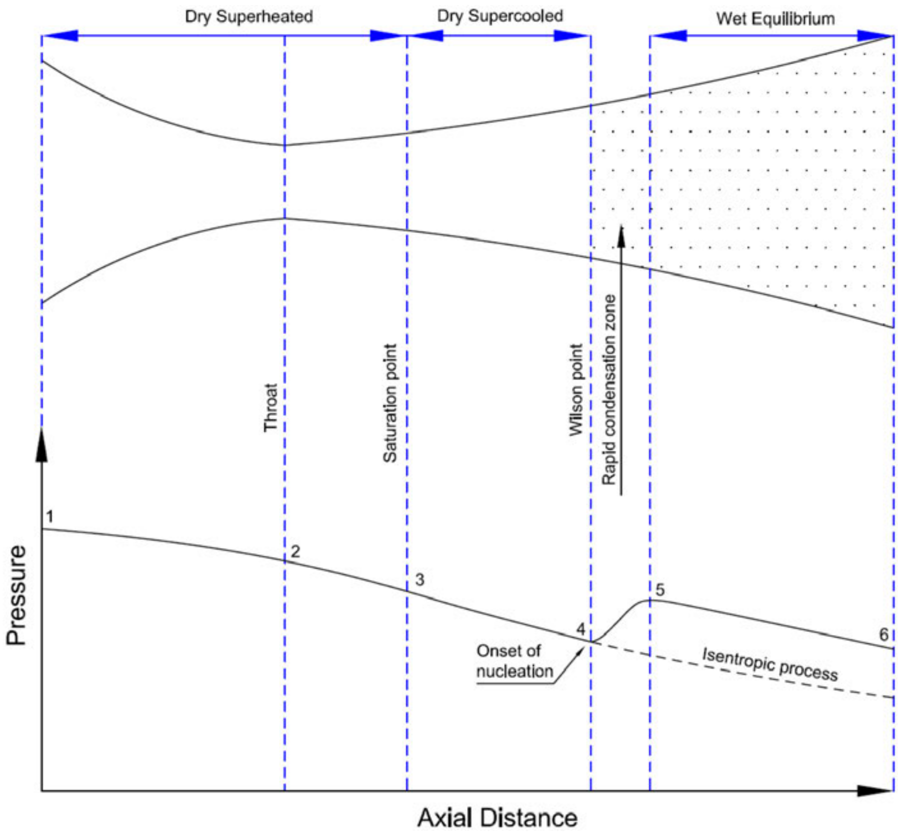

Figure 2.8: Axial pressure change and condensation development of a steam ejector (Ariafar 2016).

The nucleation rate of the droplets is very low, which typically prevents droplets from forming until point 4 shown in figure 2.8 (Wang, Lei, Dong & Tu 2012). Between points 4 and 5 a certain level of expansion is achieved that causes a rapid increase in the rate of droplet nucleation and condensation is formed in the flow (Giacomelli et al. 2016). The sudden development of condensation in the nozzle causes shock waves in the flow that reduce velocity and increase pressure and entropy and the flow returns to a state close to thermodynamic equilibrium at point 5 (Al-Manea 2019).

2.2.5 Turbulent Mixing in Steam Ejectors

Mixing of the primary and secondary flows first commences quickly after the nozzle exit which can be seen in figure 2.9. The two flows transfer energy, momentum and mass as the mixing layer develops linearly over the axial distance 'x' and expands to the wall of the throat (Tang, Liu, Li, Zhao, Fan & Chua 2021). A more rapidly developing free shear layer is desirable and has a significant effect on the performance of the ejector. A higher mixing layer growth rate means a stronger entrainment of secondary flow into the free shear layer is achieved which increases the entrainment ratio and thus improves the coefficient of performance (Ariafar 2016). The properties of the working fluid at the exit of the primary nozzle vary with the operating conditions and also have a significant impact on the growth rate.

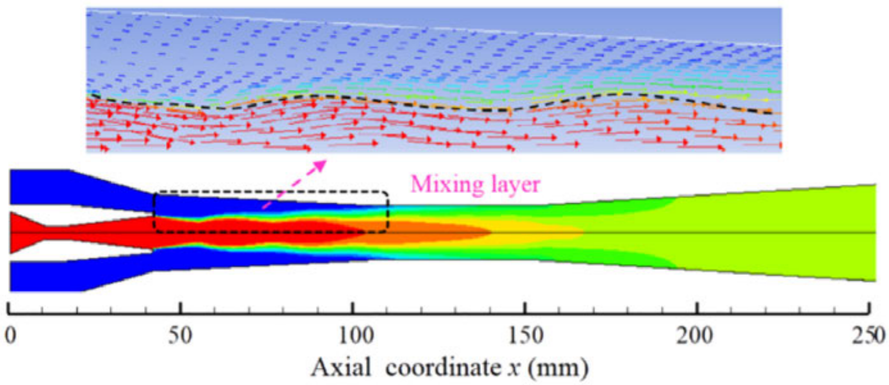

Figure 2.9: Mixing layer development between primary and secondary flow (Tang, Liu, Li, Zhao, Fan & Chua 2021).

Intense perturbation occurs as the primary flow exits the nozzle and meets the entrained fluid, resulting in a series of shock waves developing through the converging passage and into the mixing chamber (Tang, Liu, Li, Huang & Chua 2021). The shock wave chain, known as the diamond wave pattern, can be seen in figure 2.9, it is found that the mixing effect is encouraged by the shock waves as the turbulent eddies are increased (Tan, Zhang & Lv 2018). In some extreme cases the shock waves continue into the diffuser, however, greater quality mixing was observed for shorter shock wave chains (Zhu & Jiang 2014). The turbulent mixing of the supersonic primary and subsonic secondary flows in a steam ejector with non-equilibrium condensation occurring is highly complex and plays an important role in understanding the flow conditions.

The mixing process involves two types of vortices that exists in the flow field of the ejector that have a significant impact on mixing layer development. Spanwise vortices act on the axis (a vortices vector) horizontal to the direction of flow and streamwise vortices act on an axis that is parallel with the direction of flow (McMullan 2018). These vortices form as a result of the supersonic steam exiting the primary nozzle and interacting with the subsonic secondary fluid; vorticity variation occurs predominantly within the mixing chamber of the ejector (Yang, Long & Yao 2012). It is found that the streamwise vortices work to break down the spanwise vortices which promotes a stronger mixing effect. The streamwise vortices grow towards the walls of the throat while the vorticity value decays over the axial length of the ejector. Equations 2.3 and 2.4 (Yang et al. 2012) describe spanwise and streamwise vortices, respectively:

$$\Omega_{span} = \frac{D}{U_0}\sqrt{\left(\frac{\partial u}{\partial z} - \frac{\partial w}{\partial x}\right)^2 + \left(\frac{\partial v}{\partial x} - \frac{\partial u}{\partial y}\right)^2} \tag{2.3}$$

$$\Omega_{stream} = \frac{D}{U_0}\left(\frac{\partial w}{\partial y} - \frac{\partial v}{\partial z}\right) \tag{2.4}$$

Where D is the diameter of the primary nozzle exit, U_0 is the velocity of the primary fluid taken at the primary nozzle inlet and the u, v and w are the velocities for the x, y and z directions (Yang et al. 2012). The mixing efficiency has been defined by (Huang, Chang, Wang & Petrenko 1999) in terms of momentum transfer efficiency through the equation;

$$\phi_{mix} = \frac{(\dot{m}_p + \dot{m}_s)v_{mix}}{\dot{m}_p v_{pe} + \dot{m}_s v_{se}} \tag{2.5}$$

Where $\dot{m}_p$ and $\dot{m}_s$ are the primary and secondary mass flow rates, v_{pe}, v_{se} and v_{mix} are the fluid velocities at the primary nozzle exit, secondary inlet and end of the mixing chamber, respectively. It is clear that the mixing efficiency calculated through equation 2.5 is reflective of the frictional losses occurring throughout the mixing chamber.

2.3 Steam Ejector Experiments

2.3.1 Theoretical

Huang et al. (1999) developed a 1-dimensional (1D) model of an ejector focusing on the performance when operating in the choked flow region. To verify the results experimental data obtained from a test using R141b refrigerant and 11 ejectors with varying constant area section diameters and suction chamber convergence angles. With reference to figure 2.10, to simplify the theoretical analysis a number of assumptions had to be made to including:

- Ideal gas is used as the working fluid and the ejector is operating under steady flow conditions.
- The ejector operates under isentropic conditions and the internal wall of the ejector is adiabatic.
- Hypothetical throats exist at cross sections y-y (where the secondary flow becomes choked) and at s-s (where the shock wave occurs).
- Constant pressure mixing of the primary and secondary flows is completed between y-y and m-m.

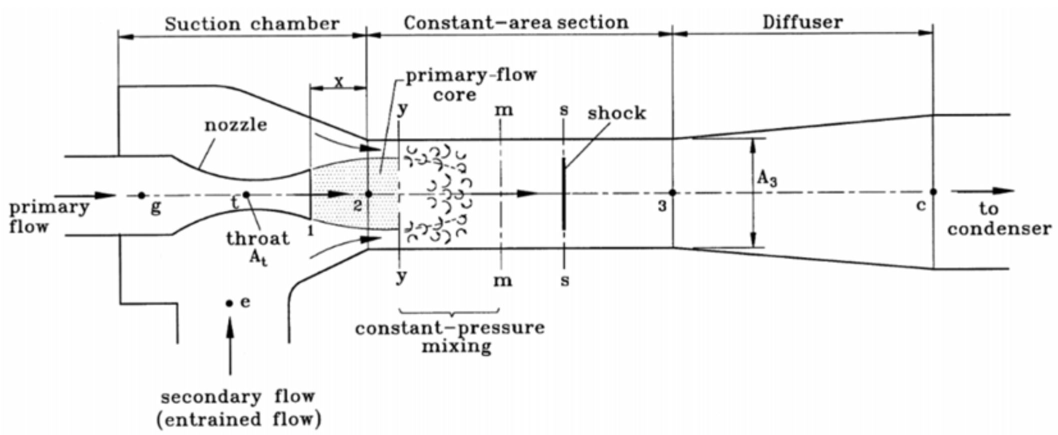

Figure 2.10: Ejector design for experimental and 1D analysis (Huang et al. 1999).

The study found that an optimal position for the primary nozzle exit with respect to the constant area section can be obtained for the greatest performance. Huang et al. (1999)

also noted that superheating the primary and secondary flows also had significant effects on the ejector performance. The study demonstrated that the 1-dimensional model could successfully produce predictions of ejector performance at an acceptable level of accuracy.

A numerical model was created for the 1D analysis of the compressible flow of R142b inside of an ejector by Ouzzane & Aidoun (2003). This study employed the same operating conditions and ejector geometry as used by Huang et al. (1999) as a method of validating the results. The model created by Ouzzane & Aidoun (2003) uses the conservation of energy, mass and momentum equations which governs the volume throughout the ejector. In order for the model to work a number of assumptions were necessary including:

- Compressible flow using a real gas for as the working fluid.
- The ejector operates under isentropic conditions and the internal walls are considered adiabatic. Friction and mixing losses are accounted for through coefficients added into the calculations.
- Mixing of the primary and secondary flow only occurs after a specifically defined point has been reached and only over a specified distance in the mixing chamber.

The results from the numerical model corresponded well with the experimental data from Huang et al. (1999), finding that the entrainment ratio and threshold temperature at the optimum operation conditions were just $3\,^{\circ}$ and $8\,^{\circ}$ error, respectively. The model showed that mixing chamber length could be used to regulate the intensity of shockwaves such that the mixed flow velocity could be reduced to almost sonic conditions and produce the maximum exit pressure at the diffuser (Ouzzane & Aidoun 2003). It was also found that the maximum isentropic compression for the model occurs in the converging section of the ejector which reduces the impact of shock and increases the final pressure at the diffuser.

Guangming, Xiaoxiao, Shuang, Lixia & Liming (2010) developed a 1D model to reflect the operation of a CO_2 ejector and investigate the influence of primary and secondary flow pressure and back pressure on the entrainment ratio. The model uses the ejector characteristic-curve equations to analyse the performance of an ejector and it is compared with experimental data obtained from a CO_2 ejector testing apparatus. The following assumptions were made for the theoretical study:

- The primary and secondary flows only mix inside the mixing chamber.
- The flow in the ejector is one dimensional and uniform.
- The kinetic energy in the primary nozzle, suction chamber and diffuser exit is insignificant and can be neglected.

The model behaved as expected as the back pressure is increased passed the critical pressure the entrainment ratio decreases rapidly. It was acknowledged, however, that the predicted entrainment ratio was higher than the experimental data, indicating that the ejector characteristic-curve equation cannot adequately simulate a 2-phase CO_2 ejector based on the assumptions made. Guangming et al. (2010) found that as the primary flow pressure is increased, the entrainment ratio would also trend higher. Results also showed that the entrainment ratio was also increased by increasing the pressure of the secondary flow.

Chen, Liu, Chong, Yan, Little & Bartosiewicz (2013) developed a numerical model for the purpose of predicting ejector performance over the entire operating range including both critical and subcritical modes of operation. A combination of the conservation of momentum, energy and mass equations is used to govern the volume throughout the ejector and dynamic gas relations are used for the isentropic flow conditions. The model also was used to analyse the effect of geometry and working fluid selection on the performance characteristics Chen et al. (2013) adopted the following assumptions for the study:

- Isentropic flow in the ejector is impacted by efficiency coefficients that account for frictional and mixing losses.
- The fluid used is an Ideal gas and the flow inside the ejector is steady and one dimensional with the internal walls considered adiabatic.
- The operation is simplified such that primary flow exits the nozzle in a wide spray and mixes with the secondary fluid until a specified point in the constant area section; from this point the mixing process occurs at a constant pressure.

The results obtained from the 1D model for the critical mode operation were compared with the experimental results from Huang et al. (1999), whilst for subcritical mode operation the model had to be validated against existing computational fluid dynamics simulation results (Hemidi, Henry, Leclaire, Seynhaeve & Bartosiewicz 2009). The geometry of the ejector, operating conditions and working fluid was adjusted for the model to correspond with Huang et al. (1999) and Hemidi et al. (2009) and a maximum error of 15% and 19.8% was observed respectively. The results suggest that the model would be suitable for estimating the performance of an ejector in all modes of operation (Chen et al. 2013).

A study similar to Chen et al. (2013) aimed to create an accurate 1D model for predicting the performance of ejectors utilising real gases (Chen, Shi, Zhang, Chen, Chong & Yan 2017). The model is applicable to both critical and subcritical operating modes and is used in this study to compare the performance characteristics of an ejector for a variety of different working fluids. To simplify the theoretical analysis a number of assumptions were made:

- Real gas is used, flow inside the ejector is 1D and the internal walls are adiabatic.
- The inlet velocities of the primary and secondary fluids are neglected.
- The primary and secondary streams are considered independent isentropic flows until a certain point within the constant area section where the flows mix under uniform pressure.

The results for the model using R141b refrigerant has a 10% margin of error when compared with Huang et al. (1999) and was accurate to approximately 20% error when compared to Aphornratana, Chungpaibulpatana & Srikhirin (2001) using R11 as the working fluid. This is a significant improvement in accuracy over models restricted to using the ideal gas assumption, particularly in the case of R11 refrigerant that does not have properties close to an ideal gas (Chen et al. 2017). Based on the 1D model, it was found that R290 and R134a refrigerants are the most suitable of those tested for the application of an ejector refrigeration system.

2.3.2 Experimental

A steam jet refrigeration system built by Sun (1997) was equipped with two 3.25kW electric heater units providing the heat source for the boiler and one unit in the evaporator.

The temperatures in the evaporator were adjusted between $5\,°C$ to $15\,°C$, from $95\,°C$ to $135\,°C$ in the boiler and from $20\,°C$ to $34\,°C$ in the condenser and were measured through local thermocouples. The results show that for constant evaporator and boiler temperatures the entrainment ratio behaves independently to the condenser temperature for subcritical values (Sun 1997). The optimum operating point of the system is when it is at critical conditions and that high evaporator temperatures will extract the best performance from the ejector. The experiment also tested three nozzles with different sizes and found that throat diameter has a significant effect on entrainment ratio.

Chang & Chen (2000) used a steam jet refrigeration test rig to experiment how the nozzle structures shown in figure 2.11 effect system performance. Several nozzles were used with varying area ratios and the generator, evaporator and condenser temperatures were adjusted to change the operating conditions. It was found that for higher area ratios the petal nozzle produced higher entrainment ratios in the ejector. Chang & Chen (2000) also noted that larger area ratios produced stronger streamwise vortices that improved the efficiency of mixing.

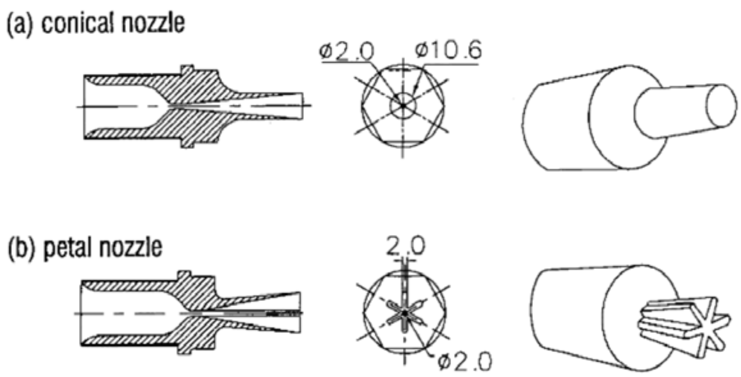

Figure 2.11: Conical and petal nozzle structures used in experimental testing (Chang & Chen 2000).

Using an experimental steam ejector refrigeration system, Chunnanond & Aphornratana (2004*b*) analysed the influence of different primary nozzle throat and exit diameters on ejector performance. The operating conditions were adjusted from $110\,°C$ to $150\,°C$ for the boiler, $5\,°C$ to $15\,°C$ for the evaporator and 25mbar to 60mbar for the condenser. The study revealed that the primary nozzles with smaller geometries produced a higher coefficient of performance and increased the systems cooling capacity (Chunnanond & Aphornratana 2004*b*). However, reducing the nozzle size could also result in a lower critical condenser pressure. Superheating the primary stream was found to have negligible impact on the coefficient of performance of the system.

Yapıcı (2008) used a vapour-jet ejector refrigeration system with R123 as the working fluid to analyse the ejector performance for different primary nozzle positions over a wide operating range. Moving the primary nozzle exit closer to the mixing chamber was found to decrease the pressure inside the suction chamber. The optimum primary nozzle position for any operating condition was determined to be the point of which the suction chamber pressure is minimised. Yapıcı (2008) found that for maximum performance, the ejector area ratio must be considered when selecting the nozzle position. The study also found that increasing the boiler temperature will result in an optimal operating temperature that if surpassed, the cooling capacity of the system is maximised and plateaus.

A study aimed to maximise pressure recovery of an ejector was performed by Del Valle, Jabardo, Ruiz & Alonso (2014) using an ejector refrigeration system and R134a working fluid. Three ejectors with different mixing chamber structures were used including a converging style and two different constant area type mixing sections (figure 2.12). It was found that the constant area mixing section type "A" and the converging style "B" performed very similarly in terms of pressure recovery while mixing chamber "C" underperformed across all of the completed tests (Del Valle et al. 2014). It was also found that for mass ratio remained constant for mixing chamber "A" when the primary nozzle position was changed, however, the mass ratio would change for mixing chambers "B" and "C".

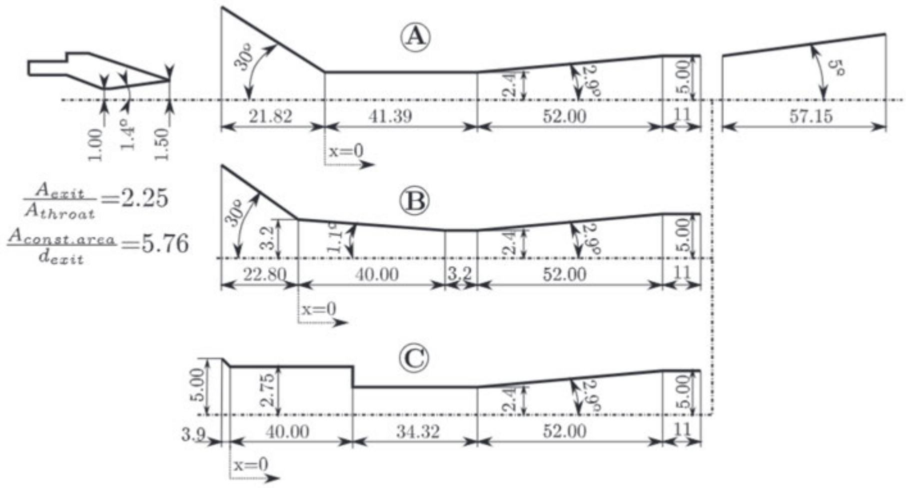

Figure 2.12: Mixing chamber geometries for enhancement of pressure recovery experiment (Del Valle et al. 2014).

A steam ejector refrigeration system using R134a shown in figure 2.13 was used to experiment with six ejectors with different throat and exit diameters and constant area section geometries (Kumar & Sachdeva 2019). The condenser and evaporator temperatures were varied through the experiment and the system performance was analysed. The results show that a lower area ratio ejector is required to achieve a higher-pressure lift which allows a wider range of condenser pressures to be used (Kumar & Sachdeva 2019). However, it is found that a lower evaporator pressure and longer mixing chamber length will increase the pressure lift for an ejector without altering the area ratio. Larger area ratios produced a higher coefficient of performance and cooling capacity for lower condenser temperatures.

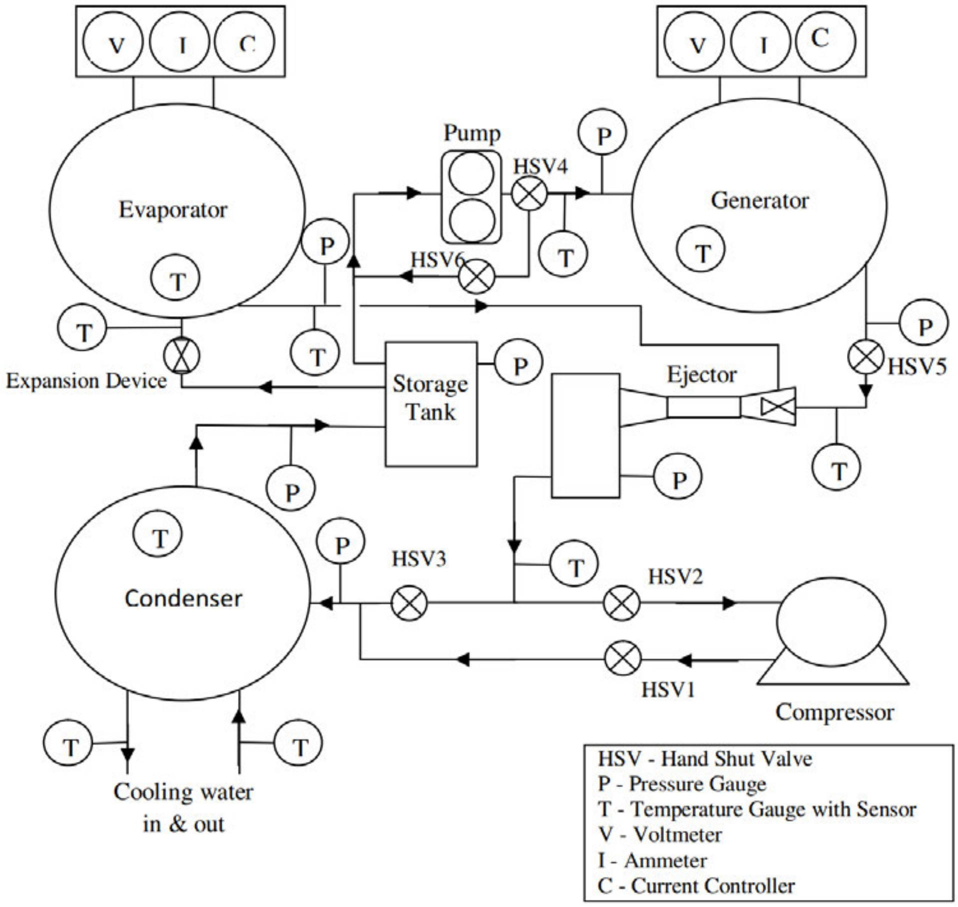

Figure 2.13: Experimental ejector refrigeration system (Kumar & Sachdeva 2019).

2.3.3 Flow Visualisation

One of the earliest recordings of the visualisation methods being used to analyse ejector performance was by Fabri & Siestrunck (1958) that used the schlieren method to analyse flow patterns and determine flow regimes for supersonic jet ejectors. This method uses light deflected from the fluid due to its refractive index gradient to visualise fine details of the flow; a typical schlieren visualisation system is depicted in figure 2.14. Matsuo, Sasaguchi, Tasaki & Mochizuki (1981) used the same visualisation method to investigate flow behaviour of an ejector with a square primary nozzle both with and without the secondary fluid. The schlieren photographs were compared with the wall static pressure distribution to better understand shock occurrences in different operating conditions.

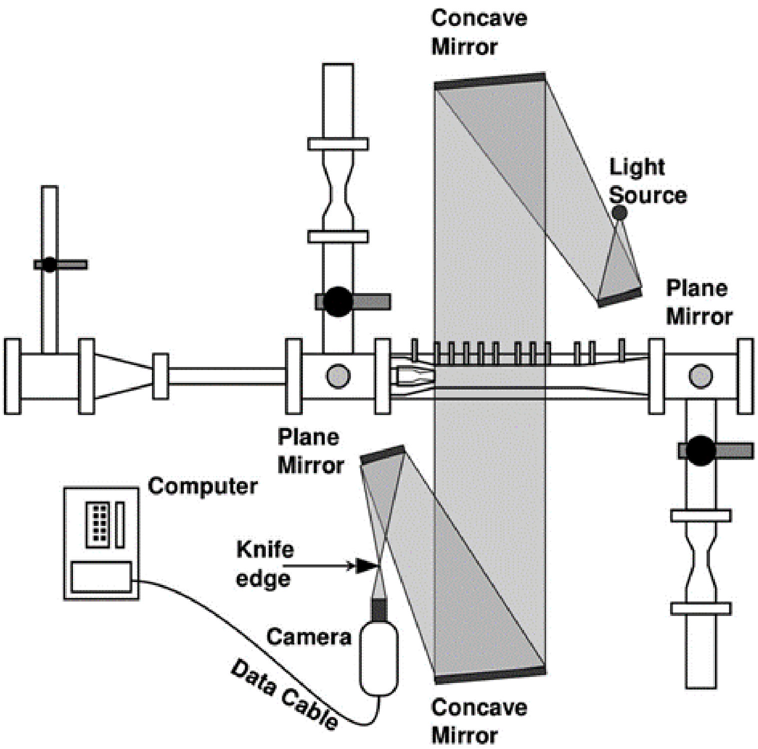

Figure 2.14: Schlieren visualisation method schematic (Rao & Jagadeesh 2014).

Hong, Alhussan, Zhang & Garris Jr (2004) incorporated supersonic rotor vane pressure exchange into an ejector refrigeration system. The new ejector design was created to increase ejector efficiency by harnessing pressure exchange through the vanes, whilst remaining simple and economical. Schlieren visualisation system and a high-speed digital camera were used to analyse the flow through the rotor-vanes in both rotating and stationary conditions (Hong et al. 2004). An experimental investigation on the influence of pressure variation of the primary, secondary and mixed flow and different primary nozzle exit positions on the entrainment ratio was completed by Arun, Tiwari & Mani (2019). The schlieren system was used to visualise the shock waves that form as a result of the velocity difference between the mixing streams were compared with computational fluid dynamics simulation results for a variety of operation conditions (see figure 2.15). It was found that the length of the resulting shock train has a significant influence on the pressure recovery and coefficient of performance of the ejector.

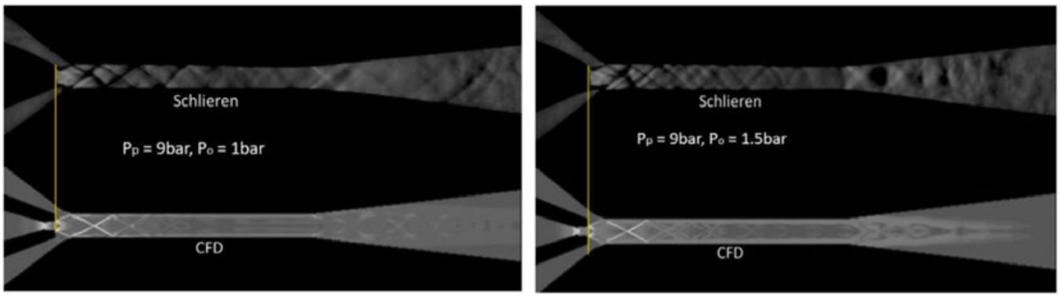

Figure 2.15: Schlieren visualitation and computational fluid dynamics results comparison (Arun et al. 2019).

Zare-Behtash & Kontis (2009) used a 2-dimensional ejector and a high-speed shadowgraph visualisation method to examine the generation of shocks and vortices and how they interact in the induced compressible flow. The shadowgraphs were found to have an error of 4% for repeatability and a lower clarity when compared to schlieren images reviewed in other literature. A transparent ejector housing and a shadowgraph system was used to visualize the primary flow nozzle and the mixing chamber for different levels of condensation (Little & Garimella 2016). The shadowgraph images were used to compare the accuracy of various turbulent computational fluid dynamics models and found that the k-ω SST model showed the best agreement.

Laser tomography visualisation methods were adopted by Bouhanguel, Desevaux & Gavignet (2011) as the schlieren and shadowgraph systems were unable to accurately visualise individual fluid streams. This method uses a pulsed laser beam that illuminates the fluid stream and high-quality camera to record the flow behaviour; a typical laser tomography system is shown in figure 2.16. Rao & Jagadeesh (2014) used both the schlieren and the laser tomography visualisation techniques to validate a k-ω Shear Stress Transport (SST) model. The results found that for lower primary stagnation pressures the laser scattering images were poor quality, whereas the schlieren images were clear for all operating conditions (Rao & Jagadeesh 2014). However, the results obtained by the two methods were in very close agreement and were within approximately 5% error for repeatability.

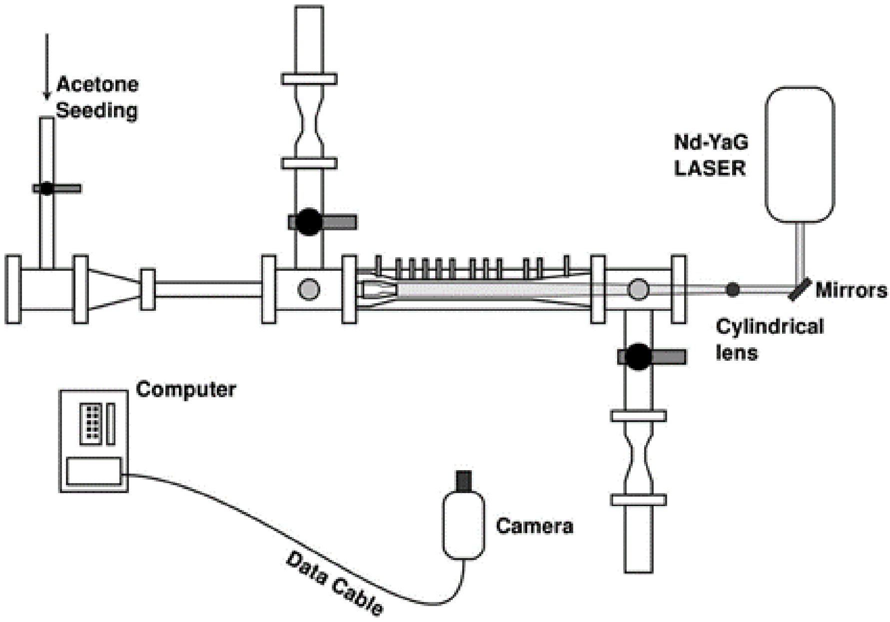

Figure 2.16: Laser tomography system schematic (Rao & Jagadeesh 2014).

Rayleigh scattering was employed by Desevaux (2001) to investigate the mixing chamber of a supersonic air ejector. The micro-droplets that form due to condensation in the mixing zone make the Planar Laser Mie Scattering (PLMS) the ideal visualisation technique, however, it is only accurate for low-speed flow and does not produce high quality images outside of the region containing condensation (Desevaux 2001). The PLMS imaging technique involves an incident laser light sheet wavelength that is smaller than the scattering particles being observed (see figure 2.17). This is considered to give higher quality images and is often preferred over the Rayleigh scattering regime by many researchers. This method was employed by Karthick, Gopalan & Reddy (2016) to visualise the fluid flow inside both a free and confined supersonic jet. Specific flow features were able to be analysed including the jet shear layer, reflecting shock, shock train length and subsonic tail waves.

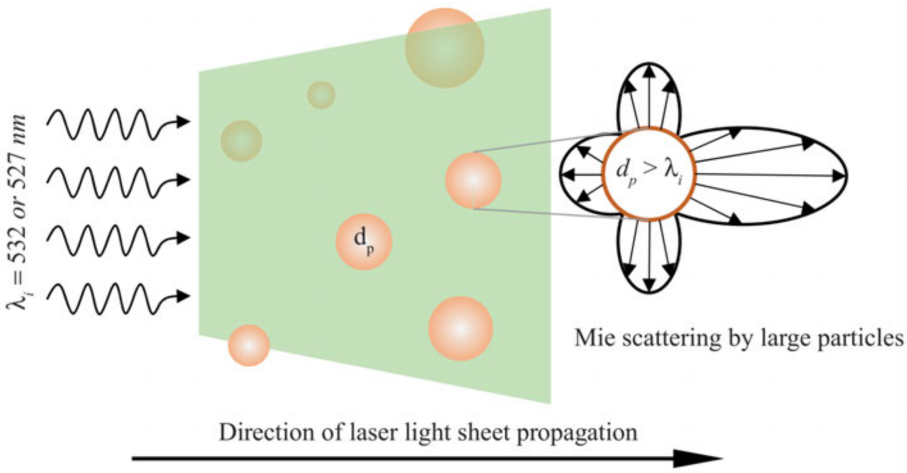

Figure 2.17: Planar Laser Mie Scattering Concept (Karthick et al. 2016).

A method that has recently become more common in flow visualisation due to the advance in camera performance is the direct photography technique. Zhu, Wang, Yang & Jiang (2017) found that the schlieren system was insufficient for capturing details in flows with CO_2 as the working fluid, thus a single-lens reflex camera and a light film was adopted. The suction and mixing chambers of a supersonic jet ejector was visualized in a number of different operating conditions. The results showed that as the secondary flow pressure was increased there was a decrease in the expansion angle of the flow after exiting the primary nozzle (Zhu et al. 2017). Direct photography was also used in a study by Palacz, Bodys, Haida, Smolka & Nowak (2022) to analyse the expansion of the primary flow and found that the expansion angle increases as the mass flow rate of the primary fluid increases. Palacz et al. (2022) also acknowledged that the mixing angle increases with the pressure lift.

2.3.4 Computational Fluid Dynamics

The accuracy of computational fluid dynamics to analyse supersonic flow in steam ejector was investigated by Sriveerakul, Aphornratana & Chunnanond (2007*a*) in a study that compared simulations with experimental data. A number of nozzles, mixing chamber and throat sections with varying geometries were experimented with. The solver Fluent 6.0 was used in pair with a realisable k-ϵ turbulence model and the steam was assumed as an ideal gas; (Sriveerakul et al. 2007*a*) explains that for low operating pressures the ideal gas assumption produces similar results to a real gas model. Static pressure profiles along the ejector wall were used to validate the two analysis methods, this comparison is shown in figure 2.18. This research was continued in Sriveerakul, Aphornratana & Chunnanond (2007*b*), through simulations it was discovered that the entrainment ratio and critical back pressure can be varied through adjusting the primary nozzle size (see table 2.1), however, they cannot be increased in unison.

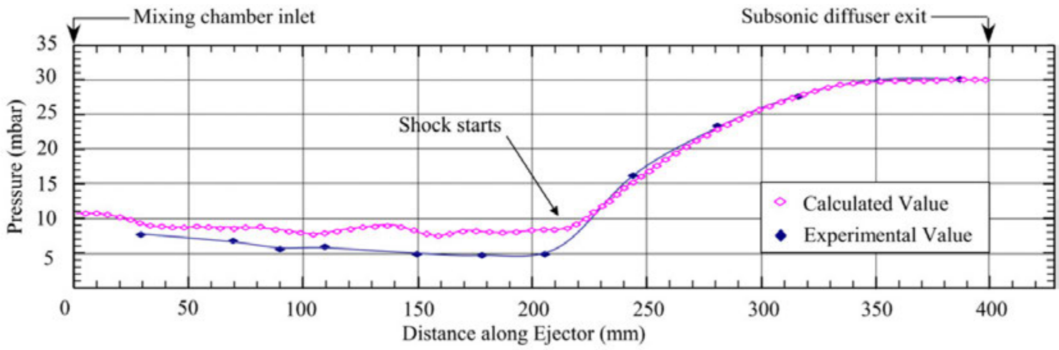

Figure 2.18: Static pressure distribution along ejector wall for simulated and experimental analysis methods (Sriveerakul et al. 2007*a*).

Parameter	Action	Performance characteristic	
		Entrainmentratio (*Rm*)	Critical backpressure (P_c)
Ejector operating pressures			
Primary fluid saturated pressure	↑	↓	↑
Secondary fluid saturated pressure	↑	↑	↑
Ejector geometries			
Primary nozzle size	↑	↓	↑
Mixing chamber inlet diameter	↑	–	Unpredictable
Ejector throat length	↑	–	↑

Table 2.1: Effect of geometry on ejector performance characteristic (Sriveerakul et al. 2007*b*).

Varga, Oliveira & Diaconu (2009*b*) used a realisable k-ϵ computational fluid dynamics model to assess the efficiencies of a steam ejector for different operating conditions. This research found that the geometrical factors with the greatest impact on ejector performance are the nozzle exit position relative to the mixing chamber, and the area ratio between the nozzle and the mixing chambers cross-sections. It was found that an optimum area ratio exists of which the maximum entrainment ratio is achieved (Varga et al. 2009*b*). Area ratios below the optimal value were found to cause over expansion of the primary flow inside the mixing chamber which reduced area availability for the secondary flow resulting in a lower entrainment ratio. Above the optimal value the secondary stream fails to reach supersonic velocity, at this point all measured efficiencies were found to decrease (Varga et al. 2009*b*).

Yang et al. (2012) experimented with a variety of different nozzle structures, using computational fluid dynamics, to identify the effect that the geometries have on the performance of the steam ejector. He used three turbulence models including the realizable k-ϵ, standard k-ϵ and RNG k-ϵ and validated them against experimental results from Sriveerakul et al. (2007a) finding that the realizable k-ϵ model was in close agreement. As shown in the simulation data in figure 2.19, it was found that the conical nozzle produced the highest critical back pressure while only the square and cross-shaped nozzles produced higher entrainment ratios. Yang et al. (2012) concluded that a nozzle structure with a greater exit perimeter and alternate geometry can produce greater streamwise and spanwise vorticity variation that can improve the mixing effect and increase the entrainment ratio. An important observation from Yang et al. (2012) research that must be considered in this dissertation is that increasing the entrainment ratio by altering the nozzle geometry can result in higher losses of mechanical energy which reduces the critical back pressure.

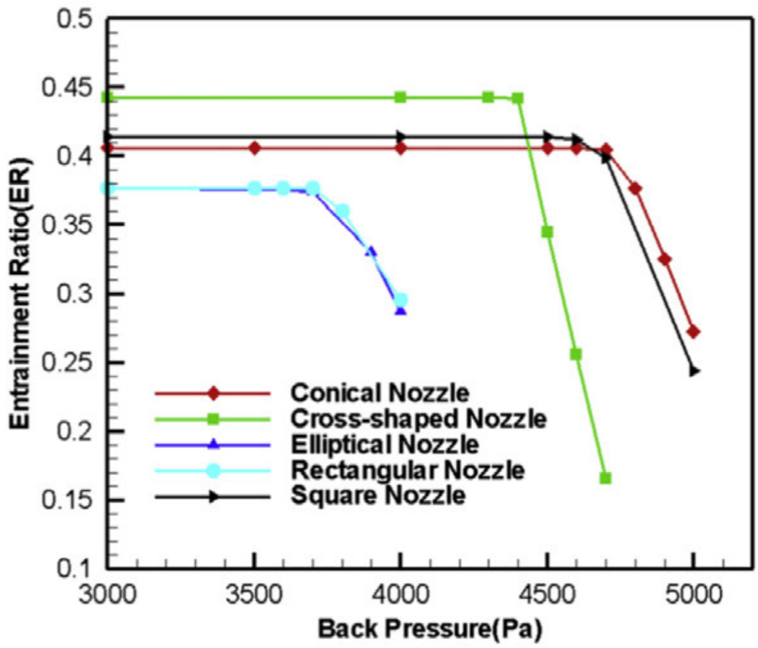

Figure 2.19: Entrainment ratio vs back pressure results (Yang et al. 2012).

Computational fluid dynamics was used to identify the correlation between primary nozzle geometry and the Mach number, primary flow pressure and mass flow rate in a study by Ruangtrakoon, Thongtip, Aphornratana & Sriveerakul (2013). A combination of the k-ω SST and realizable k-ϵ turbulence models were and compared to experimental values from Ruangtrakoon, Aphornratana & Sriveerakul (2011). The study found that the k-ϵ SST was more accurate, attributing the superiority of the k-ω SST to its ability to process complex flow behaviour such as free shear flow and mixing layer development. Primary nozzles with throat diameters varying from 1.4mm to 2.6mm were used under a fixed evaporator temperature of 7.5 °C, Mach numbers from 3 to 5.5 and boiler temperatures ranging between 110 °C and 150 °C. Two classifications of the initial shock wave from the primary nozzle were recorded from the simulations; an overexpanded wave and an under expanded wave. The over expanded wave was considered favourable and produced higher entrainment ratios. The second shock to occur in the ejector could be controlled by varying the flow rate of the mixed fluids. Ruangtrakoon et al. (2013) demonstrated how that the primary nozzle geometries and operating conditions strongly influenced the performance of the ejector.

A study implementing a Chevron style primary nozzle in a steam ejector was performed by Kong, Kim, Jin & Setoguchi (2013) that investigated the Chevrons effect on the performance characteristics. Kong et al. (2013) used a SST k-ω turbulence model in ANSYS Fluent to perform simulations for ejector models equipped with a 6 Chevron, 10 Chevron and convergent nozzle structure (figure 2.20), validating the results against existing experimental data. It was found that the ejectors with Chevrons experienced weakened shock trains and that more streamwise vortices were generated, entraining more secondary fluid, and enhancing the mixing effect (Kong et al. 2013). Compared with the convergent nozzle the fluid flow out the diffuser was lower as a result of the increased resistance introduced by the Chevrons, however, a greater pressure recovery was achieved by the 10 Chevron model. Incorporating 10 Chevrons into the primary nozzle saw, on average, a 14.8% in increase in entrainment ratio and an 8.5% improvement on pressure recovery over the convergent nozzle design (Kong et al. 2013).

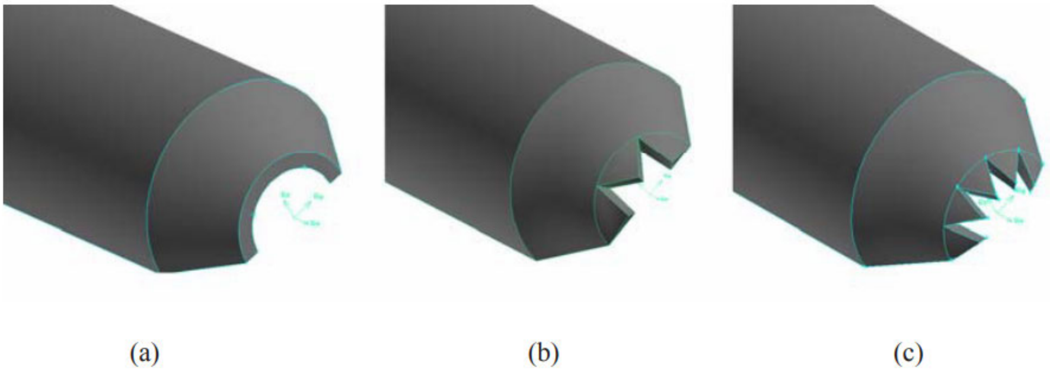

Figure 2.20: Primary Nozzle Models. a) Convergent, b) 6 Chevrons, c) 10 Chevrons. (Kong et al. 2013).

A numerical investigation using a realizable k-ϵ turbulence model conducted by Wu, Liu, Han & Li (2014), revealed that an optimum mixing chamber length and convergence angle exists that extracts the maximum performance from a steam ejector. The optimum range of L/d (ratio of mixing chamber length to primary nozzle diameter) depends on the primary flow pressure; higher primary flow pressures will have a larger optimal L/d value. For the constant operating condition used in the simulations, it was observed that the flow was choked as L/d was increased from 11 to 21 before becoming unchoked and a sharp decrease in entrainment ratio occurred. The convergent angle of the mixing chamber is dependent on its length, Wu et al. (2014) found that for small angles the entrainment ratio increases rapidly, however, once the optimal value is reached in begins to degrade. This is consistent with observations made by Ramesh & Sekhar (2018). It should be noted that for angles larger than the optimal value the secondary flow velocity is low an increase in spanwise vortices forming near the wall of the mixing chamber is observed.

An alternative ejector type known as a vortex ejector was explored in a study by Evdokimov, Piralishvili, Veretennikov & Guryanov (2018) that used computational fluid dynamic analysis methods to simulate the ejector under various conditions and comparing the results with available experimental data. This ejector types uses a swirling nozzle that generates a vortex in the ejecting flow (primary flow) that moves the passive flow (secondary fluid) as depicted in figure 2.21. This movement is created by the centrifugal force of the vortex that acts on the secondary fluid by creating a radial gradient of static pressure which is lowest in the centre of the vortex, thus motivating the passive flow (Evdokimov et al. 2018). However, it was acknowledged that the vortical flow increased the axial velocity of the primary fluid such that the Mach number shows supersonic values in some locations and the secondary fluid is entrained in an effect similar to that of a jet ejector. Evdokimov et al. (2018) concluded that the SST k-ω turbulence model used for the simulations produced adequate correlation with experimental results for a relative total back pressure value of $\pi \leq 0.15$, however, for $\pi < 0.15$ discrepancies were encountered that require additional research (Evdokimov et al. 2018).

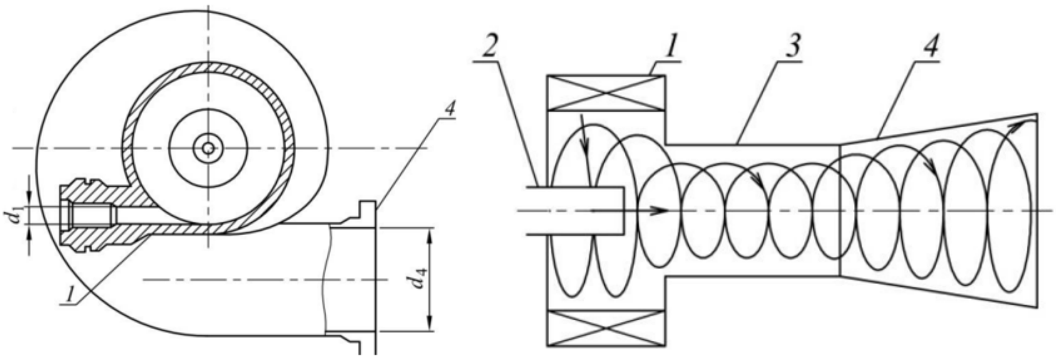

Figure 2.21: Vortex ejector (1) Primary Swirling Nozzle, (2) Secondary Passive Nozzle, (3) Mixing Chamber, (4) Diffuser (Evdokimov et al. 2018).

The effect of suction chamber angle and primary nozzle exit position (NXP) was studied by Ramesh & Sekhar (2018), comparing results from ANSYS simulations using realizable k-ϵ, RNG k-ϵ, and SST k-ω models with experimental data. A comparison of the error between the different turbulence models and the experimental results found that the SST k-ω model was the most accurate simulation. The entrainment ratio was found to decrease as the suction chamber angle was increased, however, it was observed that at 12° the entrainment ratio would improve, highlighting the importance of the entrainment diameter. According to the research, from the optimal suction chamber angle, when the primary nozzle was withdrawn from the mixing chamber the entrainment ratio would increase until a maximum point was reached, and then it would begin to decrement. Ramesh & Sekhar (2018) also discovered that the lower boiler pressure yielded the highest entrainment ratio for all tested suction chamber angles.

2.4 Steam Ejector Computational Simulations

2.4.1 Turbulence Model Selection

The high Mach and Reynolds number of the fluid flow in an ejector means that a turbulence model is required to simulate the fluid properties in ANSYS Fluent. Since the complex mixing effect that occurs within steam ejectors is viscous, the interaction type used in the model cannot treat the flow as simply inviscid or viscous-inviscid flow (Sharifi & Sharifi 2014). The turbulence model selected to simulate the flow through an ejector can have a significant effect on the accuracy of the results. There are a number of turbulence models available in ANSYS Fluent including the k-ϵ models, k-ω models, the Reynolds Stress Model (RSM), Large Eddy Simulation model (LES) and the Spalart-Allmarus model (Watanawanavet 2005). In the area of steam ejector research, a wide range of models have been explored across the literature however, no definitive turbulence model has been widely accepted.

A study conducted by Varga, Soares, Lima & Oliveira (2017) compared a variety of k-ϵ and k-ω model simulation results to experimental data to assess accuracy. It was found that the k-ϵ models were superior to the k-ω models for predicting the COP (see table 2.2) and the critical backpressure. This conclusion was also made by Hemidi et al. (2009), where the k-ϵ model would remain within 10% error across the whole operating range compared to the k-ω model that was only accurate for high primary flow pressures and heavily off-design conditions. A comparative study of the standard k-ϵ, realizeable k-ϵ and the RNG k-ϵ was made by Yang et al. (2012), finding that the realizable k-ϵ model was only 6% and 1.5% error in critical back pressure and entrainment ratio when compared with experimental data obtained in another study Sriveerakul et al. (2007*a*). It was believed that the discrepancies between the turbulence models came down to the complications surrounding the analysis of flow in the choked conditions, and the occurrence of shock waves in the experimental study (Yang et al. 2012). Other advocates for the k-ϵ model were Sriveerakul et al. (2007*a*) and Wu et al. (2014) who considered the realizable k-ϵ model the most accurate for predicting the spreading rate of fluid from the primary nozzle and also for analysing the boundary layer in the complex flow conditions.

		COP (error in %)					
T_e°C	T_g°C	k–ε	RNG k–ε	Realisable k–ε	Transition SST	k–ω	SST k–ω
5	120	0.36 (9%)	0.37 (8%)	0.35 (13%)	0.41 (2%)	0.31 (23%)	0.34 (15%)
	125	0.31 (8%)	0.31 (8%)	0.30 (12%)	0.35 (1%)	0.27 (21%)	0.29 (15%)
	130	0.27 (5%)	0.27 (5%)	0.26 (8%)	0.29 (3%)	0.23 (17%)	0.25 (12%)
	135	0.22 (11%)	0.22 (12%)	0.22 (11%)	0.24 (3%)	0.20 (19%)	0.21 (14%)
	140	0.19 (3%)	0.18 (2%)	0.19 (3%)	0.20 (13%)	0.18 (2%)	0.18 (1%)
7.5	120	0.43 (13%)	0.44 (12%)	0.41 (18%)	0.50 (0%)	0.37 (26%)	0.41 (18%)
	125	0.37 (12%)	0.38 (11%)	0.35 (16%)	0.42 (1%)	0.32 (24%)	0.35 (17%)
	130	0.32 (11%)	0.32 (11%)	0.30 (16%)	0.36 (0%)	0.28 (22%)	0.30 (17%)
	135	0.28 (8%)	0.27 (9%)	0.26 (12%)	0.30 (1%)	0.24 (19%)	0.26 (14%)
	140	0.23 (1%)	0.23 (0%)	0.23 (0%)	0.26 (11%)	0.21 (8%)	0.22 (3%)
10	120	0.54 (5%)	0.55 (3%)	0.52 (9%)	0.65 (14%)	0.50 (12%)	0.53 (7%)
	125	0.47 (14%)	0.48 (12%)	0.44 (18%)	0.55 (2%)	0.42 (22%)	0.45 (16%)
	130	0.41 (13%)	0.41 (12%)	0.39 (18%)	0.47 (0%)	0.36 (24%)	0.39 (16%)
	135	0.35 (9%)	0.36 (9%)	0.34 (14%)	0.41 (4%)	0.32 (19%)	0.34 (13%)
	140	0.31 (1%)	0.31 (1%)	0.29 (6%)	0.35 (13%)	0.28 (11%)	0.29 (6%)

Table 2.2: Error of simulations using various k-ϵ and k-ω turbulence models compared to experimental data (Varga et al. 2017).

A study performed by Bartosiewicz, Aidoun, Desevaux & Mercadier (2003) found that the standard k-ω model was ideal for the boundary layer but could be sensitive when analysing freestream conditions. The k-ω SST has the ability to use standard k-ϵ features in a k-ω formula to calculate the fluid properties in the wake region, whilst also using the standard k-ω model near the ejector walls (Bartosiewicz et al. 2003). The complex fluid interactions that occur between the supersonic shocks and mixing layer was best described by the k-ω SST model. It was acknowledged that the expansion strength could not be determined reliably which is likely due to the development of condensation in the ejector that is not accounted for by the turbulence model (Bartosiewicz et al. 2003). A similar conclusion was made by Mazzelli, Little, Garimella & Bartosiewicz (2015) who compared the accuracy of k-ω and k-ϵ model predictions against experimental data. This study found that the k-ω model typically performed the best and was particularly accurate in high primary flow pressure conditions.

The realizable k-ϵ and k-ω SST were used to model flow in a study investigating the influence of nozzle geometry on steam ejector performance (Ruangtrakoon et al. 2013). The k-ω model was superior to the k-ϵ model showing closer correspondence to experimental data (see table 2.3); this was attributed to the inability of the realizable k-ϵ model to deliver accurate performance predictions for situations involving strong adverse pressure gradients. Kong et al. (2013) also used SST k-ω model and found an error of just 4% between the ANSYS Fluent simulations and experimental data. Ramesh & Sekhar (2018) completed CFD simulations using a combination of the RNG k-ϵ, realizable k-ϵ and SST k-ω turbulence models and determined that the k-ω SST model results were the most accurate. When validated against the experimental data, the k-ω SST model had 7.7%

less error than the alternative realizable k-ϵ model.

Nozzle	T_{boiler} (°C)	Rm_{exp}	$Rm_{k\text{-}\omega\text{-}sst}$	$Rm_{k\text{-}\epsilon}$	Error[a], Rm		P_{cri} (mbar)	$P_{cri,\ k\text{-}\omega\text{-}sst}$ (mbar)	$P_{cri,\ k\text{-}\epsilon}$ (mbar)	Error[b], Pcri	
					k-ω-sst (%)	k-ε (%)				k-ω-sst (%)	k-ε (%)
d1.7M4	130	0.422	0.446	0.464	5.687	9.953	35.0	33.5	32.5	4.286	7.143
	140	0.287	0.316	0.351	10.105	22.230	45.0	44.0	42.0	2.222	6.667
	150	0.188	0.210	0.273	11.702	45.213	58.5	55.0	55.0	5.983	5.983
d1.4M4	150	0.288	0.322	0.370	11.806	28.427	44.0	42.0	37.0	4.545	15.909
d1.7M4		0.188	0.210	0.273	11.702	45.213	58.5	55.0	55.0	5.983	5.983
d2.0M4		0.102	0.125	0.171	22.549	67.647	79.0	73.0	75.0	7.595	5.063
d1.4M3	150	0.282	0.315	0.373	11.702	32.270	38.0	37.0	30.0	2.632	21.053
d1.4M4		0.288	0.322	0.370	11.806	28.472	44.0	42.0	37.0	4.545	15.909
d1.4M5.5		0.280	0.317	0.362	13.214	29.286	54.0	46.0	40.0	14.815	25.926
d1.4M4	150	0.288	0.322	0.370	11.806	28.427	44.0	41.0	37.0	6.818	15.909
d1.7M4	140	0.287	0.316	0.351	10.105	22.230	44.5	42.0	38.0	5.618	14.607
d2.0M4	130	0.286	0.312	0.320	9.091	11.888	45.0	42.5	40.0	5.556	11.111
d2.3M4	120	0.273	0.311	0.314	13.919	15.018	51.0	45.0	41.0	11.768	19.608
d2.4M4	113.6	0.267	0.308	0.315	16.854	17.978	49.5	43.0	40.0	13.131	19.191
d2.6M4	111.2	0.262	0.304	0.312	16.031	19.084	48.5	42.0	40.0	13.402	17.526

Table 2.3: Error of realizable k-ϵ and SST k-ω turbulence model simulations compared to experimental data for different nozzle geometries (Ruangtrakoon et al. 2013).

The literature typically indicates that turbulence model suitably often changes depending on whether the ejector is operating on or off-design. It can be concluded that the realizable k-ϵ and k-ω SST turbulence models are considered the most accurate and are the most frequently adopted in supersonic steam ejector research.

2.4.2 2D vs 3D Simulations

Since the geometry of the typical circular cross-section steam ejector is largely asymmetrical, 2D asymmetric modelling is commonly selected over 3D models due to the reduced computational time and memory required (Ariafar 2016). A comparison of the predication accuracy of 2D and 3D modelling methods was completed in a study by Mazzelli, Little, Garimella & Bartosiewicz (2015) using operating conditions with different primary pressures. It was found that for on-design conditions the 2D and 3D models produced results with very similar accuracy, however, for off-design conditions the 2D model was 27.8% less accurate than the 3D model (see figure 2.22). Overall, the 3D model is found to have a higher accuracy as it more precisely captures fluid interactions at the walls and accounts for more losses that occur Mazzelli et al. (2015). A similar study was performed by Sharifi & Boroomand (2013) that determined that 2D asymmetric modelling could produce sufficiently accurate results across the designed operating range; the maximum deviation of 3D and 2D models from the experimental results was 9.7% and 10.6%, respectively.

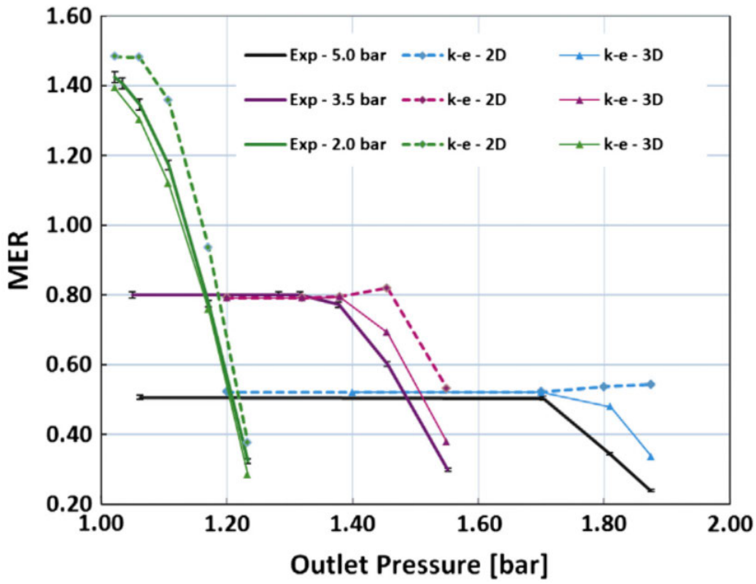

Figure 2.22: Comparison of experimental data and 2D and 3D realizable k-ϵ models for various primary pressures (Mazzelli et al. 2015).

It is clear that the advantages of using the 2D asymmetric modelling approach far outweighs the marginal reduction in accuracy compared to the 3D model. However, in some circumstances a 3D asymmetric model is used if predictions for off-design conditions are necessary or if maximum precision is desired (Hemidi et al. 2009) (Atmaca & Ezgi 2022). For nozzles with rectangular or square cross-sections it is found that the 3D approach is more suitable (Mazzelli et al. 2015). A 3D model is also necessary when complex geometries are being analysed such as the vortex ejector studied by Evdokimov et al. (2018) or the chevron style primary nozzle in the study by Kong et al. (2013).

2.4.3 Gas Model Selection

Ideal Gas Assumption

For the use of a wet fluid such as steam for the motive fluid it is common that non-equilibrium condensation develops within the steam ejector. Despite this occurrence being far from reflective of the characteristics of an ideal gas, the ideal gas assumption is commonly adapted to steam ejector research (Besagni, Cristiani, Croci, Guédon & Inzoli 2021). Whilst the clear advantages of this is a reduction in time required for simulations and increased simplicity, the ideal gas model will not account for effects such as condensation shock and other flow behaviours that occur from wet steam working fluids (Sriveerakul et al. 2007*a*). Thus, implementing the ideal gas model to simplify the analysis can come at the cost of reduced accuracy in the prediction of entrainment ratio and the critical pressure values (Wang, Dong, Li, Lei & Tu 2014).

Wet Steam Assumption

As expansion of the motive steam occurs through the primary nozzle, the fluid transitions from a gas phase in the form of water vapour, to a liquid phase in the form of water droplets. This phase change typically occurs as after the steam passes through the throat and reaches supersonic velocity, however, supersaturation can occur before the throat (Yang et al. 2019). This phenomenon cannot be captured in simulations using the ideal gas assumption and has a significant effect on the flow conditions downstream. For working fluids such as steam, a wet-steam expansion model can be applied for more accurate representation of flow conditions in ejector operation (Zhang, Dykas, Yang, Zhang, Li & Wang 2020).

There are two main numerical approaches for wet-steam models including the Eulerian-Eulerian approach and the Eulerian-Lagrangian approach. The Eulerian-Eulerian approach relies on the assumption that the liquid phase of the primary steam is distributed uniformly with the volume of the vapour. A Eulerian scheme is used to model the properties for the liquid phase and the conservation equations; this approach is commonly adopted due to its relative simplicity over alternative wet-steam models (Ariafar, Buttsworth, Sharifi & Malpress 2014)(Li, Yuen, Chen, Wang, Liu, Cao, Yang, Yeoh & Timchenko 2019)(Mazzelli, Little, Garimella & Bartosiewicz 2016). The Eulerian-Lagrangian approach also uses the Eulerian scheme to evaluate the conservation equations whilst a Langranian method is used to model the properties in the liquid phase. Despite being considered to have a higher accuracy, the Eulerian-Lagrangian is less frequently used due to being more complex, requiring more time for computation, and not being optioned in ANSYS Fluent (Sim, Im & Chung 2015).

Simulations based on a wet-steam model using the Eulerian-Eulerian approach was compared with an ideal gas model in a study conducted by Wang et al. (2014). The predicted entrainment ratio and critical pressure determined from the ideal gas model deviated from the experimental results by 20% and 6.4%, respectively. The results obtained from the wet-steam model simulations had 6.7% error for entrainment ratio and 2.1% error for critical pressure; this highlights the superiority of the wet-steam assumption over the ideal gas assumption (Wang et al. 2014). A similar conclusion was made by Wang, Dong, Zhang, Fu, Li, Han & Tu (2019), where the wet-steam model predicted a higher entrainment ratio and critical pressure in critical operating conditions compared to the ideal gas model (see figure 2.23). The improved accuracy of the wet-steam model was also identified in a comparable study performed by Mazzelli et al. (2016).

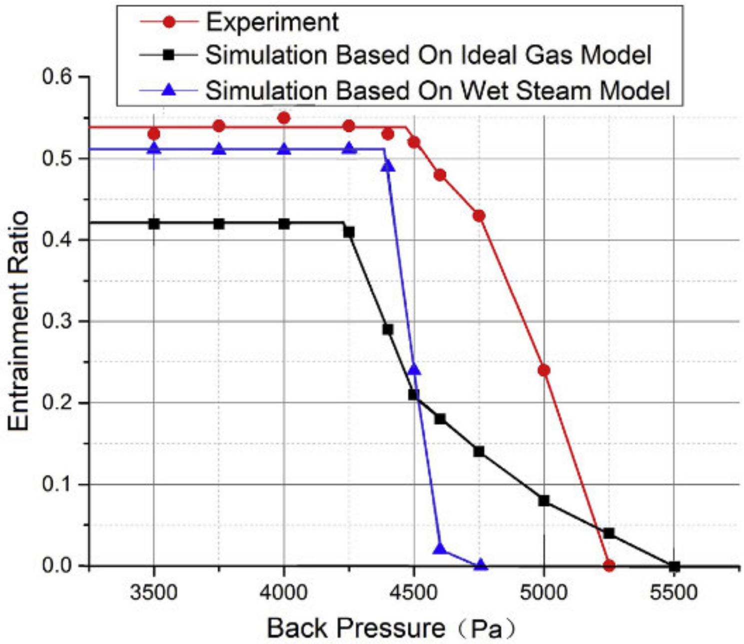

Figure 2.23: Performance predictions of ideal gas model and wet-steam model against experimental data (Wang et al. 2019).

2.5 Chapter Summary

This chapter has provided a detailed literature review on studies employing either, or a combination of, theoretical, experimental, visualisation and computational fluid dynamics analysis techniques. A strong understanding of steam ejector operation and analysis was established and important considerations, required for the computational fluid dynamics aspect of this project, are recognised.

It is acknowledged amongst the literature that key difficulties restricting the accuracy of ejector analysis exists such as non-uniform condensation, turbulent flow, and diamond wave shock trains. It has been the aim of many studies to try to improve existing analysis methods by changing gas models, turbulence models and visualisation techniques. In the area of computational fluid dynamics, significant progress has been made on increasing the accuracy of simulations for the purpose of predicting ejector performance characteristics. The literature review has revealed that there is no turbulence model that is globally accepted as being optimal for the analysis of steam ejectors. However, agreement was found with regards to the superiority of the wet-steam model over the ideal gas assumption in the selection of gas models for systems using steam as the motive fluid.

Many of the studies that were reviewed in this chapter attempted to improve the coefficient of performance by changing geometrical characteristics of the ejectors such as the nozzle shapes, NXP, mixing chamber length and expansion angle. An alternative style of ejector has been designed that generates vortex in the primary flow using a large, spiralled housing that was found to increase the velocity of the entrained fluid. The results of this literature review are particularly encouraging and revealed that there is scope to investigate the effect of a vortex inducing primary nozzle in a jet steam ejector.

Chapter 3

Research Methodology

3.1 Chapter Overview

In this chapter, the methodology process for this research project has been explained which involves: (1) generation and verification of the 2D ejector geometry; (2) specification of the boundary conditions and ANSYS Fluent setup; (3) development of the 3D standard and modified ejector CFD models; (4) accessing and implementing the UniSQ HPC. The grid independence study performed for the models has been detailed, along with the selection of the viscous turbulence model, wall functions and gas model that have been used for the simulations. A detailed explanation of the vortex generator geometry creation, and a step-by-step process for procurement and use of the HPC have been included.

3.2 2D Ejector Model

The first step in the methodology is to generate a basic 2D model of the ejector that will accurately reflect the fluid domain of the ejector described in Al-Manea (2019). By generating this 2D model, the flow of refrigerant through the ejector and thus the performance characteristics can be analysed with an acceptable level of accuracy. This model will be used to validate the ejector geometry such that it can be used in confidence for the 3D models developed later within the study.

In order to gain an understanding of how to apply ANSYS software for this analysis, a number of examples provided by USQ and the ANSYS Fluent Tutorial Guide (ANSYS 2021*a*) were completed. Once the necessary practice was completed and a fundamental understanding of the software for fluid flow analysis purpose was obtained, the geometry of the ejector could be developed. It is possible to generate the geometry through ANSYS Workbench or using external CAD software such as Creo-Parametric or SolidWorks. Both methods were tested, and it was found that for basic 2D geometry, the additional steps required to import the file from an external program into ANSYS made it unviable. In addition to this, the development of surface areas necessary for the meshing process became more complicated when importing the geometry from Creo-Parametric. Consequently, ANSYS Workbench was selected as the most suitable platform for creating the 2D model and saved significant amount of time over using a more familiar external program.

3.3 2D Geometry

The dimensions used to create the ejector geometry were obtained from Al-Manea (2019); the design dimensions used in that study are included in Appendix D. It was found that some inconsistencies existed between the detailed drawings of the components for the experimental study and the dimensions tabularised in the CFD simulation in Al-Manea (2019). These discrepancies have been corrected and the dimensions used to create the 2D geometry are provided in table 3.1 with the key ejector sections shown in figure 3.1. The geometry of the primary nozzle used in Al-Manea (2019) was obtained from Al-Doori (2013) and the detailed drawing has been included in Appendix D. The dimensions of the primary nozzle used for generating the 2D ejector model are provided in table 3.2.

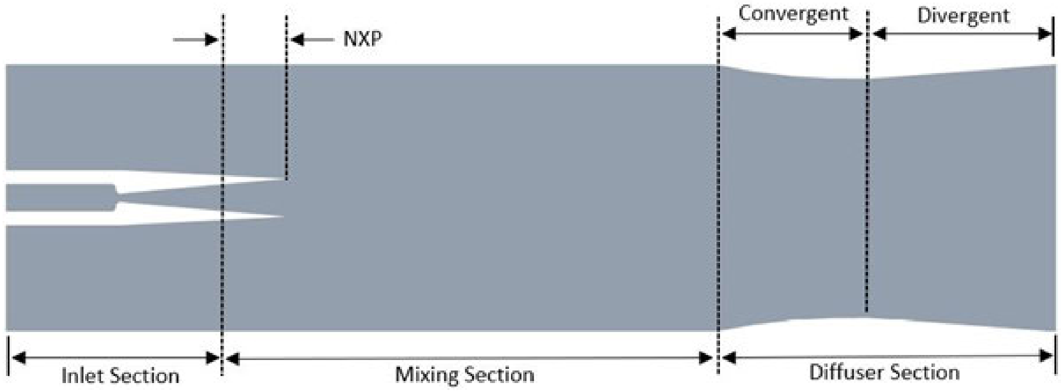

Figure 3.1: Key sections of the steam ejector.

Table 3.1: 2D ejector geometric data obtained from previous studies (Al-Manea 2019).

Geometric Parameter	Dimension
Secondary Inlet length	65.6 mm
Secondary Inlet Diameter	90 mm
NXP	+15 mm
Mixing Chamber Length	420 mm
Mixing Chamber Diameter	90 mm
Diffuser Inlet Diameter	90 mm
Diffuser Convergent Radius	730 mm
Diffuser Convergent Length	153 mm
Diffuser Throat Diameter	56 mm
Diffuser Divergent Angle	N/A deg
Diffuser Divergent Length	169 mm
Diffuser Outlet Diameter	80 mm

Table 3.2: 2D ejector nozzle geometric data obtained from previous studies (Al-Doori 2013).

Geometric Parameter	**Dimension**
Nozzle Inlet Length	65.65 mm
Nozzle Inlet Diameter	10 mm
Nozzle Inlet Fillet Radius	1.65 mm
Nozzle Throat Fillet Radius	1.8 mm
Nozzle Throat Diameter	3.2 mm
Nozzle Divergence Angle	10 deg
Nozzle Exit Length	59.5 mm
Nozzle Exit Diameter	13.6 mm

A sketch of the ejector was created in ANSYS Workbench on the XY plane as necessary for compatibility with Fluent. The model was created as a 2D asymmetric arrangement which increases simplicity and reduces the number of elements and time required for computation. The surface is generated that represents the fluid domain inside the ejector, where the primary nozzle and ejector walls are considered as the boundary surfaces. The final step in developing the ejector geometry was creating the surface regions required for mesh refinement; this was achieved using the 'Face-Split' function in ANSYS Workbench. Segmenting the nozzle and the mixing chamber allows for a finer mesh to be used in these areas that have more complex geometrical features and are key focus areas for flow behaviour in the analysis. The final 2D ejector model representation is shown in figure 3.2.

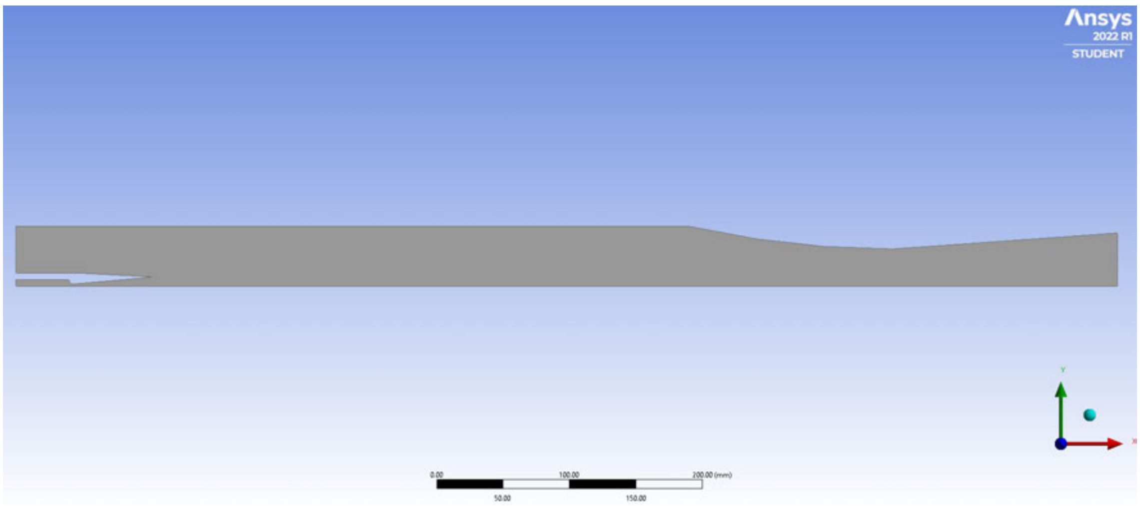

Figure 3.2: 2D ejector nozzle generated using ANSYS Design Modeller.

3.4 2D Initial Mesh

After developing an accurate 2D geometry for the ejector, the next step is to begin the meshing process in ANSYS. Developing a high-quality mesh for this model is important as it ensures that the results obtained from the Fluent simulations are an accurate reflection of reality. If the generated mesh is not sufficient it is also likely that the results will vary significantly from those achieved by Al-Manea (2019) even if the geometry is correct.

The mesh described in this section was developed using the Al-Manea (2019) tutorial guide, USQ course material and with guidance from the project supervisor. Observing the meshes used throughout the literature was also helpful for distinguishing key focus areas within the ejector that require a more refined mesh. The first setting that must be considered when beginning the mesh set up is the selection of the physics preference. There are multiple options for physics preference which include: mechanical, non-linear mechanical, electromagnetic, hydrodynamics, CFD and explicit. Since this project is focusing on the analysis of fluid behaviour inside the ejector, the CFD option was selected for this application.

The solver preference must also be selected in the meshing process, with Fluent, CFX and Polyflow being provided as the options within ANSYS. Each solver preference option has different default meshing values such as the transition ratio and have different exporting capabilities. For this situation, the CFX and fluent options were identified in the literature as the most suitable, however, fluent offers more solution approaches which allows for more versatility. Additionally, fluent is also the solver used by Al-Manea (2019) which made it the obvious selection for modelling the 2D ejector.

3.4.1 Details of Mesh

The default mesh created in ANSYS is extremely rough and has significant inconsistencies in element shapes and sizing that make it unusable, even for very preliminary testing. Thus, it the default mesh settings must be adjusted to create a more appropriate mesh that can act as the foundation for further mesh refinements. This section will mainly discuss the settings that were modified, with the majority of the default settings being left as standard.

3.4.2 Sizing

The first modification that is made is changing the element size, which increases the number of elements used in the default mesh. Due to the complex curvature in the primary nozzle, the element size was reduced to 1mm to provide a closer representation of the curve. Adaptive sizing is activated to allow the software to automatically adjust the element size as appropriate to suit the ejector geometry. Increasing the resolution setting to 4 also improved the effectiveness of the mesh around the throat of the primary nozzle. The span angle center has the option of being coarse, medium or fine and allows the developed mesh to be structured into curved regions until the curvature is covered with elements. This is not as necessary for the large radius of the diffuser convergent; however, the fine "Span Angle Center" setting is useful for representing the tighter curves in the primary nozzle.

3.4.3 Quality

Inside the "Quality" settings the smoothing has the option to be changed between low, medium and high. Selecting the high option improves the mesh quality across the surface of the model and resolves some of the inconsistencies in the mesh that can be seen in figure 3.3. Inside this setting the skewness and the aspect ratio can be observed which are parameters that can be used to gauge the quality of the mesh. The skewness and aspect ratio for this modified default mesh was 0.67 and 2.94, respectively; these are acceptable values with the ideal aspect ratio being close to 1 and less than 0.9 for skewness (ANSYS 2021*a*).

Significant improvement can be observed when comparing the mesh before and after the adjustments to the default settings are made (see figures 3.3 and figure 3.4). It is clear from figure 3.4 that there are some distorted cells and some cells that are oriented approximately 45 degrees to the flow direction. It is important that the cell face is normal to the flow direction vector; this is due to the way in which flux is calculated by the software using the normal component of the velocity vector. Despite the inconsistencies in this mesh, the modifications have provided an initial mesh that acts as a good foundation for further mesh refinements that will be made.

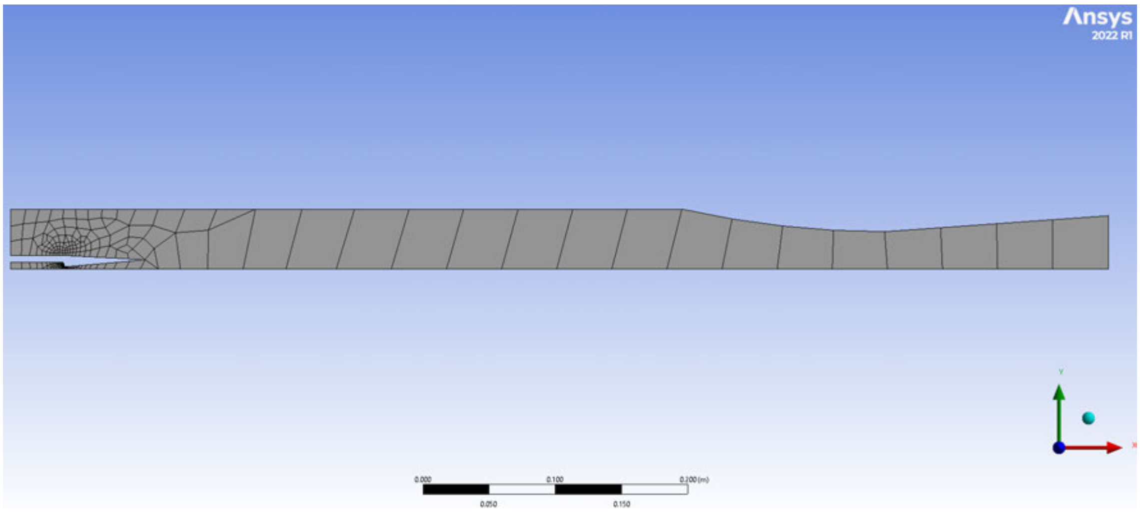

Figure 3.3: 2D ejector model default mesh.

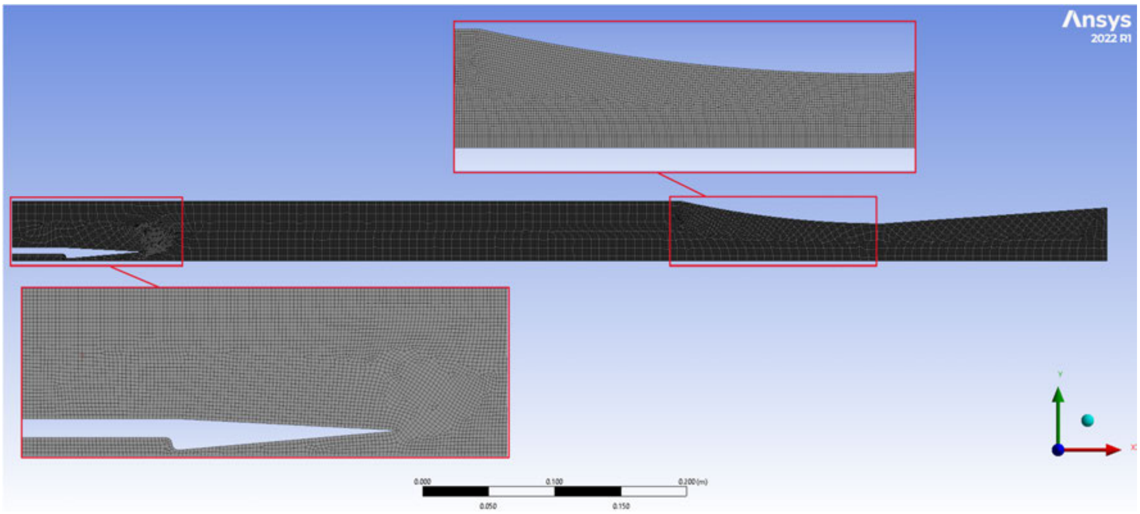

Figure 3.4: 2D ejector initial mesh created using default mesh controls.

3.5 2D Mesh Independence

The cell shape selected to mesh the fluid domain was the structured quadrilaterals which was a common selection throughout the literature and consistent with that used by (Al-Manea 2019). As shown in figure 3.5, the mesh throughout the primary nozzle is the most refined section as a smaller element size will allow the best representation of the nozzle throat to be achieved. The complex flow behaviour that is expected to occur in the mixing chamber means that particular focus is made on the mesh from the exit of the primary nozzle to a distance of 300mm into the mixing chamber. The refinement of this area is shown in figure 3.5 and follows a similar structure as used by (Al-Manea 2019).

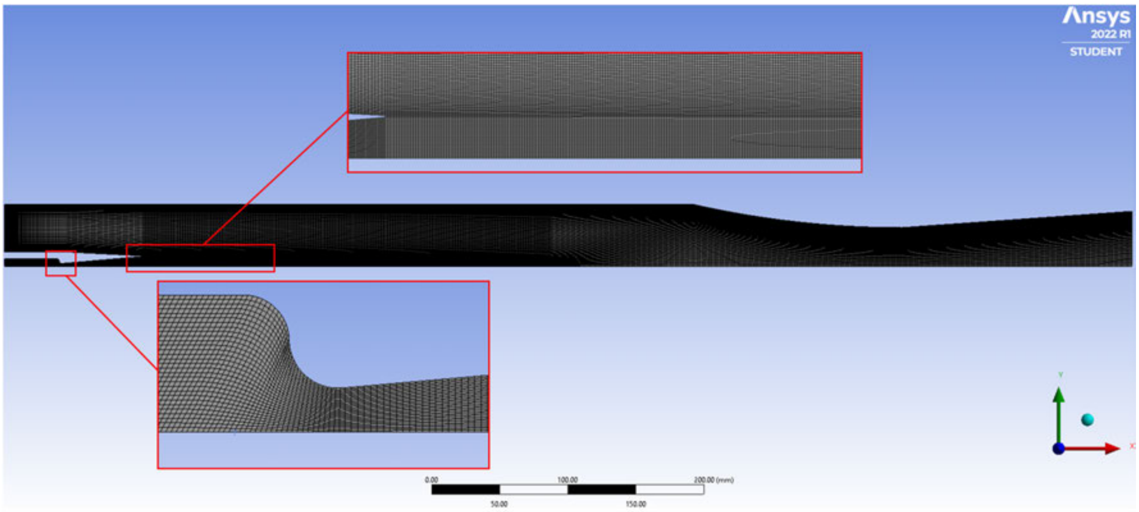

Figure 3.5: Final 180,000 element mesh resolution with nozzle throat and 300mm section of mixing chamber refinement enhanced.

Further refinement must be applied to the area close to the ejector walls, including the walls inside the primary nozzle. This is due to the difference in behaviour of the fluid in the boundary layer as it transitions to turbulent flow. The y+ value must be refined appropriately to allow the selected wall function to account for the difference between the flow viscous sublayer and the log law layer (ANSYS 2021*a*). This is a factor the must be considered during the meshing process and is important for determining which wall function should be implemented in ANSYS Fluent to obtain accurate results.

Table 3.3: Mesh Statistics recorded for the three mesh resolutions of the 2D ejector model.

Resolution	**Number of Cells**	**y+**	**Max Ascpect Ratio**	**Max Skewness**
Coarse	92422	4.16	7.6646	0.71638
Medium	182524	2.47	12.11	0.72313
Fine	378570	1.23	10.325	0.70577

The model was developed with 3 levels of discretization to confirm mesh independence: the coarse mesh with 90,000 cells, the medium mesh with 180,000 cells and the fine mesh with 300,000 cells. The details of the mesh structure for each of these grid levels is provided in table 3.4, with figure 3.6 identifying the block segments that have been created in the ejector model for the mesh refinement process. The number of elements in each of the block segments was controlled using the edge sizing function in ANSYS meshing and a face mesh was applied to the whole ejector surface to improve the distribution of cells.

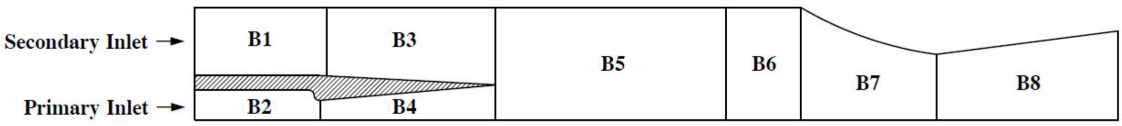

Figure 3.6: 2D ejector divided into blocks used for the mesh independence study.

Table 3.4: Number of elements in the axial and radial directions of the 2D ejector model for each resolution of mesh.

Block Number	Resolution					
	Coarse		Medium		Fine	
	X-Axis	R-Axis	X-Axis	R-Axis	X-Axis	R-Axis
B1	70	64	120	104	140	144
B2	120	20	180	30	220	40
B3	60	64	100	104	110	144
B4	100	20	250	30	350	40
B5	500	86	640	136	710	187
B6	100	86	200	136	250	187
B7	130	86	220	136	300	187
B8	150	86	280	136	450	187

In order to confirm that the results obtained from the simulations are independent of the mesh size, the Mach number profile along the centreline of the ejector for each resolution has been extracted and is shown in figure 3.7. It is recommended by ANSYS (2021*a*) that for a model to be considered mesh independent the percentage difference between the values should be within 5%. The medium and fine meshes were found to be in good agreement, with the difference in Mach number being consistently below 1%. The course mesh was outside of the acceptable range of error, with values exceeding 8% in variation from the medium mesh, and would not produce reliable results. This conclusion was also made when observing the velocity magnitude through the centreline of the ejector, shown in figure 3.8.

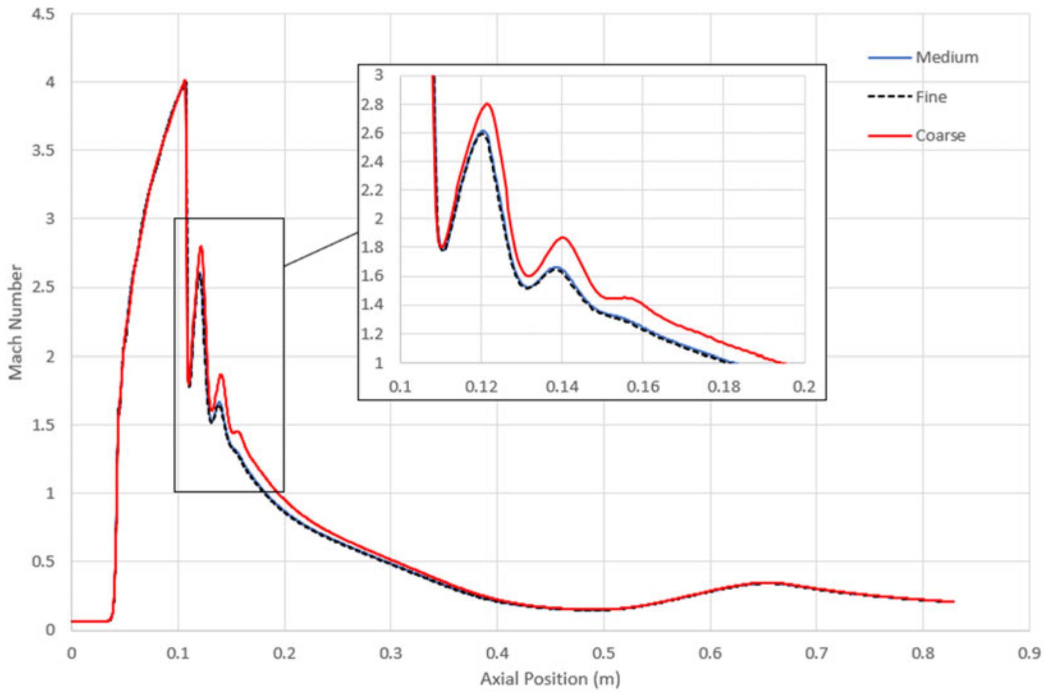

Figure 3.7: The variation in Mach number through the centreline of the ejector for the three mesh resolutions.

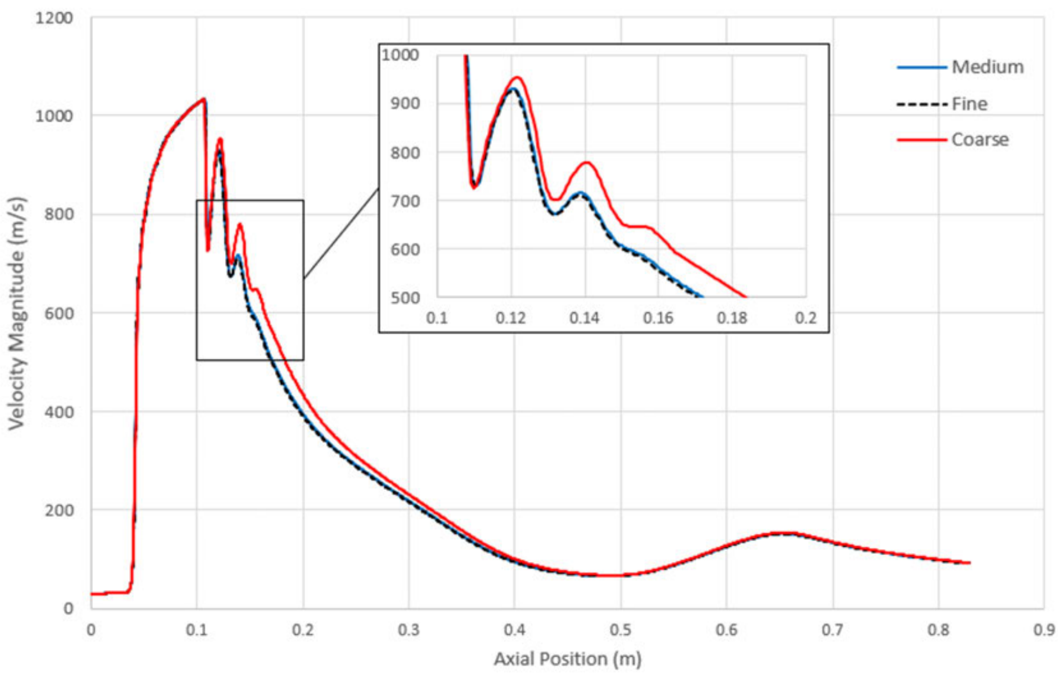

Figure 3.8: The variation in velocity magnitude through the centreline of the ejector for the three mesh resolutions.

The total pressure over the centreline of the ejector was also used to gauge mesh independency, and showed the greatest variation in results (see figure 3.9). The medium and fine meshes had a maximum variation of approximately 3%, whilst the coarse mesh differed by over 20% in some positions. Thus, it can be concluded that the medium mesh level is adequate for the simulations and will provide results with an acceptable level of accuracy.

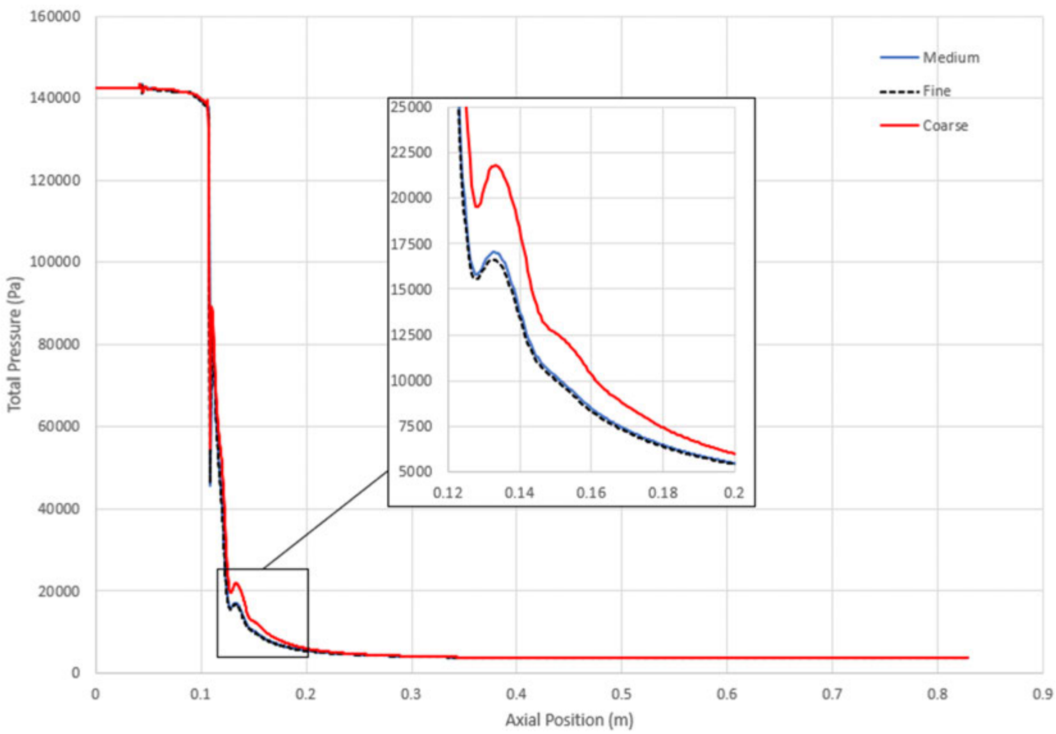

Figure 3.9: The variation in total pressure through the centreline of the ejector for the three mesh resolutions.

3.6 2D Initial Fluent Setup

After establishing a suitable mesh for conducting the simulations, the next step is to transfer the model to ANSYS Fluent and set up the simulation environment. In this part of the methodology process, the details provided in Al-Manea (2019) were used as a guide for creating the initial fluent model setup (see table 3.5) and establishing preliminary boundary conditions. The set-up was not covered in-depth by Al-Manea (2019); thus, they must be modified in a trial by error approach to determine the correct setup. This approach involves repeatedly changing one element of the set-up at a time and running the simulation, with each change determined based on the result of the previous simulation. This process is repeated until the simulations produce results that reflect the expected flow behaviour.

Table 3.5: Sample of the key Fluent setups used during the trial-and-error attempts to achieve correct flow behaviour.

Parameter	**Setting**		
	Inital	**Change 7**	**Change 29**
Solver Type	Density Based	Density Based	Pressure Based
2D Space	Axisymmetric	Axisymmetric	Axisymmetric
Time	Steady State	Steady State	Steady State
Energy Equation	Activated	Activated	Activated
Turbulence Model	Realizable k-ϵ	Realizable k-ϵ	Realizable k-ϵ
Wall Function	Standard	Standard	Advanced
Materials	Air (Ideal Gas)	Air (Ideal Gas)	Water-Vapour (Ideal Gas)
Primary Inlet	Mass Flow Inlet	Pressure Inlet	Pressure Inlet
Secondary Inlet	Mass Flow Inlet	Pressure Inlet	Pressure Inlet
Outlet	Pressure Outlet	Pressure Outlet	Pressure Outlet
Discretization	1st Order	1st Order	1st Order
Residuals	1e-3	1e-3	1e-6
Initialisation	Hybrid	Hybrid	Hybrid
Iterations	10,000	10,000	10,000

To determine the optimal setup for the model an initial setup, shown in table 3.5, was chosen as the foundation for making changes. Examining the simulation results for the initial setup, as the flow passes through the primary nozzle and enters the mixing chamber, it does not reach supersonic velocity as it should (see figure 3.10). To improve this, the primary and secondary inlets were changed to pressure inlets (see change 7 in table 3.5) and their values set to 148000Pa and 2800Pa, respectively, and the operating pressure changed to zero. This resulted in the supersonic flow at the primary nozzle exit, however, observing figure 3.11 it is clear from the shock intensity and train length, as well as the maximum velocity, that further modifications were required.

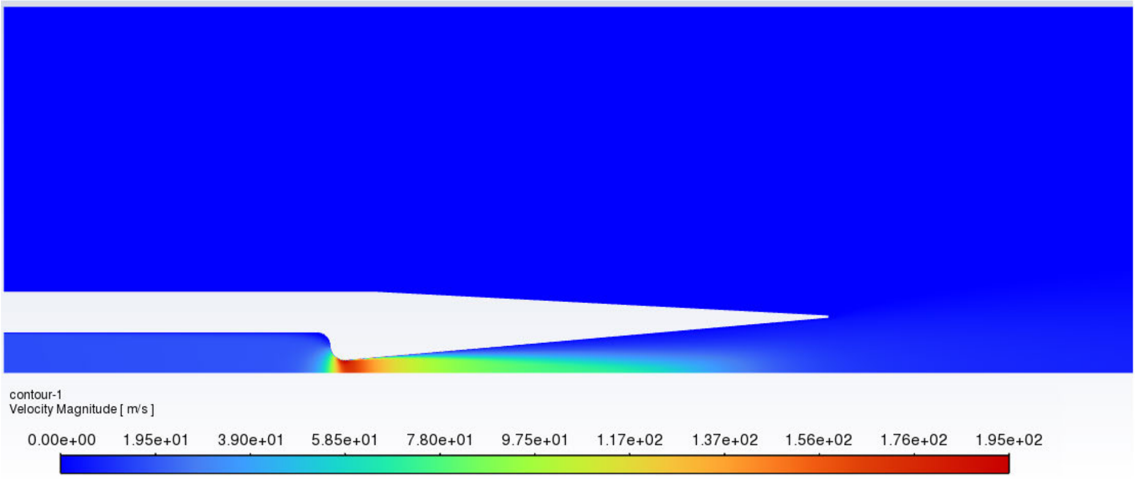

Figure 3.10: Velocity magnitude contour plot for simulations of the initial Fluent setup with the primary inlet at 1.8g/s, secondary inlet at 6.5g/s, outlet at 2000Pa and operating pressure at 101325Pa.

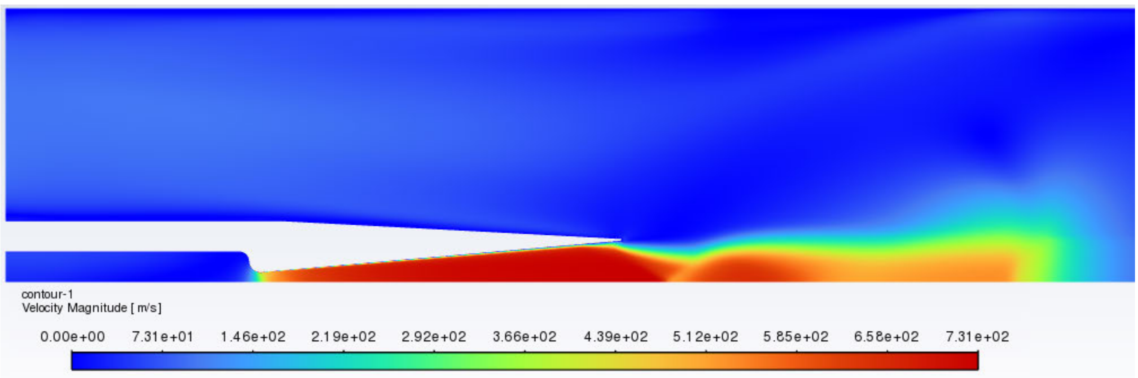

Figure 3.11: Velocity magnitude contour plot for simulations of the Change 7 fluent set-up with the primary inlet at 148500Pa, Secondary inlet at 2800Pa, outlet at 2000Pa and operating pressure at 0Pa.

Once the ejector was operating correctly using air for both the primary and secondary inlets, the fluid material was changed to water-vapour. The solver type, wall function, discretization and residuals were also modified (See change 29 in table 3.5) to improve the flow behaviour and increase calculation accuracy. The results in figures 3.12 and 3.13 show that the flow characteristics, operating condition, and mass flow rates are much more consistent with that specified by Al-Manea (2019).

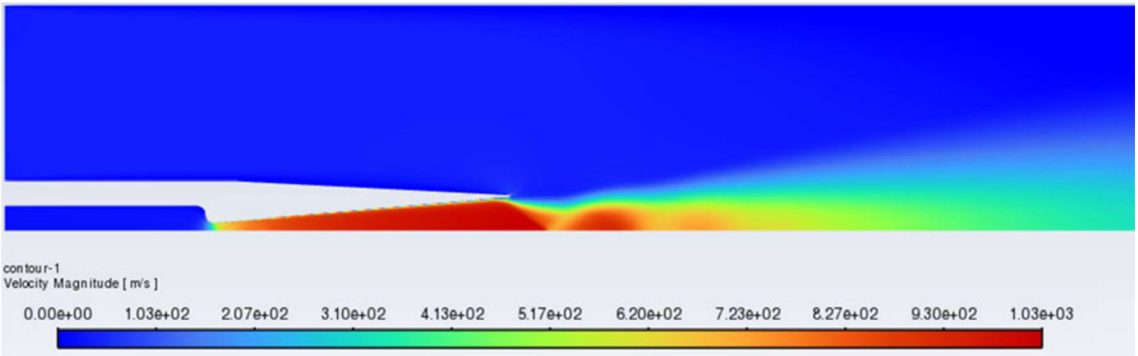

Figure 3.12: Velocity magnitude contour plot for simulations of the change 29 fluent set up with the primary inlet at 142500Pa, Secondary inlet at 3400Pa, outlet at 3500Pa and operating pressure at 0Pa.

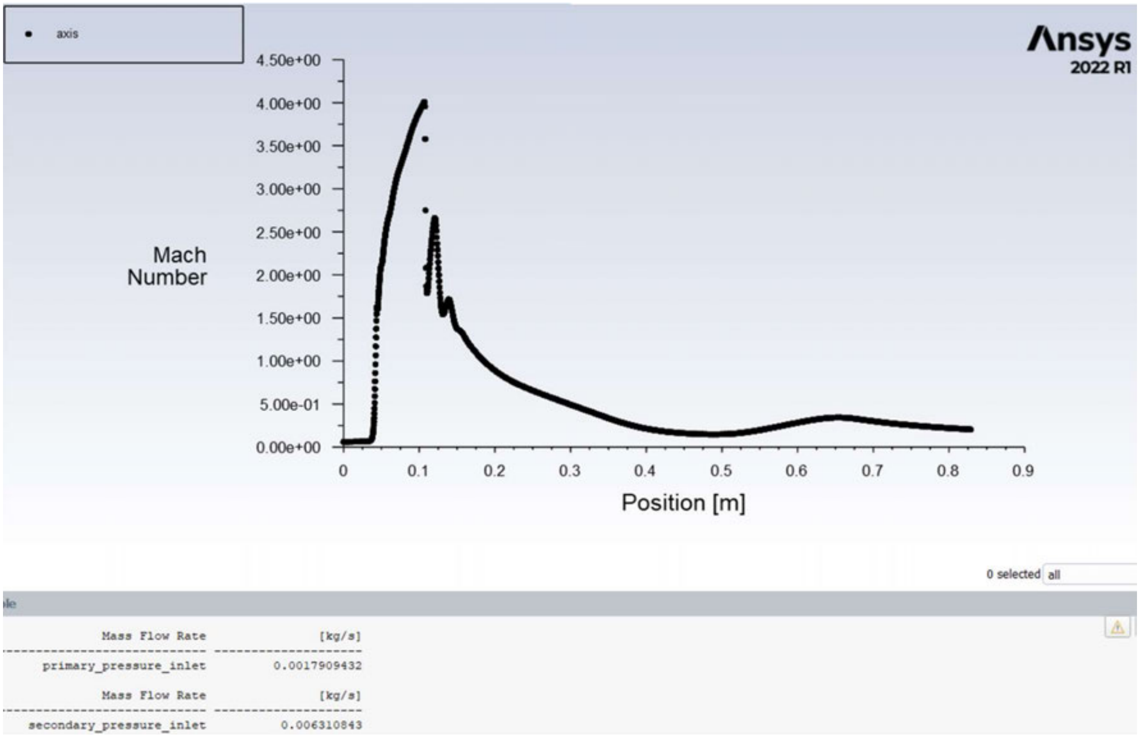

Figure 3.13: Mach plot and mass flow rate results for change 29 with the primary inlet at 142500Pa, Secondary inlet at 3400Pa, outlet at 3500Pa and operating pressure at 0Pa.

3.7 2D Final Fluent Setup

For this research, it is assumed that the flow inside the ejector is compressible, steady state conditions and governed by the energy and continuity equations. The reasoning behind the final set-up selection is discussed in this section, with the final fluent set-up summarised in table 3.6.

3.7.1 General Settings and Model Selection

The density-based solver was selected by Al-Manea (2019) and is recommended by ANSYS (2021*b*) for use with high velocity, compressible flows, particularly flows with a Mach number greater than 1.5. The pressure-based model is typically used for low velocity, incompressible flow, however, it can be used in place of the density-based model but can result in a lower accuracy solution (ANSYS 2021*b*). In this case, it was found that the pressure-based model had very little variation in results compared to the density solver and converged more quickly, thus, it was selected for the final model. With this type of solver, the coupled scheme is selected for pressure-velocity coupling which solves the governing equations simultaneously. Whilst this requires more memory usage, the convergence rate of the simulation is improved significantly. For the discretization, second order upwind is used to reduce numerical diffusion, except for the turbulent kinematic energy which follows the first order upwind scheme similar to Al-Manea (2019).

The flow through the steam ejector has a high velocity and Reynolds number and therefore requires the use of a turbulence model. Across the literature, variations of the k-ϵ and k-ω models are most commonly implemented to govern the turbulence characteristics of ejector flow. The realizable k-ϵ model is selected for this research as it is consistent with that used by Al-Manea (2019). This model is also deemed superior to other turbulence models for simulating swirling flows, or situations where the boundary layer endures recirculation, separation or significant adverse pressure gradients. When selecting the wall function to use with the realizable k-ϵ model, the wall y+ value for 2D ejector model must be considered for accurate results (see table 3.3). According to ANSYS (2021*b*), the wall y+ value must be within the range of $\sim 1 < y+ < 300$ to be considered acceptable for use with the enhanced wall treatment option for the k-ϵ model. This wall function was selected as it is specifically recommended by ANSYS (2021*b*) for use with the k-ϵ models. Finally, the energy equation was activated which is required for compressible flows and includes the conservation of mass, momentum and energy necessary for modelling the flow field inside the ejector.

3.7.2 Materials

For the final fluent setup, the primary and secondary inlets use water-vapour and nitrogen respectively, which is consistent with Al-Manea (2019). This is achieved by activating the species transport model and selecting inert gas as the working fluid. Water-vapour is then assigned to the primary inlet by changing the mole amount to '1' in the species tab of the boundary conditions. With the ejector operating under compressible flow, the density of the working fluid changes as a function of the velocity and temperature. Thus, the density is obtained by the ideal gas relationship, which is activated in the fluid properties for the inert gas. To ensure fluent uses the correct fluid, the surface body must be set to fluid and inert gas must be selected in the cell zone conditions. Since only the fluid domain of the ejector is modelled, solid materials are not required. As a default setting, ANSYS uses aluminium as the solid material for the model; this is removed by changing the wall thermal properties to the fluid used for this model.

3.7.3 Boundary Conditions

The boundary conditions for the primary and secondary inlets are set as pressure inlets and the outlet is set to a pressure outlet; this allows the pressure for these areas to be controlled and set as constants. With the operating pressure set as zero, the gauge pressure for each of the inlets and the outlet can be set as the absolute pressure. The supersonic, or initial gauge pressure, for the inlets is estimated to be very close to the actual gauge pressure, due to the flow at the inlet being subsonic and having a very low Mach number. The pressure values were adjusted to map the operating range of the ejector based on the values used by Al-Manea (2019); this is discussed further in the following section.

Table 3.6: Summary of the final fluent setup used for the 2D model.

Parameter	**Setting**
Solver Type	Pressure Based
2D Space	Axisymmetric
Time	Steady State
Energy Equation	Activated
Turbulence Model	Realizable k-ϵ
Wall Function	Advanced
Materials	Inert Gas (Ideal Gas)
Primary Inlet	Pressure Inlet
Secondary Inlet	Pressure Inlet
Outlet	Pressure Outlet
Discretization	2nd Order
Residuals	1e-6
Initialisation Method	Hybrid
Number of Iterations	2500

3.8 2D Simulations

In order to determine the operating range of the ejector, the primary inlet was set to 150kPa, while the secondary inlet pressure and condenser pressure were set to values within the range used by Al-Manea (2019). The final boundary conditions used for mapping the operating range of the ejector are summarised in table 3.7. The secondary inlet pressure and the condenser pressure were adjusted based on the observations:

a) Recirculation in the diffuser - condenser pressure too low.

b) Reversed flow in the secondary inlet - condenser pressure too high.

Table 3.7: Final boundary conditions selected to map the operating range of the 2D ejector model.

Boundary Condition	Primary Inlet	Secondary Inlet	Outlet
Gauge Pressure (Pa)	150000	2400	1500-2700
Initial Gauge Pressure (Pa)	149000	2300	-
Temperature (°C)	120	34	-
Operating Pressure (Pa)	0		

The operating range can be seen in figure 3.14 and was established for the ejector by determining the secondary mass flow rate over a range of different condenser pressures. The critical point can be identified at approximately 2.2kPa, where the mass flow rate of the secondary fluid begins to decay with further increases of the condenser pressure. The break down point was identified at approximately 2.65kPa where the further condenser pressure increases would result in reversed flow in the secondary inlet and failure of the system.

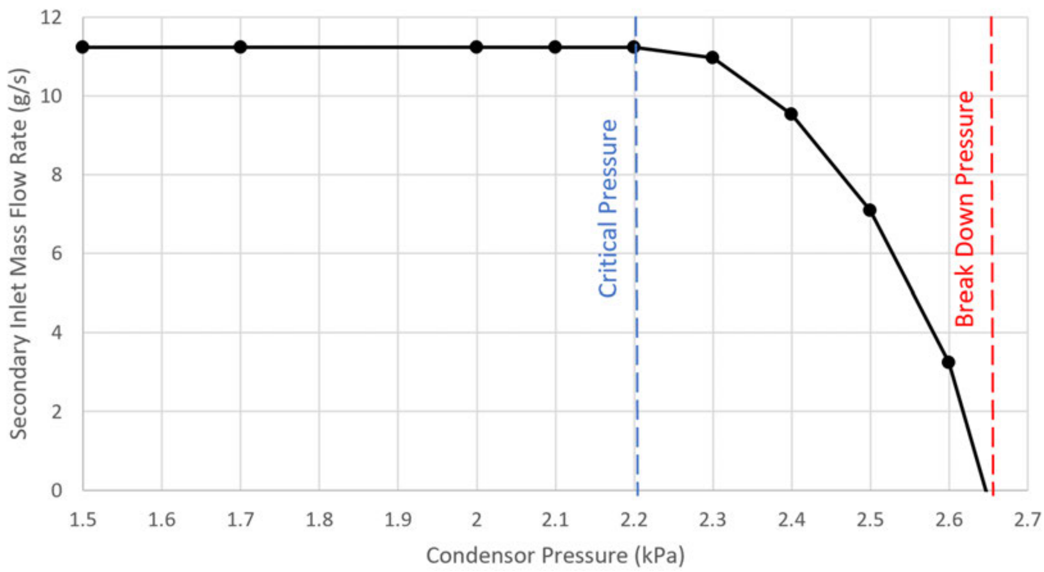

Figure 3.14: Effect of condenser pressure on the secondary inlet mass flow rate with the critical and break down pressures indicated by dashed lines.

When the ejector was operating in the chocked condition the mass flow rate of the secondary flow was approximately 11.2 g/s; this is the point in the operating range of which the ejector is performing at its most efficient. When the ejector is operating in the unchoked condition, the fluid is subsonic in the diffuser and the entrained flow is reduced; this can be observed in figures 3.15 and 3.16. The reverse flow condition occurs when the ejector is operating above the break down pressure and is failing. The difference in behaviour of the choked, unchoked and reversed flow operating conditions can be seen clearly in figures 3.15 and 3.16.

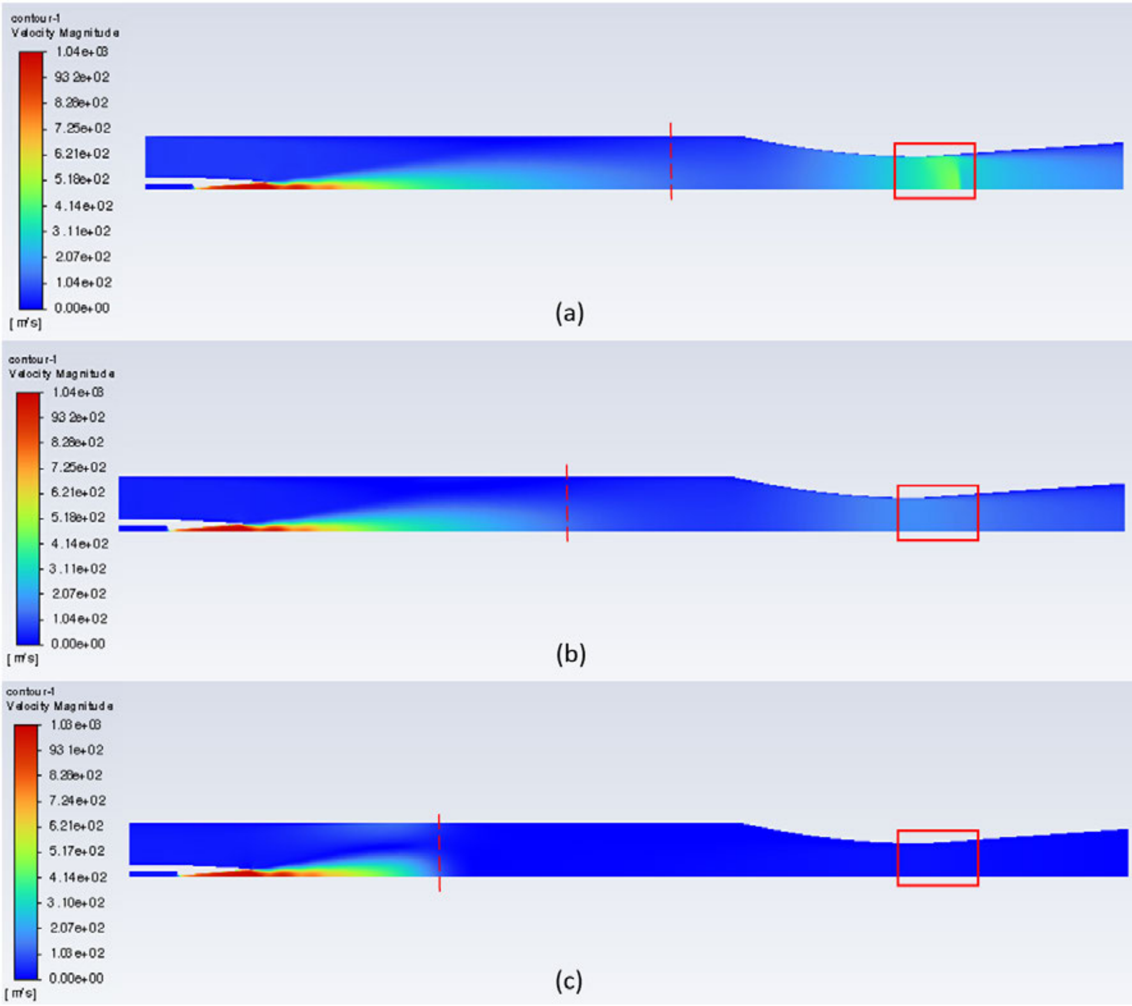

Figure 3.15: Comparision of the ejector operating in (a) choked at 2.1kPa, (b) Unchoked at 2.5kPa, and (c) Reverse flow conditions 2.7kPa.

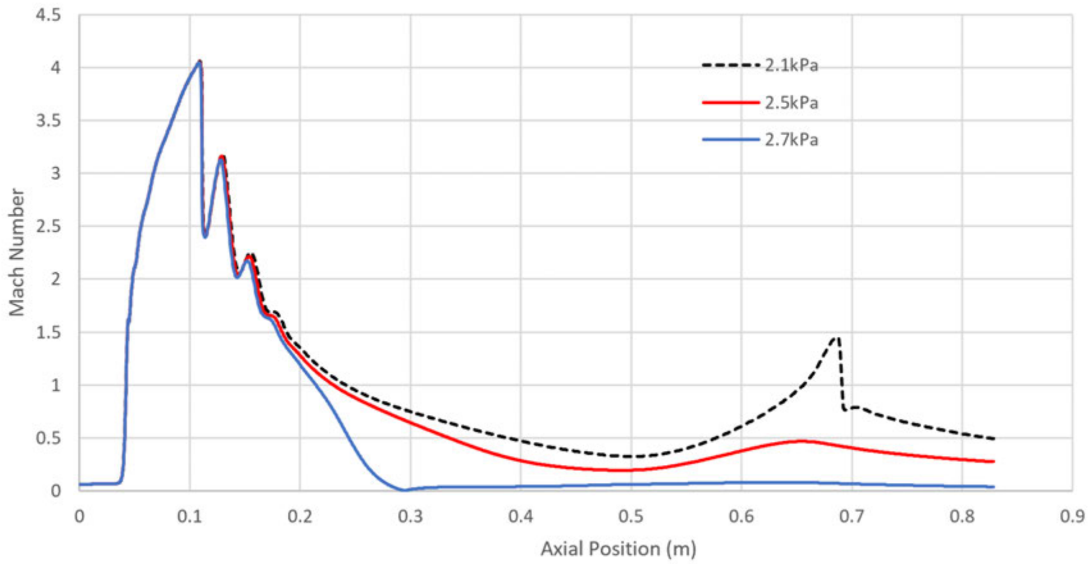

Figure 3.16: Comparison of the Mach numbers for the ejector operating in choked, unchoked and reverse flow conditions.

3.9 2D Model Validation

In order to validate the model, the simulations were completed using the same boundary conditions as used by Al-Manea (2019) for the ideal gas model. The primary inlet pressure was set to 150kPa, secondary inlet pressure to 3.4kPa and the condenser ranging between 2-4kPa. The results provided by Al-Manea (2019) showed that for boundary conditions in this range, the primary mass flow rate would be 1.8g/s and the secondary mass flow rate would be within the range of 5.5-6.5g/s. Figure 3.17 shows the that at a condenser pressure of 3.55kPa the secondary mass flow rate was within the specified range and the primary mass flow rate was within 5% of Al-Manea (2019).

Comparing the Mach number in the diffuser throat in figure 3.17 and 3.18, it is clear that the ejector is operating in the unchoked region at 3.55kPa which consistent with Al-Manea (2019). The higher magnitude of Mach number recorded for this research using the ideal gas model compared to the wet-steam model used by Al-Manea (2019) is expected and is reported across the literature. In the wet-steam model, the fluid mixture increases in humidity and temperature as a result of the condensation effect which causes a lower Mach number (Han et al. 2020) (Poorasadion, Alishiri & Saadatmand 2013).

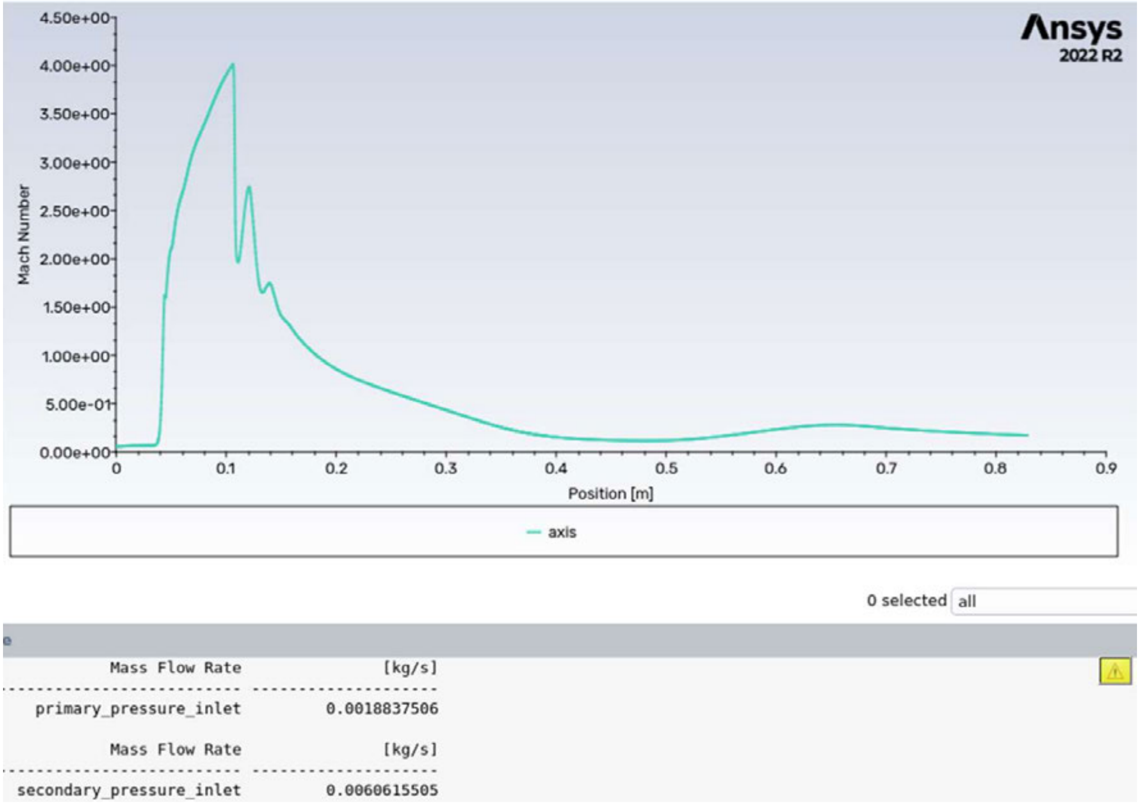

Figure 3.17: Mach number over the ejectors axial length and mass flow rate results for the simulations with the primary inlet pressure set to 150kPa, the secondary inlet pressure set to 3.4kPa and the condenser pressure set to 3.55kPa.

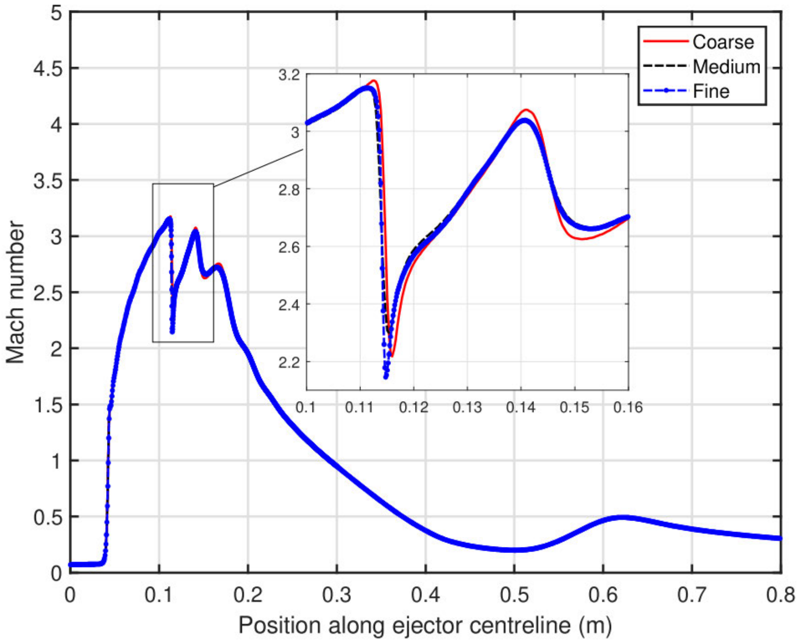

Figure 3.18: Mach number across the ejector centreline for wet steam simulations (Al-Manea 2019).

The general behaviour of the ejector aligns with typical ejector flow observed in the literature and is also similar to that of Al-Manea (2019). The shock train proceeding the nozzle exit for this research and Al-Manea (2019) can be observed in figures 3.19 and 3.20. The similarity in the velocity of the fluid mixture at the condenser pressure of 2.5kPa in unchoked conditions can also be noticed.

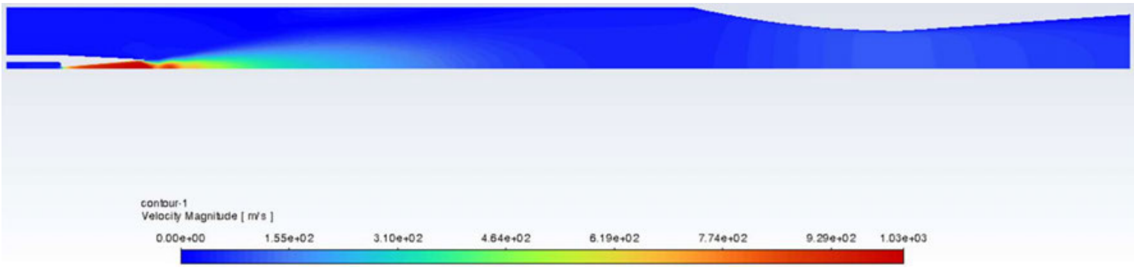

Figure 3.19: Ejector flow behaviour for operating conditions with the condenser pressure at 2.5kPa.

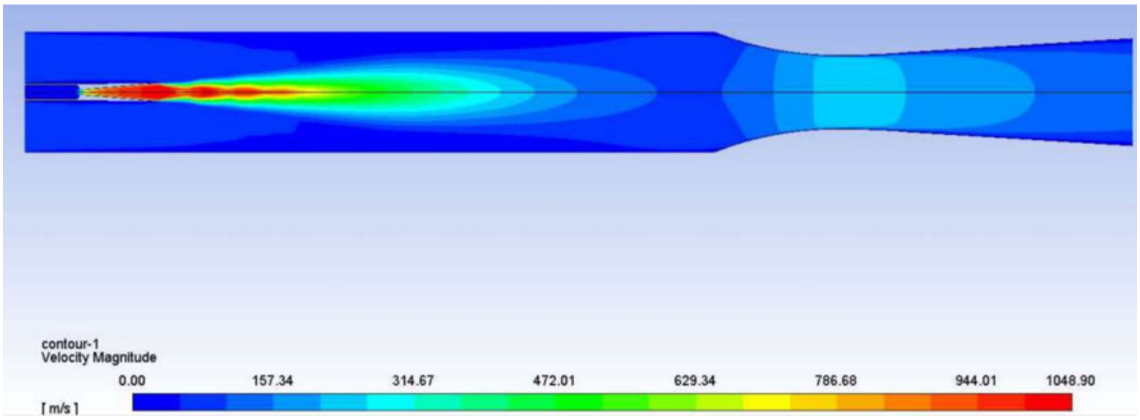

Figure 3.20: Ejector flow behaviour for operating conditions with the condenser pressure at 2.5kPa (Al-Manea 2019).

The objective of the ideal gas model used by Al-Manea (2019) was to design a new ejector geometry to reduce the recirculation that occurs in the mixing chamber as a result of the primary nozzle flow. Observing figure 3.22, it can be seen that the recirculation region achieved in the design for Al-Manea (2019) (see figure 3.21) is also present for condenser pressures over 3000Pa. Both ejectors pictured in figures 3.21 and 3.22 are operating in unchoked conditions.

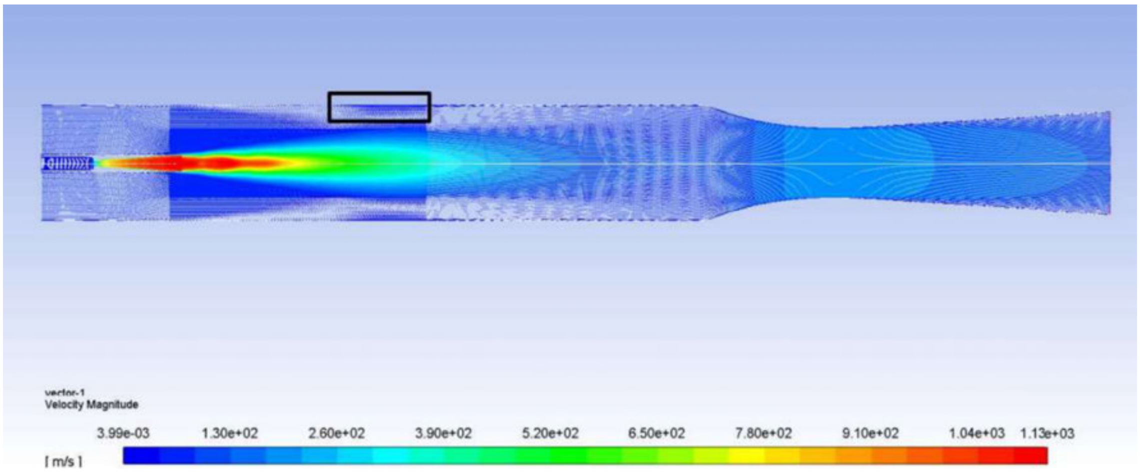

Figure 3.21: New ejector geometry showing recirculation occurring in the mixing chamber with a condenser pressure at 3kPa (Al-Manea 2019).

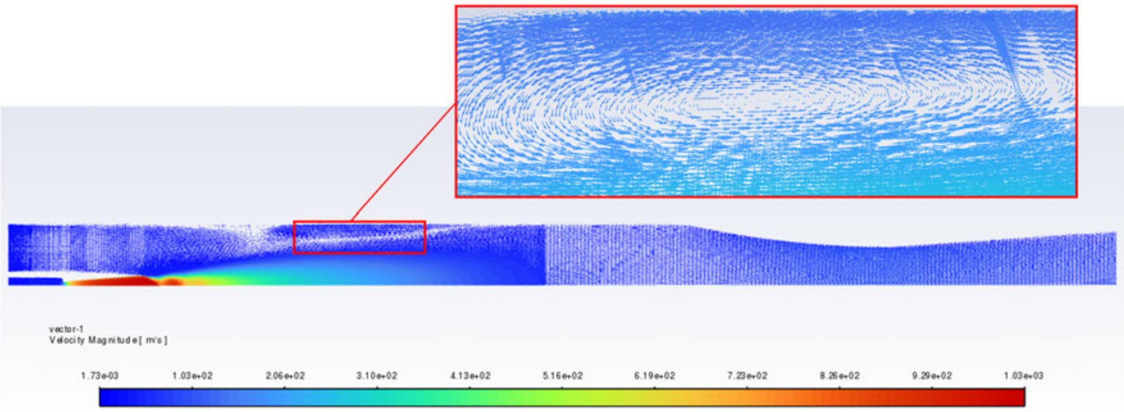

Figure 3.22: Recirculation observed in mixing chamber for simulation results with a condenser pressure of 3.55kPa.

In conclusion, the model is in reasonable agreement with Al-Manea (2019), displaying similar flow behaviours such as recirculation and oblique shock waves across the ejectors whole operating range. The variation that is observed in the operating range of the ejector can be attributed to differences in the meshing and Fluent setups used, and not related to the accuracy of the ejector geometry. With the ejector model functioning in accordance with typical ejector operation outlined in the literature review, the 2D model geometry and the Fluent setup can be considered reliable for further application in this project.

3.10 3D Ejector Model

The vortex generator that is being integrated into the primary nozzle is a 3D feature and, therefore, cannot be represented in a 2D model. The literature review revealed that using a 3D model has the advantage of providing higher accuracy results across all operating conditions for steam ejector. This does, however, come at the cost of a significant increase in computational effort and memory requirements that come with meshing and simulating the 3D models. These disadvantages are often compensated for by applying symmetry lines to make a half or quarter 3D model, which reduces the number of cells that the computer must process to obtain the results. Unfortunately, this method is not possible in this circumstance due to the modified primary nozzle being asymmetric; a full model must be used to analyse influence of the vortex generator on the flow through ejector. With the geometry of the ejector verified by the 2D ejector study, the 3D ejector model can be generated with confidence that an accurate reflection of the real system is being achieved.

It was found that while developing the standard ejector model using was a simple process, incorporating the complex helical feature for the vortex generator in the primary nozzle was very difficult. Using a more familiar and user-friendly modelling software rather than ANSYS design modeller decreased the time spent creating the models significantly. Creo-Parametric is a common substitute for ANSYS Design Modeller amongst the literature and has a reliable interface with ANSYS Workbench. To reduce the possibility of inconsistencies, both the standard and modified 3D models were generated using Creo-Parametric version 8.0.

3.11 3D Geometry

The strategy used for creating the 3D model is to break the ejector down into parts and create an assembly file to compile all of the individual parts in Creo-Parametric; this is presented in figure 3.23. This method is necessary to optimise the mesh refinement in the model to better capture the flow behaviour through the mixing chamber section, particularly where the shock waves were identified in the 2D simulations (see figure 3.19). Each part of the model was first created as a 2D sketch, following the dimensions provided in tables 3.1 and 3.2. The sketch for each part was then revolved around the axis of symmetry to generate the 3D component. Once the ejector assembly was created, it was then imported into ANSYS Design Modeller as shown in figure 3.24.

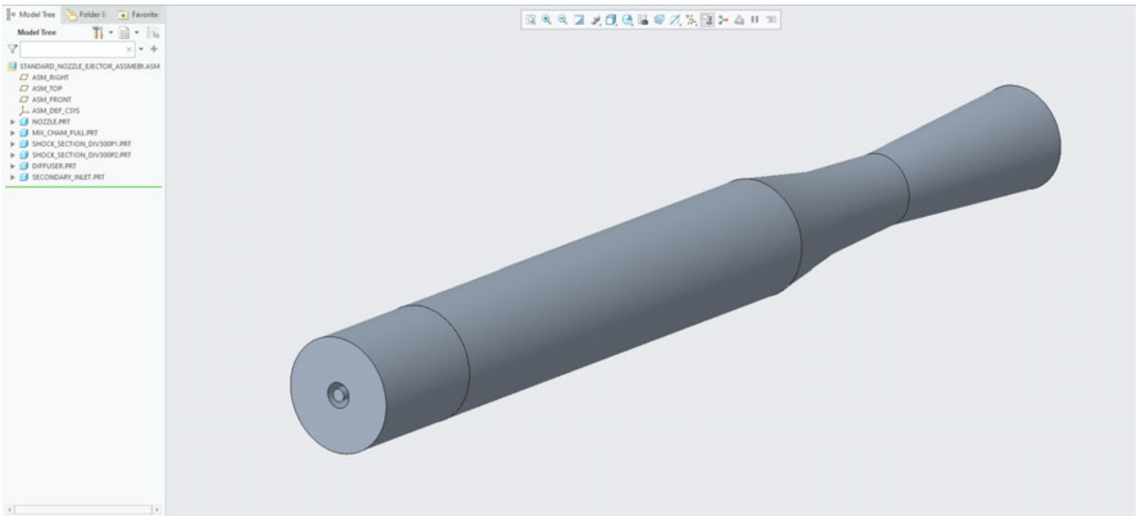

Figure 3.23: Creo-parametric assembly of final 3D model arrangement.

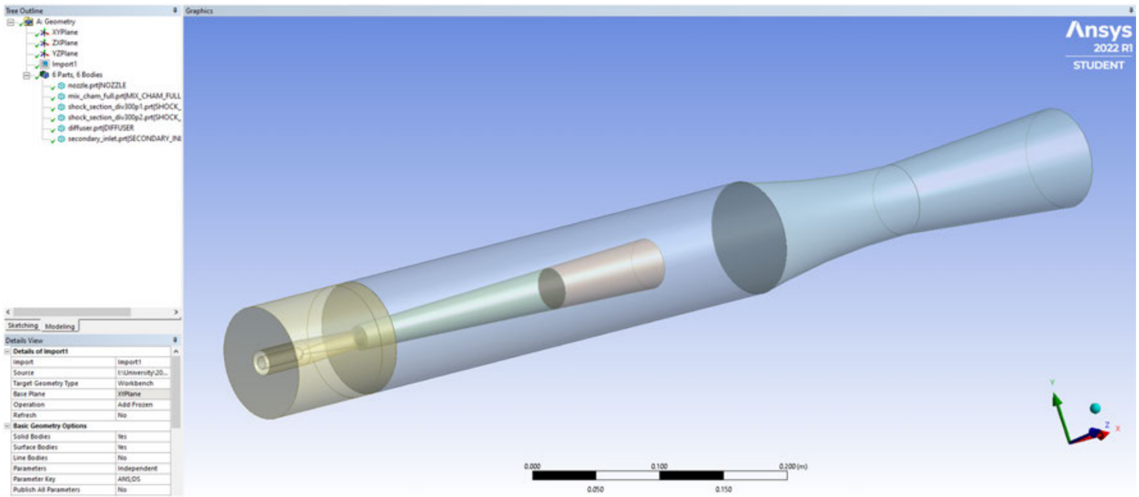

Figure 3.24: 3D model of the third mixing chamber variation transferred to ANSYS design modeller.

Three different ejector models were initially created, each of them using different method to model the section of the mixing chamber experiencing supersonic flow. The subsequent meshing process was a key consideration for the mixing chamber designs, acknowledging the importance of minimising the element count, maintaining a high-quality mesh, and producing results with a clear resolution. The first version involved a 30mm diameter cylinder of length 300mm that would be used for capturing the supersonic flow out of the primary nozzle. It was discovered after initial fluent simulations that the cylinder was too narrow to model the shear layer and had unacceptable level of clarity (see figure 3.25), thus it was removed from consideration for the remainder of the study.

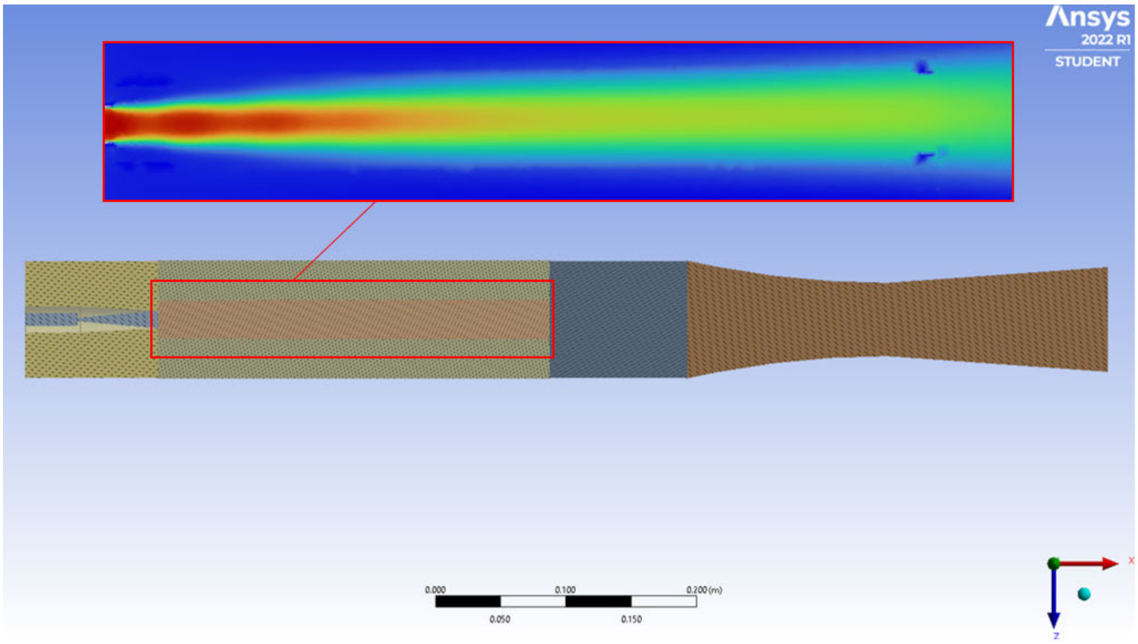

Figure 3.25: Segments of the first variation mixing chamber ejector assembly: Grey – Primary Nozzle; Yellow – Secondary Inlet; Orange – Cylinder; Dark Yellow/Dark Grey – Mixing Chamber; Brown – Diffuser.

To rectify the problems observed in the first model, the second variation of the mixing chamber used a 40mm to 60mm expanding section to model the supersonic region in the mixing chamber (see figure 3.26). This resulted in much clearer visualisation of the fluid behaviour; however, this design would significantly increase the element count. The third design incorporated two solid bodies in the mixing chamber: a 30mm to 40mm expanding body divided into a 200mm and 100mm long segments (See Figure 3.27). This design will use a more advanced meshing method allowing a reduced mesh count and maintaining a high-quality resolution. Both the second and third models will be explored in the following mesh independence study to determine the optimal mixing chamber variation.

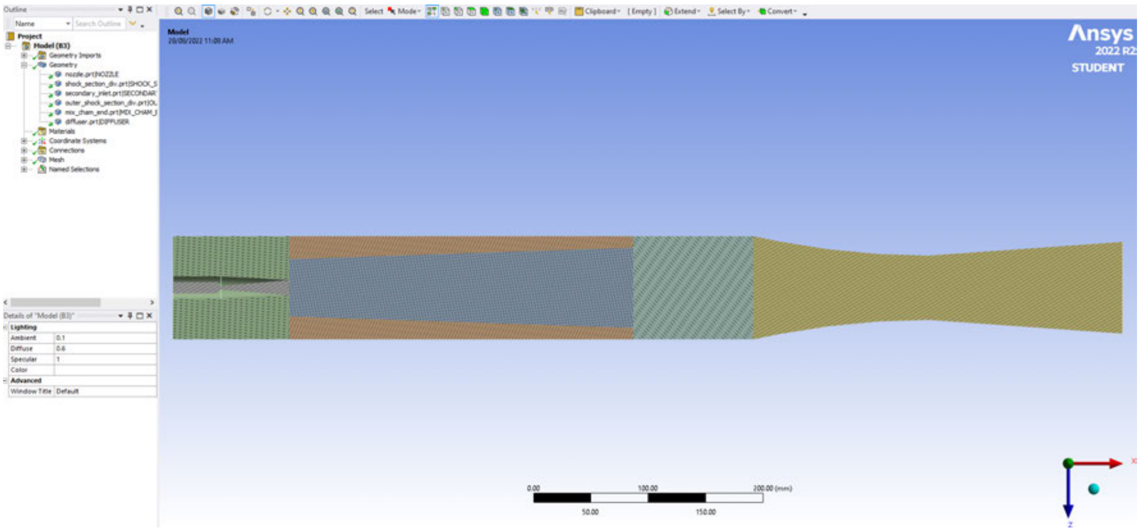

Figure 3.26: Segments of the second variation mixing chamber ejector assembly: Grey – Primary Nozzle; Green – Secondary Inlet; Blue – Expanding Section; Orange/Dark Green – Mixing Chamber; Yellow – Diffuser.

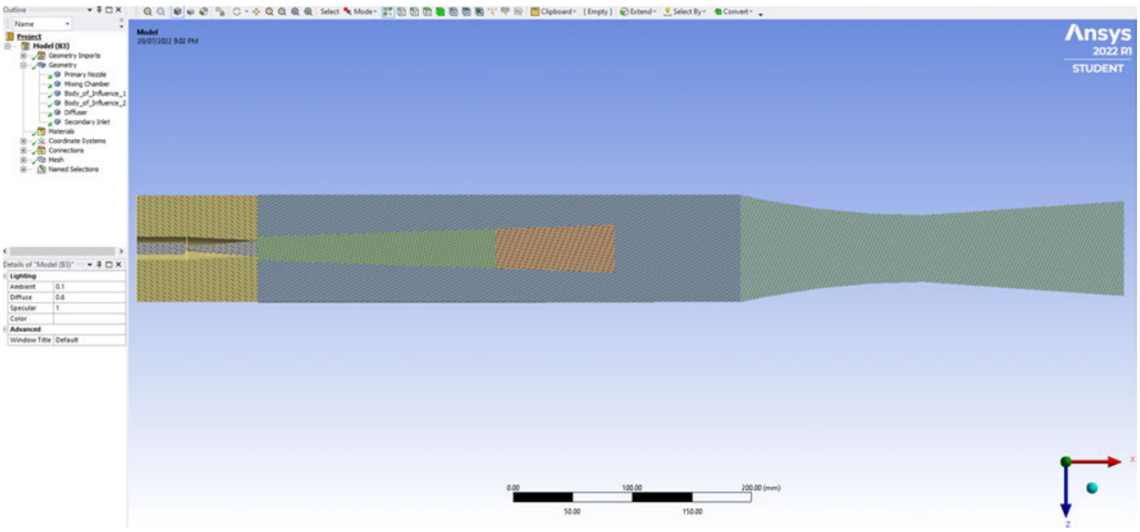

Figure 3.27: Segments of the third variation mixing chamber ejector assembly: Grey – Primary Nozzle; Yellow – Secondary Inlet; Green – Body of Influence 1; Orange – Body of Influence 2; Blue – Mixing Chamber; Dark Green – Diffuser.

3.12 3D Initial Mesh

Once the model variations are assembled and imported to ANSYS workbench, the meshing process could be commenced. The default mesh generated by ANSYS, as shown in figure 3.28, uses hexahedral elements to cover the fluid domain. Whilst a hexahedron mesh can offer an improved resolution for visualisation purposes, it is often not ideal for models containing significant small radius curvature. As a result, default mesh is a very low-quality representation of the fluid domain and must be modified using the default mesh settings within ANSYS to create an acceptable initial mesh that can be used as the foundation for applying advanced mesh settings in the independence study.

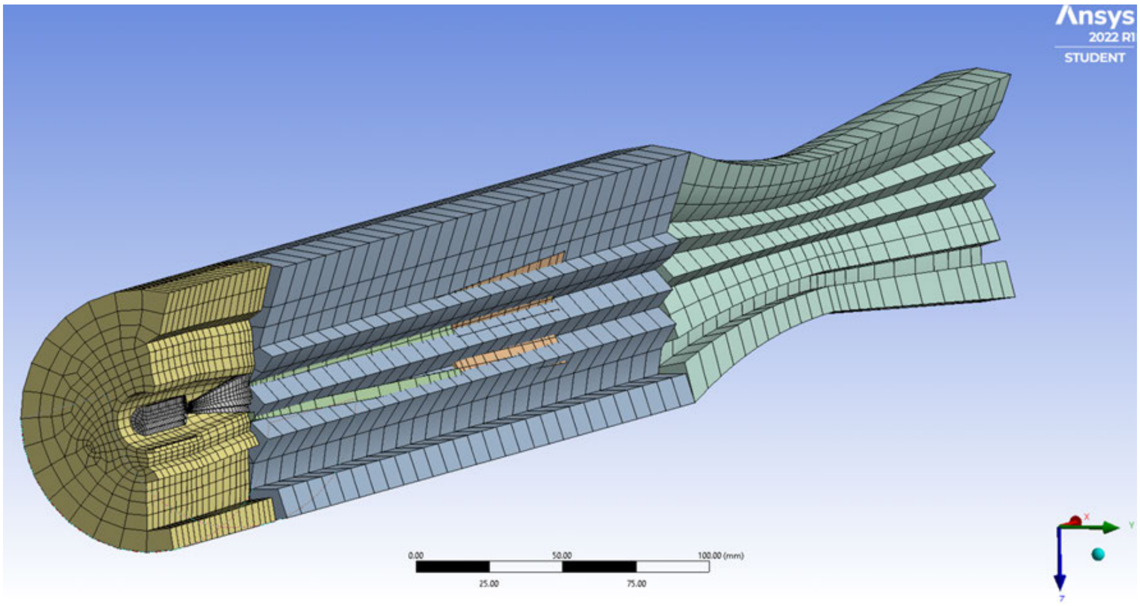

Figure 3.28: Third variation 3D ejector model equipped with the default mesh.

In the case of the 3D models, the default mesh settings do not require significant adjustment since the mesh for each of the parts in the ejector assembly is modified independently with the advanced meshing procedures. A patch conforming method is applied to the ejector assembly which allows a tetrahedral mesh to be selected; this provides a higher quality mesh distribution (see figure 3.29) and more accurately represents the complex curvature in the model. The global element size was reduced to 4mm, and the high smoothing setting was selected which further improved the mesh quality, with the skewness and aspect ratio for the initial mesh displayed in figure 3.29 being 0.79 and 9.9, respectively. The initial mesh outlined in this section is applied to both the second and third variations of the ejector for the ensuing mesh independence studies.

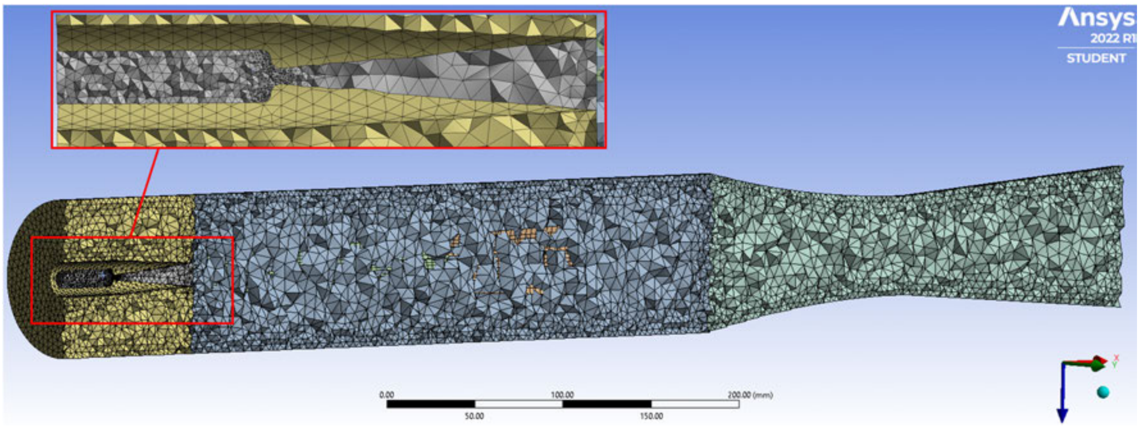

Figure 3.29: Third variation 3D ejector model equipped with the initial mesh created using basic mesh settings.

3.13 3D Mesh Independence

With the initial mesh constructed for the 3D ejector models, an independence study must be performed. A similar strategy as outlined in the 2D independence study is also applied for the 3D models, beginning with developing a more appropriate mesh to the fluid domain. When creating the mesh not only is the accuracy of results important but the computational efficiency of the model when running simulations. Having access to the university's HPC means that this is less of a concern and more priority can be made to maximising accuracy; more detail on the use of the HPC for this research is provided at the end of this chapter.

3.13.1 Details of Mesh Refinement

The number of elements for each of the second and third variation models were adjusted primarily through the global mesh controls and within the body sizing and face sizing settings for areas where significant refinement is required. With the ejector models being imported to ANSYS as an assembly, contact sizing was applied between each section of the ejector which created a more blended transition between different element sizes and increased the resolution quality. Inflation was applied the for the walls of the ejector to model boundary layer development, which involves setting values for the transition ratio, growth rate and number of layers. The transition ratio is the volume ratio between the first element layer and the last element layer and was set at 0.77. The growth rate controls the increase in element size with each layer of elements and was set to 1.1. The number of inflation layers chosen for the mesh was 7, which was found to provide y+ values within the range required for the wall function options of the k-ϵ turbulence model.

3.13.2 Mixing Chamber Variation 2

In order to identify the most suitable mesh, simulations must be performed comparing the different mesh resolutions at a constant set of boundary conditions. The boundary conditions selected for the simulations were the same as those used for the 2D mesh independence study (shown in Change 29 table 3.5) so the results can be validated. With the HPC in use, simulations were not restricted by processing speed, and could be run until the residuals stabilised or converged. The mass flow imbalance between the inlets and outlet of the ejectors should be equal to zero to ensure the model follows the conservation of mass law. It was observed in the study that decreasing the mesh size reduced the mass flow imbalance, with values around $1e^{-6}$ recorded for the fine meshes.

The skewness and aspect ratio for the different mesh resolutions were recorded in table 3.8; this was done to monitor the quality of the mesh. It can be interpreted that as the element size is reduced, the maximum skewness observed in the model increases. This likely occurs as the disparity between element sizes increases as the mesh gets finer, so the skewness values of the cells increase at the interfaces of the ejector sections.

Table 3.8: Mesh statistics for the second mixing chamber variation independence study.

Resolution	**Global Size**	**Skewness Max**	**Skewness Avg**	**Element Count**
Coarse	8	0.81881	0.20867	1.25×10^6
Medium	6	0.81996	0.19406	2.5×10^6
Fine	4	0.87393	0.18974	5×10^6

The simulation results for each of the resolutions were compared to determine to margin of error between them; the comparison of the Mach number profile over the centreline of the ejector is derived from ANSYS and plotted in figure 3.30. For second mixing chamber arrangement (see figure 3.26), the maximum difference between the values for the medium and fine meshes was exceeding 10%. It was identified in the results that areas within the ejector experiencing significant pressure or velocity changes were more sensitive to the mesh resolution. Figure 3.30 shows that the section from 0.1 to 0.3 metres exhibits the most error, and further refinement is required.

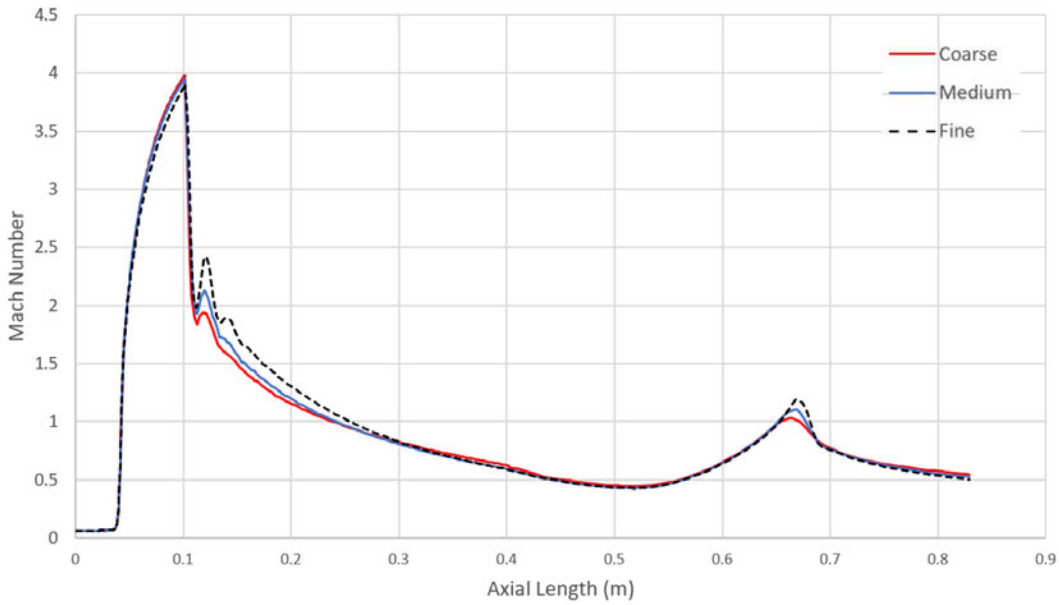

Figure 3.30: Mach Number over ejector centreline for second mixing chamber variation.

Initially, the element size for the shock section included in the geometry was reduced incrementally until the error margin was reduced to within 5%. However, due to the large size of this shock section, this resulted in the coarse mesh increasing to over 6 million elements which more than doubled the runtime required to complete the simulations. Additionally, the disparity between mesh sizes for the shock section and the mixing chamber required a more advanced growth rate control that could not be achieved using contact sizing; this resulted in a higher skewness value of over 0.9 for the coarse mesh. The second mixing chamber design and the mesh can be observed in figure 3.31.

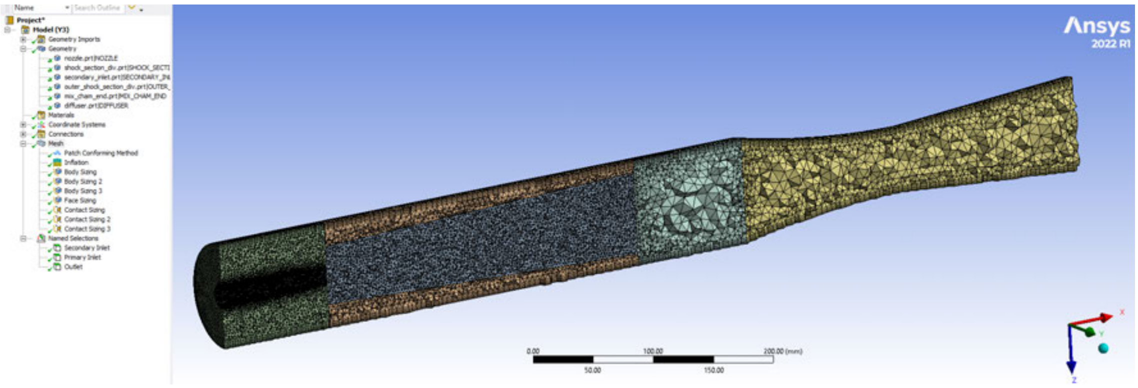

Figure 3.31: Mesh used for the second mixing chamber variation independence study.

3.13.3 Mixing Chamber Variation 3

To rectify the issues observed the second mesh, a reconstructed mixing chamber arrangement was produced, incorporating two bodies of influence in the mixing chamber (see figure 3.27). Rather than acting as a separate section of the ejector, the bodies are able to be used to focus mesh refinements to the key areas of the mixing chamber section. Using the body of influence mesh setting also allowed for targeted control of the growth rate between the smaller elements and the larger elements within the mixing chamber. The growth rate for both bodies of influence was set to 0.8, which resulted in a better mesh resolution and improved skewness values. The reviewed mixing chamber design and the mesh can be observed in figure 3.32.

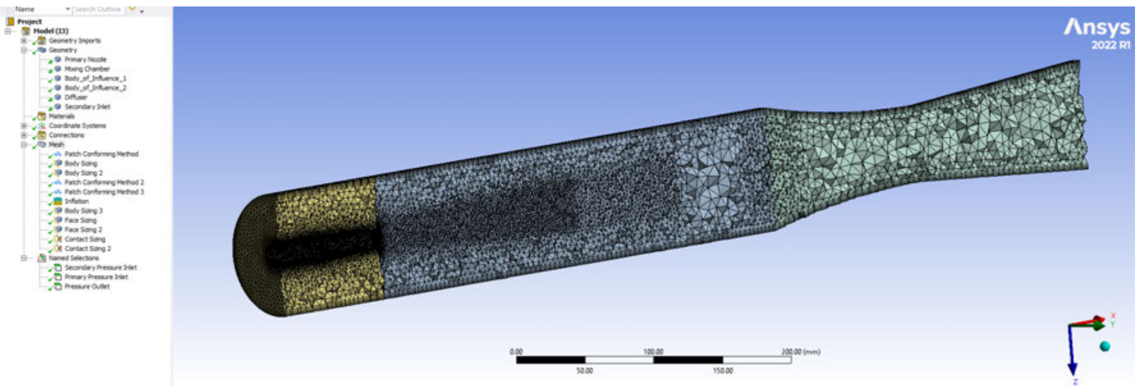

Figure 3.32: Mesh used for the third mixing chamber variation independence study.

A mesh independence study was performed on the new mixing chamber arrangement, this followed the same procedure as outlined for the previous model. The mesh statistics for this independence study are shown in table 3.9 and the Mach number over the centreline of the ejector for the different mesh resolutions is extracted from ANSYS Fluent and is shown in figure 3.33. The medium and fine meshes were found to have error values typically lower than 1%. The coarse mesh was also within the acceptable range of error with values around 3% variation from the medium mesh.

Table 3.9: Mesh statistics for the third mixing chamber variation independence study.

Resolution	Global Size	Y+	Skewness Max	Skewness Avg	Element Count
Coarse	5	2.682	0.79514	0.10852	3×10^6
Medium	4	1.3308	0.79613	0.20446	5.5×10^6
Fine	3	1.064	0.79928	0.20062	11×10^6

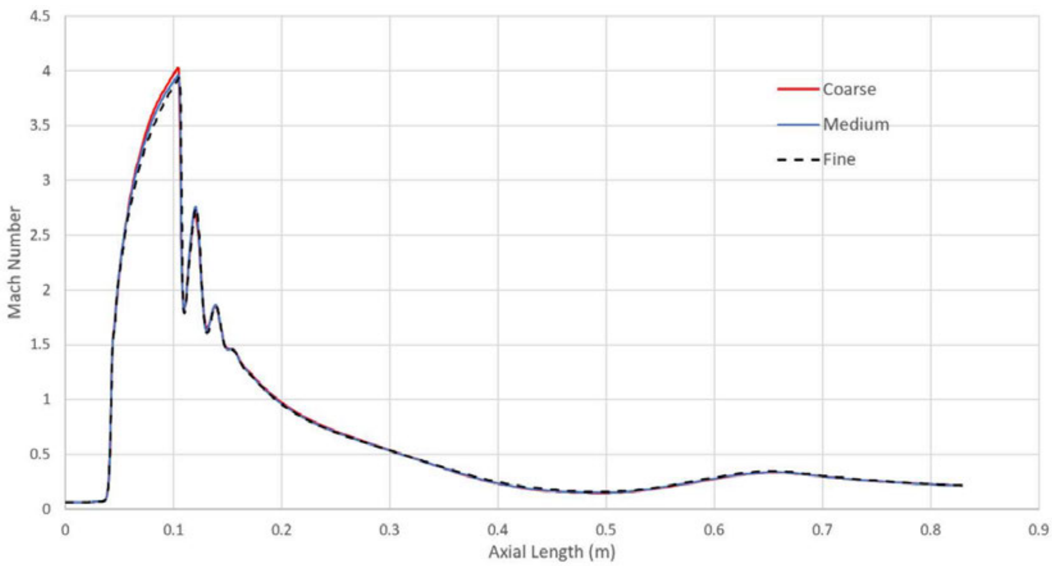

Figure 3.33: Mach number over the ejector centreline for the third mixing chamber variation mesh independence study.

Whilst the ejector shows an acceptable margin of error for the velocity and Mach number, it was found that the independence of the primary nozzle mesh is best determined by observing the total pressure over the centreline of the ejector. From figure 3.34, it is clear that the variation between the pressure through the divergent section of the primary nozzle exceeds 10% in some locations. To combat this, a separate independence study was performed on the primary nozzle component.

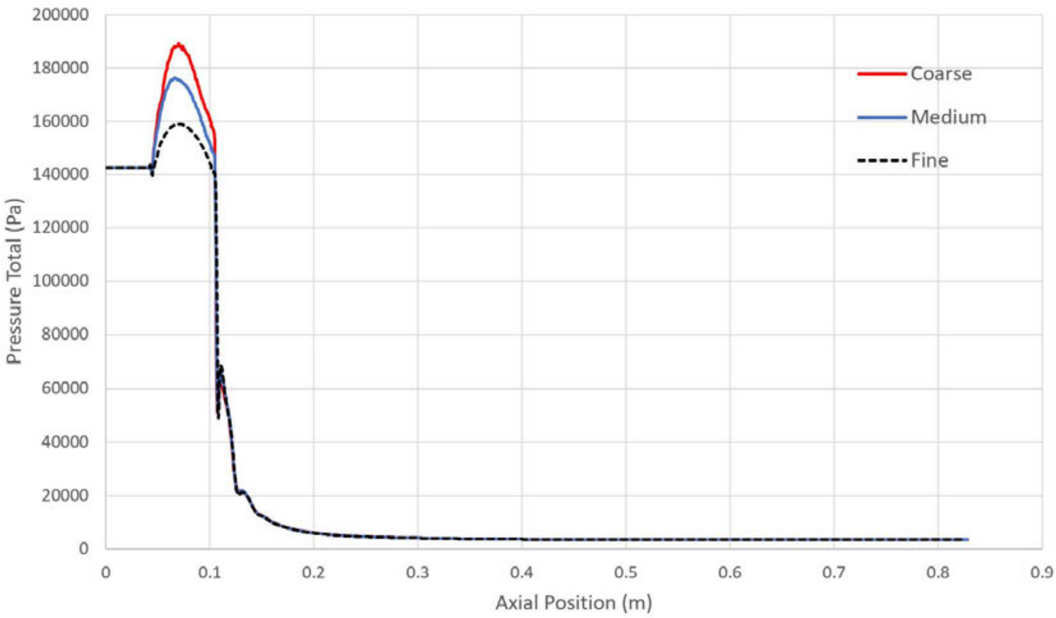

Figure 3.34: Total pressure variation over the centreline of the ejector for the third variation independence study.

The boundary conditions used for the simulations of the primary nozzle remained the same, with the nozzle outlet set to the values of the diffuser outlet for simplicity. The element size in the throat and the diverging section of the nozzle is controlled using the sphere of influence (SOI) mesh setting. This requires a new co-ordinate system to be created at halfway into the divergent area; the radius of the sphere is set to a constant value of 33mm. Table 3.10 lists the resolutions used in the simulations with the results for the total pressure over the axial length of the ejector depicted in figure 3.35.

Table 3.10: Mesh statistics for the standard primary nozzle independence study.

Resolution	Global Size	SOI Element Size	Element Count
Coarse	1	0.5	262000
Medium	0.7	0.4	531000
Fine	0.5	0.3	$1.26{\times}10^6$
Extra Fine	0.4	0.25	$2.17{\times}10^6$

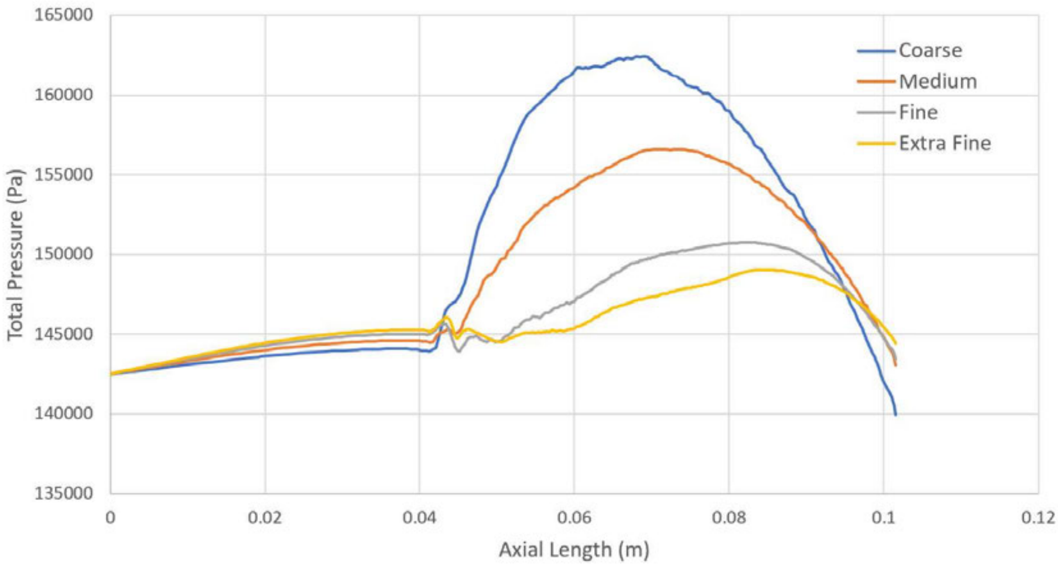

Figure 3.35: Pressure variation between meshes for the standard nozzle.

The simulation results determined that the coarse and medium meshes had less than 5% error. The fine and extra fine meshes were typically within 2% variation (see figure 3.35). It was decided that the fine mesh would be selected for use in the model despite the higher element count. This decision was made due to inflation causing blending problems at the interface between the secondary inlet, nozzle, and the mixing chamber. It was also found that inflation would cause mesh failure for the modified models, therefore, it could not be applied to the nozzle walls. Using the fine mesh was found to provide enough cells within the boundary layer to deliver an acceptable representation. The final mesh utilising tetrahedral elements is shown in figure 3.36, highlighting the mesh structure in the primary nozzle.

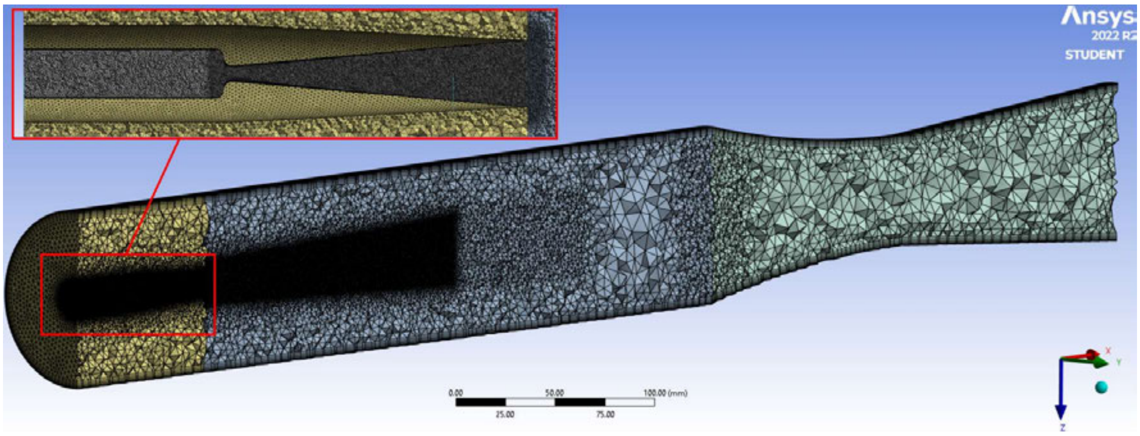

Figure 3.36: 3D ejector model with final tetrahedral mesh refinements with an enhanced view of the primary nozzle mesh.

The final modification made to the mesh was activating the polyhedral mesh setting; this option is automatically generated within the ANSYS Fluent program. The key advantage of polyhedral elements is reducing the number of elements required in the model which decreases the computational effort required to run the simulations. This is because they are obtained directly from the tetrahedral elements by producing polygons around the individual nodes within the tetrahedral mesh. The increased number of nodes in the polyhedral mesh means that more information can be extracted for each cell in the simulations, thus, improving the accuracy of results. Throughout the meshing process it was also found that simulations using the polyhedral mesh would require far fewer iterations to reach convergence compared to the tetrahedral mesh. The polyhedral mesh is depicted in figure 3.37 consisting of approximately 9.8×10^5 elements, significantly less than the 6.2×10^6 elements of the final tetrahedral mesh.

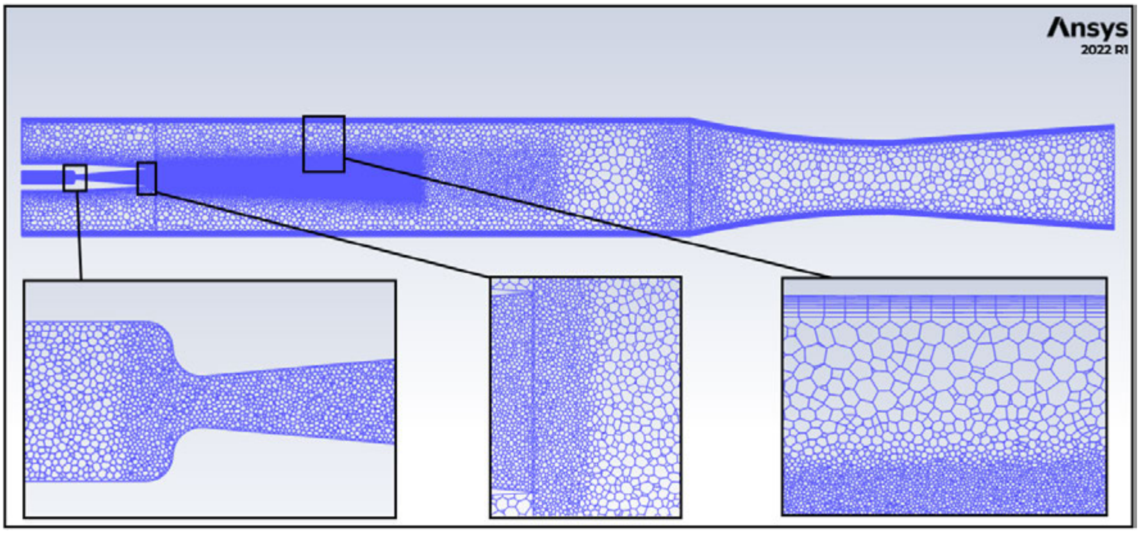

Figure 3.37: 3D ejector model with final Polyhedral mesh.

3.13.4 Turbulence Model Selection

With the mesh independence study completed and the optimal mesh selected, the appropriate turbulence model must be determined. To achieve this, the simulation results from the 2D model and a variety of 3D models utilising different turbulence model options are analysed. The model that most closely aligns with the 2D results is accepted as the most accurate option. The literature review revealed that the k-ϵ and k-ω turbulence models are most suitable for calculating the fluid properties of jet ejector flow. For this reason, all the options available in Fluent for the k-ϵ and k-ω models were selected for comparison alongside the transition SST turbulence model.

The results displayed in figure 3.38 show the variation between the six turbulence models and the 2D simulation results at the same operating conditions (see Change 29 table 3.5). It is clear that the k-ϵ models offer the greatest uniformity, however, the Realizable k-ϵ option is in the closest agreement with the 2D simulation results. This is expected as the k-ϵ realizable turbulence model was also used in that study. According to the literature, differences between 2D and 3D results are common, particularly when the ejector is operating in unchoked conditions (Wang et al. 2019). For turbulence modelling in swirling flows, the RNG k-ϵ, RSM, and the Realizable k-ϵ models are recommended by (ANSYS 2021*a*). With the vortex generators expected to increase the swirling flow in the ejector, the Realizable k-ϵ model is selected as the appropriate turbulence model for this research project.

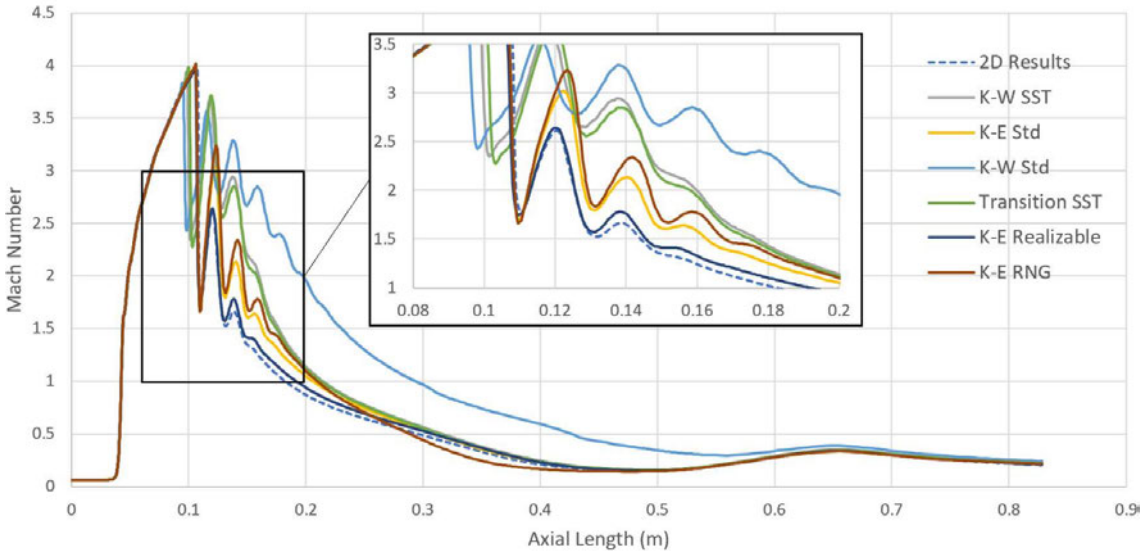

Figure 3.38: Mach number over the axial length of the ejector for varying turbulence models.

3.13.5 3D Fluent Model Setup

Since the 2D and 3D simulations are shown to be producing similar results, the final fluent setup used for the 2D model (see table 3.6) can be adapted for the 3D model. The key parameters governing the fluent simulation are listed in table 3.11; notice that the 3D space is now used with a full model in place of the axisymmetric model from the 2D set up. (ANSYS 2021*b*) cautions that the 3D model is more vulnerable to inaccuracies when using the first order upwind scheme, so all discretization is adjusted to second order for the 3D simulations. The boundary conditions used for the 3D model also remain the same as used in the 2D model. It was found that the number of iterations required for the system to converge or for the residuals to flatten out with no change was consistently within 3000 iterations across the ejectors entire operating range. Thus, the final parameter introduced to the 3D model set up is the number of iterations which is listed as 3000.

Table 3.11: Final fluent settings used for the study.

Parameter	Setting
Solver Type	Pressure Based
3D Space	Full Model
Time	Steady State
Energy Equation	Activated
Turbulence Model	Realizable k-ϵ
Wall Function	Advanced
Materials	Inert Gas (Ideal Gas)
Primary Inlet	Pressure Inlet
Secondary Inlet	Pressure Inlet
Outlet	Pressure Outlet
Discretization	2nd Order
Residuals	1e-6
Initialisation Method	Hybrid
Iterations	3000

3.13.6 3D Simulations

The boundary conditions used for the 3D simulations will be the same as the 2D simulations presented in table 3.7. This allows for further validation of the standard 3D model by comparing the operating range against that determined for the 2D model. Figure 3.39 shows that the 2D and 3D models typically are within 1% of each other within the choked region. Up to 10% error is observed between the models within the unchoked range, which aligns with observations made in the literature. Further results for the simulations of the standard nozzle ejector are included in Chapter 5 of this dissertation.

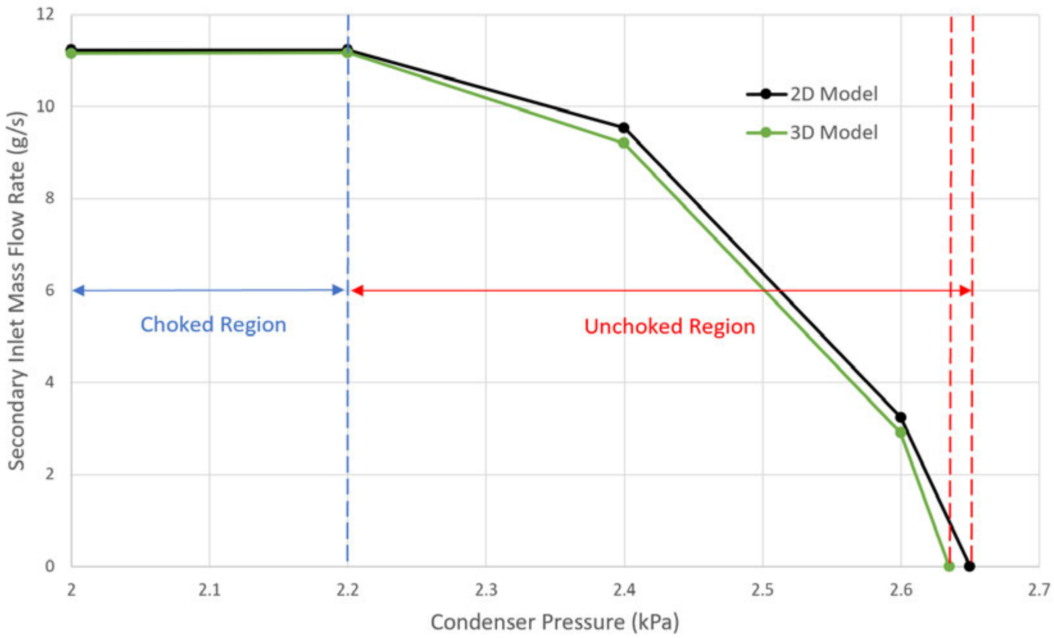

Figure 3.39: Comparison of the 2D and 3D models secondary mass flow rates determined for choked and unchoked condenser operating pressures.

3.13.7 Model Limitations

When completing a computational analysis, it is expected that limitations will arise due to assumptions or simplifications that must be made to allow progression of the research. As for the CFD analysis described within this chapter, the fundamental limitation that separates this model from reality is the use of an ideal gas model in place of the wet-steam model. This decision was made to primarily to simplify the model due to time constraints related to the project. The use of the ideal gas model means that the effects of condensation, that occurs within the primary nozzle in actual steam ejector operation, is disregarded in the simulations. As explained previously in this chapter, the condensation droplets have been shown to impinge on the velocity of the primary flow. This simplification was justified by the detailed literature review that concluded that the ideal gas model could provide an acceptable depiction of real ejector flow and greater computational efficiency. The effects of the condensation in a nozzle equipped with a vortex generator is unknown and is not within the scope of this study.

3.14 Vortex Generator

The complex helical feature of the vortex generator was difficult to create using ANSYS Design Modeller directly. Alternatively, Creo-Parametric 8.0 3D modelling software was used, and the modified nozzle was added to an assembly before being imported to ANSYS workbench. This section of the methodology outlines the process followed to create the vortex generator geometry in Creo-Parametric. The general mesh that was used for the primary nozzle models that incorporate the vortex generators is also detailed in this section. The different vortex generator variations and justifications have been described in the parametric study in Chapter 4.

3.14.1 Generator Geometry

The geometry begins using the standard nozzle model that was revolved from a 2D sketch on the XY plane. The first step involved creating a trajectory for the generator to follow. The divergent face of the nozzle was selected as a reference for the sketch; figure 3.40 shows the trajectory of the generator created using a sketch. Curving the line at either end allowed the tails of the generator to finish flush with the fluid surface.

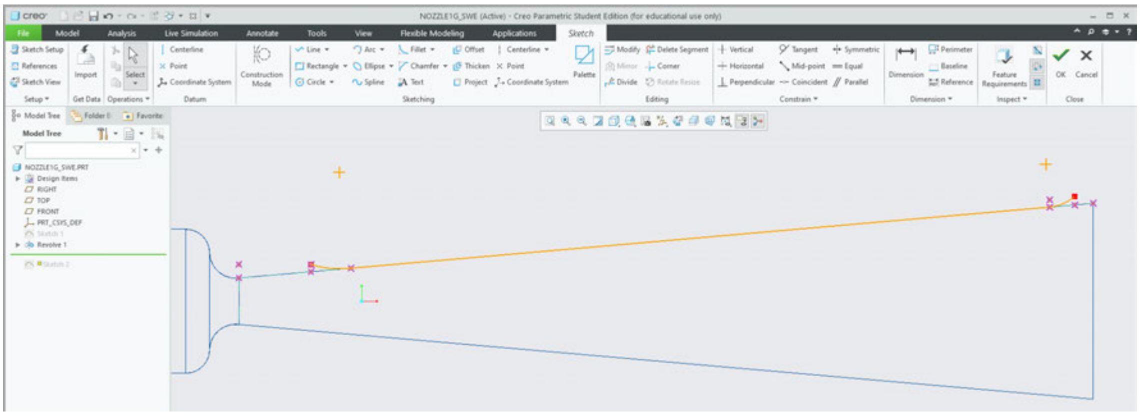

Figure 3.40: Sketch created for the trajectory of the vortex generator.

Next, the helical sweep option was selected from the shapes tab in the ribbon. The trajectory sketch and the X-axis was selected as the references and the section of the helix was created as a sketch (see figure 3.41). It was important that the section was oriented normal to the trajectory to avoid distortion of the helix profile when it was generated.

In settings, remove material was activated so the profile of the generator was subtracted from the fluid domain. The final adjustment for the helical sweep was the pitch option, which was adjusted according to the values discussed in Chapter 4.

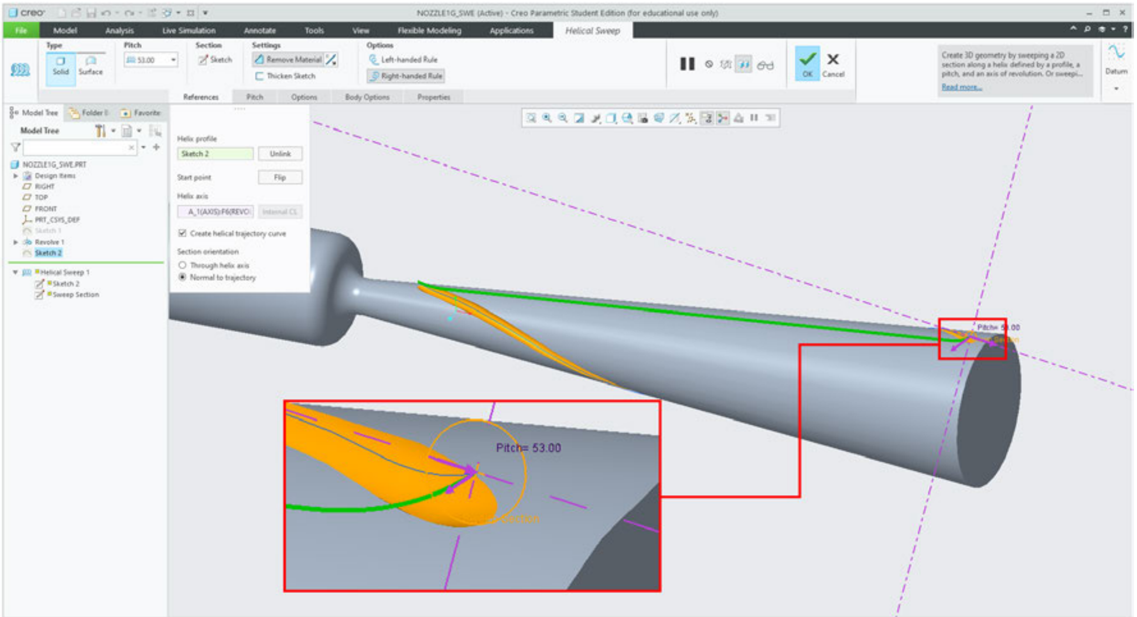

Figure 3.41: Helical sweep settings used to create the vortex generator with section creation enhanced.

For developing nozzles equipped with multiple generators, the pattern option was selected from the editing tab in the ribbon. The type option was changed to axis and the X-axis is selected as the reference. In the settings options, the first direction members input value was equivalent to the number of generators required and the angle between members was determined accordingly. Figure 3.42 shows the settings selected to create a nozzle with three vortex generators.

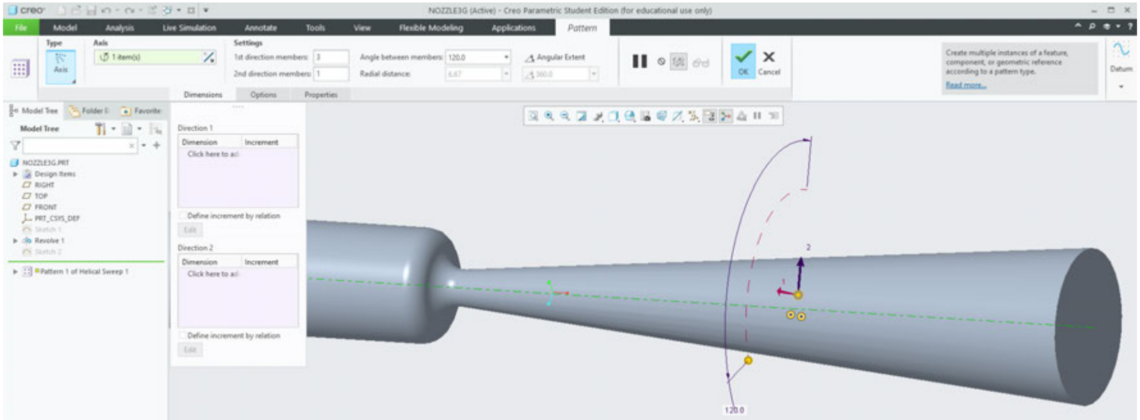

Figure 3.42: Pattern settings applied to the helical sweep to create multiple vortex generators.

The final feature applied to the model was the round option which was accessed from the engineering tab in the ribbon. The edges of helical sweep feature were selected as the references for the rounding effect (see figure 3.43). The radius of the round was controlled through the dimension scheme option in the ribbon; further details of the dimensions have been included in Chapter 4.

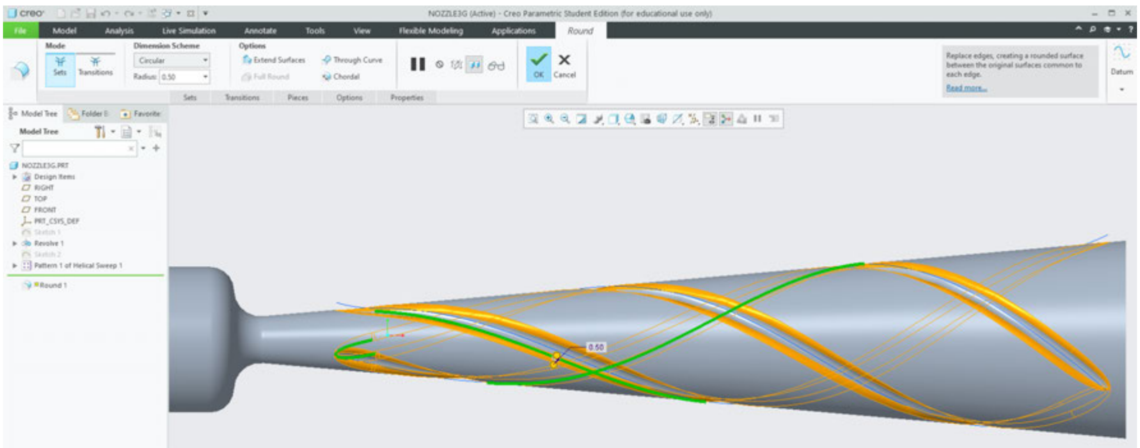

Figure 3.43: Rounding settings applied to the edges of the vortex generators.

3.14.2 Generator Mesh Independence

The addition of the vortex generators to the primary nozzle means that the mesh used for the standard nozzle was no longer suitable. The radius of the rounding used for the generators was 0.5mm and the element size used for the standard nozzle divergent was 0.3mm. Figure 3.44 shows that the 0.3mm element size was not fine enough to accurately represent the curvature of the vortex generator. To repair this, a mesh independence study of a primary nozzle equipped with a single vortex generator was conducted, testing the effect of three different element sizes on simulation results.

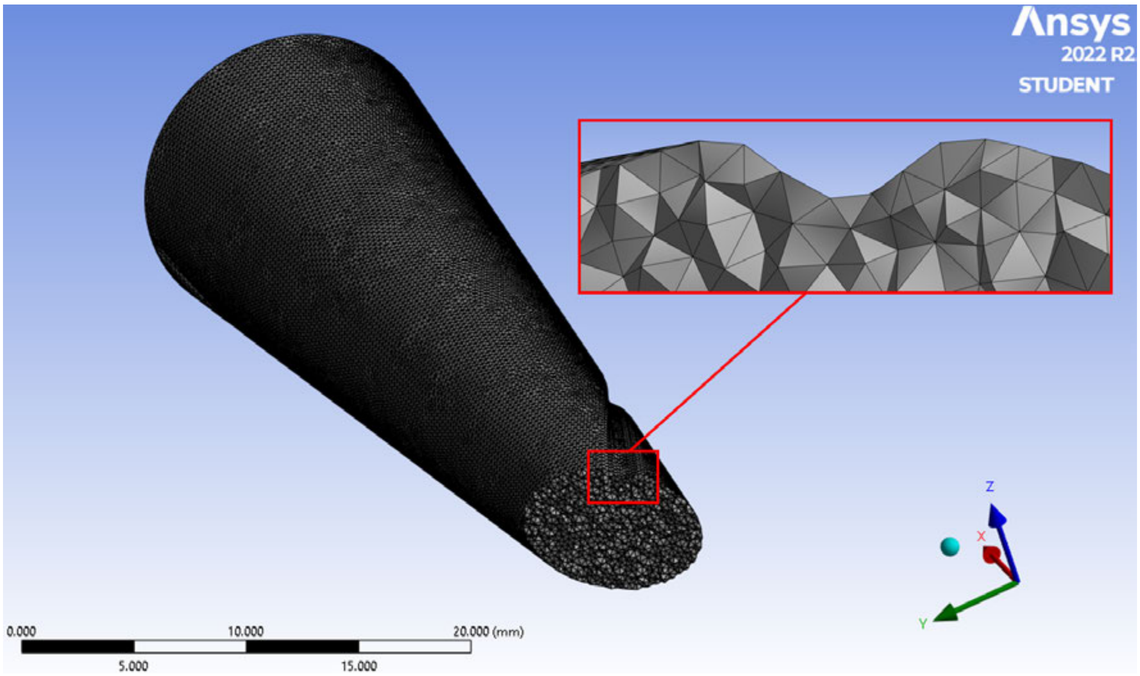

Figure 3.44: Unacceptable representation of the small radius curvature of a vortex generator using the standard nozzle mesh.

The face sizing mesh function in ANSYS was used to control the element size used for the vortex generators. A 0.2mm, 0.1mm, and 0.05mm element size was tested in the study, with the results for the total pressure variation displayed in figure 3.45. It was observed that the coarsest mesh predicts the peak pressure to occur at an earlier location in the nozzle than the medium and fine meshes. This indicated that there was a significant difference between the fluid domain modelled by the 0.2mm mesh compared to the finer meshes. The margin of error between the medium and fine mesh was typically less than 2%. Thus, the 0.2mm mesh was considered adequate for the research and would provide results with an acceptable level of accuracy.

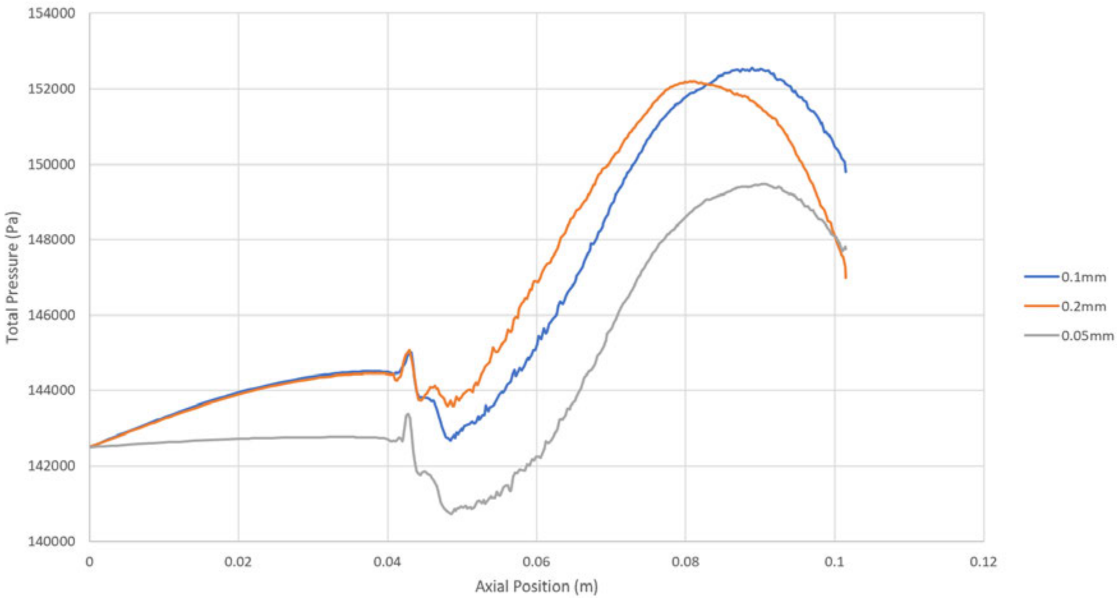

Figure 3.45: Effect of mesh size on total pressure variation over through the centreline of a single generator nozzle.

The tetrahedral mesh using the 0.2mm face mesh on the vortex generator curvature can be seen in figure 3.46. Comparing this mesh to the standard mesh (see figure 3.44) it was found that the 0.1mm produced a much closer representation of the vortex generator profile. The final polyhedral mesh applied to nozzle in ANSYS Fluent can also be seen in figure 3.44.

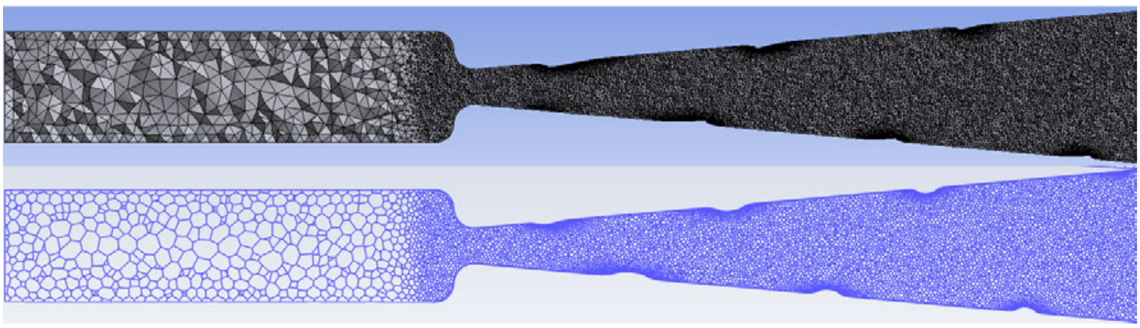

Figure 3.46: Final tetrahedral and polyhedral meshes applied to a three generator primary nozzle.

3.15 High Performance Computations

In scientific research involving simulations, it is often found that significant computational power is required in order to work effectively and obtain results quickly. In these circumstances, a HPC can be utilised, which has substantially higher processing potential than that of a common desktop machine. For CFD research, the processing time of the simulation is heavily influenced by the number of elements in the model. The university's desktops are limited to 23hrs of usage per day; with the expected computational times for some of the models exceeding this limit, the HPC was essential to complete the research. This section of the methodology provides the process followed to access and use the UniSQ HPC.

3.15.1 HPC Account and Software

The first step involves submitting a HPC account request which can be selected from the service catalogue on USQhub. This involves specifying the software required and intended use of the HPC, as well as approval from the project supervisor. Once the account is activated by the university's HPC Systems engineer, the software necessary to connect to the HPC must be downloaded. For postgraduate research students using an assigned university desktop computer the software is accessed through the UniSQ software portal. However, for undergraduate students, the software must be downloaded directly from the software provider's website onto a personal computer device. The required software packages include:

1. PuTTY – A Secure Shell (SSH) client for Windows platforms necessary to connect with the HPC.
2. Notepad++ – Implemented as the default code editor for PuTTY and FileZilla and supports a wide range of programming languages.
3. Strudel – A Scientific Remote User Desktop Launcher (STRUDEL) that configures and implements an SSH tunnel and connects with the Virtual Network Computing (VNC) viewer.
4. TurboVNC – An X server and windows viewer used by Strudel to display an X-window output under Windows when running a Linux program.

5. FileZilla – A Secure File Transfer Protocol (SFTP) client that is necessary to safely move files between the HPC and a windows desktop.

6. Cisco AnyConnect – The secure mobility client used to connect to the UniSQ Virtual Private Network (VPN).

3.15.2 University VPN

Once the appropriate software is installed, the first step is to connect to the university's server by entering the VPN address into Cisco AnyConnect. Successful connection with the university server is confirmed by the Cisco AnyConnect prompt window and can also be checked using the computers command prompt window as shown in figure 3.47.

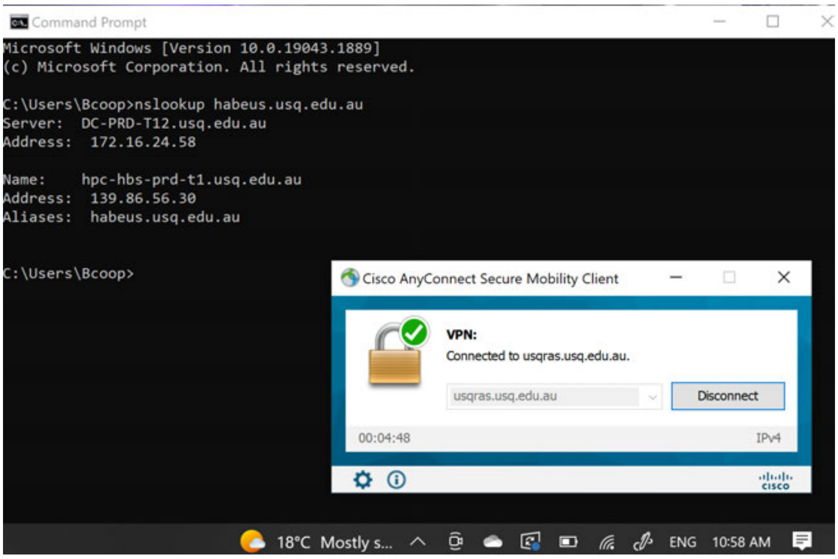

Figure 3.47: Confirmation of connection to the UniSQ VPN.

Once the VPN is connected the users HPC account can be verified by searching for the strudel.json file in a preferred web browser. If the site cannot be reached, this is due to the systems firewall that requires undergraduate student access to be granted by the University's Information and Communications Technology (ICT) department. Figure 3.48 shows the file the strudel.json file that should appear, indicating the HPC account has the necessary approval to access the HPC.

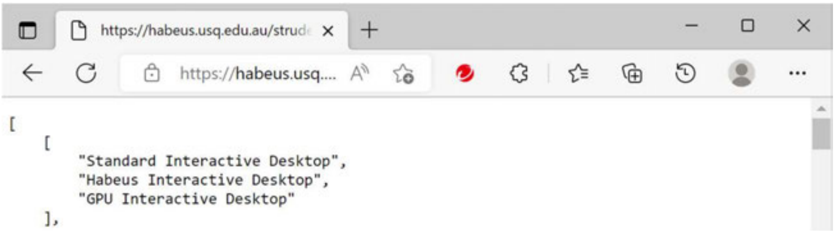

Figure 3.48: Confirmation of connection to the UniSQ HPC.

3.15.3 File Transfer Client

The next step is to set up the SFTP client. First, the “Default editor” must be changed to a custom editor in the FileZilla settings. The location of the Notepad++ exe file must be selected as shown in figure 3.49.

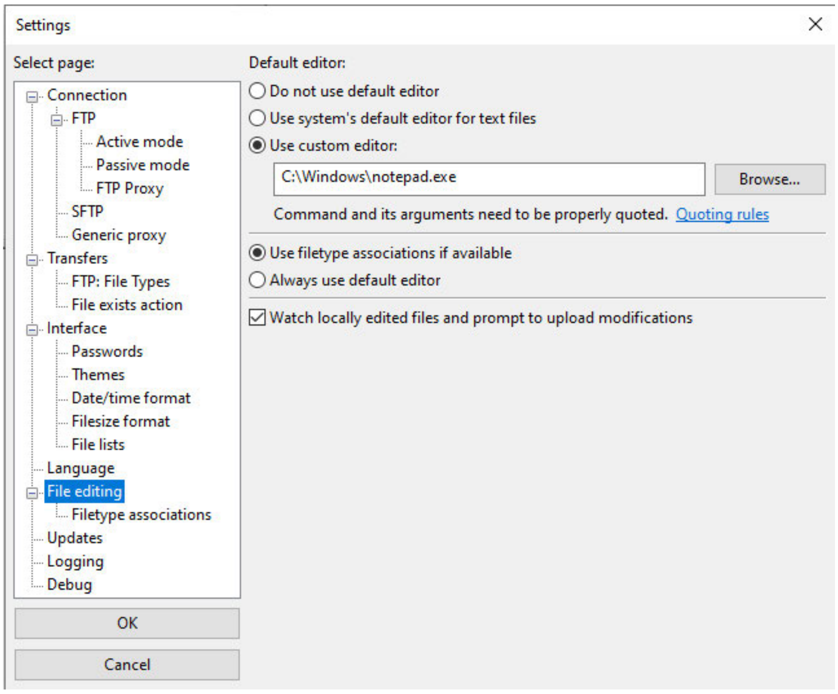

Figure 3.49: Change of the default editor for Filezilla configuration.

The server details must be entered into the program and a connection with the HPC file directory will be established (see figure 3.50). A new file can be created to the HPC directory to organise the jobs for the research project. Files are transferred between the local and remote site windows by clicking and dragging them to the desired location. Figure 3.50 shows FileZilla running on a Windows platform transferring an ANSYS job

File from the HPC.

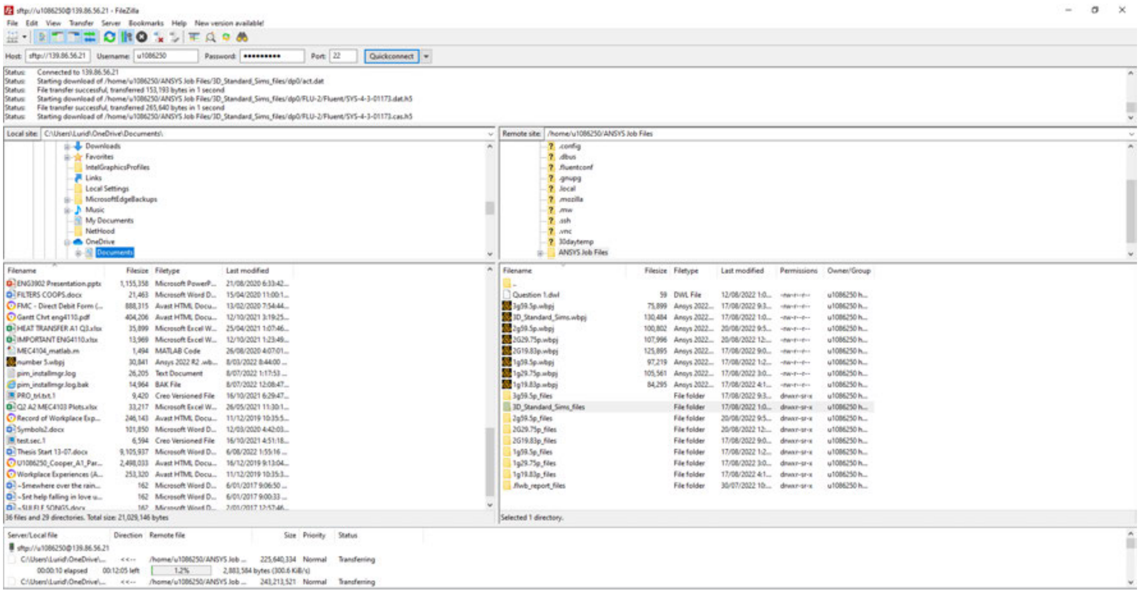

Figure 3.50: FileZilla connected with the HPC, transferring job files between the local and remote sites.

3.15.4 Graphical Interface

The details of the configuration server for the HPC must be added to the "Available Sites" and activated in the strudel configuration window as shown in figure 3.51.

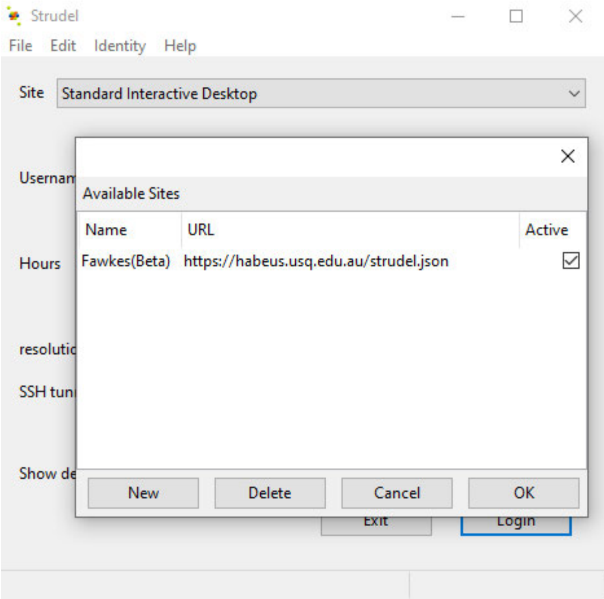

Figure 3.51: Details of the configuration server activated in Strudel.

Next, the "Show Advanced Options" must be selected and the "SSH Tunnel Cipher" changed to aes128-ctr. The user's student number is entered as the "Username" and the required number of "Hours", "Memory" and "CPUs" are assigned. For this research project 72 hours and 64GB was sufficient and 64 CPUs was selected to ensure the simulations were being run at maximum efficiency (see figure 3.52).

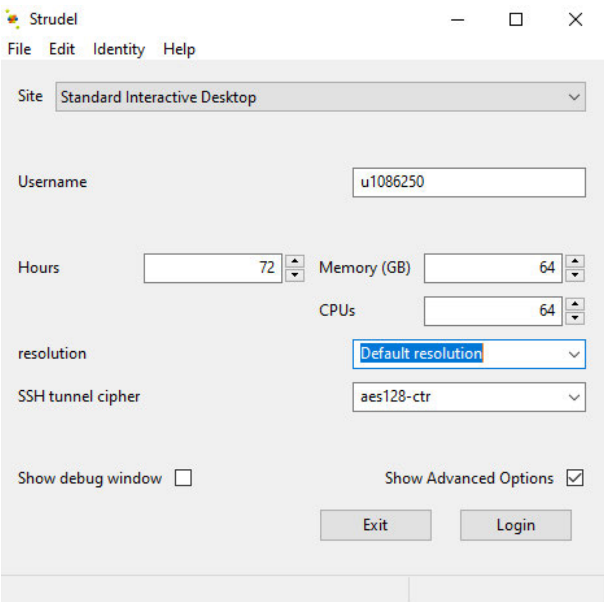

Figure 3.52: Hours, Memory and CPU inputs used in Strudel for the simulations.

Once the configuration and login is completed, Strudel will create an SSH tunnel using PuTTY and open a virtual desktop session with TurboVNC (see figure 3.53). The command terminal can be selected from the desktop and ANSYS Workbench 2022 R2 can be opened as shown in figure 3.53.

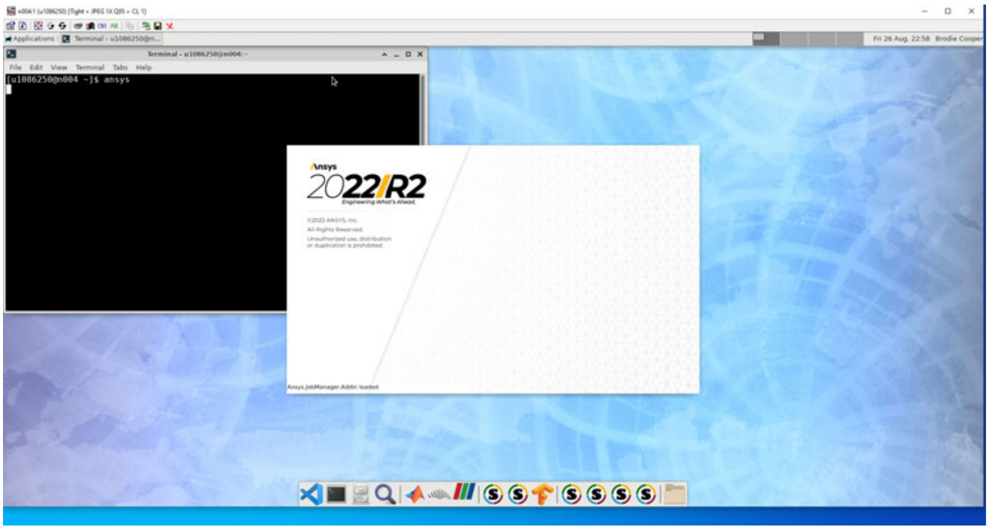

Figure 3.53: Strudel virtual desktop with the command terminal used to open Ansys 2022 R2.

3.15.5 ANSYS Fluent Simulations

Execution of the simulations is accomplished in the same way as on a standard desktop with each job being ran one at a time and the results analysed upon completion. The final mesh independence study for the 3D ejector model was completed using both the desktop and the HPC to allow a comparison to be made on the computational efficiency which is shown in table 3.12. It is clear that without the HPC, the computation times required for the medium and fine elements is unacceptable.

Table 3.12: Comparison of computation times for the 3D mesh independence study using the HPC and desktop.

Number of Elements	Iterations	Desktop Time (hrs)	HPC Time (hrs)
3million	1000	3.5	0.25
5.5million	1000	7	0.52
11.5million	500	16	1.5

3.15.6 Running Ansys Case Files

As an alternative to using strudel, the case file for a CFD model can be saved in ANSYS Fluent and ran directly from the Linux environment using PuTTY. However, since the jobs are only executed in series and the ANSYS licence possessed by UniSQ is restricted to 4 CPUs, the computational efficiency is not increased. The key advantage of this method is that the jobs do not require user input to run or save; this means that all the jobs can be uploaded, and an email alert will be sent to the user when the simulations are complete. The case file solutions can then be opened for review, either through strudel on the HPC or by transferring the file back to the local directory and viewing through a desktop.

3.16 Chapter Summary

The methodology process has been covered in depth by this chapter, beginning with the development and validation of a 2D CFD model against previous research conducted by Al-Manea (2019). With the geometry of the ejector verified, the 3D model creation using Creo-Parametric 8.0 software was detailed along the steps followed to transfer the models to ANSYS Workbench and develop an initial mesh. The mesh independence studies performed to determine the necessary mesh resolutions are detailed and the final mesh utilising polyhedral elements is provided. The selection process for the optimal turbulence model and wall function is outlined and the final boundary conditions and fluent settings to be used for the parametric study are confirmed. Furthermore, this chapter has provided a step by step process of the vortex generator creation and a detailed description of how the HPC was setup and used to optimise the efficiency of the CFD simulations.

Chapter 4

Parametric Study of Vortex Generators

4.1 Chapter Overview

After the geometry of the standard ejector design was validated against previous research, modifications to the primary nozzle can be made with relative confidence. A parametric study was conducted to determine the dimensions and configurations of the vortex generators that will be used for this research. The characteristics to be modified were determined through discussion with the project supervisor and also influenced by observations made throughout the literature review process. This chapter focuses on the parametric study and provides details and justification of the different variations of vortex generator used in the primary nozzle. It also follows on from section 3.14 of the methodology which outlines the steps followed to create the vortex generator geometry in Creo-Parametric modelling software. A summary of the key vortex generator characteristics that are modified and their corresponding values obtained through the parametric study is included in table 4.1.

Table 4.1: A summary of the different vortex generator characteristics used in the study.

Number of Generators	**Profile (mm)**	**Pitch (mm)**
1	1	53, 26.5, 17.5
2	1	53, 26.5, 17.5
3	1	53, 26.5, 17.5

4.2 Generator Profile

The sectional shape that is cut into the fluid domain to represent the vortex generator is referred to in this study as the generators profile. The shape of the generator is designed to be a subtle and smooth transition for the fluid as is it leaves the throat of the primary nozzle. To achieve this, a rounded generator profile with a gradual rise and fall from the nozzle surface at each end is used; these features can be seen clearly in figure 4.1. Avoiding sharp and abrupt edges reduces the unintentional generation of turbulent eddies or obstructions in the fluid flow, and also simplifies the meshing process.

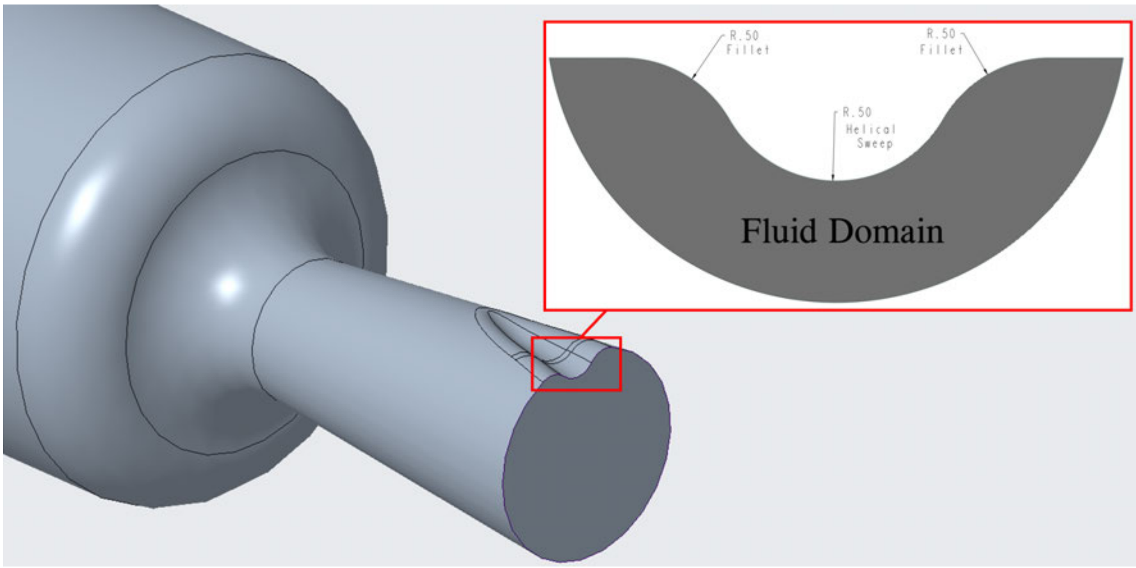

Figure 4.1: Vortex generator profile.

When determining the dimensions for the generator profile there were a number of a factors to consider including; geometrical restrictions and software limitations. The diameter of the nozzle, particularly around the throat (see table 3.2), was a key consideration for determining the final generator profile to ensure that the generator is protruded enough to influence the flow but not restrict it and hinder the performance. The profile was limited to a circular shape due to the way the section does not rotate when the helical sweep is generated as outlined in section 3.14 of the methodology. As a result, a 0.5mm radius section with a 0.5mm rounding applied to the edges was selected. Figure 4.1 shows the dimensions of the final sectional profile used for the vortex generators.

The radius used to create the progressive rise from the surface at each end of the generator is shown in figure 4.4. By using a large radius at the nozzle throat end, the divergent section increases as the full profile of the generator is gradually introduced to the fluid domain. The outlet end was initially going to share the same radius, however, an error related to the interface between ANSYS 2022 R1 and Creo-Parametric 8.0 occurred for the model that distorted the cells for this feature (see figure 4.2). This prevented the generator surface from being properly selected during the meshing process and resulted in a defect in the fluid domain that would impact flow behaviour. This issue was resolved for most of the nozzle variations by adjusting the radius for the profile at the outlet end to values between 7mm and 8mm.

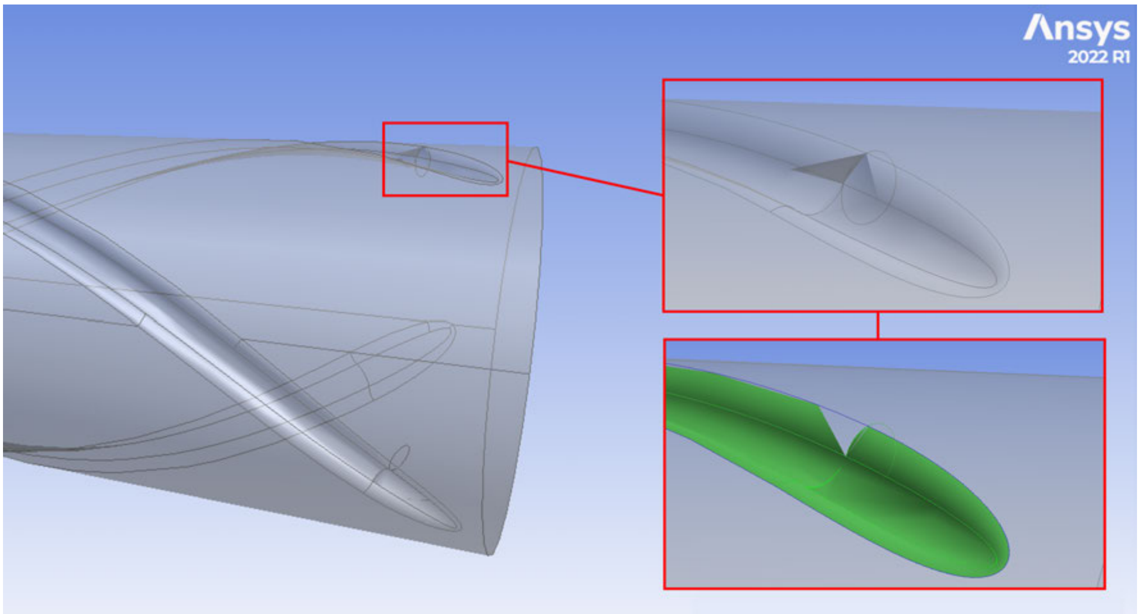

Figure 4.2: Cell defect that occurs due to an error in the interface between ANSYS and Creo-Parametric.

The cell distortion issue was encountered for the all variations of the three generator nozzle; the 26.5mm and 17.5mm pitch variations could not be remedied by adjusting the profile dimensions. In ANSYS, model defects are typically resolved using the repair tools within the software, however, this issue did not fall under any categories of the tool options. Therefore, an alternative profile end was used for these models which is shown in figure 4.3. By extending the trajectory to the end of the nozzle, the cell distortion issue was eliminated. This design was considered for all models initially, however, it was predicted that the sharper edges would create unwanted spanwise vortices at the nozzle exit. Conversely, it is theorised that the design would reduce the decay of the induced vortex that may occur when the generator ends before the nozzle exit. Thus, while consistency of the generator profile was preferred, the design shown in figure 4.3 will yield valuable results.

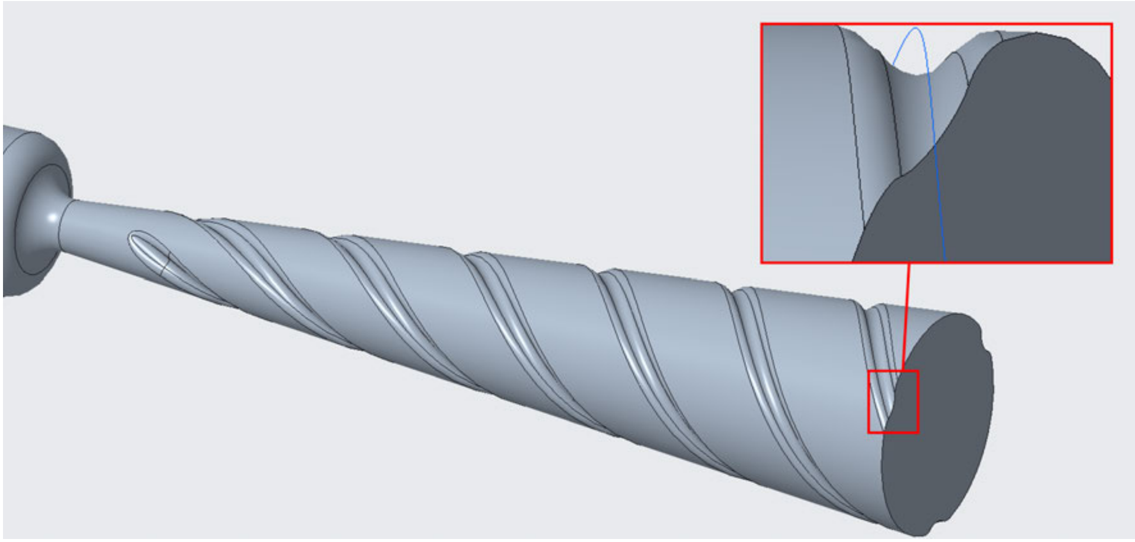

Figure 4.3: End location of the 26.5mm and 17.5mm pitch three vortex generator primary nozzles.

4.3 Helix Pitch

The pitch values shown in table 4.1 were determined by taking the length of nozzle covered by the generator and dividing by the desired number of helical rotations. The effective length can be deduced from the dimensions shown in figure 4.4. The starting location for the vortex generator, as shown in figure 4.4, was selected to avoid restricting the flow and to allow the flow to develop in the divergent section before introducing the generator.

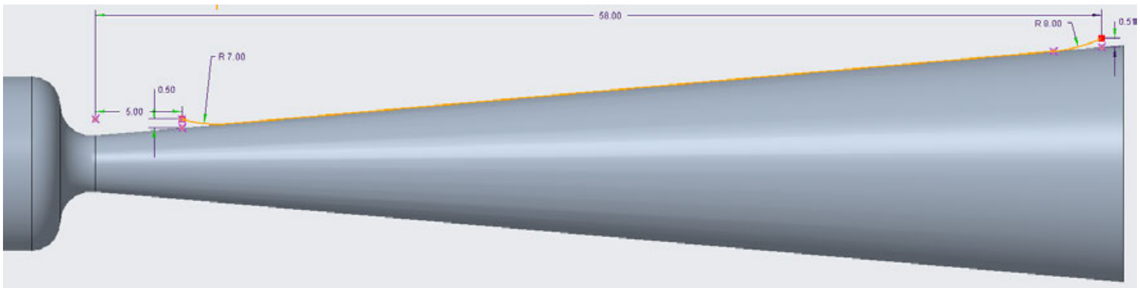

Figure 4.4: Dimensions of the vortex generator including the total profile length and the radius of each end.

When determining the number of helical rotations that would be used in the study, the pitch angle had to be considered. The pitch angle can be described as the angle between the direction of fluid flow and the trajectory of the generator. Increasing the number of helical rotations decreases the pitch value and increases the pitch angle. The larger the pitch angle the more abruptly the fluid has to change direction to follow the helical trajectory of the vortex generator. With the primary fluid flow at such a high velocity, sudden changes in direction would likely force the fluid to flow over the generators rather than follow them, resulting in disrupted flow rather than guided flow. Thus, the number of rotations in the nozzle was restricted to one, two, and three; a single vortex generator nozzle set to the final pitch values are shown in figure 4.5.

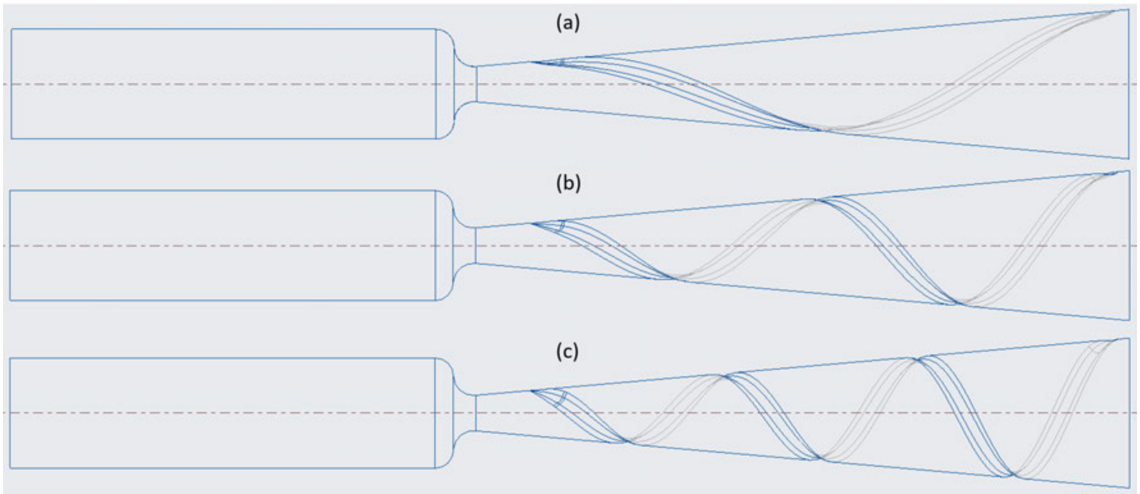

Figure 4.5: A single vortex generator primary nozzle with pitch values of : (a) 53mm, (b) 26.5mm, and (c) 17.5mm.

4.4 Number of Generators

It is theorised that by increasing the number of generators inside the nozzle, more fluid is in contact with a generator surface which would result in a stronger influence on the fluid flow. However, it also also noted that by increasing the number of generators in the nozzle the volume of the nozzle will decrease. This means that the mass flow rate may also decrease, which could have a negative affect on the performance of the ejector. The number of generator that can be used is also limited by the nozzle's geometry. The small diameter, and subsequently small circumference, restricts the amount of generators that can be included in the nozzle without them over lapping or without having to reduce the radius of the generator profile. With these factors taken into consideration, a maximum of three vortex generators will be used in the nozzles (see figure 4.6).

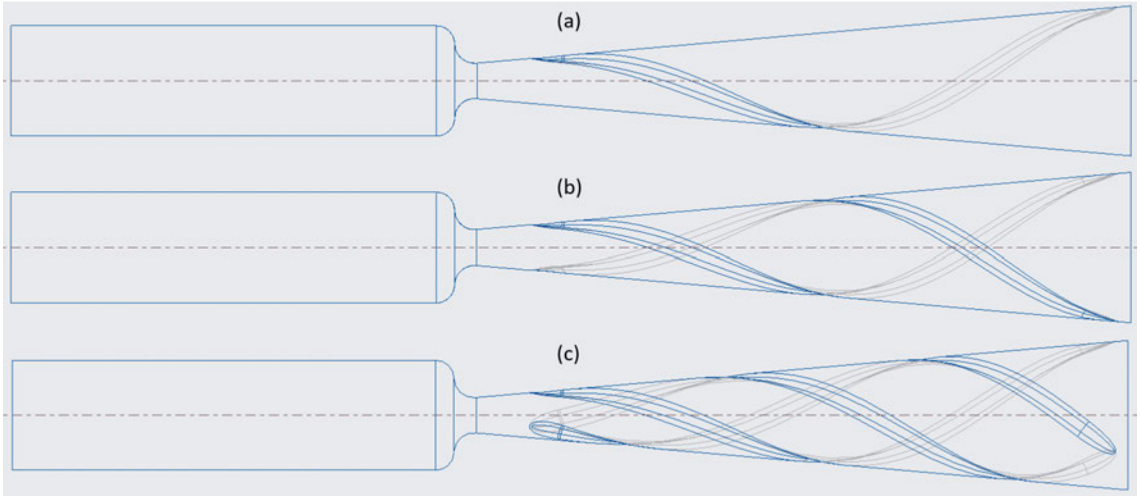

Figure 4.6: A primary nozzle with the number of vortex generators: (a) One, (b) Two, and (c) Three. All generators pictured have a 53mm pitch value.

4.5 Chapter Summary

The characteristics of the vortex generators that are modified in the parametric study have been summarised in this chapter. The key dimensions as well as limitations and constraints surrounding the vortex generator designs have been settled. This chapter has also explained and justified the generator designs. The final variations of the vortex inducing primary nozzle that will be used to generate the results in Chapter 5 have been sufficiently detailed.

Chapter 5

Results

5.1 Chapter Overview

This chapter presents the results obtained through the parametric study outlined in Chapter 4. The simulations carried out in the parametric study used the same boundary conditions and fluent settings as the standard model for consistency of results. The structure used to deliver the results is based on the number of vortex generators implemented in the primary nozzle. Thus, the influence of the pitch and profile variations can be more easily observed. This chapter provides the key images used to analyse the results, which have been referred to throughout the discussion in Chapter 6. Since the main objective of this study was to investigate the effect of vortex generators on the ejectors maximum operating efficiency, the results delivered in this section focused primarily on the choked operating conditions. The full results used to plot the operating ranges have been included in Appendices E through to H.

5.2 Standard Nozzle Ejector Design

The results presented within this section are for the unmodified 3D ejector model simulations as outlined in Chapter 3. These results were used as the standard for comparison for all other variations of the ejector equipped with vortex generators. Figures 5.1 to 5.3 clearly characterise the flow behaviour of the standard 3D ejector model at the optimal operating conditions.

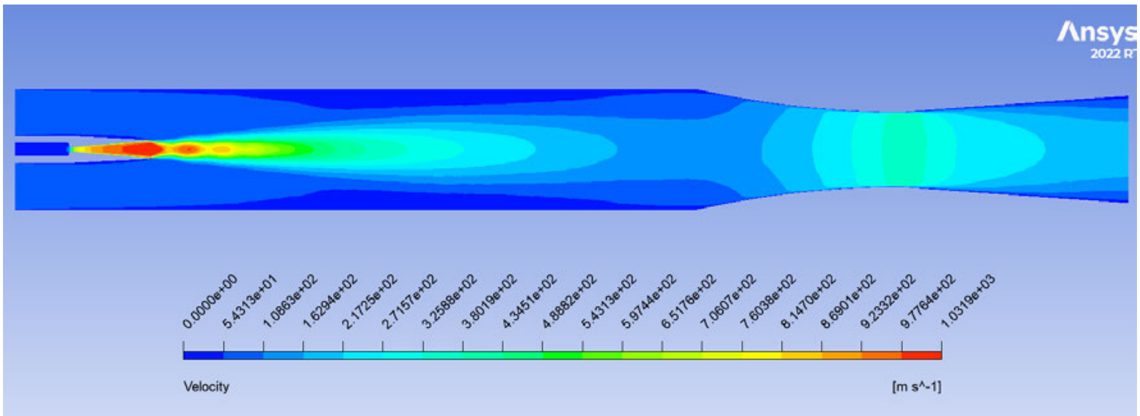

Figure 5.1: Velocity map of standard nozzle operating at 2.2kPa condenser pressure.

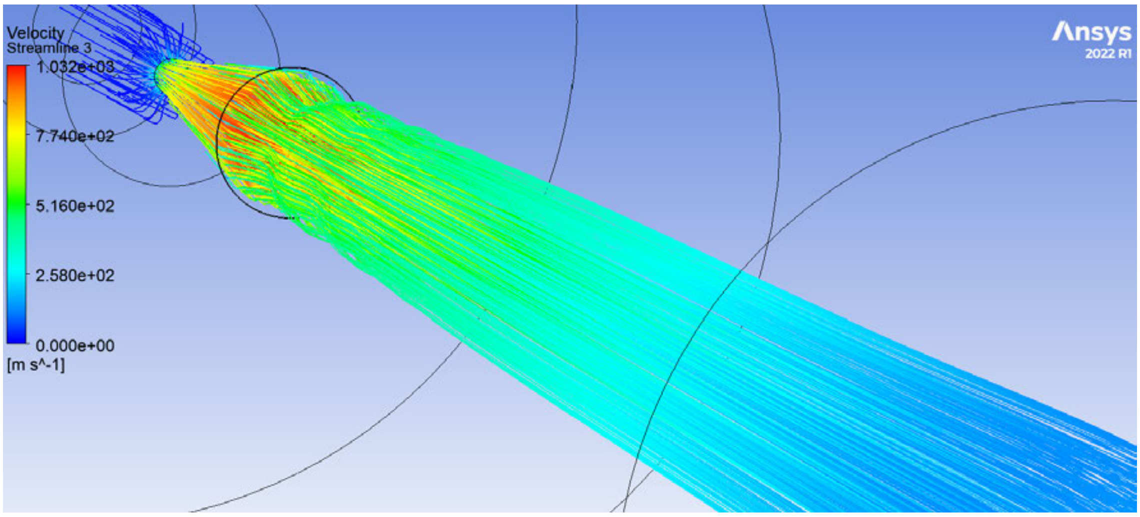

Figure 5.2: Velocity streamlines of the jet core for the standard ejector at 2.2kPa condenser pressure.

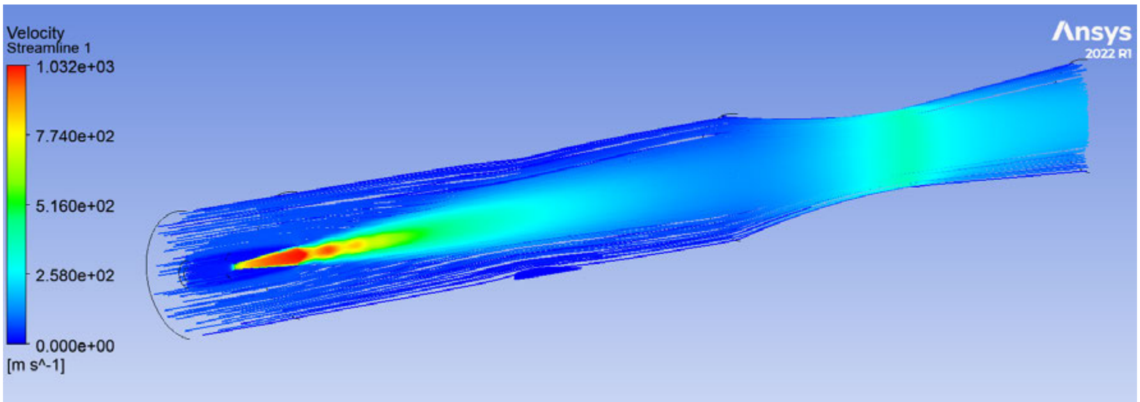

Figure 5.3: Velocity streamlines of mixing chamber recirculation for the standard ejector at 2.2kPa condenser pressure.

The graphs shown in figures 5.4 and 5.5 have been used as key performance metrics for gauging the influence of the modified nozzles on the ejector. The entrainment ratio is representative of the operational performance of the ejector; figure 5.4 plots the entrainment ratio for 2-2.8 kPa condenser pressures and indicates the critical and breakdown pressure points. Figure 5.5 is based on equation 2.5 and was used alongside fluid particle distribution in ANSYS Fluent to understand the vortex generators affect on mixing. The numerical data extracted for figures 5.4 and 5.5 can be found in Appendix E.

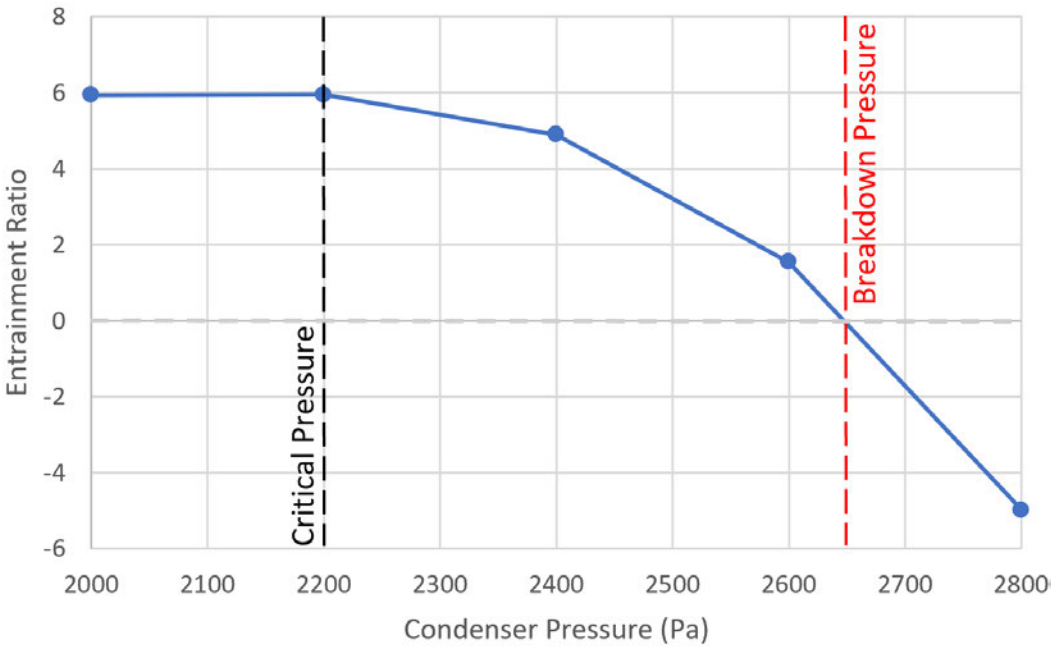

Figure 5.4: Standard nozzle entrainment ratio results for 2kPa to 2.8kPa condenser pressures.

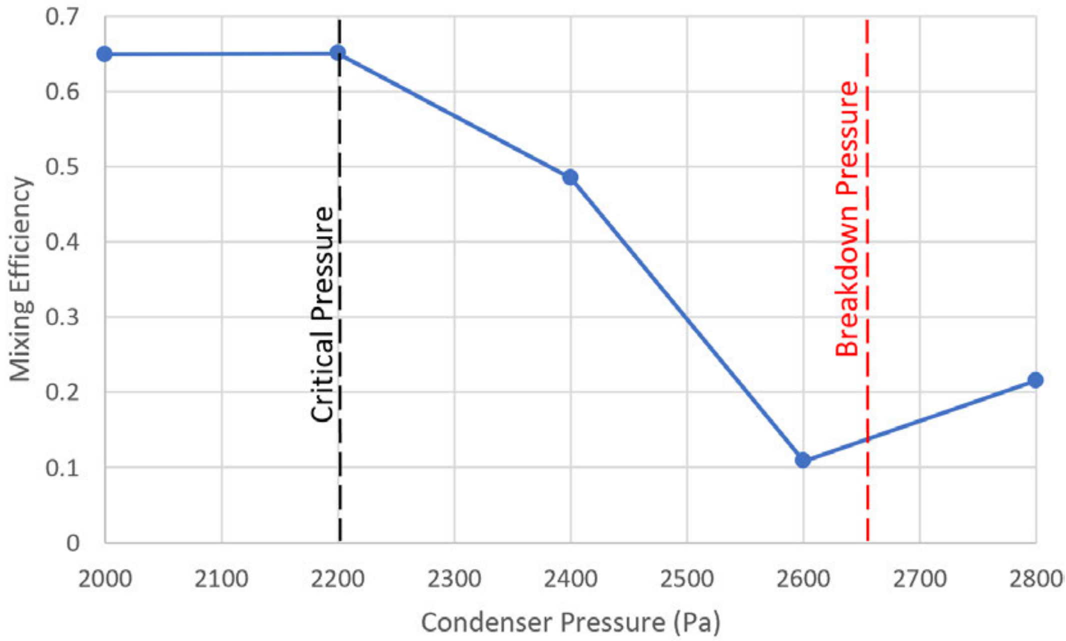

Figure 5.5: Standard nozzle mixing efficiency plot for the 2kPa to 2.8kPa condenser pressures.

5.3 One Vortex Generator Nozzle

Simulation results for the modified nozzles equipped with one vortex generator have been presented in this section. Figures 5.6 to 5.9 show, through visual post-processing methods, the key observations including recirculation, oblique shock waves, jet core shape and flow trajectory for the one generator nozzle variations. The arrangement of the figures allows a comparison to be made between the 17.5mm, 26.5mm and 53mm pitches tested in the parametric study. A centreline has been included into the contour plots in figure 5.6 to highlight the off-centre trajectory of the flow as a result of the one generator design. These observations have been further discussed in Chapter 6.

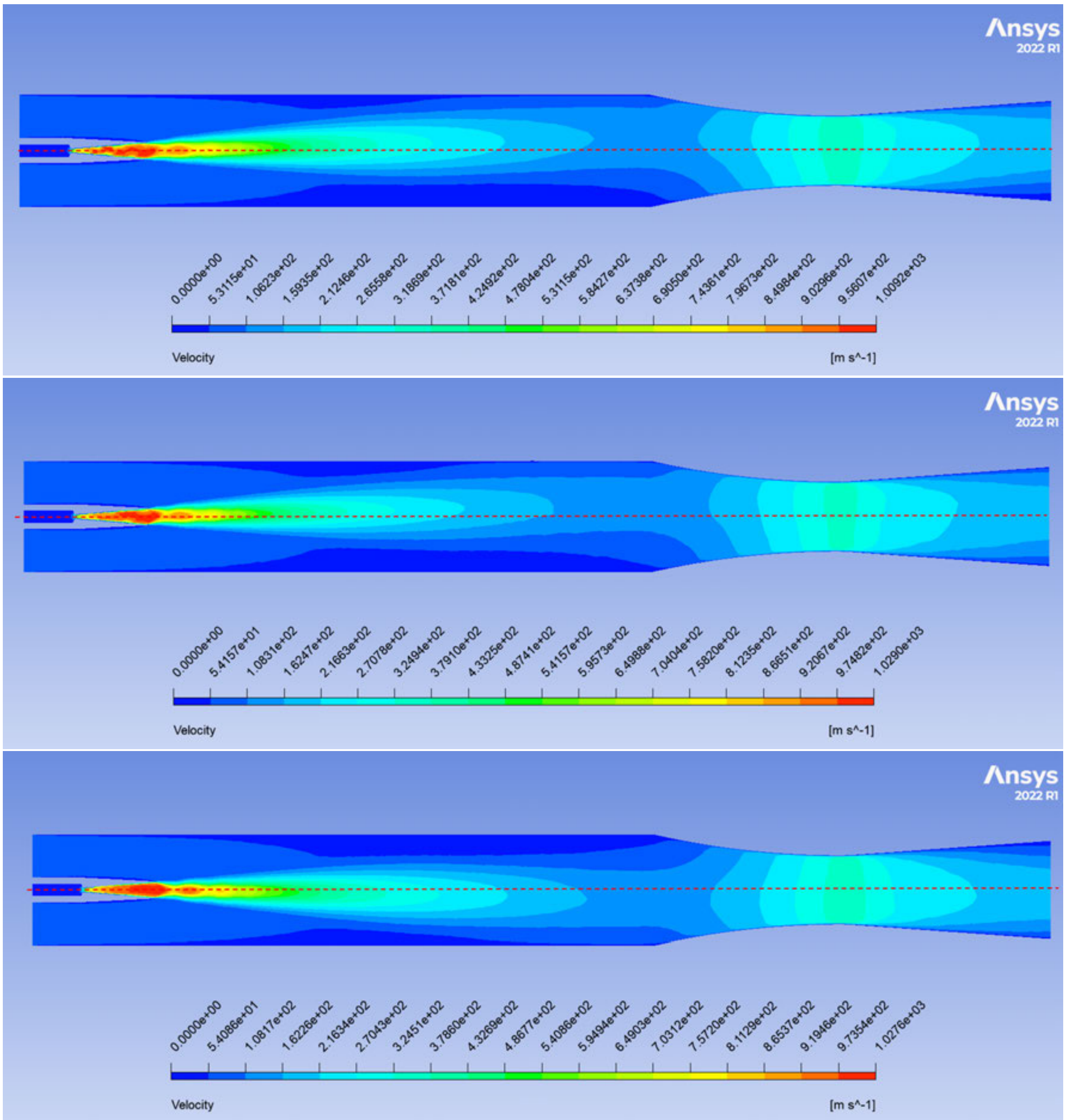

Figure 5.6: Velocity map comparison of one generator nozzle variations operating at 2.2kPa condenser pressure. Pitch sizes: 17.5mm (top), 26.5mm (middle), 53mm (bottom).

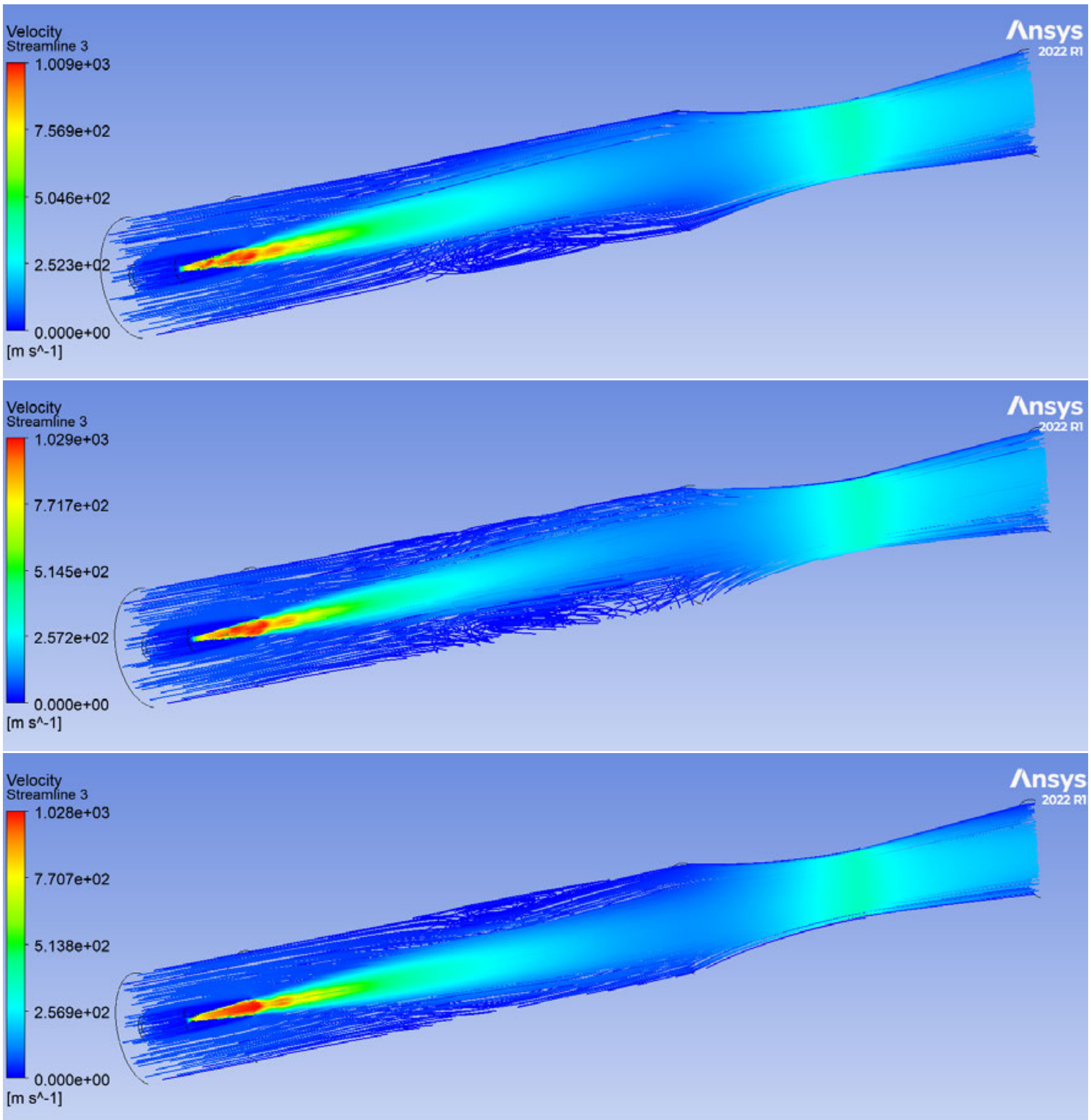

Figure 5.7: Velocity streamlines of mixing chamber recirculation for the one generator nozzle variations at 2.2kPa condenser pressure. Pitch sizes: 17.5mm (top), 26.5mm (middle), 53mm (bottom).

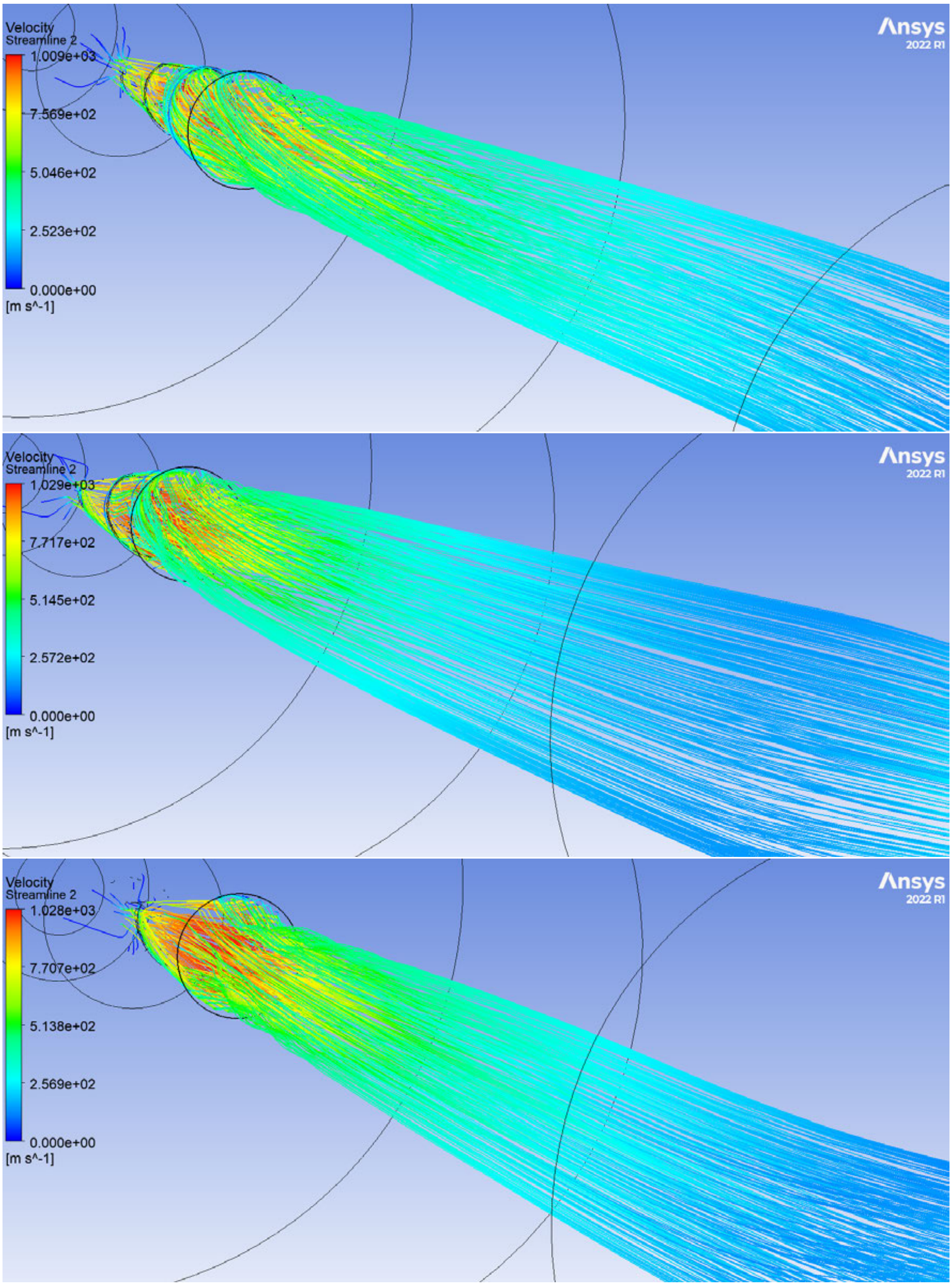

Figure 5.8: Velocity streamlines of the jet core for the one generator nozzle variations at 2.2kPa condenser pressure. Pitch sizes: 17.5mm (top), 26.5mm (middle), 53mm (bottom).

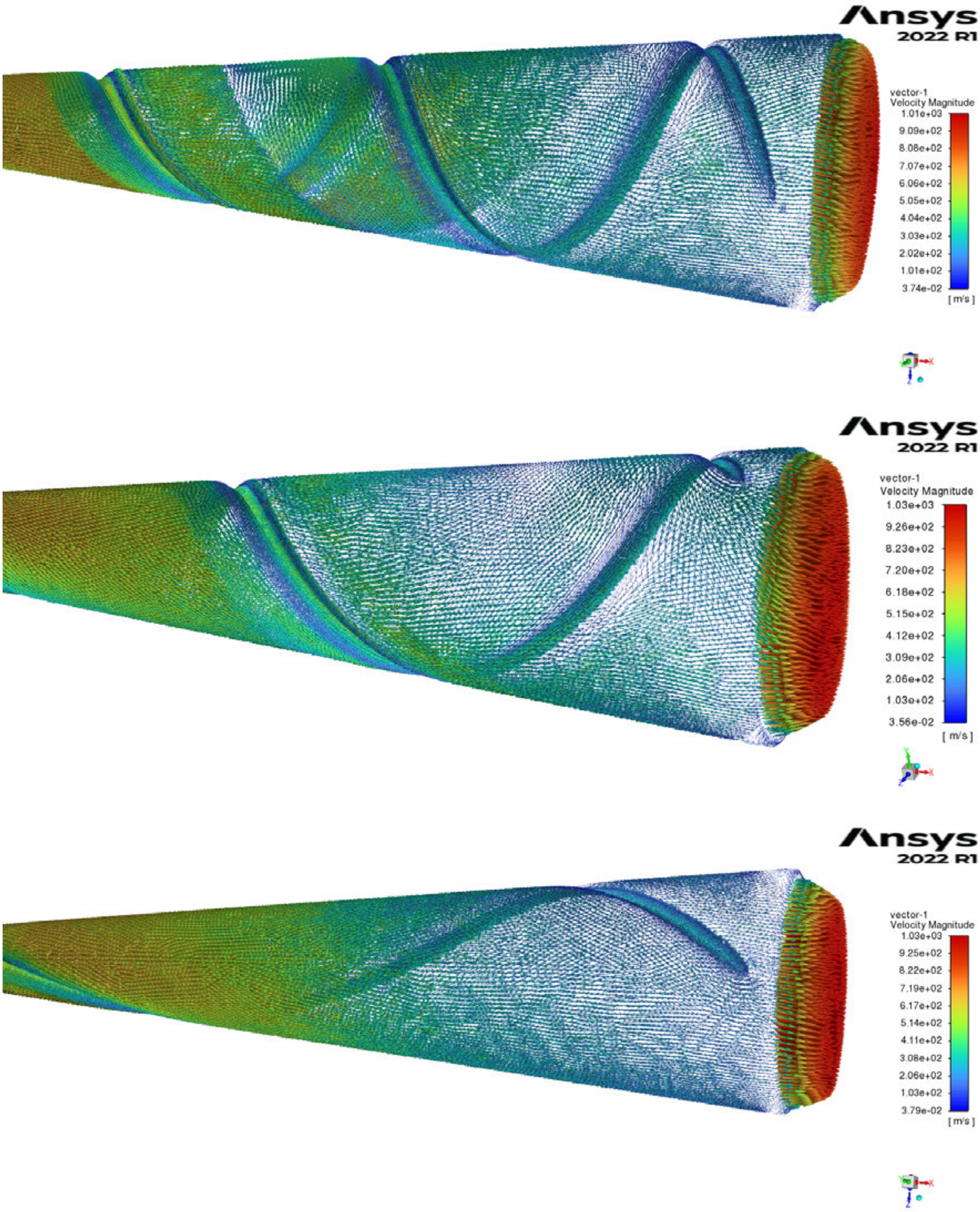

Figure 5.9: Velocity vectors showing flow behaviour in the primary nozzle at critical condenser pressure for all one generator nozzle variations. Pitch sizes: 17.5mm (top), 26.5mm (middle), 53mm (bottom).

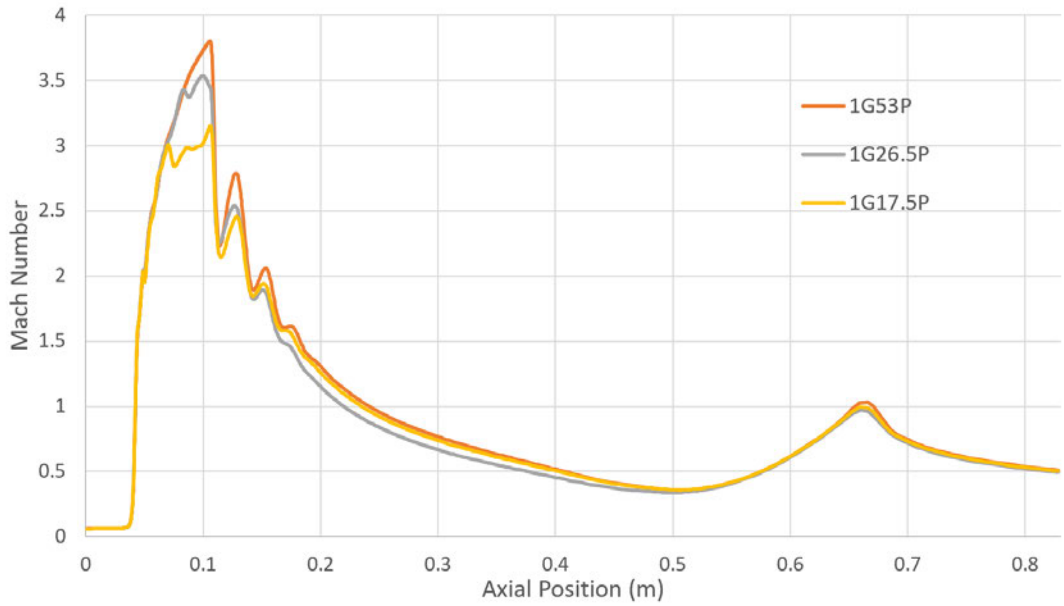

Figure 5.10: Comparison of the Mach number over the ejector centreline for the one generator nozzle variations at 2.2kPa condenser pressure. Notation: 1G53P represents 1 generator with 53mm pitch. Notation: 1G53P represents 1 generator with 53mm pitch.

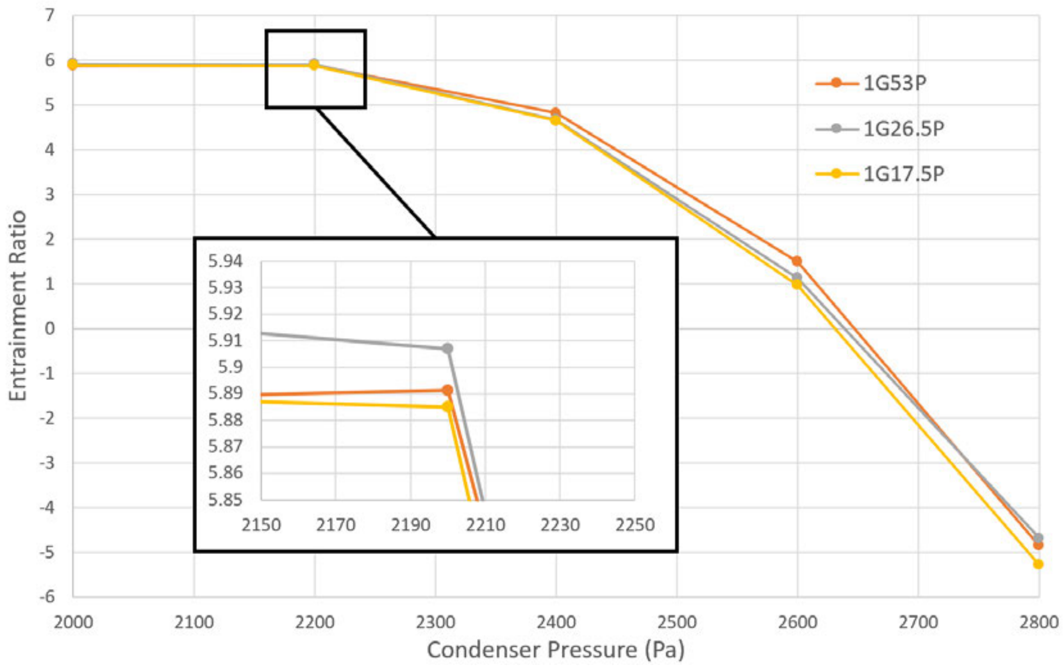

Figure 5.11: Entrainment ratio results plot for the one generator nozzle variations at 2kPa to 2.8kPa condenser pressures. Notation: 1G53P represents 1 generator with 53mm pitch.

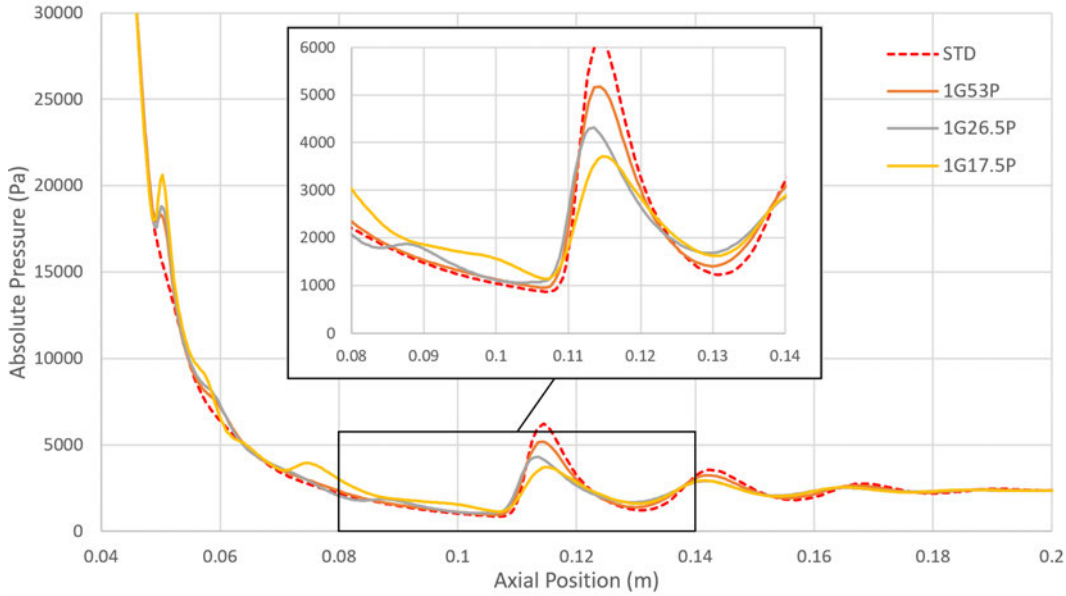

Figure 5.12: Comparison of the absolute pressure over the ejector centreline for the one generator nozzle variations. Notation: 1G53P represents 1 generator with 53mm pitch, STD represents the standard model.

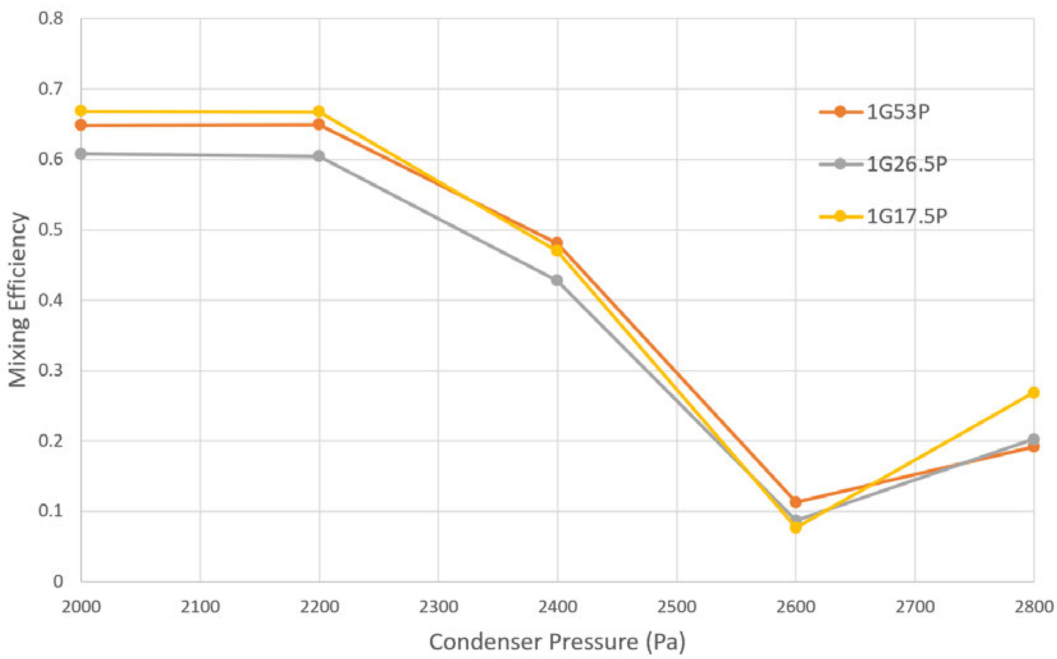

Figure 5.13: Mixing efficiency results plot for the one generator nozzle variations at 2kPa to 2.8kPa condenser pressures. Notation: 1G53P represents 1 generator with 53mm pitch.

In figure 5.10, the Mach number over the ejector centreline for each of the one generator nozzle variations has been plotted alongside the standard nozzle results. The difference in absolute pressure over the ejector centreline compared to the standard nozzle is shown in figure 5.12. These results provide a clear representation of how the modified nozzles affected the pressure and velocity at key locations within the ejector. The operating range of the one generator nozzle variations have been plotted in terms of both entrainment ratio (see figure 5.11) and mixing efficiency (see figure 5.13); this was a key point of analysis covered in the following chapter. The full results extracted from Fluent for the entrainment ratio and mixing efficiency can be found in Appendix F.

5.4 Two Vortex Generator Nozzle

Simulation results for nozzle variations equipped with two vortex generator have been presented within this section. The velocity streamlines presented in figures 5.14 and 5.15 effectively show how using two generators affected the jet core shape, flow trajectory and the recirculation within the mixing chamber, providing a comparison of the results for all generator pitch values used. The comparison of velocity vectors in figure 5.16 show the interaction between the steam and the generators for different pitch values, which has been discussed in further detail in Chapter 6. The combination of these results demonstrates effectiveness of the vortex generators at inducing the desired swirling flow in the mixing chamber.

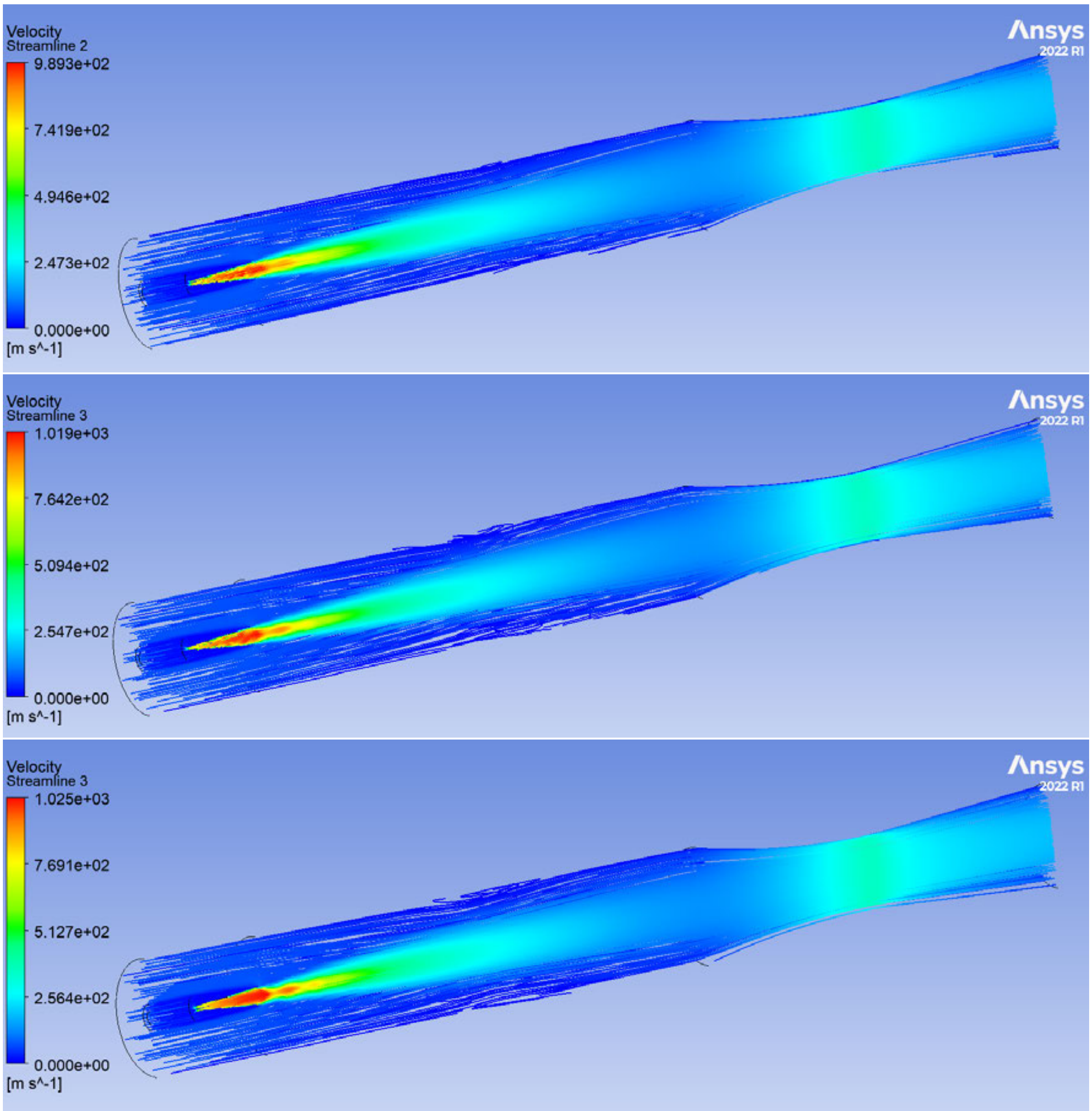

Figure 5.14: Velocity streamlines of mixing chamber recirculation for the two generator nozzle variations at 2.2kPa condenser pressure. Pitch sizes: 17.5mm (top), 26.5mm (middle), 53mm (bottom).

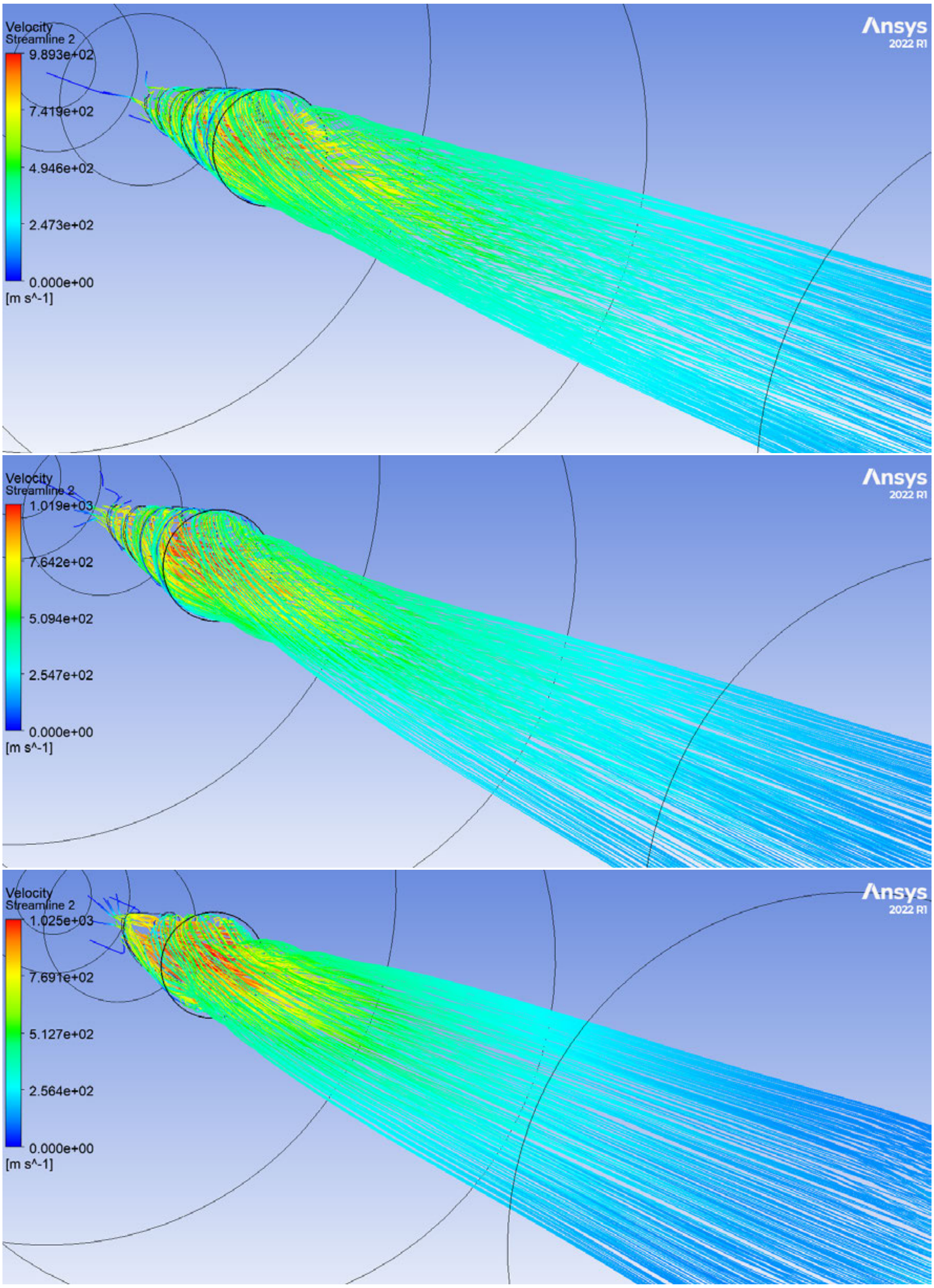

Figure 5.15: Velocity streamlines of the jet core for the two generator nozzle variations at 2.2kPa condenser pressure. Pitch sizes: 17.5mm (top), 26.5mm (middle), 53mm (bottom).

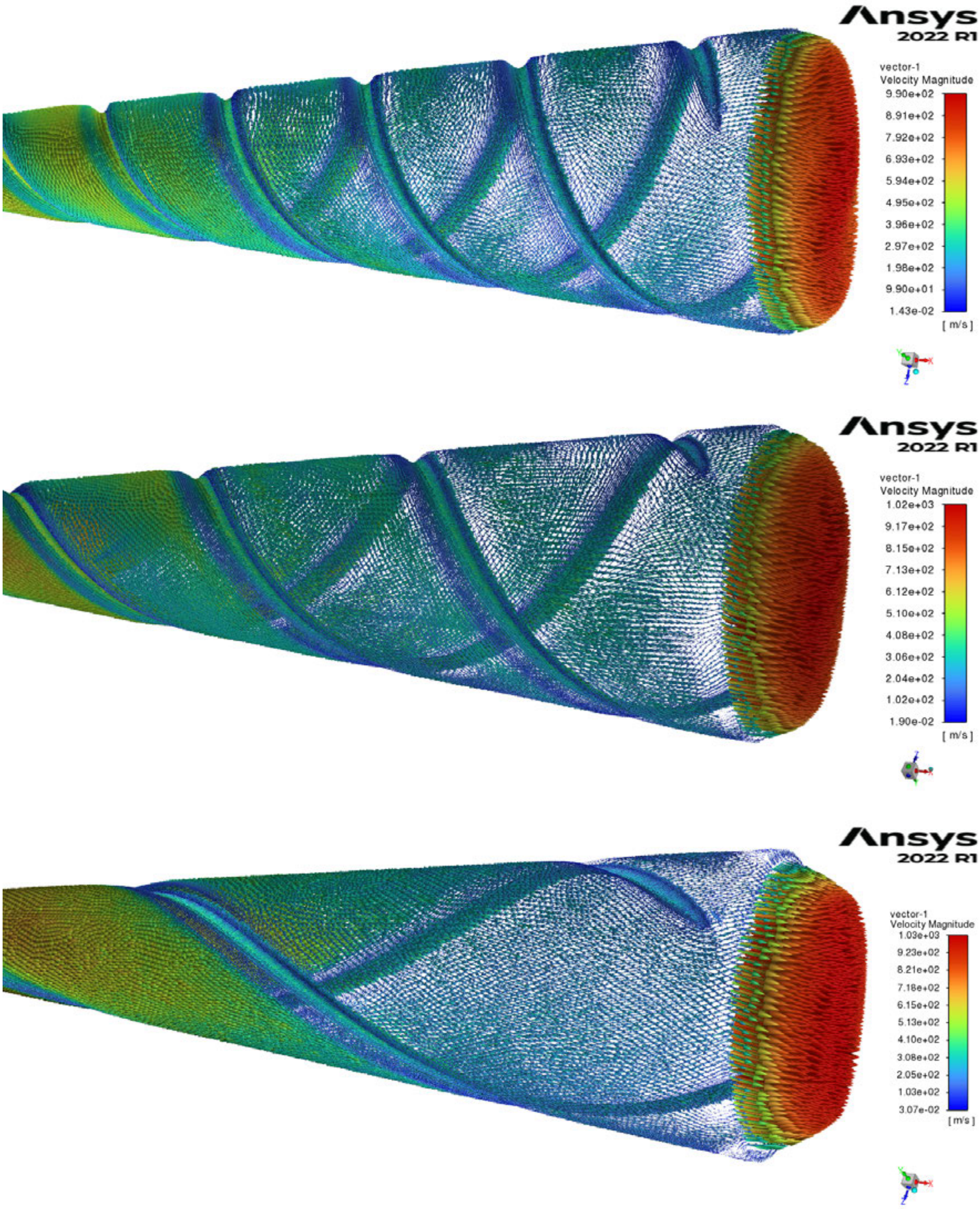

Figure 5.16: Velocity vectors showing flow behaviour in the primary nozzle at critical condenser pressure for all two generator nozzle variations. Pitch sizes: 17.5mm (top), 26.5mm (middle), 53mm (bottom).

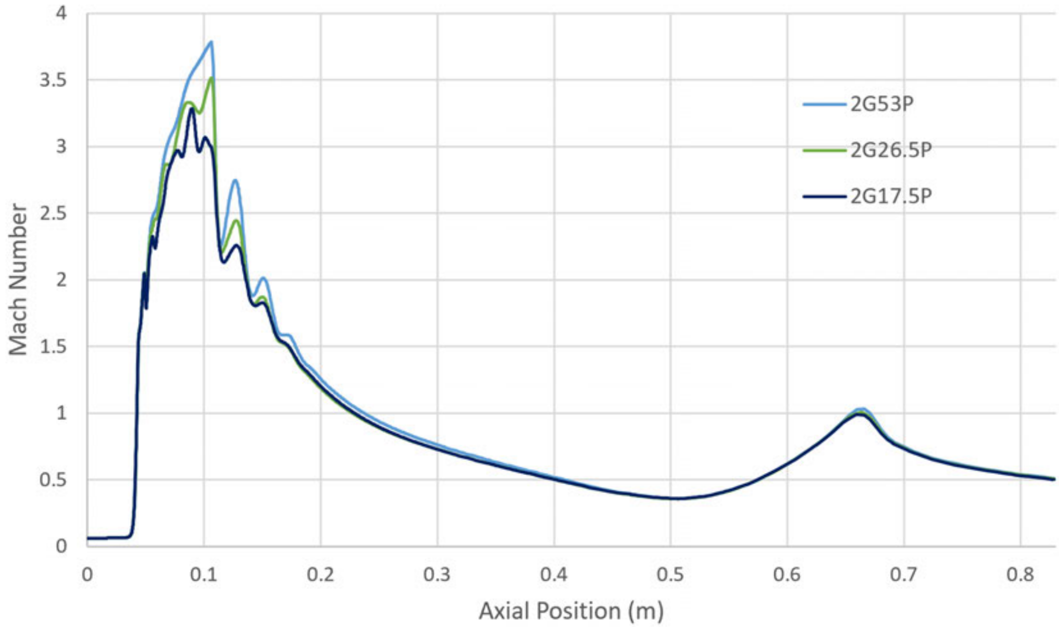

Figure 5.17: Comparison of the Mach number over the ejector centreline for the two generator nozzle variations at 2.2kPa condenser pressure. Notation: 2G53P represents 2 generators with a 53mm pitch.

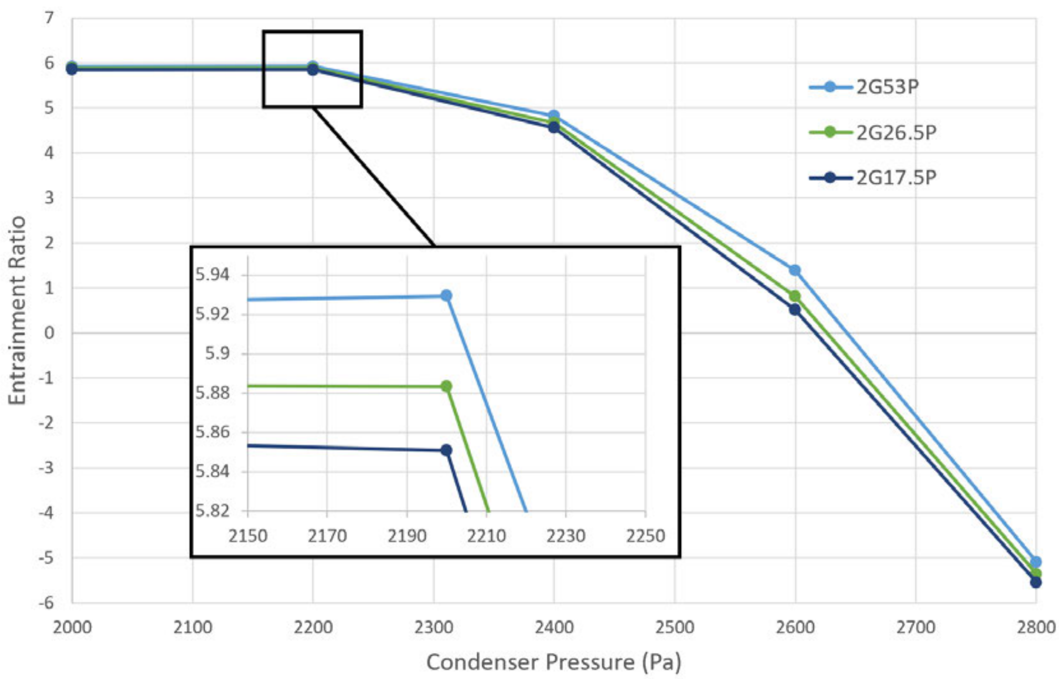

Figure 5.18: Entrainment ratio results for the two generator nozzle variations at 2kPa to 2.8kPa condenser pressures. Notation: 2G53P represents 2 generators with a 53mm pitch.

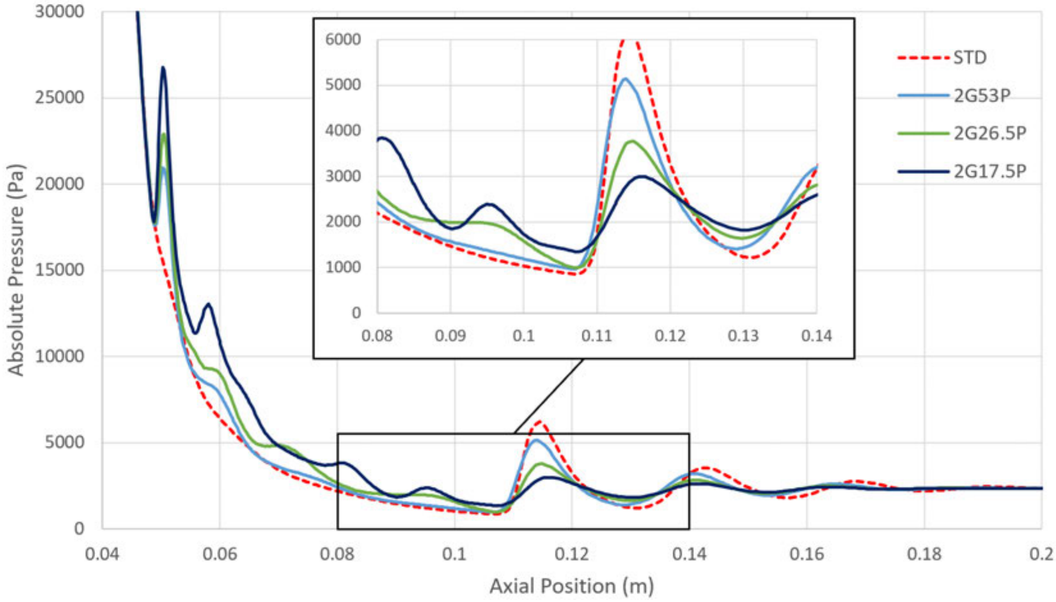

Figure 5.19: Comparison of the absolute pressure over the ejector centreline for the two generator nozzle variations. Notation: 2G53P represents 2 generators with a 53mm pitch, STD represents the standard model.

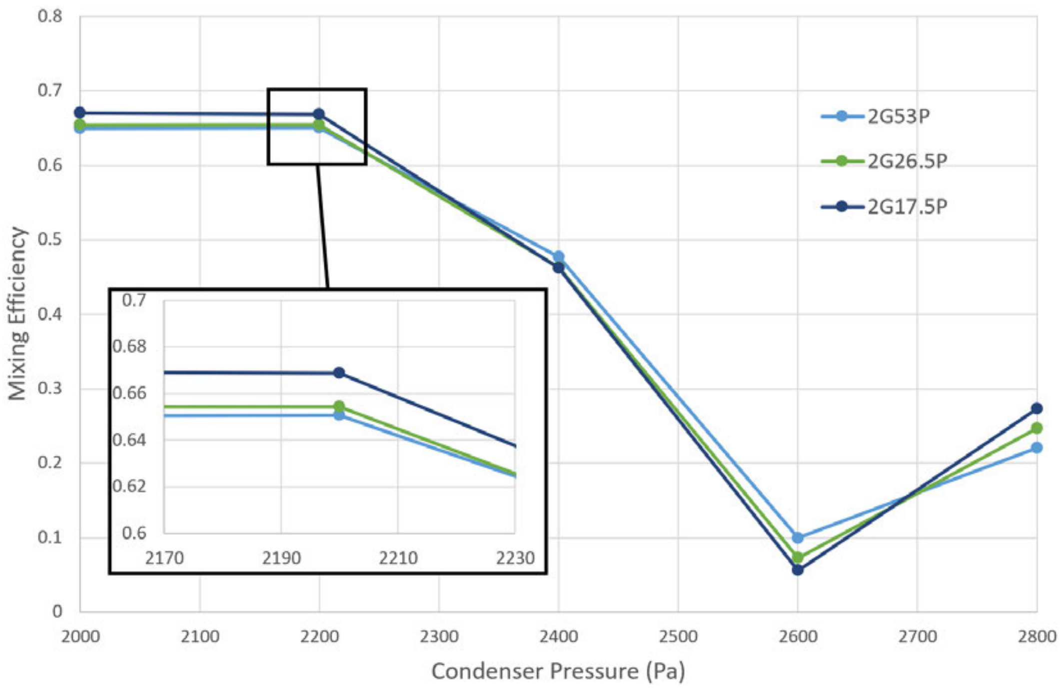

Figure 5.20: Mixing efficiency results plot for the two generator nozzle variations at 2kPa to 2.8kPa condenser pressures. Notation: 2G53P represents 2 generators with a 53mm pitch.

The Mach number over the centreline plot shown in figure 5.17 shows the shock wave effect that occurred in the nozzle as the steams velocity decreased over the generator profile. The contour plots for the two generator models are also included in appendix G and provide a clearer visualisation of shock waves observed within the nozzle and into the mixing chamber. Figure 5.19 has been used to indicate the influence of the two generator variations on pressure difference compared to the standard nozzle design. The entrainment ratio and mixing efficiencies determined for the modified nozzles over the 2kPa to 2.8kPa condenser pressure range has been shown in figures 5.18 and 5.20 with the full data provided in Appendix G.

5.5 Three Vortex Generator Nozzle

Simulation results for the three vortex generator nozzle variations have been presented in this section. Graphical representations of the results are provided in figures 5.21, 5.22, 5.23 to compare the affects of the different pitch sizes on flow behaviour for a nozzle with three generators. The influence of the alternate end profile used for the 26.5mm and 17.5mm pitch variations on the flow trajectory can be seen in figure 5.24. A full analysis of these results has been presented in the discussion in Chapter 6.

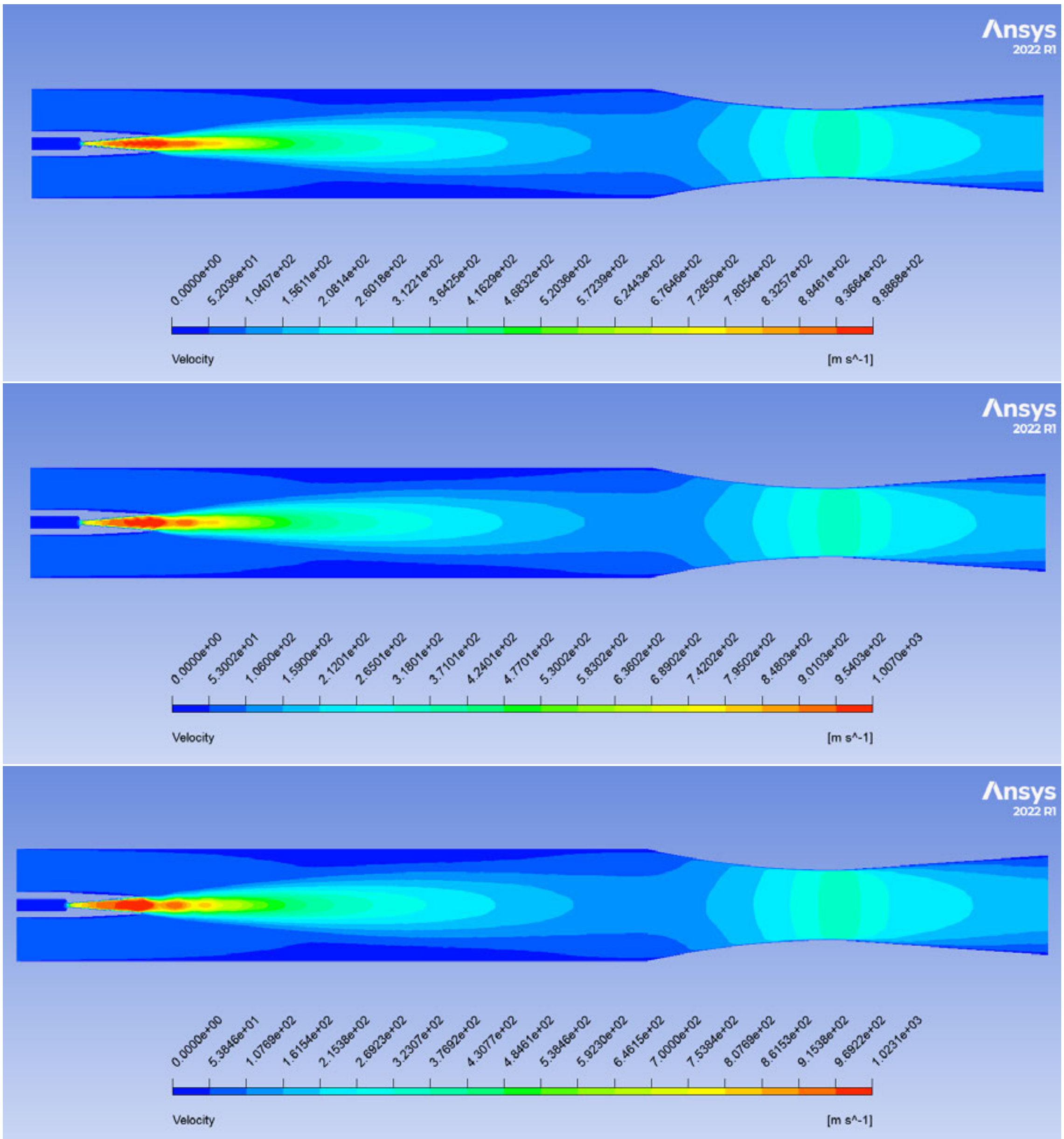

Figure 5.21: Velocity map comparison of three generator nozzle variations operating at 2.2kPa condenser pressure. Pitch sizes: 17.5mm (top), 26.5mm (middle), 53mm (bottom).

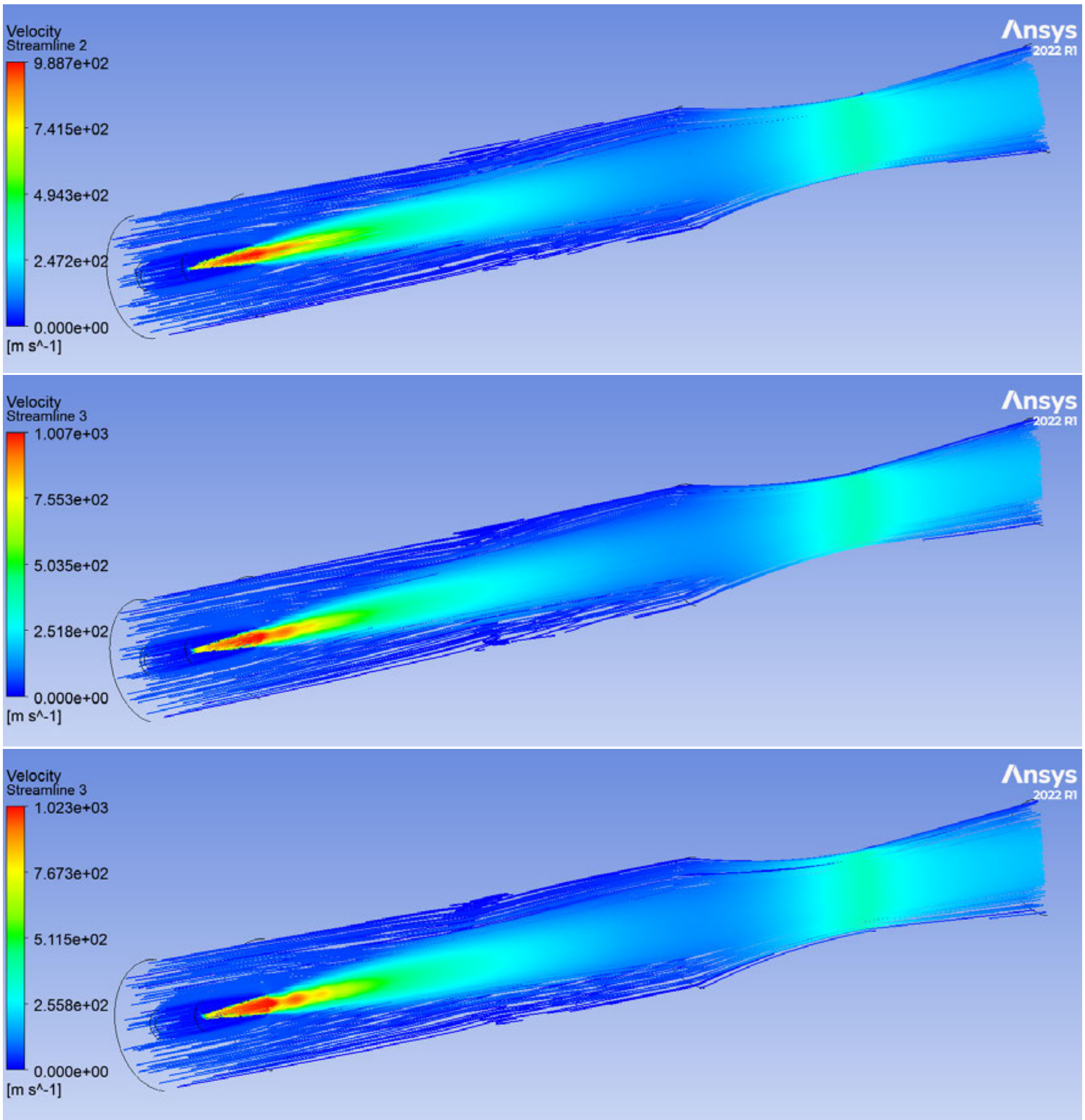

Figure 5.22: Velocity streamlines of mixing chamber recirculation for the three generator nozzle variations at 2.2kPa condenser pressure. Pitch sizes: 17.5mm (top), 26.5mm (middle), 53mm (bottom).

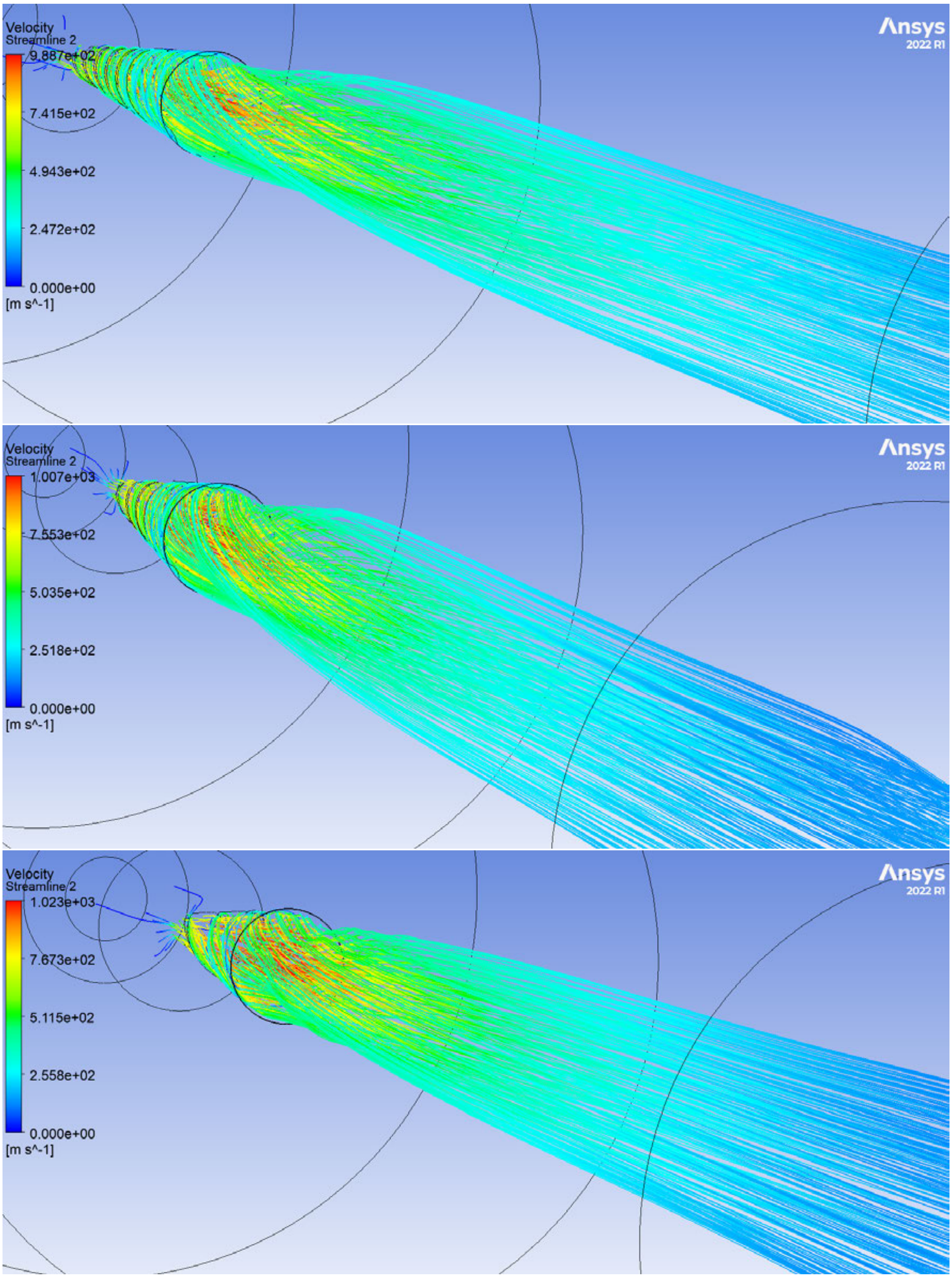

Figure 5.23: Velocity streamlines of the jet core for the three generator nozzle variations at 2.2kPa condenser pressure. Pitch sizes: 17.5mm (top), 26.5mm (middle), 53mm (bottom).

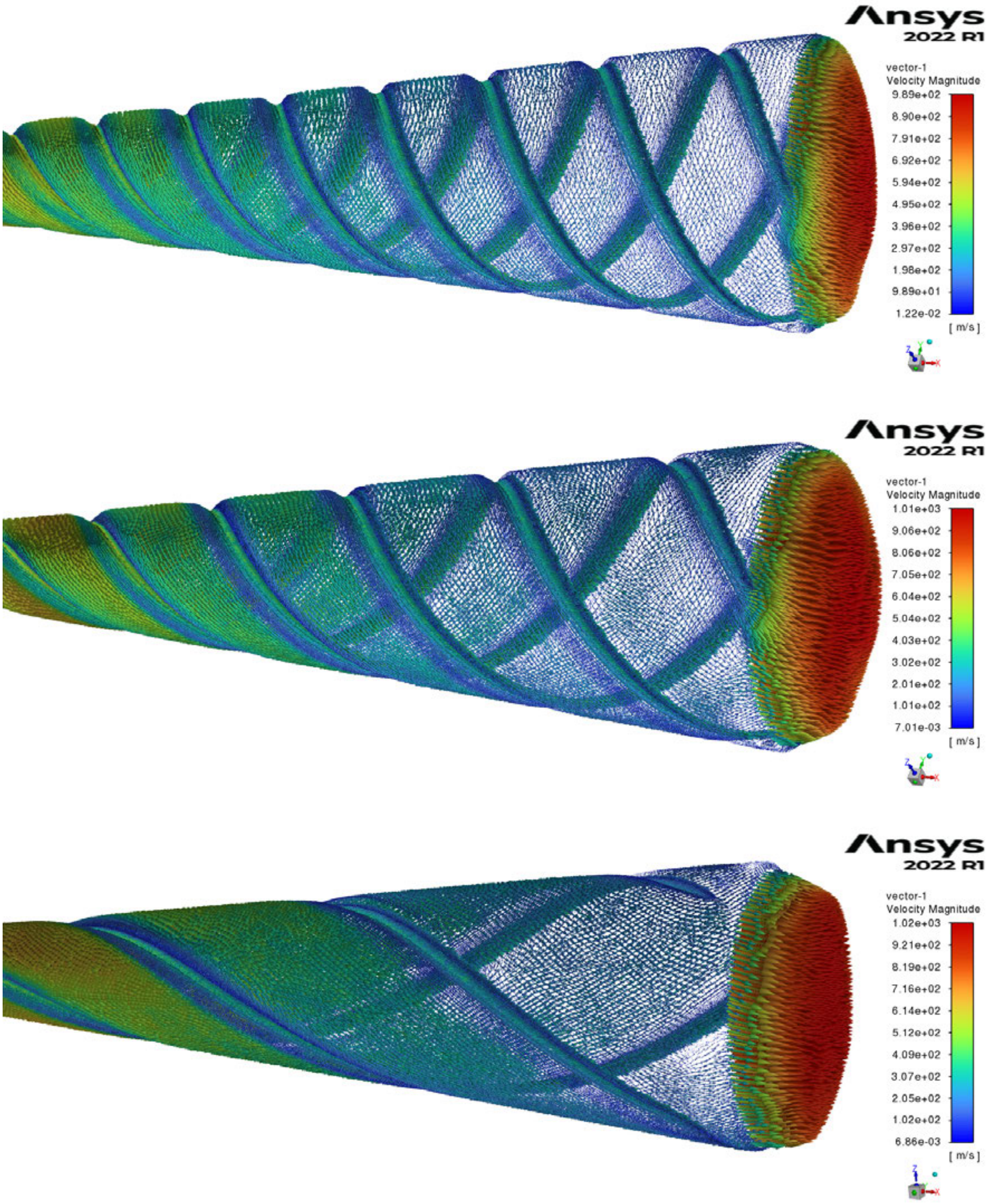

Figure 5.24: Velocity vectors showing flow behaviour in the primary nozzle at critical condenser pressure for all three generator nozzle variations. Pitch sizes: 17.5mm (top), 26.5mm (middle), 53mm (bottom).

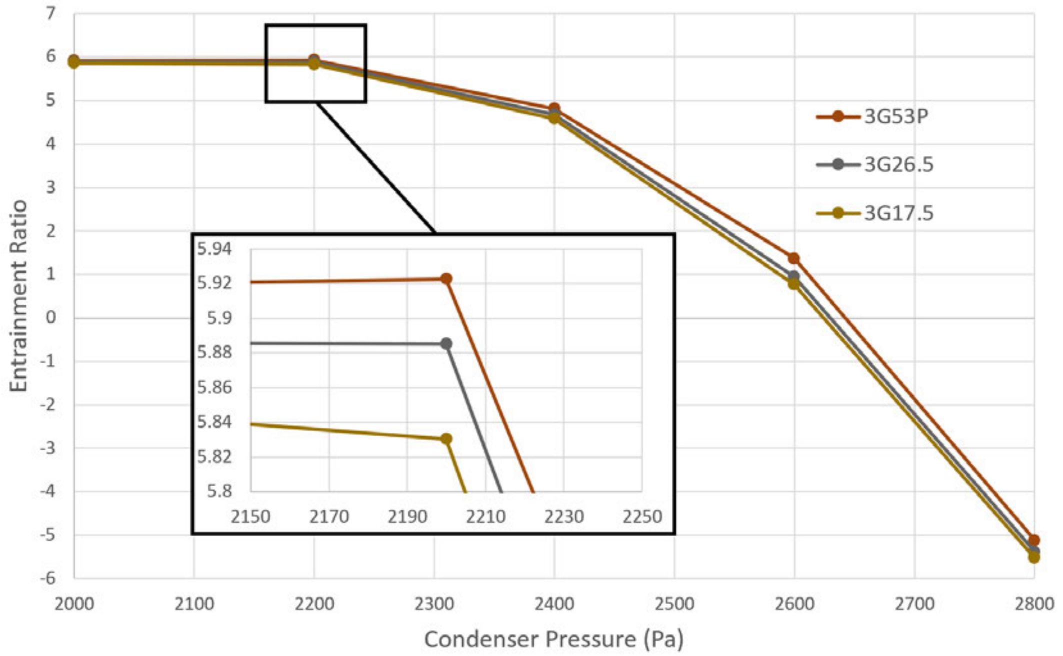

Figure 5.25: Entrainment ratio results plot for the three generator nozzle variations at 2kPa to 2.8kPa condenser pressures. Notation: 3G53P represents 3 generators with a 53mm pitch.

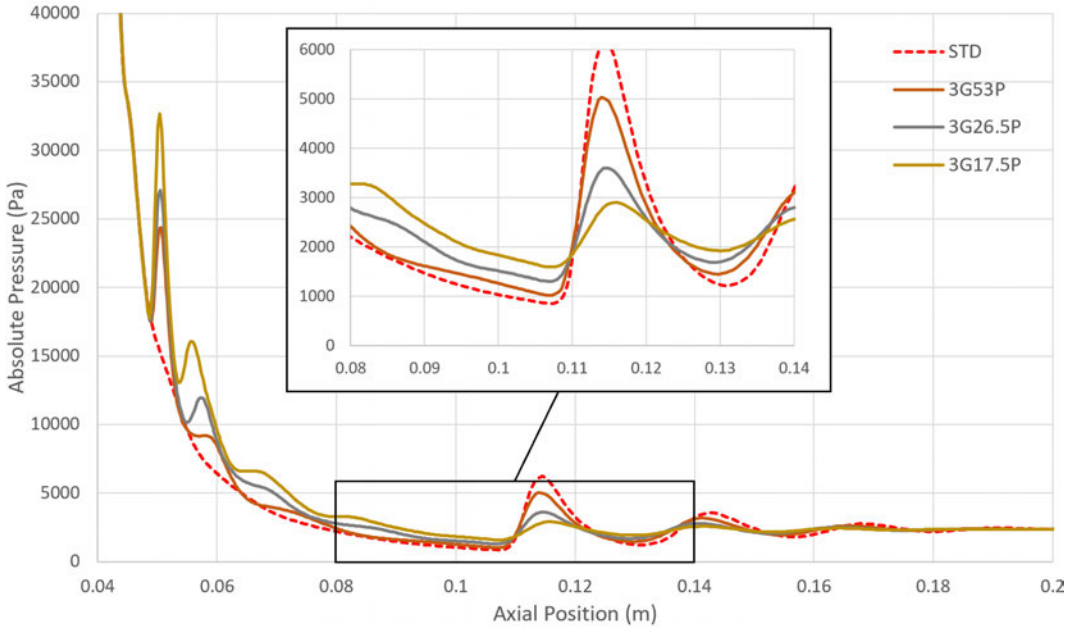

Figure 5.26: Comparison of the absolute pressure over the ejector centreline for the three generator nozzle variations. Notation: 3G53P represents 3 generators with a 53mm pitch, STD represents the standard model.

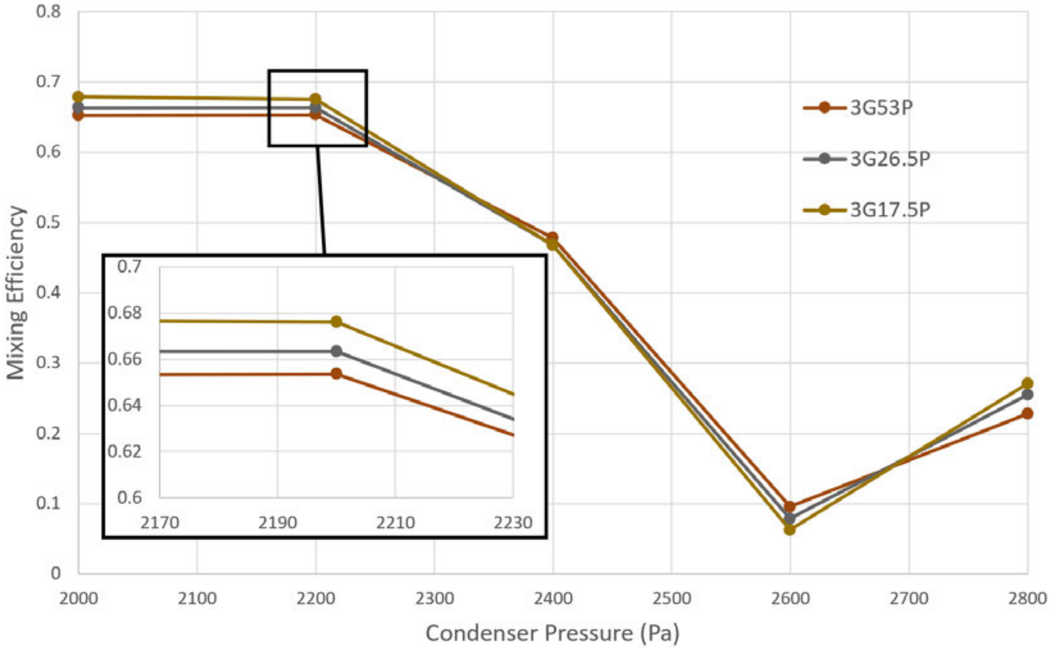

Figure 5.27: Mixing efficiency results plot for the three generator nozzle variations at 2kPa to 2.8kPa condenser pressures. Notation: 3G53P represents 3 generators with a 53mm pitch.

The plot presented in figure 5.26 shows the significant change in minimum pressure observed for the three generator models compared to the standard nozzle; the affect this had on the ejectors performance has been discussed in depth in Chapter 6. A comparison of the Mach number over the ejector centreline for the models has been included in the Appendix H along with the full entrainment ratio and mixing efficiency data relative to figures 5.25 and 5.27.

5.6 Chapter Summary

This chapter has delivered results obtained from the fluent simulations for the standard ejector model defined in Chapter 3 and those found through the parametric study carried out in Chapter 4. The results presented have provided a detailed perspective on the affects of the vortex generators on flow behaviour and ejector performance. A number of methods were used to convey the results such as streamlines, velocity vectors, contour plots and graphs. These figures are referred to in Chapter 6 as the results are analysed and implications are discussed.

Chapter 6

Discussion

6.1 Chapter Overview

This chapter delivers a discussion on the results, outlined in Chapter 5, obtained throughout the parametric study. Due to the significant number of models, this chapter segregates the results based on the number of generators in the primary nozzle and compares them to the standard ejector model. The trends observed for the modified nozzles are highlighted and the results are evaluated to determine the influence of the vortex generators on flow behaviour and ejector performance. The outcomes are compared to initial expectations and justification for the results is made based on evidence obtained in the CFD analysis. The reliability of the results produced from this research is also covered at the end of this chapter.

6.2 Standard Primary Nozzle Model

The simulations for the standard 3D ejector model demonstrated strong agreement with the 2D ejector model analysed as part of the methodology process in Chapter 3 (see figure 3.39). Observing the contour plot in figure 5.1 the oblique shocks are present subsequent to the primary nozzle exit as the high velocity of the steam decays into the mixing chamber. The first supersonic shock wave begins to form right at the end of the nozzle just before the exit. For the ensuing discussion, it is also worth noting that the primary stream shares a similar cross-sectional shape as the nozzle exit, which can be seen clearly by the streamlines shown in figure 5.2.

As the steam and nitrogen transfer energy, mass and momentum the mixing layer can be seen developing linearly over length of the mixing chamber, expanding outwards to the walls of ejector. The shear layer becomes fully developed right at the beginning of the diffuser in the convergent section; it is from this interaction with the wall and the reduced cross-sectional area that the recirculation in the mixing chamber originates. The recirculation is seen more clearly when analysing the flow using streamlines as shown in figure 5.3; where the radial vortex forms around the circumference at approximately midway of the mixing chamber. It was found during the simulations that the recirculation in the mixing chamber increases in unchoked operating conditions, which correlates with observations documented in the literature.

Conducting the simulations in ANSYS Fluent allowed the key performance characteristics to be extracted for each of the models. In order to gauge the effectiveness of the radial pressure gradient induced by the vortex generators, the data for absolute pressure across the centreline of the standard ejector was extracted and used as the standard of comparison in figures 5.12, 5.19 and 5.26. It was found that a minimum pressure of 902.38Pa occurred at approximately NXP +3mm which corresponds with the location that the peak Mach number of 3.96 is observed. This is an important factor, as a greater pressure difference to the secondary inlet promotes a stronger entrainment of passive flow.

Plotting the operating range of the standard ejector (see figure 5.4) revealed that it operates at its highest efficiency when the condenser pressure was set close to the critical pressure at approximately 2200Pa. At this pressure, the mass flow rates determined by Fluent for the primary and secondary flows were 1.8797 g/s and 11.17818 g/s, respectively. Using these values the maximum entrainment ratio for the model can be calculated as:

$$\omega_0 = \frac{\dot{m}_s}{\dot{m}_p} = \frac{11.17818}{1.8797} = 5.9467 \tag{6.1}$$

The entrainment ratio is consistently used throughout literature to gauge ejector performance as it is the driving factor for the coefficient of performance (see equation 2.2). The mixing efficiency of the ejector was also determined for the model and is plotted for over the whole operating range in figure 5.5. Predictably, the maximum mixing efficiency of the ejector was identified at the same back pressure as the maximum entrainment ratio. Extracting the necessary velocity values from the fluent results, the mixing efficiency observed for the the optimal condenser pressure can be calculated through equation 2.5 as:

$$\phi_{mix} = \frac{(\dot{m}_p + \dot{m}_s)v_{mix}}{\dot{m}_p v_{pe} + \dot{m}_s v_{se}} = \frac{(1.8797 + 11.1781) \times 138.2483}{(1.8797)(1024.9871) + (11.1781)(75.1110)} \tag{6.2}$$

$$\Rightarrow = 0.6495$$

Overall, the results obtained for the standard ejector simulations were congruent with expectations and provided a reliable foundation for comparison for the parametric study.

6.3 One Vortex Generator Primary Nozzle Models

In analysing the velocity vectors in fluent where the steam accelerates from the nozzle throat and meets the vortex generator, it is seen that the flow adapts to the generator profile smoothly, as designed. Boundary layer separation over the generator surface is, however, seen to increase throughout nozzle as fluid velocity increases (see figure 6.1). The resulting flow recirculation and wake regions on the down stream side of the generator is also intensified; this effect becomes stronger with the 17.5mm and 26.5mm pitches. This behaviour is known to negatively influence drag, which is evident in this case as the maximum velocity observed in the nozzle decreases with pitch size. A decrease in velocity at the primary nozzle exit is recorded for all one generator nozzles with a maximum reduction of 5.5% observed when compared with the standard nozzle.

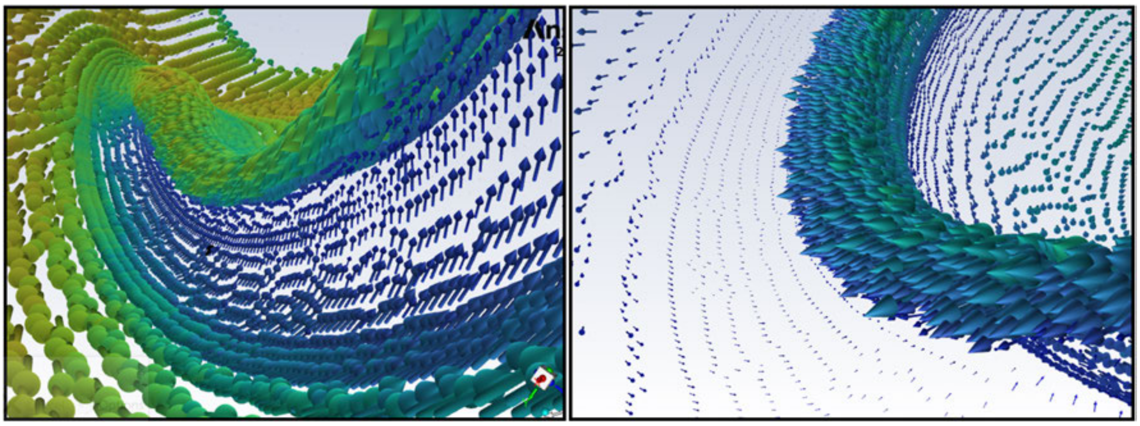

Figure 6.1: Wake region formed on downstream side of generator (26.5mm pitch) by boundary layer separation. At location: throat (left), outlet (right).

Another resultant of the generator can be seen when observing Mach number in figure 5.10. The decreased maximum velocity explains the reduction in peak Mach number by up to 20% compared to the standard nozzle, however, a shock wave type pattern begins to appear inside the nozzle. This is an effect that can be related back to the drag caused by the boundary separation where the generator forces the steam to quickly decelerate in a similar way to when it interacts with the passive fluid at the nozzle exit. This results in a shock wave type behaviour, shown visually in figure 5.6, which increases in intensity with the smaller pitch values.

Where the generator regresses at the end of the nozzle, figure 5.9 shows that the fluid following the vortical trajectory rapidly straightens before the nozzle exit. This effect is weaker on the flow for smaller pitches; it is expected that this occurs as more fluid particles are slowed down and are travelling in direction closer to the pitch. Further visualisation of this is shown in figure 5.8, where the streamlines show that the smaller pitch values produce a stronger swirling effect and maintain their trajectory for longer.

For the one generator design, the jet core is off-centre leading into the mixing chamber, as shown in figure 5.6. Analysing this behaviour using the streamlines, it was found that the jet core leaving the nozzle keeps the nozzle's relative cross sectional shape, maintaining a divot in the flow from the generator profile. Since the single generator does not have a symmetric influence on the flow, the jet core exits the nozzle at an angle in the direction opposite the end point of the generator; the angle was increased for smaller pitches. This is an undesirable effect, and is believed to contribute significantly to the poor performance that was recorded for the one generator models.

Another byproduct of off-centre flow is that the recirculation in the mixing chamber was almost completely eradicated on one side and is significantly increased on the opposite side compared to the standard nozzle (see figure 5.7 and 5.3). It can be seen that this recirculation intensifies as the pitch is reduced and flow becomes more off-centre. Furthermore, the analysis revealed that reversed flow was present in the diffuser across the entire operating range of the ejector, this behaviour has been captured in figure 6.2. This is believed to occur due the jet core from the nozzle being directed into the wall, and an infliction point is created in the divergent section of the diffuser where the flow detaches, initiating recirculation. The maximum reversed flow values in the choked conditions were recorded at the lowest condenser pressure for all models; the highest value was 3.9% recorded for the 26.5mm pitch model.

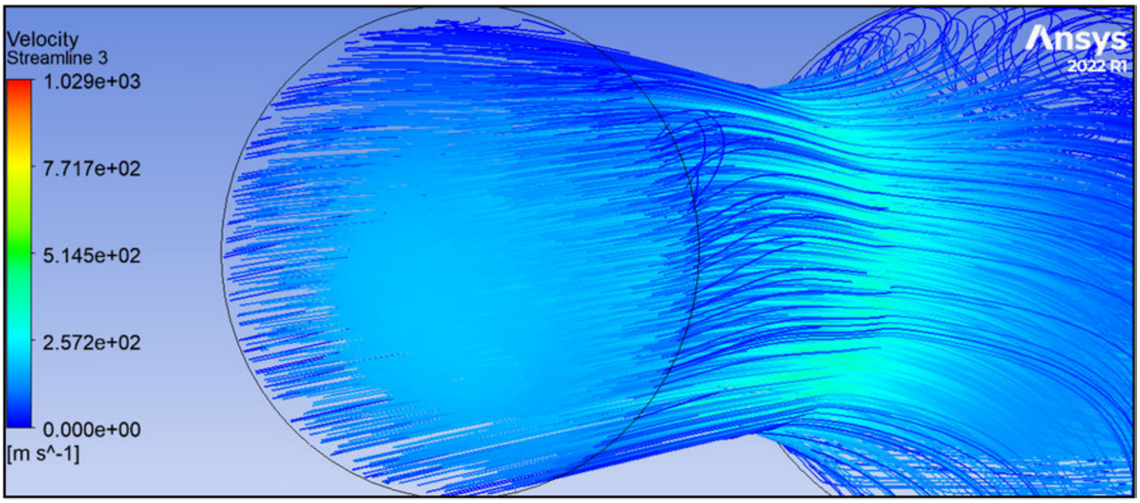

Figure 6.2: Velocity vectors showing the reversed flow occurring in the diffuser for the one generator model with a 26.5mm pitch.

The operating ranges for the one generator equipped nozzles plotted in figure 5.11 revealed that the resulting change was exiguous. The optimal operating condition was selected as the point with the lowest reversed flow recorded in the diffuser before the critical point; this was identified at 2200Pa condenser pressure. It was found that the entrainment ratio was reduced by more than 0.3% for all one generator models, indicating that the coefficient of performance was hindered compared to the standard nozzle. The minimum pressure on the ejector centreline was actually increased by 133.3 Pa for 53mm and up to 177.8 Pa for 17.5mm (see figure 5.12); this explains the reduced secondary entrainment that was observed.

The mixing efficiency calculations appear off-trend which is believed to be due to the complex flow behaviour caused by the off-centre jet core trajectory and the method used to extract the velocity value from a point on the centreline at the end of the mixing chamber. Figure 5.13 shows that the maximum mixing efficiency appears to decrease for the 53mm pitch and more substantially for the 26.5mm pitch, however, increases for the 17.5mm pitch. In order to gauge the effectiveness of the mixing, a visual comparison observing the mole mass fraction distribution in ANSYS Fluent was used that suggested the mixing was less effective than for the standard nozzle.

In conclusion, the one generator nozzle design was found to negatively impact almost all aspects of the ejectors performance. The off-centre jet core created a number issues as discussed above, making the one generator model clearly unviable for application or further consideration. The analysis of these results supported the initial expectation that multiple generators would be a better platform for improving ejector performance.

6.4 Two Vortex Generator Primary Nozzle Models

Analysing the fluid flow from the beginning of the vortex generators, it is seen that the initial contact with the generator profile is clean, and not abrupt or disruptive. Velocity vectors revealed that the boundary separation commenced at an earlier location than previously observed with the one generator nozzle. Additionally, for the 59.5mm pitch variation, the fluid particles appear to follow the generators more effectively (see figure 5.16), travelling more consistently with the smaller helix angle. Looking further up the divergent nozzle, the disparity between vector paths became visibly worse for both the 26.5 and 17.5mm pitches. This was attributed to the fact that as pitch angle increases more fluid is forced over the top of the generator, relying more on the guided flow to change its trajectory.

The shock wave effect was present inside the primary nozzle for all two generator variations; where the Mach number and maximum recorded velocity were reduced as a result. This was worsened with smaller pitches, as the fluid impacts the generator at a more direct angle which increases the period of boundary layer separation that occurs before reattachment. Inspecting the results for the 17.5mm pitch, the velocity through the nozzle was reduced by 4.4% and over 19% for Mach number when compared to the standard nozzle (refer to figure 5.17). At the end of the generators in the nozzle, the flow quickly begins to straighten; this behaviour increases in prominence for smaller pitch angles (see figure 5.16). The cause of this is the large volume of high velocity fluid particles travelling through the centre of the nozzle that are not directly influenced by the generators.

The streamlines shown in figure 5.15 reveal that the desired swirling effect looks to rapidly decay after exiting the nozzle, lasting noticeably longer for smaller pitch values. In the case of the nozzle with a 17.5mm pitch, the flow appears to have completely straightened by approximately NXP+ 200mm into the mixing chamber. Similar to the observation of the one generator nozzle, the profile of the generators are imprinted on the shape of the jet core (see figure 6.3). Where the core cross section is deformed into an flattened oval shape, however, the trajectory of the flow is more centred for the two generator nozzles.

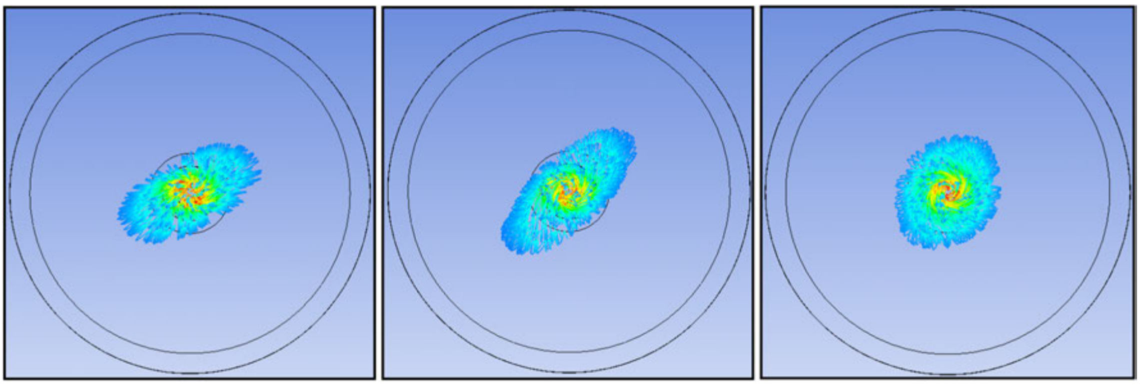

Figure 6.3: Jet core cross sections created by the two generator nozzle variations. Pitch sizes: 53mm (Left), 26.5mm (Middle), 17.5mm (Right).

Further examination of the streamlines also showed that the recirculation is increased in the mixing chamber compared to the standard nozzle. In the case of the two generator models, the recirculation improves with pitch decrease as the flat shape of the core starts to become more circular, however, the streamlines appear more turbulent and unpredictable (see figure 5.14). The same trend was also observed for the reversed flow occurring in the diffuser at condenser pressures lower than the critical pressure. This was similar to that of the standard nozzle, however, it was present for all of the tested condenser values lower than 2200Pa.

The operating range plotted in figure 5.18 and 5.20 shows that for the 17.5mm and 26.5mm pitch models, the highest entrainment ratio and mixing efficiency values are seen at 2000Pa condenser pressure. This was also recorded for the standard ejector at 1800Pa, however, at this pressure 0.4% reversed flow occurs in the diffuser which contradicts the boundary conditions set for the diffuser outlet, potentially reducing the accuracy of the result. Thus, the optimal operating condition is taken as the first point in the choked region that no reversed flow is detected in the diffuser.

The entrainment ratio of the ejector was found to decrease for all two generator models; the 17.5mm pitch nozzle showed the worst result with a 2% decrease compared to the standard nozzle. Moreover, the minimum absolute pressure over the centreline (refer to figure 5.19) was found to be increased compared to the standard nozzle, increasing more for larger pitch values. This is explained by Bernoulli's equation which states that as velocity decreases the pressure will increase; the maximum velocity is reduced by using smaller pitches as mentioned previously. This agrees with the findings that secondary mass flow rate is reduced for the two generator models and that the performance is subsequently hindered.

The calculations determined that the 59.5mm pitch reduced the mixing efficiency, whilst the 26.5mm and 17.5mm pitches saw improvement over the standard nozzle. At a condenser pressure of 2200Pa, the mixing efficiency for the 17.5mm generator pitch experienced a 2% increase over the standard nozzle. From the results collected in this research, it could be concluded that the method of calculation for the mixing efficiency becomes more reliable with symmetrical shaped jet cores travelling along the centreline.

In conclusion, it can be said that the two generator nozzle models negatively impact the coefficient of performance of the ejector, however, they provide a better mixing efficiency compared to the standard nozzle. These results formed the expectation that perhaps a nozzle equipped with three generators would create a stronger and longer lasting swirling effect to reduce the pressure at the nozzle outlet.

6.5 Three Vortex Generator Primary Nozzle Models

From the previous observations, it was expected that increasing the number of generators in the divergent nozzle would result in a slightly more turbulent initial transition for the fluid. The velocity vectors in figures 5.24 show this to be true, with the boundary layer separation initiating almost immediately after the generator is fully protruded for the 59.5mm pitch and before this point for the smaller pitches. This trend continues throughout the length of the generator, with the wake regions enlarging for larger pitch angles; this is shown clearly in the contour plots in figure 5.21.

Once again the shock wave effect is identified within the nozzle and a 0.93%, 12.8% and 19.8% decrease in maximum Mach number observed for the 17.5, 26.5 and 53mm pitch models, respectively. On the basis of that, it was expected that a velocity loss through the nozzle also occurs for the three generator nozzle variations which recorded a maximum of 43m/s (or 4.2%) slower over the standard nozzle. Referring back to Chapter 4, the 53mm pitch three generator nozzle followed the same end profile as the previous models, which figure 5.24 shows the flow begins to straighten after the generator ends in the nozzle. The

26.5 and 17.5mm pitch nozzles required an alternative generator end profile that extends to the end of the nozzle. This design reduced the straightening effect, however, a significant recirculation region appeared on the downstream side of the generator right at the nozzle exit; this is shown more clearly in figure 6.4.

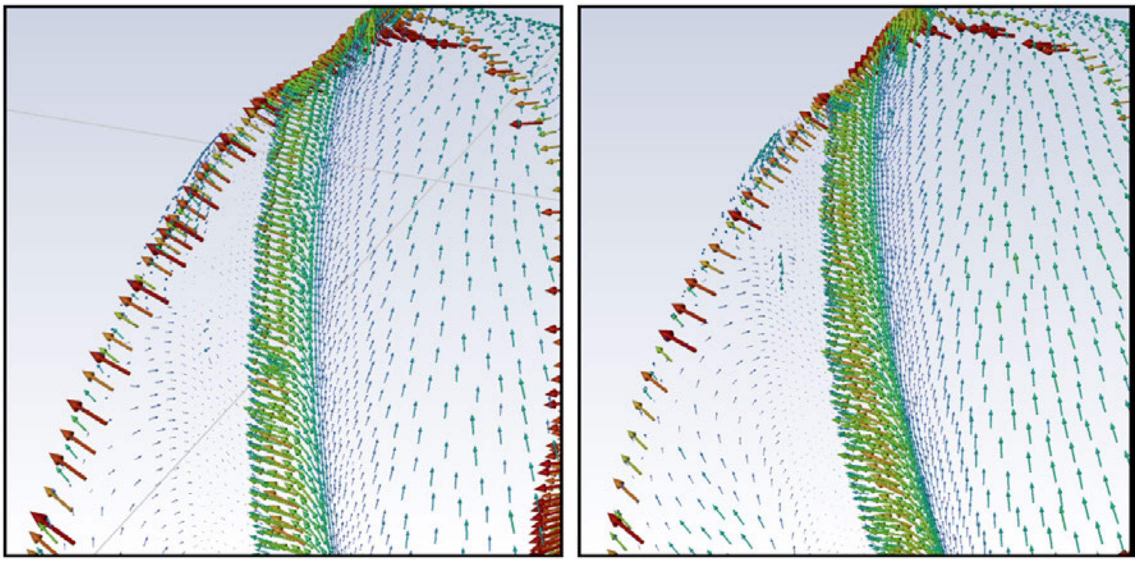

Figure 6.4: Velocity vectors showing the flow trajectory and recirculation at the nozzle exit for the three generator nozzles. Pitch sizes: 17.5mm (Left), 26.5mm (Right).

Additionally, it can be seen that slight recirculation is observed right around the circumference of the nozzle exit (see figure 6.4) for all models. This is believed to be an effect of largest shock wave leading into the mixing chamber that begins just inside the nozzle exit. The shock train into the mixing chamber can be seen clearly in figure 5.21, where magnitude of each wave is visibly reduced as a result of decreasing the pitch.

Even with three vortex generators influencing the flow it is found that the swirling trajectory of the steam begins to relapse shortly after exiting the nozzle and a full vortical rotation is not achieved inside the mixing chamber. This is shown most clearly in the streamlines in figure 5.23. It can also be seen that the three generator configuration produces a triangular shaped jet core, however, it maintains a centred trajectory over the entire length of the ejector.

Further analysis of flow behaviour through the streamlines in figure 5.22 show the influence of the three generator variations on recirculation in the mixing chamber. Initially, it was assumed that the streamwise vortex induced by the generators would break down the radial vortices in the mixing chamber, however, the recirculation was increased. This may be due to the generators not creating a long lasting vortex and reducing the flow velocity, where it was found in the standard model that reducing the velocity (ie. in the unchoked region) actually increased recirculation. Similarly to the two generator nozzle, the recirculation appeared more turbulent with larger radial vortices forming on the sides of the cores triangular shape (refer to figures 5.22). Another observation was that the odd the shape of the jet core caused increased recirculation in the diffuser in choked conditions.

The operating range plotted in figure 5.25 determined that there didn't appear to be a significant shift in operating range when compared to the standard nozzle. It was found that the critical point remains at approximately the same location for the modified nozzles as for the standard nozzle. Since minimal fluctuation in secondary entrainment occurs within choked operating conditions, the optimal operating point was taken at the condenser pressure of 2200Pa , which recorded no reversed flow.

Figure 5.25 shows that the maximum entrainement ratio was reduced by between 0.4% and 2% for the three generator nozzles; decreasing in performance with the lower pitch values. Once again, it was found that the absolute pressure reading on the centreline at the nozzle exit was increased by up to 46.1% compared to the standard nozzle (refer to figure 5.26). Analysing the results for mixing efficiency (see figure 5.27) calculated using equation 2.5, it was determined that increasing the pitch would see an improvement of up to 2.66%. Where the mixing efficiency appears to increase for nozzles using a smaller generator pitch.

Overall, the results indicate that the performance of the ejector would be reduced if any of the three vortex generator variations were implemented in the primary nozzle. The only potential improvement that was observed was an increased mixing efficiency over the standard ejector; the potential implications of this result will be discussed further in the following section.

6.6 Modified Nozzle Comparison

In summary, when comparing all variations of the one, two, and three generator models it is clear that they exhibit similar trends regarding their influence on flow behaviour. The smooth transition of the flow from the nozzle throat to the vortex generator observed for all models indicates that the gradual rise and profile of the generators is appropriate for the application. It was a common finding that the boundary layer separation increased over the surface of the generators further down the nozzle and was worsened as the pitch was increased and also as more generators were added. This was supported by observing the maximum velocities through the nozzle, with also tended to decreased as lower pitches and more generators were used.

With regards to vortex longevity, it was found that decreasing pitches and increasing the number of generators improved the longevity. The 26.5mm and 17.5mm pitched three generator models using the alternative profile reduced the amount of angle lost in the nozzle and showed to increase the duration of the swirling trajectory. The shape of the jet core and its trajectory relative to the centreline was found to have a significant influence on recirculation in the mixing chamber and reversed flow in the diffuser. In the case of the one and two generator models this proved to be a major issue, with the three generator design confirming that more generators result in a better shape and more centralised trajectory that reduces turbulence and unpredictability in the mixing chamber.

By analysing the key performance characteristics from the results, clear trends can be identified; where the impact of the vortex generator variations on the maximum entrainment ratio is the main focus of this research. Thus far in the discussion it has been a common trend that smaller pitch values have reduced the performance, and when comparing the one, two and three generator model's entrainment ratios it is clear that including more generators further decreases the entrainment ratio. This is shown clearly in figure 6.5 which outlines the percentage difference for each model compared the the standard ejector. The exception to this trend was the one generator design, which produced significantly more unstable flow behaviour compared to the two and three generator design, as discussed previously.

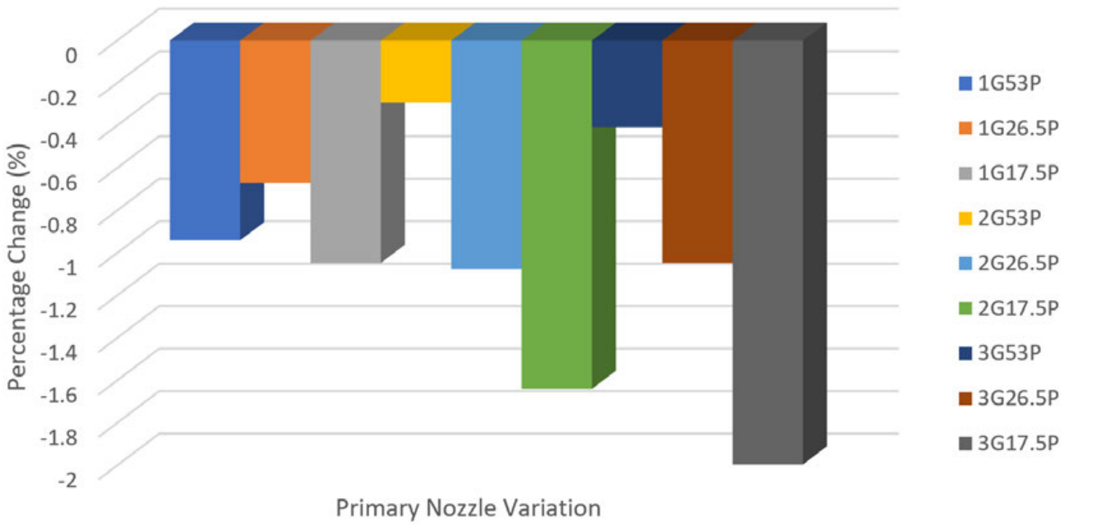

Figure 6.5: Percentage change of the entrainment ratio for all of the vortex generator variations compared to the standard nozzle. Where: Percentage Change (%) $= \frac{Standard-Modified}{Standard} \times 100$.

This decrease in entrainment ratio is not unexpected when the velocity and pressure differences are analysed for the modified nozzles compared to the standard nozzle. Its clear that increasing the pitch and number of generators shows a decrease maximum velocity and, concomitantly, an increase in minimum pressure. This indicates that the restriction caused by the vortex generators has a greater influence than the radial pressure gradient effect created by them, ultimately resulting in a decreased entrainment ratio. The analysis of the streamlines from Chapter 5 supports this, showing that the even for three generator nozzle the induced vortex was weak and faded rapidly inside the mixing chamber.

One of the main outcomes initially expected from the vortex generators was an enhanced mixing effect between the primary and secondary streams. The mixing efficiency determined at maximum operating conditions increased in most cases; figure 6.6 shows that smaller pitches and more generators tended to produce a higher percentage change. Once again, the one generator results appear off trend for reasons discussed earlier in this chapter. With the mixing efficiency calculation based on momentum transfer, the positive trend indicates that less frictional losses are incurred in the mixing chamber. The fundamental cause of this, was found to be the decreased primary flow velocity which was observed as a direct result of the vortex generators in the nozzle.

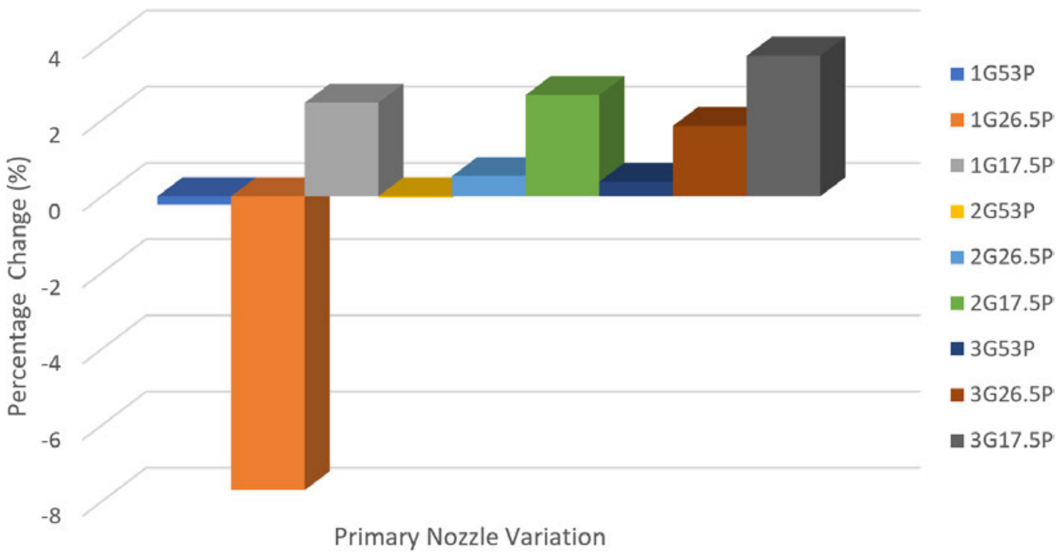

Figure 6.6: Percentage change of the mixing efficiency for all of the vortex generator variations compared to the standard nozzle. Where: Percentage Change (%) $= \frac{Standard - Modified}{Standard} \times 100$.

To further investigate the influence of the vortex generators on mixing, the mass fraction of nitrogen was taken at a point at the end of the mixing chamber at the optimal operating conditions for all models. For the standard nozzle ejector, area-weighted average of 0.84567 for nitrogen and 0.1547 for water-vapour was measured at the location. Figure 6.7 shows, the concentration of nitrogen appears to decrease for all modified nozzles, indicating that the mixing quality is consistently reduced.

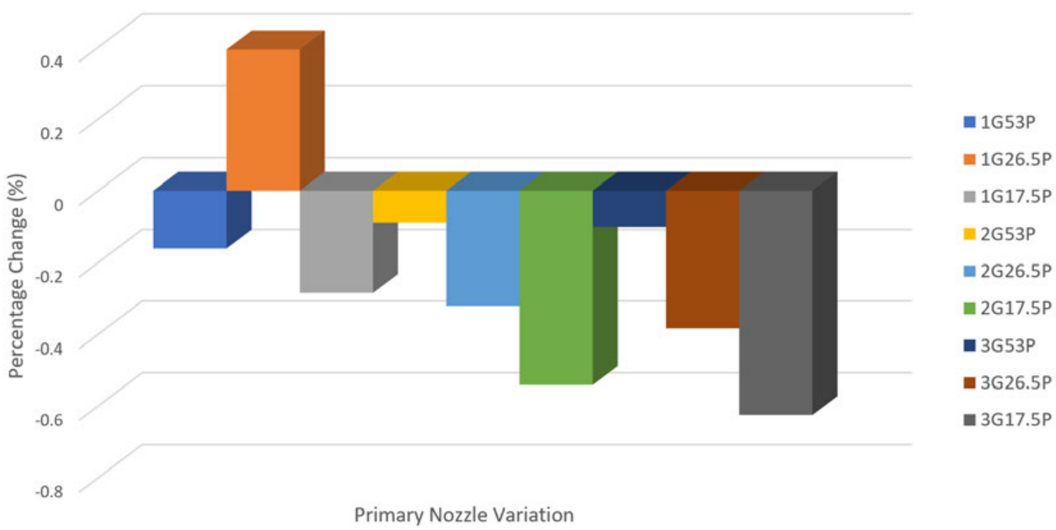

Figure 6.7: Percentage change of the mass fraction of nitrogen at the end of the mixing chamber for all of the vortex generator variations compared to the standard nozzle. Where: Percentage Change (%) $= \frac{Standard - Modified}{Standard} \times 100$.

The integrity of these results is strengthened by the increase in recirculation in the mixing chamber observed across the board, with recirculation being reported in the literature as a factor leading to a lower mixing quality. Interestingly, these results indicate that the quality of the mixture actually decreases with more generators, despite the streamlines indicating the opposite trend for recirculation. Through these results, a relationship between the reduced mixing quality and the lower frictional losses and velocities have been drawn, where another key indicator of mixing quality is the mixing layer development. Whilst the differences in the rate of development were difficult to detect from the simulations, the literature review revealed that reduced velocities are linked to a slower mixing layer growth rate and, therefore, a reduced mixing quality (Al-Manea 2019) .

Based on the entrainment ratios recorded for each of the modified nozzles, it can be concluded that the performance of the ejector is hindered by all combinations of the vortex generators. In general, the entrainment ratio is found to be reduced as the pitch is decreased and as more generators are added. The opposite effect has been observed for the maximum mixing efficiency, with improvement over the standard nozzle being recorded consistently for the two and three generator nozzles. Conversely, analysis of the simulation results indicated that quality of the fluid mixture decreased with smaller pitches and more generators.

6.7 Results Reliability

The reliability of CFD modelling, specifically in ANSYS Fluent, is largely dependent on the controls put in place by the user. Without a process for ensuring dependable results, the research could be misleading and could potentially be dangerous. For this study, the CFD model, mesh independence and boundary conditions were key considerations regarding the reliability. Additionally, analysis of the residuals throughout the simulations is another crucial aspect to ensuring the results are an acceptable level of accuracy.

The geometry validation, model descritization and boundary condition selection process was discussed in detail throughout Chapter 3. The results found maximum percentage change of entrainment ratio 2% was observed for the modified nozzles, producing realistic values when compared to experimental and CFD results obtained by studies investigated throughout the literature review. Furthermore, the mixing efficiency of ejectors typically fall within the $50 - 70\%$ range throughout the literature which is consistent with results found in this study. With differences between values occurring at the 4th or 5th significant figure in some cases, the results could be vulnerable to numerical error which should be acknowledged as a possible reason for unexpected deviations from trends.

Another important part of the reliability management is monitoring the residuals when running the simulations. Although the residuals were set to converge at 1e-6, this was not always achieved in the simulations and was found to be affected greatly by the boundary conditions. As the condenser pressure approached the breakdown pressure the residuals were often flattening earlier; this was most prevalent in the one generator models and models with smaller generator pitches. In these circumstances, typically the continuity equation, which is reflective of the conservation of mass in the model, would be the only residual not to reach 1e-6 for convergence. Thus, the most reliable and accurate results are those taken at pressures closest to the critical point. At this range the residuals converged or reached at least 3e-6 for all modified models; aligning with the recommendations of ANSYS (2021*b*).

With the focus of this study primarily on the choked region of operation, the accuracy of the simulation results can be considered acceptable and the results reliable enough to deliver a conclusion on the topic. The key limitations encountered during the research is discussed in more detail the conclusion presented in Chapter 7.

6.8 Chapter Summary

This chapter has discussed the results presented within Chapter 5, and provided insight to the process followed and methods used to analyse the results. Each variation of the modified ejectors was discussed based on the number of generators in the primary nozzle and compared to the results obtained for the standard 3D nozzle. The overall influence of the generator variations on the performance of the ejector was discussed in terms of flow behaviour, entrainment ratio and mixing efficiency, and quality. Finally, considerations regarding the reliability and accuracy of the results were also addressed.

Chapter 7

Conclusions

7.1 Motivation

Steam jet ejectors are a promising replacement for compressors in air conditioning and refrigeration applications due to their relative simplicity, high reliability and low capital costs. A fundamental reason ejectors have not yet been completely adopted is their low efficiency when compared to the standard mechanical compressor; this is attributed to the effects of supersonic mixing. Extensive research exists within the literature regarding geometric modifications and experiments with operational factors aimed at improving the coefficient of performance of the traditional jet ejector with few significant breakthroughs.

This dissertation aimed to influence a vortex in the motive flow using guide vane style generators in the primary nozzle. The ideal outcome of this modification was to generate a greater pressure gradient between the primary and secondary flows, promoting an increase in the entrainment ratio. The findings of this paper are intended to contribute to journal proceedings currently being prepared by the University of Southern Queensland.

7.2 Project Conclusions

The completed dissertation successfully showed the influence of a primary nozzle vortex generator on the performance of an ejector. This involved initially the generation and verification of a 2D CFD model based on the UniSQ steam ejector refrigeration apparatus against previous research conducted by Al-Manea (2019) and Al-Doori (2013). This 2D model achieved within 5% agreement for the primary and secondary mass flow rates obtained by Al-Manea (2019) in unchoked conditions. Following this, the baseline ejector was successfully characterised as a 3D CFD model in ANSYS Fluent following an extensive discretization process. The 2D and 3D models simulation results were within 1% variation in choked conditions and 10% in unchoked conditions. The operating range was defined through simulations at a constant primary pressure of 150kPa and secondary pressure of 2.4kPa and varying condenser pressure between 1.8kPa and 2.8kPa. The maximum entrainment ratio of approximately 5.95 at 2.2kPa back pressure was recorded and set as the standard for comparison. Simulations were performed using the UniSQ HPC which maximised computational efficiency and increased the depth of the research.

The main focus of this research is the parametric study conducted on the primary nozzle vortex generator design that delivered results specific to different combinations of profiles, pitches and quantity. Varying the pitch between 59.5mm and 17.5mm and the number of generators from 1 to 3, was found to largely cause a decrease in the entrainemnt ratio; with the reduction of between $0.67-2\%$ observed over the standard model. Simulations revealed that the mixing efficiency, based on momentum conservation, could be increased by between $0.22-3.7\%$ with the maximum increase obtained by incorporating three vortex generators with 17.5mm pitches into the primary nozzle. A decline in mixing quality of up to 0.6% was observed for modified nozzles with lower pitches and more generators. Overall, the results of the computational analysis indicated that the vortex generator designs used in this study had a negative influence on steam ejector performance for refrigeration applications.

7.3 Final Statements

An increased pressure at the nozzle outlet due to the interaction of the high velocity steam with the vortex generators in the nozzle, resulted in a decreased entrainment ratio and overall performance compared to the existing UniSQ ejector model. Some general summarising statements are delivered reflecting the results found and discussed in this dissertation:

1. A gradually introduced and large radius curvature used for the generator profile

produced a smooth transition for the steam.

2. Extending the end profile of a generator through to the nozzle exit increased vortex longevity and reduced decay.
3. More vortex generators increased vortex longevity and provided a rounder jet core shape that produced less turbulent behaviour across the operating range compared to nozzles equipped with less generators.
4. Use of one generator caused an asymmetric, off-centre jet core that enhanced recirculation in mixing chamber and diffuser.
5. Lower pitch values increased boundary layer separation and wake regions, reducing flow velocity.
6. Lower pitch values increased the vortex longevity into the mixing chamber.

7.4 Project Limitations and Further Work

This dissertation has delivered highly theoretical results that adds further understanding of ejector operation and can be used to guide the direction of future research on steam ejector performance. Whilst all initially specified project aims and objectives were met, due to the theoretical nature of this research there are limitations regarding its use. There also remains a range of potential areas of future research that could be conducted to further strengthen the hypothesis of this research and also to investigate other possible avenues for improving the performance of ejectors through vortex generators.

7.4.1 Project Limitations

Modified CFD Models

Although a grid independence study was conducted for one of the modified nozzles, this mesh was used universally across all modified variations of the primary nozzle and is identified as a potential limitation. Due to the substantial amount of simulations required in the parametric study alone, time did not allow for an individualised mesh to be generated for each model. Ensuring mesh independence is achieved is imperative for maintaining a high level of accuracy and reliability in results.

Data Collection

Another key limitation that can be found in the results is the range of data collected. The significant workload and computational size of the models posed time restraints on the amount of simulations that could be performed. Additionally, the time taken to gain access and familiarise with the HPC environment detracted significantly from the time allowance. This has been addressed within Chapter 3 and a detailed guide has been included in this dissertation to aid future undergraduate research. It is possible that collating more data points could result in the formation of new trends and, consequently, affect the outcome of the results.

7.4.2 Further Work

Alternate Generator Geometry

Analysis of the streamlines during post-processing indicate that the effect of boundary layer separation over the generator surface reduces flow velocity. It is suggested that in future work, the cross section of the generator is altered to include a larger radius or more gradual decline on the downstream side. This modification could combat the recirculation and wake region typically observed in that area, thus helping to reduce the drag through the nozzle. Other geometrical changes such as increased pitch values and more subtle generator profiles may also be worth investigating for this purpose.

Model Selection and Boundary Conditions

A recommendation for future work includes employing a wet steam model for the analysis of the supersonic steam ejectors. The use of the wet steam model allows for the simulation of the condensation phenomenon that occurs inside the nozzle as the steam changes phase. Whilst this model provides a number of benefits including a more accurate reflection of reality, it was not considered necessary to achieve the reliable outcomes required for this dissertation. Furthermore, experimenting with alternate boundary conditions, such as lower primary pressures, would determine if the generators are more effective with lower velocities. This feedback would provide insight into whether alternate generator geometries are an avenue worth further investigation for high velocity flow.

Experimental Investigation

Development of physical models of the modified nozzles and fitting them to the UniSQ steam ejector refrigeration apparatus to conduct experimental testing would significantly help the verification of the results. Additionally, pairing this with visualisation techniques such as TDLAS, PLMS or the Schlieren method would provide a more detailed understanding of the influence of the generators on flow behaviour. This of course is not feasible until further CFD analysis on the areas mentioned above has been completed and results are obtained indicating the possibility of improved ejector performance.

References

Abdulateef, J., Sopian, K., Alghoul, M. & Sulaiman, M. (2009), 'Review on solar-driven ejector refrigeration technologies', *Renewable and Sustainable Energy Reviews* **13**(6-7), 1338–1349. DOI: .org/10.1016/j.rser.2008.08.012.

Al-Doori, G. F. L. (2013), Investigation of Refrigeration System Steam Ejector Performance through Experiments and Computational Simulations, Master's thesis, University of Southern Queensland, Toowoomba, Australia. `https://eprints.usq.edu.au/23675/1/Al-Doori_2013_whole.pdf`.

Al-Manea, A. R. H. (2019), Supersonic Condensing Steam Jet Measurements Using TDLAS, PhD thesis, University of Southern Queensland, Toowoomba, Australia. `https://eprints.usq.edu.au/43755/1/Ahmedthesis_revised_final%20version.pdf`.

Alsagri, A. S., Alrobaian, A. A. & Almohaimeed, S. A. (2020), 'Concentrating solar collectors in absorption and adsorption cooling cycles: An overview', *Energy Conversion and Management* **223**, 1–27. DOI: .org/10.1016/j.enconman.2020.113420.

ANSYS (2021*a*), *ANSYS Fluent Tutorial Guide*.

ANSYS (2021*b*), *ANSYS Fluent User's Guide*.

Aphornratana, S., Chungpaibulpatana, S. & Srikhirin, P. (2001), 'Experimental investigation of an ejector refrigerator: effect of mixing chamber geometry on system performance', *International journal of energy research* **25**(5), 397–411. DOI: 10.1002/er.689.

Aravind, T., Reddy, P. R. & Baserkoed, S. (2014), 'Thermal analysis of steam ejector using cfd', *International Journal of Innovative Research in Science, Engineering and Technology* **3**(12), 18311–18318. DOI: 10.15680/IJIRSET.2014.0312076.

Ariafar, K. (2016), Simulation and measurement of condensation and mixing effects in steam ejectors, PhD thesis, University of Southern Queensland, Toowoomba, Australia. `https://eprints.usq.edu.au/32860/1/Ariafar_2016.pdf`.

Ariafar, K., Buttsworth, D., Sharifi, N. & Malpress, R. (2014), 'Ejector primary nozzle steam condensation: area ratio effects and mixing layer development', *Applied thermal engineering* **71**(1), 519–527. DOI: 10.1016/j.applthermaleng.2014.06.038.

Arun, K. M., Tiwari, S. & Mani, A. (2019), 'Experimental studies on a rectangular ejector with air', *International Journal of Thermal Sciences* **140**, 43–49. DOI: 10.1016/j.ijthermalsci.2019.02.014.

Atmaca, M. & Ezgi, C. (2022), 'Three-dimensional cfd modeling of a steam ejector', *Energy Sources, Part A: Recovery, Utilization, and Environmental Effects* **44**(1), 2236–2247. DOI: 10.1080/15567036.2019.1649326.

Bartosiewicz, Y., Aidoun, Z., Desevaux, P. & Mercadier, Y. (2003), Cfd-experiments integration in the evaluation of six turbulence models for supersonic ejectors modeling, *in* 'Integrating CFD and Experiments Conference, Glasgow, UK', Citeseer. DOI: 10.1.1.584.3454.

Berk, Z. (2009), Chapter 2: Fluid flow, *in* 'Food Process Engineering and Technology', Academic Press, San Diego, pp. 27–68. DOI: 10.1109/TIE.2015.2495292. **URL:** *https://www.sciencedirect.com/science/article/pii/B9780123736604000028*

Besagni, G., Cristiani, N., Croci, L., Guédon, G. R. & Inzoli, F. (2021), 'Computational fluid-dynamics modelling of supersonic ejectors: Screening of modelling approaches, comprehensive validation and assessment of ejector component efficiencies', *Applied Thermal Engineering* **186**, 116431. DOI: 10.1016/j.energy.2014.10.004.

Bouhanguel, A., Desevaux, P. & Gavignet, E. (2011), 'Flow visualization in supersonic ejectors using laser tomography techniques', *International journal of refrigeration* **34**(7), 1633–1640. DOI: 10.1016/j.ijrefrig.2010.08.017.

Britannica (2019), 'Injector — Encyclopedia Britannica', `https://www.britannica.com/technology/injector`. [Online; accessed March-2022].

Chang, Y.-J. & Chen, Y.-M. (2000), 'Enhancement of a steam-jet refrigerator using a novel application of the petal nozzle', *Experimental Thermal and Fluid Science* **22**(3-4), 203–211. DOI: 10.1016/S0894-1777(00)00028-5.

Chen, J., Havtun, H. & Palm, B. (2014), 'Screening of working fluids for the ejector refrigeration system', *International Journal of Refrigeration* **47**, 1–14. DOI: 10.1016/j.ijrefrig.2014.07.016.

Chen, W., Liu, M., Chong, D., Yan, J., Little, A. B. & Bartosiewicz, Y. (2013), 'A 1d model to predict ejector performance at critical and sub-critical operational regimes', *International journal of refrigeration* **36**(6), 1750–1761. DOI: 10.1016/j.ijrefrig.2013.04.009.

Chen, W., Shi, C., Zhang, S., Chen, H., Chong, D. & Yan, J. (2017), 'Theoretical analysis of ejector refrigeration system performance under overall modes', *Applied Energy* **185**, 2074–2084. DOI: 10.1016/j.apenergy.2016.01.103.

Chunnanond, K. & Aphornratana, S. (2004*a*), 'Ejectors: applications in refrigeration technology', *Renewable and sustainable energy reviews* **8**(2), 129–155. DOI: 10.1016/j.rser.2003.10.001.

Chunnanond, K. & Aphornratana, S. (2004*b*), 'An experimental investigation of a steam ejector refrigerator: the analysis of the pressure profile along the ejector', *Applied thermal engineering* **24**(2-3), 311–322. DOI: 10.1016/j.applthermaleng.2003.07.003.

Del Valle, J. G., Jabardo, J. S., Ruiz, F. C. & Alonso, J. S. J. (2014), 'An experimental investigation of a r-134a ejector refrigeration system', *International journal of refrigeration* **46**, 105–113. DOI: 10.1016/j.ijrefrig.2014.05.028.

Desevaux, P. (2001), 'A method for visualizing the mixing zone between two co-axial flows in an ejector', *Optics and Lasers in engineering* **35**(5), 317–323. DOI: 10.1016/S0143-8166(01)00020-3.

Elbel, S. (2011), 'Historical and present developments of ejector refrigeration systems with emphasis on transcritical carbon dioxide air-conditioning applications', *International Journal of Refrigeration* **34**(7), 1545–1561. DOI: .org/10.1016/j.ijrefrig.2010.11.011. **URL:** *https://www.sciencedirect.com/science/article/pii/S0140700710002720*

Evdokimov, O., Piralishvili, S. A., Veretennikov, S. & Guryanov, A. (2018), Cfd simulation of a vortex ejector for use in vacuum applications, *in* 'Journal of Physics: Conference Series', Vol. 1128, IOP Publishing, p. 012127. DOI: 10.1088/1742-6596/1128/1/012127.

Fabri, J. & Siestrunck, R. (1958), 'Supersonic air ejectors', *Advances in applied mechanics* **5**, 1–34. DOI: 10.1016/S0065-2156(08)70016-4.

Ghorbanian, S. & Nejad, S. J. (2011), 'Ejector modeling and examining of possibility of replacing liquid vacuum pump in vacuum production systems', *International Journal of Chemical Engineering and Applications* **2**(2), 91. http://ijcea.org/papers/82-A563.pdf.

Giacomelli, F., Biferi, G., Mazzelli, F. & Milazzo, A. (2016), 'Cfd modeling of the supersonic condensation inside a steam ejector', *Energy Procedia* **101**, 1224–1231. DOI: 10.1016/j.egypro.2016.11.137.

Graham Corporation (2022), 'Ejector Applications', `https://www.graham-mfg.com/graham-steam-jet-ejectors-applications`. [Online; accessed March-2022].

Guangming, C., Xiaoxiao, X., Shuang, L., Lixia, L. & Liming, T. (2010), 'An experimental and theoretical study of a co2 ejector', *International journal of refrigeration* **33**(5), 915–921. DOI: 10.1016/j.ijrefrig.2010.01.007.

Han, Y., Wang, X., Yuen, A. C. Y., Li, A., Guo, L., Yeoh, G. H. & Tu, J. (2020), 'Characterization of choking flow behaviors inside steam ejectors based on the ejector refrigeration system', *International Journal of Refrigeration* **113**, 296–307. DOI: 10.1016/j.enconman.2006.10.009.

Hemidi, A., Henry, F., Leclaire, S., Seynhaeve, J.-M. & Bartosiewicz, Y. (2009), 'Cfd analysis of a supersonic air ejector. part ii: Relation between global operation and local flow features', *Applied Thermal Engineering* **29**(14-15), 2990–2998. DOI: 10.1016/j.applthermaleng.2009.03.019.

Hong, W. J., Alhussan, K., Zhang, H. & Garris Jr, C. A. (2004), 'A novel thermally driven rotor-vane/pressure-exchange ejector refrigeration system with environmental benefits and energy efficiency', *Energy* **29**(12-15), 2331–2345. DOI: 10.1016/j.energy.2004.03.050.

Huang, B., Chang, J., Wang, C. & Petrenko, V. (1999), 'A 1-d analysis of ejector performance', *International journal of refrigeration* **22**(5), 354–364. DOI: 10.1016/S0140-7007(99)00004-3.

International Institute of Refrigeration (2015), 'The Role of Refrigeration in the Global Economy', `https://sainttrofee.nl/wp-content/uploads/2019/`

`01/NoteTech_29-World-Statistics.pdf#:~:text=Refrigeration%20and%20energy%20Electricity%20consumption%20for%20refrigeration%20and,about%2017%25%20of%20the%20overall%20electricity%20used%20worldwide.` [Online; accessed March-2022].

Karthick, S., Gopalan, J. & Reddy, K. (2016), 'Visualization of supersonic free and confined jet using planar laser mie scattering technique', *Journal of the Indian Institute of Science* **96**(1), 29–46.

Kong, F. S., Kim, H. D., Jin, Y. & Setoguchi, T. (2013), 'Application of chevron nozzle to a supersonic ejector–diffuser system', *Procedia Engineering* **56**, 193–200. DOI: 10.1016/j.proeng.2013.03.107.

Kumar, V. & Sachdeva, G. (2019), Experimental investigation of an ejector refrigeration system using r-134a, *in* 'Journal of Physics: Conference Series', Vol. 1240, IOP Publishing, p. 012168. DOI: 10.1088/1742-6596/1240/1/012168.

Li, A., Yuen, A. C. Y., Chen, T. B. Y., Wang, C., Liu, H., Cao, R., Yang, W., Yeoh, G. H. & Timchenko, V. (2019), 'Computational study of wet steam flow to optimize steam ejector efficiency for potential fire suppression application', *Applied Sciences* **9**(7), 1486. DOI: 10.3390/app9071486.

Little, A. B. & Garimella, S. (2016), 'Shadowgraph visualization of condensing r134a flow through ejectors', *International journal of refrigeration* **68**, 118–129. DOI: 10.1016/j.ijrefrig.2016.04.018.

Matsuo, K., Sasaguchi, K., Tasaki, K. & Mochizuki, H. (1981), 'Investigation of supersonic air ejectors: Part 1. performance in the case of zero-secondary flow', *Bulletin of JSME* **24**(198), 2090–2097. DOI: 10.1299/jsme1958.24.2090.

Mazzelli, F., Little, A. B., Garimella, S. & Bartosiewicz, Y. (2015), 'Computational and experimental analysis of supersonic air ejector: Turbulence modeling and assessment of 3d effects', *International Journal of Heat and Fluid Flow* **56**, 305–316. DOI: 10.1016/j.ijheatfluidflow.2015.08.003.

Mazzelli, F., Little, A., Garimella, S. & Bartosiewicz, Y. (2016), Condensation in supersonic steam ejectors: comparison of theoretical and numerical models, *in* 'International Conference on Multiphase Flow, ICMF'.

McMullan, W. (2018), 'Spanwise domain effects on streamwise vortices in the plane turbulent mixing layer', *European Journal of Mechanics-B/Fluids* **67**, 385–396. DOI: 10.1016/j.euromechflu.2017.10.007.

Meyer, A., Harms, T. & Dobson, R. (2009), 'Steam jet ejector cooling powered by waste or solar heat', *Renewable Energy* **34**(1), 297–306. DOI: 10.1016/j.renene.2008.03.020.

Milazzo, A. & Rocchetti, A. (2015), 'Modelling of ejector chillers with steam and other working fluids', *International Journal of Refrigeration* **57**, 277–287. DOI: 10.1016/j.ijrefrig.2015.05.015.

Ouzzane, M. & Aidoun, Z. (2003), 'Model development and numerical procedure for detailed ejector analysis and design', *Applied Thermal Engineering* **23**(18), 2337–2351. DOI: 10.1016/S1359-4311(03)00208-4.

Palacz, M., Bodys, J., Haida, M., Smolka, J. & Nowak, A. J. (2022), 'Two-phase flow visualisation in the r744 vapour ejector for refrigeration systems', *Applied Thermal Engineering* **210**, 118322. DOI: 10.1016/j.applthermaleng.2022.118322.

Poorasadion, S., Alishiri, S. & Saadatmand, M. (2013), Cfd simulation of condensing phenomena in the steam ejector by wet steam model, *in* 'The International Desalination Association World Congress on Desalination and Water Reuse', pp. 1–9.

Ramesh, A. & Sekhar, S. J. (2018), 'Experimental and numerical investigations on the effect of suction chamber angle and nozzle exit position of a steam-jet ejector', *Energy* **164**, 1097–1113. DOI: 10.1016/j.energy.2018.09.010.

Rao, S. M. & Jagadeesh, G. (2014), 'Observations on the non-mixed length and unsteady shock motion in a two dimensional supersonic ejector', *Physics of Fluids* **26**(3), 036103. DOI: 10.1016/j.ijrefrig.2010.08.017.

Ruangtrakoon, N., Aphornratana, S. & Sriveerakul, T. (2011), 'Experimental studies of a steam jet refrigeration cycle: effect of the primary nozzle geometries to system performance', *Experimental Thermal and Fluid Science* **35**(4), 676–683. DOI: 10.1016/j.expthermflusci.2011.01.001.

Ruangtrakoon, N., Thongtip, T., Aphornratana, S. & Sriveerakul, T. (2013), 'Cfd simulation on the effect of primary nozzle geometries for a steam ejector in refrigeration cycle', *International Journal of Thermal Sciences* **63**, 133–145. DOI: 10.1016/j.ijthermalsci.2012.07.009.

Sahlot, M. & Riffat, S. B. (2016), 'Desiccant cooling systems: a review', *International Journal of Low-Carbon Technologies* **11**(4), 489–505. DOI: :10.1093/ijlct/ctv032.

Sharifi, N. & Boroomand, M. (2013), 'An investigation of thermo-compressor design by analysis and experiment: Part 1. validation of the numerical method', *Energy conversion and management* **69**, 217–227. DOI: 10.1016/j.enconman.2012.12.009.

Sharifi, N. & Sharifi, M. (2014), 'Reducing energy consumption of a steam ejector through experimental optimization of the nozzle geometry', *Energy* **66**, 860–867. DOI: 10.1016/j.energy.2014.01.055.

Sim, J., Im, H. G. & Chung, S. H. (2015), 'A computational study of droplet evaporation with fuel vapor jet ejection induced by localized heat sources', *Physics of Fluids* **27**(5), 1–16. DOI: 10.1063/1.4919809.

Sriveerakul, T., Aphornratana, S. & Chunnanond, K. (2007*a*), 'Performance prediction of steam ejector using computational fluid dynamics: Part 1. validation of the cfd results', *International Journal of Thermal Sciences* **46**(8), 812–822. DOI: 10.1016/j.ijthermalsci.2006.10.014.

Sriveerakul, T., Aphornratana, S. & Chunnanond, K. (2007*b*), 'Performance prediction of steam ejector using computational fluid dynamics: Part 2. flow structure of a steam ejector influenced by operating pressures and geometries', *International Journal of Thermal Sciences* **46**(8), 823–833. DOI: 10.1016/j.ijthermalsci.2006.10.012.

Sun, D.-W. (1997), 'Experimental investigation of the performance characteristics of a steam jet refrigeration system', *Energy Sources* **19**(4), 349–367.

Sun, D.-W. (1999), 'Comparative study of the performance of an ejector refrigeration cycle operating with various refrigerants', *Energy conversion and management* **40**(8), 873–884.

Sun, W., Ma, X., Zhang, Y., Jia, L. & Xue, H. (2021), 'Performance analysis and optimization of a steam ejector through streamlining of the primary nozzle', *Case Studies in Thermal Engineering* **27**, 1–13. DOI: 10.1016/j.csite.2021.101356.

Tan, J., Zhang, D. & Lv, L. (2018), 'A review on enhanced mixing methods in supersonic mixing layer flows', *Acta Astronautica* **152**, 310–324. DOI: 10.1016/j.actaastro.2018.08.036.

Tang, Y., Liu, Z., Li, Y., Huang, Z. & Chua, K. J. (2021), 'Study on fundamental link between mixing efficiency and entrainment performance of a steam ejector', *Energy* **215**, 1–14. DOI: 10.1016/j.energy.2020.119128.

Tang, Y., Liu, Z., Li, Y., Zhao, F., Fan, P. & Chua, K. J. (2021), 'Mixing process of two streams within a steam ejector from the perspectives of mass, momentum and energy transfer', *Applied Thermal Engineering* **185**, 1–13. DOI: 10.1016/j.applthermaleng.2020.116358.

Valenti, M. (1998), 'Vacuum degassing yields stronger steel', *Mechanical Engineering* **120**(04), 54–58. /doi.org/10.1115/1.1998-APR-1.
URL: *https://asmedigitalcollection.asme.org/memagazineselect/article/120/04/54/367692*

Varga, S., Oliveira, A. C. & Diaconu, B. (2009*a*), 'Analysis of a solar-assisted ejector cooling system for air conditioning', *International Journal of Low-Carbon Technologies* **4**(1), 2–8. DOI: 10.1093/ijlct/ctn001.

Varga, S., Oliveira, A. C. & Diaconu, B. (2009*b*), 'Numerical assessment of steam ejector efficiencies using cfd', *International Journal of Refrigeration* **32**(6), 1203–1211. DOI: 10.1016/j.ijrefrig.2009.01.007.

Varga, S., Soares, J., Lima, R. & Oliveira, A. C. (2017), 'On the selection of a turbulence model for the simulation of steam ejectors using cfd', *International Journal of Low-Carbon Technologies* **12**(3), 233–243. DOI: 10.1093/ijlct/ctx007.

Victoria State Government (2015), 'Computer Related Injuries — Better Health Channel', `https://www.betterhealth.vic.gov.au/health/healthyliving/computer-related-injuries`. [Online; accessed March-2022].

Wang, X.-D., Lei, H.-J., Dong, J.-L. & Tu, J.-y. (2012), 'The spontaneously condensing phenomena in a steam-jet pump and its influence on the numerical simulation accuracy', *International journal of heat and mass transfer* **55**(17-18), 4682–4687. DOI: 10.1016/j.ijheatmasstransfer.2012.04.028.

Wang, X., Dong, J., Li, A., Lei, H. & Tu, J. (2014), 'Numerical study of primary steam superheating effects on steam ejector flow and its pumping performance', *Energy* **78**, 205–211. DOI: 10.1016/j.energy.2014.10.004.

Wang, X., Dong, J., Zhang, G., Fu, Q., Li, H., Han, Y. & Tu, J. (2019), 'The primary pseudo-shock pattern of steam ejector and its influence on pumping efficiency based on cfd approach', *Energy* **167**, 224–234. DOI: 10.1016/j.energy.2018.10.097.

Watanawanavet, S. (2005), Optimization of a high-efficiency jet ejector by computational fluid dynamic software, PhD thesis, Texas A&M University. `https://oaktrust.library.tamu.edu/handle/1969.1/2432`.

Wu, H., Liu, Z., Han, B. & Li, Y. (2014), 'Numerical investigation of the influences of mixing chamber geometries on steam ejector performance', *Desalination* **353**, 15–20. DOI: 10.1016/j.desal.2014.09.002.

Yang, X., Long, X. & Yao, X. (2012), 'Numerical investigation on the mixing process in a steam ejector with different nozzle structures', *International journal of thermal sciences* **56**, 95–106. DOI: 10.1016/j.ijthermalsci.2012.01.021.

Yang, Y., Zhu, X., Yan, Y., Ding, H. & Wen, C. (2019), 'Performance of supersonic steam ejectors considering the nonequilibrium condensation phenomenon for efficient energy utilisation', *Applied Energy* **242**, 157–167. DOI: 10.1016/j.apenergy.2019.03.023.

Yapıcı, R. (2008), 'Experimental investigation of performance of vapor ejector refrigeration system using refrigerant r123', *Energy Conversion and Management* **49**(5), 953–961. DOI: 10.1016/j.enconman.2007.10.006.

Yu, J., Ren, Y., Chen, H. & Li, Y. (2007), 'Applying mechanical subcooling to ejector refrigeration cycle for improving the coefficient of performance', *Energy Conversion and Management* **48**(4), 1193–1199. DOI: 10.1016/j.enconman.2006.10.009.

Zare-Behtash, H. & Kontis, K. (2009), 'Compressible flow structures interaction with a two-dimensional ejector: a cold-flow study', *Journal of Propulsion and Power* **25**(3), 707–716. DOI: 10.2514/1.39315.

Zhang, G., Dykas, S., Yang, S., Zhang, X., Li, H. & Wang, J. (2020), 'Optimization of the primary nozzle based on a modified condensation model in a steam ejector', *Applied Thermal Engineering* **171**, 115090. DOI: 10.1016/j.applthermaleng.2020.115090.

Zhu, Y. & Jiang, P. (2014), 'Experimental and analytical studies on the shock wave length in convergent and convergent–divergent nozzle ejectors', *Energy Conversion and Management* **88**, 907–914. DOI: 10.1016/j.enconman.2014.09.023.

Zhu, Y., Wang, Z., Yang, Y. & Jiang, P.-X. (2017), 'Flow visualization of supersonic two-phase transcritical flow of co2 in an ejector of a refrigeration system', *International journal of refrigeration* **74**, 354–361. DOI: 10.1016/j.ijrefrig.2016.11.012.

Appendix A

Project Specification

ENG 4111/2 Research Project

Project Specification

For:	**Brodie Cooper**
Topic:	CFD Analysis of a Primary Nozzle Vortex Generator on Steam Ejector Performance.
Supervisors:	Dr Khalid Saleh
Sponsorship:	Faculty of Health, Engineering & Sciences
Project Aim:	To investigate whether generating a vortex in the steam exiting the primary flow nozzle will produce a larger pressure difference between the primary and secondary flows, thereby increasing the flow rate of the steam drawn from the condensor, reducing shock waves and improving the mixing of the steam inside the mixing chamber.

Program:

1. Learn Ansys software and familiarise with the fundamental concepts of the steam ejector.
2. Develop a 2D model of the existing USQ steam ejector in ANSYS Fluent, verifying its accuracy against previous studies.
3. Conduct background research regarding the optimisation of steam ejector and the application of vortex generators in different flow conditions. Identify geometric characteristics for the vortex generators that will be suitable for the primary flow nozzle of the ejector.
4. Create a 3D model of the existing USQ steam ejector in ANSYS Fluent, run simulations and anlayse the performance characteristics of the ejector prior to modification of the primary nozzle.
5. Create multliple 3D ejector models modifed primary nozzles varying in a) number of vortex generators, b) generator helix angles, and c) generator shape profiles.
6. Simulate the steam ejector with each variation of the vortex inducing nozzle in ANSYS Fluent; conducting each simulation approximately 3 - 5 times.
7. Analyse the results of the simulations and identify whether a) the vortex generator enhances or hinders ejector performance, and b) which vortex generator characteristics have the greatest effect on the coefficient of peformance.

As time and resources permit:

1. From the simulation results, generate a 3D model of the ejector with an optimised primary nozzle vortex generator.
2. Simulate the optimised 3D model in ANSYS Fluent.
3. Analyse the results and determine the overall feasibility of the design.

Resource Requirements:

Table 1: List of resources necesary for completion of the project.

Item/Resource	**Quantity**	**Cost**	**Source**
ANSYS Student Software	1	Nil	Free downloand for students and available on university computers
ANSYS Tutorials and Users Guide	1	Nil	Available free online and from MEC5100 course material
Guidance of Project Supervisor	N/A	Nil	Dependent on the availability of the Supervisor
Time to Conuct the Research	N/A	Nil	Research wil likely require all of the allocated time
Internet Access for Literature	1	Nil	Universtiy has unlimited WiFi
Unlimited Access to a Computer	1	Nil	Unlimited access to personal computer and university computers

Appendix B

Risk Assessment

University of Southern Queensland

Generic Risk Management Plan

Workplace (Division/Faculty/Section):		
204070 - School of Mechanical and Electrical Engineering		
Assessment No (if applicable): 1	Assessment Date: 14/03/2022	Review Date: (5 years maximum) 12/12/2024
Context: What is being assessed? Describe the item, job, process, work arrangement, event etc: Computational Fluid Dynamics research using university desktop computers in an office setting at the Toowoomba campus.		
Assessment Team – who is conducting the assessment?		
Assessor(s): Brodie Cooper Others consulted: (eg elected health and safety representative, other personnel exposed to risks) Dr Khalid Saleh		

The Risk Management Process

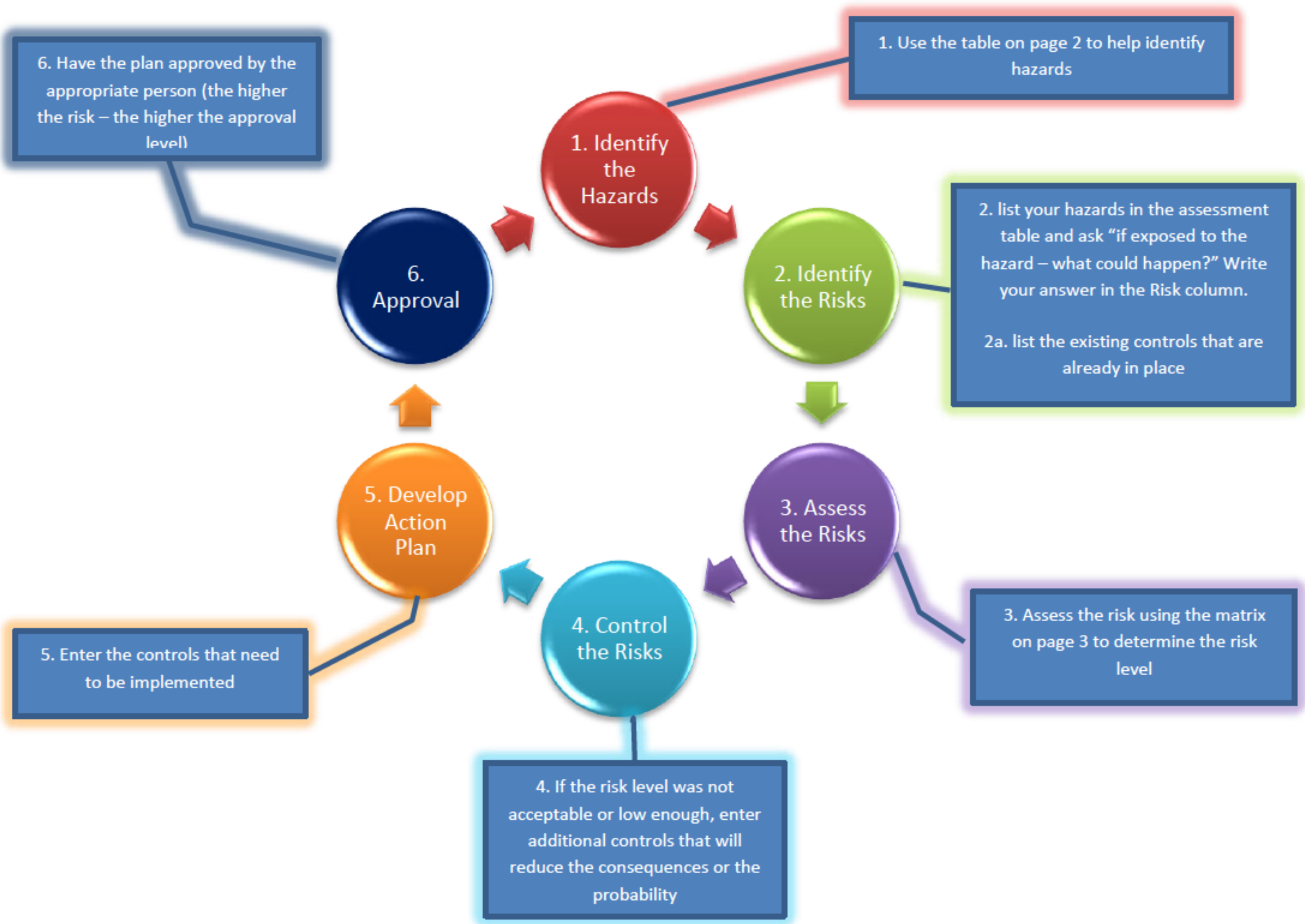

Step 1 - Identify the hazards (use this table to help identify hazards then list all hazards in the risk table)		
General Work Environment		
☐ Sun exposure	☐ Water (creek, river, beach, dam)	☐ Sound / Noise
☐ Animals / Insects	☐ Storms / Weather/Wind/Lightning	☐ Temperature (heat, cold)
☐ Air Quality	☒ Lighting	☐ Uneven Walking Surface
☒ Trip Hazards	☐ Confined Spaces	☐ Restricted access/egress
☐ Pressure (Diving/Altitude)	☐ Smoke	☐
Other/Details:		
Machinery, Plant and Equipment		
☐ Machinery (fixed plant)	☐ Machinery (portable)	☐ Hand tools
☐ Laser (Class 2 or above)	☐ Elevated work platforms	☐ Traffic Control
☐ Non-powered equipment	☐ Pressure Vessel	☐ Electrical
☐ Vibration	☐ Moving Parts	☐ Acoustic/Noise
☐ Vehicles	☐ Trailers	☐ Hand tools
Other/Details:		
Manual Tasks / Ergonomics		
☐ Manual tasks (repetitive, heavy)	☐ Working at heights	☐ Restricted space
☐ Vibration	☐ Lifting Carrying	☐ Pushing/pulling
☐ Reaching/Overstretching	☐ Repetitive Movement	☐ Bending
☒ Eye strain	☐ Machinery (portable)	☐ Hand tools
Other/Details:		
Biological (e.g. hygiene, disease, infection)		
☐ Human tissue/fluids	☒ Virus / Disease	☐ Food handling
☐ Microbiological	☐ Animal tissue/fluids	☐ Allergenic
Other/Details:		
Chemicals Note: Refer to the label and Safety Data Sheet (SDS) for the classification and management of all chemicals.		
☐ Non-hazardous chemical(s)	☐ 'Hazardous' chemical (Refer to a completed hazardous chemical risk assessment)	
☐ Engineered nanoparticles	☐ Explosives	☐ Gas Cylinders
Name of chemical(s) / Details:		
Critical Incident – resulting in:		
☒ Lockdown	☒ Evacuation	☒ Disruption
☐ Public Image/Adverse Media Issue	☐ Violence	☐ Environmental Issue
Other/Details:		
Radiation		
☐ Ionising radiation	☐ Ultraviolet (UV) radiation	☐ Radio frequency/microwave
☐ infrared (IR) radiation	☐ Laser (class 2 or above)	☐
Other/Details:		
Energy Systems – incident / issues involving:		
☐ Electricity (incl. Mains and Solar)	☐ LPG Gas	☐ Gas / Pressurised containers
Other/Details:		
Facilities / Built Environment		
☐ Buildings and fixtures	☐ Driveway / Paths	☐ Workshops / Work rooms
☐ Playground equipment	☐ Furniture	☐ Swimming pool
Other/Details:		
People issues		
☒ Students	☒ Staff	☒ Visitors / Others
☒ Physical	☒ Psychological / Stress	☐ Contractors
☒ Fatigue	☒ Workload	☐ Organisational Change
☐ Workplace Violence/Bullying	☐ Inexperienced/new personnel	☐
Other/Details:		

Step 1 (cont) Other Hazards / Details (enter other hazards not identified on the table)
Unreliable results or methodology
Car accident during travel to univeristy campus

Risk Matrix

Eg 1. Enter Consequence

	Consequence				
Probability	**Insignificant** No Injury 0-$5K	**Minor** First Aid $5K-$50K	**Moderate** Med Treatment $50K-$100K	**Major** Serious Injuries $100K-$250K	**Catastrophic** Death More than $250K
Almost Certain 1 in 2	M	H	E	E	E
Likely 1 in 100	M	H	H	E	E
Possible 1 in 1000	L	M	H	H	H
Unlikely 1 in 10 000	L	L	M	M	M
Rare 1 in 1 000 000	L	L	L	L	L

Eg 2. Enter Probability

Recommended Action Guide
E=Extreme Risk – Task ***MUST NOT*** proceed
H=High Risk – Special Procedures Required (See USQSafe)
M=Moderate Risk – Risk Management Plan/Work Method Statement Required
L=Low Risk – Use Routine Procedures

Eg 3. Find Action

Risk register and Analysis

Step 1 (cont)	Step 2	Step 2a	Step 3			Step 4				
Hazards: From step 1 or more if identified	**The Risk:** What can happen if exposed to the hazard with existing controls in place?	**Existing Controls:** What are the existing controls that are already in place?	**Risk Assessment:** (use the Risk Matrix on p3) Consequence x Probability Risk Level			**Additional controls:** Enter additional controls if required to reduce the risk level	**Risk assessment with additional controls:** (use the Risk Matrix on p3 – has the consequence or probability changed?)			Controls Implemented? Yes/No
			Consequence	Probability	Risk Level		Consequence	Probability	Risk Level	
Example										
Working in temperatures over 35^0 C	Heat stress/heat stroke/exhaustion leading to serious personal injury/death	Regular breaks, chilled water available, loose clothing, fatigue management policy.	catastrophic	possible	high	temporary shade shelters, essential tasks only, close supervision, buddy system	catastrophic	unlikely	mod	Yes
Poor Lighting entering Room	Injury from walking into surroundings in the dark.	Light switches at door before entry.	Minor	Possible	Moderate	Use a phone torch to navigate dark areas.	Insignificant	Unlikely	Low	Yes
Tripping using Stairs	Injury, ie. Cuts, bruises, broken bones.	Use handrails, watch footing, walk slowly.	Moderate	Possible	High	Use the elevator.	Minor	Rare	Low	Yes
Eye Strain	Visual impairment, reduced productivity and quality of work.	Take regular breaks from study to refocus eyes.	Moderate	Possible	High	Adjust computer and room lightingto minimise glare, adjust the font size and maintain a distance of 60cm from the screen.	Moderate	Rare	Low	Yes
Lockdown /evacuation /disruption	Risk of physical harm, dissruption of productivity.	Alarms and signage around the building.	Major	Unlikely	Moderate	Learn and understadning the evaculation plan and route that is provided in th foyer, memorise the assembly point.	Moderate	Rare	Low	Yes
Students / Staff/ Visitors	Dissuption of other classes or own productivty.	Class Schedules, notices on doors and desktops.	Minor	Likely	High	Communicate with staff/students/visitors in the room to gain permission, organise to be in other rooms during times that the room is booked.	Insignificant	Unlikely	Low	Yes
Physical	Muscle and joint pain, poor posture habbits.	Ergonimic office equipment available.	Moderate	Possible	High	Ensure a comfortbale chair and desk height, take regular breaks for exercise and stretching.	Minor	Unlikely	Low	Yes
Psychologic Stress	Anxiety, decreased health, reduced work quality.	Regular contact with supervisor, course examinar, detailed schedule.	Major	Possible	High	Access to counseller and support from friends and family.	Minor	Unlikely	Low	Yes
Fatigue	Decreased health, reduced quality of work.	Take regular work breaks.	Moderate	Possible	High	Maintain a consistent sleep schedule, work for set time periods between breaks.	Minor	Unlikely	Low	Yes
Workload	Decreased quality of work, Incomplete work.	Discuss aims and objecties with supervisor.	Moderate	Possible	High	Update project objectives as needed throughout the duration.	Minor	Unlikely	Low	Yes

Step 1 (cont)	Step 2	Step 2a	Step 3			Step 4				
Hazards: From step 1 or more if identified	**The Risk:** What can happen if exposed to the hazard with existing controls in place?	**Existing Controls:** What are the existing controls that are already in place?	**Risk Assessment:** (use the Risk Matrix on p3) Consequence x Probability Risk Level			**Additional controls:** Enter additional controls if required to reduce the risk level	**Risk assessment with additional controls:** (use the Risk Matrix on p3 – has the consequence or probability changed?)			Controls Implemented? Yes/No
			Consequence	Probability	Risk Level		Consequence	Probability	Risk Level	
Example										
Working in temperatures over 35º C	Heat stress/heat stroke/exhaustion leading to serious personal injury/death	Regular breaks, chilled water available, loose clothing, fatigue management policy.	catastrophic	possible	high	temporary shade shelters, essential tasks only, close supervision, buddy system	catastrophic	unlikely	mod	Yes
Unreliable Results/methodology	Distribution of misleading results and information.	Dissertations limitations of use and disclaimer included, Work overseen by supervisor.	Major	Unlikely	Moderate	Dissertation written with integrity.	Major	Unlikely	Moderate	Yes
Car accident	Injury/ Fatality/ Damage to property.	Roadworthy vehilce, roadrules.	Major	Unlikely	Moderate	Ensure unfatigued, plan route, stay focused, obey road rules and use available safety equipment.	Major	Unlikely	Moderate	Yes
Corona Virus	Flu like symtoms, hospitalisation, lost time due illness.	Wipe down desktop before use, wash and sanitise hands, use face mask, social distancing.	Major	Possible	High	Double Vaccination	Minor	Unlikely	Low	Yes
			Select a consequence	Select a probability	Select a Risk Level		Select a consequence	Select a probability	Select a Risk Level	Yes or No
			Select a consequence	Select a probability	Select a Risk Level		Select a consequence	Select a probability	Select a Risk Level	Yes or No
			Select a consequence	Select a probability	Select a Risk Level		Select a consequence	Select a probability	Select a Risk Level	Yes or No
			Select a consequence	Select a probability	Select a Risk Level		Select a consequence	Select a probability	Select a Risk Level	Yes or No
			Select a consequence	Select a probability	Select a Risk Level		Select a consequence	Select a probability	Select a Risk Level	Yes or No
			Select a consequence	Select a probability	Select a Risk Level		Select a consequence	Select a probability	Select a Risk Level	Yes or No
			Select a consequence	Select a probability	Select a Risk Level		Select a consequence	Select a probability	Select a Risk Level	Yes or No
			Select a consequence	Select a probability	Select a Risk Level		Select a consequence	Select a probability	Select a Risk Level	Yes or No
			Select a consequence	Select a probability	Select a Risk Level		Select a consequence	Select a probability	Select a Risk Level	Yes or No
			Select a consequence	Select a probability	Select a Risk Level		Select a consequence	Select a probability	Select a Risk Level	Yes or No
			Select a consequence	Select a probability	Select a Risk Level		Select a consequence	Select a probability	Select a Risk Level	Yes or No
			Select a consequence	Select a probability	Select a Risk Level		Select a consequence	Select a probability	Select a Risk Level	Yes or No
			Select a consequence	Select a probability	Select a Risk Level		Select a consequence	Select a probability	Select a Risk Level	Yes or No
			Select a consequence	Select a probability	Select a Risk Level		Select a consequence	Select a probability	Select a Risk Level	Yes or No

Step 5 – Action Plan (for controls not already in place)			
Control Option	**Resources**	**Person(s) responsible**	**Proposed implementation date**
Appropriate Training for Posture	Online / Internet	Brodie Cooper	14/03/2022

Step 6 – Approval

Drafter's Comments:

The risks and hazards associated with the project have been considered in depth and the processes put in place to ensure the safety of those involved are acceptable. I am confident the project can be undertaken safely.

Drafter Details:

Name: Brodie Cooper Signature [redacted] **Date**: 14/03/2022

Assessment Approval: (Extreme or High = VC, Moderate = Cat 4 delegate or above, Low = Manager/Supervisor)

I am satisfied that the risks are as low as reasonably practicable and that the resources required will be provided.

Name: Khalid Saleh Signature: [redacted] Date: 12/10/2022

Position Title: Lecturer

Appendix C

Dissertation Schedule

Project Timeline:

Table 2: Key Components of the Proposed Research Project

Phase 1	**Initial Preparation**
1A	Project Approval: Complete the project proposal forms and obtain official approval for the research topic.
1B	Resource Acquisiton: Gain access to all necessary resources
1C	Intial Research: Obtain important data and geometric values required for developing the models of the ejector design and familiarise with ANSYS Workbench/Fluent.
1D	Project Specificaiton: Collaborate with the project supervisor and develop a project specification.
1E	Literature Review: Develop a deep understanding of the topic by reviewing relevent literature and identify important chracteristics and key variables that should be considered throughout the completion of this project.
Phase 2	**CFD Analysis**
2A	Generate 2D Geometry: Create the 2D models of the ejector design in ANSYS Workbench based on data obtained from the initial research
2B	Confirm Model Accuracy: Simulate the flow conditions using the 2D model and validate the results against the data obtained in intial research.
2C	Generate 3D Geometries: Create the 3D models of the ejector for each variation of primary nozzle design in ANSYS Workbench.
2D	Generate Meshes: Conduct a grid independence study on the 3D models in ANSYS Fluent and generate appropriate meshes.
2E	Simulations: Using ANSYS Fluent, simulate the flow through the 3D ejector models.
2F	Results and Analysis: Anlayse the behaviour of the fluid and identify the effect that the vortex generator is having on the ejectors performance. Determine which vortex generator characteristics offer the greatest improvement on the ejector performance and propose the optimal design.
Phase 3	**Dissertation Writing and Presentation**
3A	Project Progress Report: This document will inlcude the introduction, literature review, research methodology ect. and must be submitted as part of ENG4111.
3B	Draft Disertation: Prepare a draft dissertation to submit to the project supervisor for feedback.
3C	Professional Practice 2 Presentation: Prepare a 15-minute oral presentation delivering the results of the research project.
3D	Edit and Finalise Dissertation: Make any changes based on the feedback from Phase 3B and produce a final copy of the dissertation.

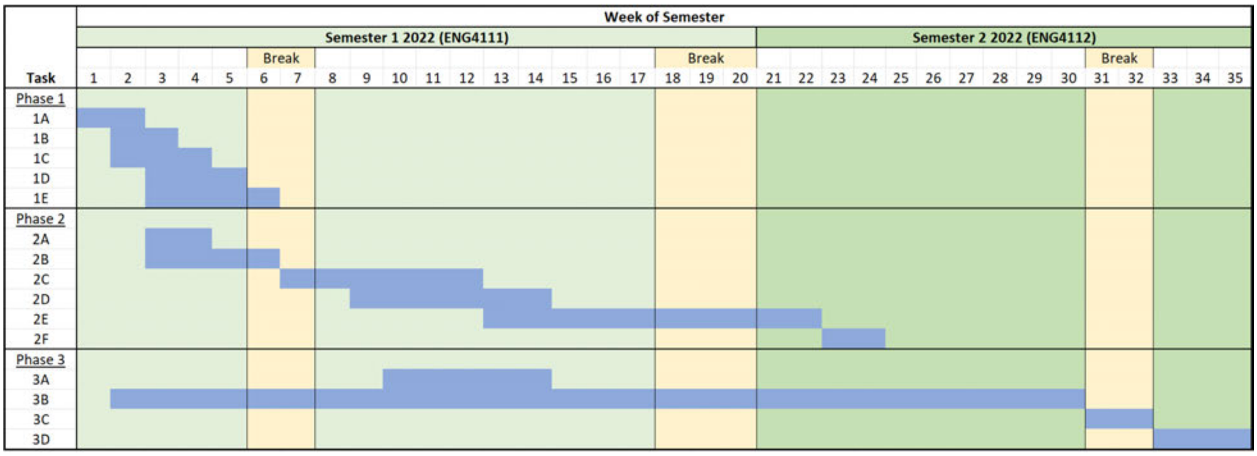

Figure 1: Gandt Chart for the Research Project's Timeline of Significant Events.

Appendix D

UniSQ Ejector Dimensions

D.1 UniSQ Steam Ejector Geometry

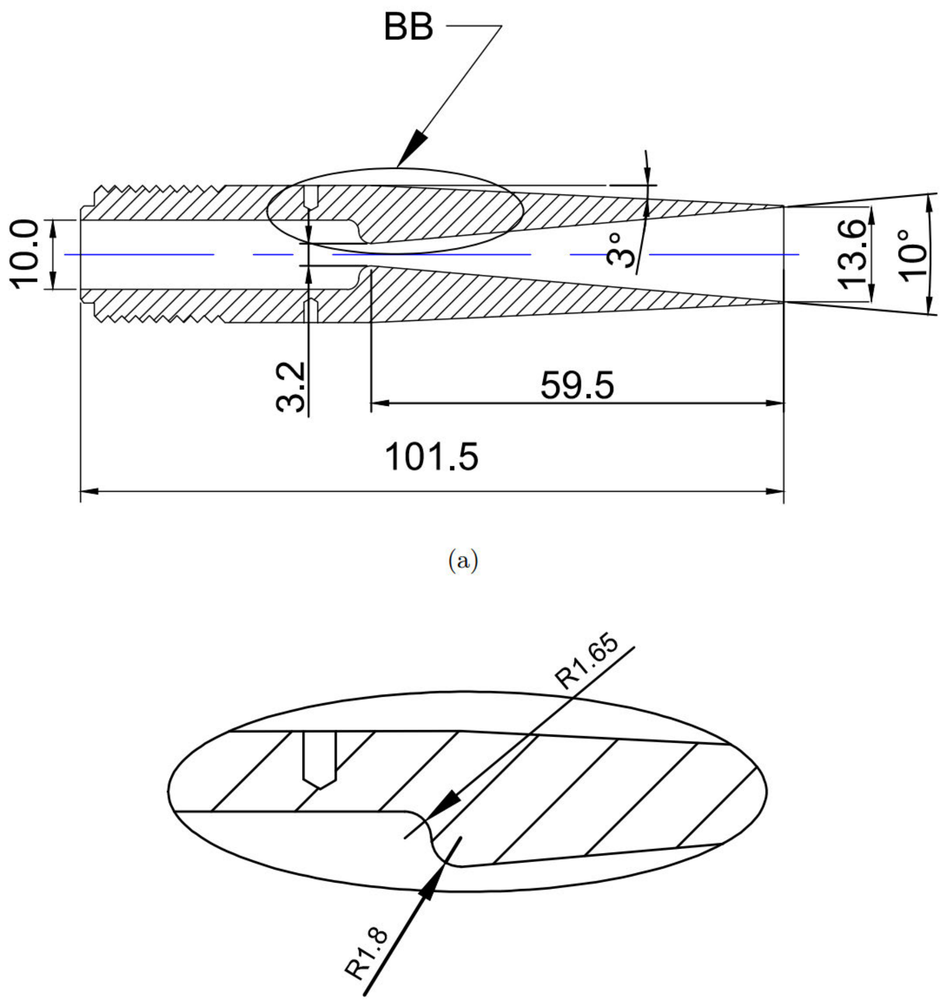

(a)

(b)

Figure D.1: Detailed drawing of the UniSQ steam ejector showing: (a) Overall nozzle dimensions, (b) details of nozzle throat. (Al-Doori 2013)

Geometric parameters	(a) Old design in mm	(b) New design in mm
Diameter of the secondary inlet	37	90
Nozzle Exit Position (NXP)	+15	+15
Mixing chamber length	420	420
Mixing chamber diameter	90	90
Diffuser inlet diameter	80	90
Diffuser throat diameter	22	28
Diffuser outlet diameter	80	94
Diffuser convergent length	20	153
Diffuser divergent length	270	169

Figure D.2: Dimensions of the new and old UniSQ steam ejector (Al-Manea 2019).

Appendix E

Standard Nozzle Additional Data

E.1 Numerical Results Data

Back Pressure (Pa)	Primary MFR (g/s)	Secondary MFR (g/s)	Rev Flow (%)	Vmix (m/s)	Vpe (m/s)	Vse (m/s)	ER	ME%
2000	1.8797244	11.159766	0	137.96606	1024.987	75.577621	5.93691607	0.6494325
2200	1.8797224	11.17818	0	138.24832	1024.987	75.703125	5.94671852	0.6510238
2400	1.8797244	9.1995892	0	109.4077	1024.987	62.391134	4.89411597	0.4847358
2600	1.8797244	2.902179	0	45.24	1024.987	21.66347	1.54393857	0.108734
2800	1.8797244	-9.365	100%	-73.3832	1024.987	-65.9696	-4.9821133	0.215875

Figure E.1: Standard Nozzle Operating Range Results Data.

Appendix F

One Generator Supporting Documents

F.1 Numerical Results Data

Back Pressure (Pa)	Primary MFR (g/s)	Secondary MFR (g/s)	Rev Flow (%)	Vmix (m/s)	Vpe (m/s)	Vse (m/s)	ER	ME%
2000	1.8935688	11.143265	1.50%	137.73961	1020.73961	75.026486	5.88479542	0.648525
2200	1.8935688	11.155644	1%	137.92855	1020.7565	75.111047	5.89133281	0.6495846
2400	1.8935696	9.136027	0.30%	108.7888	1020.7565	61.468338	4.8247643	0.4810265
2600	1.8935696	2.848484	1.30%	45.84895	1020.7549	-2.9668342	1.50429327	0.1129786
2800	1.8935696	-9.1880378	100%	-71.569053	1020.7565	-84.980915	-4.8522314	0.1923801

Figure F.1: 1 Generator 53mm Pitch Operating Range Results Data.

Back Pressure (Pa)	Primary MFR (g/s)	Secondary MFR (g/s)	Rev Flow (%)	Vmix (m/s)	Vpe (m/s)	Vse (m/s)	ER	ME%
2000	1.8790737	11.143257	3.90%	127.64737	1009.0954	75.244938	5.93018624	0.607856
2200	1.8790737	11.099816	2.70%	127.04309	1009.0954	74.950239	5.90706793	0.6044057
2400	1.8790737	8.7813809	1.60%	97.09325	1009.0953	59.58648	4.67324986	0.4278132
2600	1.8790737	2.1363484	1.30%	42.443979	1009.0916	30.605608	1.1369157	0.086886
2800	1.8790737	-8.8093961	100%	-68.132922	1009.0953	-49.24864	-4.6881589	0.2026524

Figure F.2: 1 Generator 26.5mm Pitch Operating Range Results Data.

Back Pressure (Pa)	Primary MFR (g/s)	Secondary MFR (g/s)	Rev Flow (%)	Vmix (m/s)	Vpe (m/s)	Vse (m/s)	ER	ME%
2000	1.8791561	11.073788	1.50%	136.54966	968.44815	74.514098	5.89295801	0.6686986
2200	1.8791561	11.059073	0.90%	136.32628	968.44815	74.414264	5.88512737	0.6674015
2400	1.8791561	8.7402009	0.50%	103.35305	968.44813	58.964796	4.65113085	0.4699936
2600	1.8791561	1.828644	1.20%	38.204025	968.44459	14.07989	0.9731198	0.0767514
2800	1.8791561	-9.9233262	100%	-78.742711	968.44804	-54.038476	-5.2807354	0.2688417

Figure F.3: 1 Generator 17.5mm Pitch Operating Range Results Data.

Back Pressure (Pa)	Standard	1G53P	Change (%)	1G26.5P	Change (%)	1G17.5P	Change (%)
2000	5.936916071	-0.05212	-0.88568333	-0.00673	-0.1134843	-0.043958	-0.7459421
2200	5.946718515	-0.05539	-0.94012182	-0.03965	-0.6712396	-0.061591	-1.0465558
2400	4.894115967	-0.06935	-1.43741053	-0.22087	-4.7261781	-0.242985	-5.224216
2600	1.543938569	-0.03965	-2.63547692	-0.40702	-35.800619	-0.570819	-58.658633
2800	-4.982113335	0.129882	2.67674732	0.293954	6.2701465	-0.298622	-5.6549339

Figure F.4: Percentage Change Data for 1 Generator Entrainment Ratio.

Back Pressure (Pa)	Stand	1G53P	Change (%)	1G26.5P	Change (%)	1G17.5P	Change (%)
2000	0.649432534	-0.00091	-0.13993529	-0.04158	-6.8398682	0.019266	2.88112283
2200	0.651023779	-0.00144	-0.22155994	-0.04662	-7.7130459	0.0163777	2.45394928
2400	0.484735778	-0.00371	-0.77110986	-0.05692	-13.305467	-0.014742	-3.1366693
2600	0.10873401	0.004245	3.756968246	-0.02185	-25.145622	-0.031983	-41.670324
2800	0.215874956	-0.02349	-12.2127497	-0.01322	-6.5247606	0.0529668	19.7018452

Figure F.5: Percentage Change Data for 1 Generator Mixing Efficiency.

Appendix G

Three Vortex Generator Supporting Data

G.1 Numerical Results Data

Back Pressure (Pa)	Primary MFR (g/s)	Secondary MFR (g/s)	Rev Flow (%)	Vmix (m/s)	Vpe (m/s)	Vse (m/s)	ER	ME%
2000	1.8796875	11.132114	1.30%	137.15953	1017.6652	74.958388	5.92232166	0.649608
2200	1.8796875	11.145458	0	137.36362	1017.6652	75.049273	5.92942071	0.6507649
2400	1.8796875	9.0837963	0	107.41978	1017.6652	61.197954	4.83260984	0.4770309
2600	1.8796875	2.6216868	0	43.479509	1017.6648	19.029557	1.39474609	0.0997144
2800	1.8796875	-9.5712452	100%	-75.351485	1017.6652	-74.566956	-5.0919343	0.2206549

Figure G.1: 2 Generator 53mm Pitch Operating Range Results Data.

Back Pressure (Pa)	Primary MFR (g/s)	Secondary MFR (g/s)	Rev Flow (%)	Vmix (m/s)	Vpe (m/s)	Vse (m/s)	ER	ME%
2000	1.8801426	11.064143	1.20%	136.986	1001.2681	74.64	5.88473608	0.6547097
2200	1.8801426	11.061619	0	136.94767	1001.2681	74.625888	5.88339363	0.6544821
2400	1.8801426	8.7904399	0	104.39887	1001.2681	59.382261	4.67541127	0.4632922
2600	1.8801426	1.5202817	0	41.402683	1001.2696	37.305377	0.80859915	0.0725987
2800	1.8801426	-10.075951	100%	-80.199857	1001.2681	-77.188929	-5.3591419	0.2470804

Figure G.2: 2 Generator 26.5mm Pitch Operating Range Results Data.

Back Pressure (Pa)	Primary MFR (g/s)	Secondary MFR (g/s)	Rev Flow (%)	Vmix (m/s)	Vpe (m/s)	Vse (m/s)	ER	ME%
2000	1.8799079	11.017593	1.20%	138.31955	979.97412	74.307509	5.86070892	0.6704282
2200	1.8799079	10.998982	0	138.03642	979.97412	74.180668	5.85080897	0.6687886
2400	1.8799079	8.5811408	0	103.2906	979.9706	57.968776	4.56466022	0.4618247
2600	1.8799079	0.96236609	0	36.919998	979.97809	31.3261	0.51192194	0.0560435
2800	1.8799079	-10.427829	100%	-83.658488	979.97382	-74.338218	-5.5469893	0.2732075

Figure G.3: 2 Generator 17.5mm Pitch Operating Range Results Data.

Back Pressure (Pa)	Stand	2G53P	Change (%)	2G26.5P	Change (%)	2G17.5P	Change (%)
2000	5.936916071	-0.01459	-0.24643053	-0.05218	-0.8867006	-0.076207	-1.300306
2200	5.946718515	-0.0173	-0.29172834	-0.06332	-1.0763326	-0.09591	-1.6392528
2400	4.894115967	-0.06151	-1.27273117	-0.2187	-4.6777638	-0.329456	-7.2175307
2600	1.543938569	-0.14919	-10.6967479	-0.73534	-90.939921	-1.032017	-201.59649
2800	-4.982113335	-0.10982	-2.15676263	-0.37703	-7.0352414	-0.564876	-10.183469

Figure G.4: Percentage Change Data for 2 Generator Entrainment Ratio.

Back Pressure (Pa)	Stand	2G53P	Change (%)	2G26.5P	Change (%)	2G17.5P	Change (%)
2000	0.649432534	0.000175	0.027006333	0.005277	0.8060305	0.0209956	3.13167701
2200	0.651023779	-0.00026	-0.03978303	0.003458	0.528409	0.0177649	2.65627443
2400	0.484735778	-0.0077	-1.6151709	-0.02144	-4.628521	-0.022911	-4.9609788
2600	0.10873401	-0.00902	-9.04545506	-0.03614	-49.773968	-0.052691	-94.017131
2800	0.215874956	0.00478	2.166266841	0.031205	12.629664	0.0573326	20.9849895

Figure G.5: Percentage Change Data for 2 Generator Mixing Efficiency.

G.2 Graphical Results

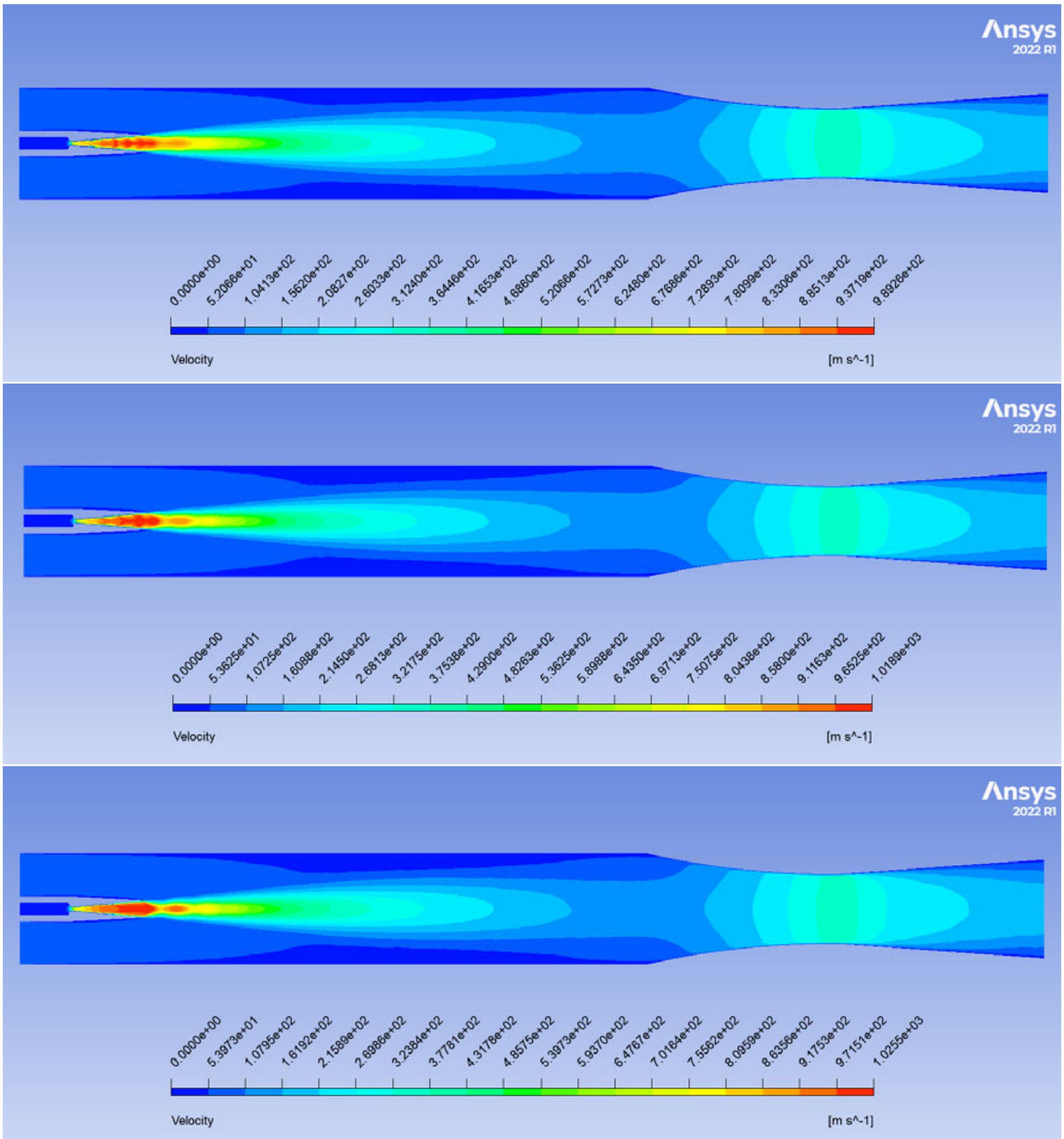

Figure G.6: Velocity map comparison of two generator nozzle variations operating at 2.2kPa condenser pressure. Pitch sizes: 17.5mm (top), 26.5mm (middle), 53mm (bottom).

Appendix H

Three Vortex Generator Supporting Data

H.1 Numerical Results Data

Back Pressure (Pa)	Primary MFR (g/s)	Secondary MFR (g/s)	Rev Flow (%)	Vmix (m/s)	Vpe (m/s)	Vse (m/s)	ER	ME%
2000	1.8805011	11.124656	1.50%	137.45748	1014.1067	74.88321	5.9157934	0.6524105
2200	1.8805011	11.137501	0	137.65335	1014.1067	74.970678	5.92262403	0.6535237
2400	1.8805011	9.0576711	0	107.59679	1014.1067	61.003112	4.81662632	0.4785023
2600	1.8805011	2.567539	0	42.1067	1014.1067	18.968457	1.36534831	0.0957659
2800	1.8805011	-9.6258767	100%	-75.858726	1014.1067	-69.888191	-5.1187828	0.2277551

Figure H.1: 3 Generator 53mm Pitch Operating Range Results Data.

Back Pressure (Pa)	Primary MFR (g/s)	Secondary MFR (g/s)	Rev Flow (%)	Vmix (m/s)	Vpe (m/s)	Vse (m/s)	ER	ME%
2000	1.879263	11.062788	1.30%	138.8317	1001.8606	74.582594	5.88676944	0.6635398
2200	1.879263	11.059753	0	138.78515	1001.8606	74.561925	5.88515445	0.6632732
2400	1.879263	8.7793174	0	105.6306	1001.8606	59.264059	4.67168108	0.4685166
2600	1.879263	1.7780207	0.10%	41.504603	1001.861	26.467127	0.94612659	0.0786572
2800	1.879263	-10.108954	100%	-80.541203	1001.8606	-70.746894	-5.379212	0.2551368

Figure H.2: 3 Generator 26.5mm Pitch Operating Range Results Data.

Back Pressure (Pa)	Primary MFR (g/s)	Secondary MFR (g/s)	Rev Flow (%)	Vmix (m/s)	Vpe (m/s)	Vse (m/s)	ER	ME%
2000	1.8799036	11.024232	1.30%	140.63771	985.57855	74.375976	5.86425389	0.679009
2200	1.88799036	11.007752	0	140.38325	985.57855	74.263597	5.83040689	0.6759467
2400	1.8799036	8.6031399	0	105.07227	985.57855	58.121566	4.57637291	0.4681518
2600	1.8799036	1.43776829	0	35.345632	985.57782	15.358548	0.76480958	0.0625457
2800	1.8799036	-10.383743	100%	-83.223533	985.57858	-73.462022	-5.5235508	0.270576

Figure H.3: 3 Generator 17.5mm Pitch Operating Range Results Data.

Back Pressure (Pa)	Stand	3G53P	Change (%)	3G26.5P	Change (%)	3G17.5P	Change (%)
2000	5.936916071	-0.02112	-0.35705556	-0.05015	-0.8518531	-0.072662	-1.2390695
2200	5.946718515	-0.02409	-0.40682115	-0.06156	-1.046091	-0.116312	-1.9949144
2400	4.894115967	-0.07749	-1.608795	-0.22243	-4.7613457	-0.317743	-6.94312
2600	1.543938569	-0.17859	-13.0801977	-0.59781	-63.1852	-0.779129	-101.87228
2800	-4.982113335	-0.13667	-2.66996036	-0.3971	-7.3820966	-0.541437	-9.802344

Figure H.4: Percentage Change Data for 3 Generator Entrainment Ratio.

Back Pressure (Pa)	Stand	3G53P	Change (%)	3G26.5P	Change (%)	3G17.5P	Change (%)
2000	0.649432534	0.002978	0.456455705	0.014107	2.1260641	0.0295764	4.35582275
2200	0.651023779	0.0025	0.382527491	0.012249	1.8468164	0.0249229	3.68711574
2400	0.484735778	-0.00623	-1.30270803	-0.01622	-3.4618247	-0.016584	-3.5424393
2600	0.10873401	-0.01297	-13.5415007	-0.03008	-38.237911	-0.046188	-73.847381
2800	0.215874956	0.01188	5.216183444	0.039262	15.388542	0.0547011	20.2165209

Figure H.5: Percentage Change Data for 3 Generator Mixing Efficiency.

H.2 Graphical Results

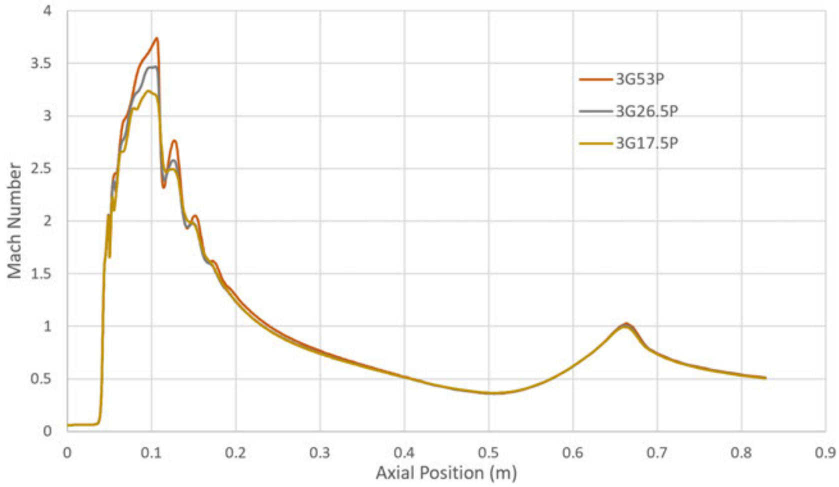

Figure H.6: Comparison of the Mach number over the ejector centreline for the three generator nozzle variations at 2.2kPa condenser pressure. Notation: 3G53P represents 3 generators with a 53mm pitch.